ACOUSTICAL PROPERTIES OF CLASSICAL OTTOMAN MOSQUES SIMULATION AND MEASUREMENTS

A THESIS SUBMITTED TO
THE GRADUATE SCHOOL OF NATURAL AND APPLIED SCIENCE
OF
THE MIDDLE EAST TECHNICAL UNIVERSITY

BY

İ. LEVENT TOPAKTAŞ

IN PARTIAL FULFILLMENT OF THE REQUIREMENTS FOR THE DEGREE
OF
DOCTOR OF PHILOSOPHY

IN

BUILDING SCIENCE, ARCHITECTURE

JULY 2003

Approval of the Graduate School of Natural and Applied Science

Prof.Dr.Canan Özgen
Director

I certify that this thesis satisfies all the requirements as a thesis for the degree of Doctor of Philosophy

Assoc.Prof.Dr. Selahattin Önür
Head of the Department

This is to certify that we have read this thesis and that in our opinion it is fully adequate, in scope and quality, as a thesis for the degree of Doctor of Philosophy.

Prof.Dr. Mehmet Çalışkan
Co-Supervisor

Prof.Dr. Ömür Bakırer
Supervisor

Examining Committee Members

Prof.Dr. Ömür Bakırer

Prof.Dr. Mehmet Çalışkan

Assoc.Prof.Dr. Demet Irklı Eryıldız

Assist.Prof.Dr. Nimet Özgönül

Assist.Prof.Dr. Soofia Tahira Elias-Özkan

ABSTRACT

ACOUSTICAL PROPERTIES OF CLASSICAL OTTOMAN MOSQUES: SIMULATION AND MEASUREMENTS

TOPAKTAŞ, İ.Levent

Ph.D., Building Science, Department of Architecture

Supervisor: Prof.Dr. Ömür Bakırer

Co-supervisor: Prof.Dr. Mehmet Çalışkan

July 2003, 234 pages

In this study, acoustical properties of XVI Century Classical Ottoman Mosques have been examined by using geometrical room acoustics techniques. This golden period of mosque architecture in Ottoman history reached to the summit with the beautiful art pieces, all designed and built by Sinan the Architect (Mimar Sinan). Süleymaniye, Rüstem Pasa, Mihrimah Sultan (Edirnekapı) in Istanbul and Cenabi Ahmet Pasa in Ankara have been selected for measurements and acoustical simulation. Each mosque chosen in the study has different architectural features and properties, which are important from the acoustical analysis point of view. Süleymaniye has the largest inner space compared to others. It has two semi-domes and it has mainly plaster and stone interior surfaces. Rüstem Pasa is relatively small mosque with highly reflective tile-covered inner surfaces. Mihrimah Sultan has full glass windows on its walls and, finally, Cenabi Ahmet Pasa possesses plaster covered inner surfaces. Sound propagation inside these holy spaces has been simulated by ray tracing technique. For the diffuse sound field simulation radiosity approach has been employed throughout the acoustical modeling. Sound measurements have also been recorded and analyzed later for comparative evaluation. Important acoustical properties of these mosques such as energy decay curves, reverberation times, clarity and definition are estimated and compared within themselves. The acoustical importance of dome shape and surface materials are emphasized in terms of functional and acoustical requirements for such spaces. Also, in this thesis, analytical photogrammetry technique has been applied to define accurate three dimensional graphical model of a mosque.

Keywords: Acoustics of Mosque Architecture, Acoustics of Holy Spaces, Geometrical Room Acoustics, Acoustical Simulation Methods, Ray tracing, Radiosity.

ÖZ

KLASİK OSMANLI CAMİLERİNİN AKUSTİK ÖZELLİKLERİNİN BENZETİM VE ÖLÇÜMLERLE BELİRLENMESİ

TOPAKTAŞ, İ.Levent

Doktora, Yapı Bilgisi Anabilim Dalı, Mimarlık Bölümü

Tez Yöneticisi: Prof.Dr. Ömür Bakırer

Ortak Tez Yöneticisi: Prof.Dr. Mehmet Çalışkan

Temmuz 2003, 234 sayfa

Bu çalışmada XVI. yüzyıl klasik Osmanlı camilerinin akustik özellikleri, geometrik oda akustiği tekniği ile incelenmektedir. Bu dönem Osmanlı tarihi cami mimarisinde altın dönem olarak bilinir ve Mimar Sinan tarafından tasarlanmış ve inşa edilmis tüm bu eşsiz sanat eserleri zirvede ki haklı yerlerini almışlardır. İstanbul'da Süleymaniye, Rüstem Paşa, Mimhimah Sultan (Edirnekapı) ve Ankara'da Cenabi Ahmet Paşa camileri bu tez kapsamında akustik ölçümler ve benzetim çalışmaları için seçilmişlerdir. Seçilen her bir cami akustik analiz bakış açısından farklı özelliklere ve unsurlara sahiptirler. Örneğin, Süleymaniye camisi diğerlerine kıyasla en büyük iç hacme ve iki büyük yarı kubbeye sahip olup mermer ve sıva yüzeylere sahiptir. Rüstem Paşa camisi ise

göreceli olarak daha az hacme sahip ve iç yüzeylerde bol miktarda seramik kullanılmıştır. Mihrimah Sultan camisi ise cok sayıda pencereye sahiptir ve son olarak Cenabi Ahmet Paşa camisi ise sıva kaplı yuzeylerle kaplıdır. Örnek mekanlarda ses dalgalarının yayılımı ışın izleme tekniği ile bilgisayar benzeşimi gerçekleştirilmiştir. Dağınık ses benzeşiminde radiosite yaklaşımı kullanılmıştır. Gerçek zamanlı frekans analiz cihazı ile ses ölçümleri de kayıt edilmiş ve daha sonra analiz edilmiştir. Enerji sönümlenmesi, çınlama süreleri, 'clarity' ve 'definition' gibi önemli akustik özellikler bu tez sonucunda elde edilmiş ve karşılaştırılmıştır. İç yüzey malzemelerin ve kubbenin akustik önemi vurgulanmıştır. Ayrıca, bu tez çalışmasında analitik fotogrametri tekniği, üç boyutlu çizim modelini hasas bir şekilde oluşturulması aşamasında uygulanmıştır.

Anahtar kelimeler: Cami Mimarisi Akustiği, Kutsal Mekan Akustiği, Geometrik oda akustiği, Akustik Benzetim Yöntemleri, Işın izleme, Radiosite.

To My Dear Wife

ACKNOWLEDGEMENTS

The author would like to express his deepest gratitude and appreciation to his supervisor, Dr. Mehmet Çalışkan, Professor of the Mechanical Engineering Department, M.E.T.U., for his continuous help, guidance and encouragement throughout this study.

The author also extends his sincere thanks to his supervisor Prof.Dr. Ömür Bakırer for her encouragement and invaluable help for completion of this study.

The author would like to thank Mr. Ashoki Sujanani of Intergraph Middle East, for his kind consideration all the time and encouragement for this study.

The author would also like to express his thanks to Mr. Murat Özgümüş, Mr. Şinasi Özkılıç and Mr. Kemar Gülcen for their help during measurements.

The Presidency of Religious Affairs (Diyanet İşleri Başkanlığı) and the the General Directorate of Foundations (Vakıflar Genel Müdürlügü) are gratefully acknowledged for the permision to make measurements in these mosques.

Finally, thanks are also to his family for their continous support and patience.

TABLE OF CONTENTS

LIST OF TABLES

Table

LIST OF FIGURES

Figure

CHAPTER 1

INTRODUCTION

In this thesis acoustical characteristics of XVI century classical Ottoman mosques is analyzed using a software developed called BASS which is the implementation of a combined geometrical room acoustics and radiosity techniques. The software development has been started during the Master of Science study of the author and it’s been evolved and reached its current status through this study.

One of the most important reasons of studying mosque acoustics is the rarity and inadequacy of studies on the subject. Inadequacy is better observed when the studies on church acoustics are compared with the ones on mosques. A literature survey on mosque acoustics also show how rare the studies are on the subject when compared to the ones done for the church acoustics. Consequently, this study has originated from the need of a detailed and comprehensive study on mosque acoustics.

The aim of the study is to draw out main acoustical design principles through an analysis on acoustics of historical mosques. Additionally, the study aims to provide additional knowledge to those in search of reaching a consensus on mosque acoustics. The results of this study may serve as a reference for future studies. Especially, in the mosques where acoustical measurements have been made, very detailed documentation has been done and presented in the appendix of this study.

The mosque architecture in Ottoman history reached it's summit in this XVI. century with the art pieces, all designed and built by Sinan the Architect (Mimar Sinan). Süleymaniye, Selimiye, Sehzade Mehmet, Rüstem Pasa, Mihrimah Sultan mosques are some examples built by Mimar Sinan in this period. Some mosques of the period were selected to study acoustical properties of the mosque architecture. Each mosque chosen in the study has different architectural features and properties, which are important from the acoustical analysis point of view. Also, the main reason of choosing Sinan's mosques to be analyzed, relies on the belief that in his superiority in mosque design and their perfectness in acoustical terms. The target will be reached by analyzing the master's monuments.

In Chapter 2, methods developed for the analysis of sound fields inside enclosed spaces are discussed with a special emphasis on geometrical room acoustics techniques. Existing literature on ray tracing, method of images, beam tracing and radiosity is reviewed. Amongst available methods of analysis, the geometrical room acoustics has proven to be a viable and powerful tool. It has been extensively used to characterize both transient and steady-state acoustical behavior of enclosed spaces.

The XVI century is the golden period of Ottoman architecture and it reached it's zenith with by Sinan the Architect. It is necessary to give some background information to emphasize the historical and architectural importance of the selected mosques for case studies in this thesis. Chapter 3 is, basically, a historical survey which gives a brief life story of Sinan the Architect and summarize his art and works. This chapter also looks through the historical context of mosque architecture. Mosques in general, pre-Ottoman mosques and mosques before Sinan the Architect are discussed briefly in this Chapter 3 as well. Since one of the objectives in this thesis is to analyze the effect of dome structure on the acoustics inside the mosque, it is important to see the historical and architectural transition to single domed mosques from multiple domes or from other variations.

In Chapter 4, the theory behind the ray tracing and radiosity is given in detail with some mathematical background. This chapter also presents the computer implementation of the methods used in the developed software. The algorithm and some techniques are explained in this chapter too. In order to use radiosity technique form factors should be determined in advance. The form factor determination is the basic problem in radiosity approach. This chapter fully describes determination of form factors for such a complex enclosed spaces like mosque architecture.

In Chapter 5, results of selected case studies carried to demonstrate the strength and flexibility of the methods are discussed. The selected case studies are Süleymaniye Mosque, Rüstem Pasa Mosque, Mihrimah Sultan Mosque and Cenabi Ahmet Pasa Mosque. These selected mosques are located in Istanbul except the last one which is in Ankara. They are all designed and built by Sinan the Architect in XVI century and they represent the level of art in that period. Each one has different characteristics and properties. For example, Süleymaniye has huge interior space, Rüstem Pasa has beautiful ceramic tiles which used almost entire interior surfaces of the mosque and Mihrimah Sultan has enormous number of windows which makes this mosque different than the other in terms of light and acoustics. The final one, Cenabi Ahmet Pasa has no specific difference than the others. The reason why it is included in this thesis is that the use of photogrammetry in order to define precisely the geometry of the mosque. Photogrammetrical plots are employed to draw the three dimensional model of the mosque and then, acoustical analysis techniques are implemented. Also, sound measurements are performed inside the mosques. These are full spectrum measurements and used to compare and validate the simulation results. These measurements could also be used in future studies since they are considered as invaluable documentation about acoustical characteristics of these mosques. The measurement data and its graphical form are presented in appendices.

Summary and conclusions drawn from the evaluation of case studies are outlined in Chapter 6. Also, recommendations for the future work in the field are stated in this last chapter.

CHAPTER 2

PREVIOUS WORKS

2.1 Introduction

This chapter will look through literature in two different aspects, namely techniques in geometrical room acoustics and literature in holy space acoustics.

There are mainly two major methods developed to analyze sound field inside enclosed spaces; geometrical room acoustics and analytical methods. Analytical methods like finite elements, boundary elements and finite differences can be applied to more simple geometries like rectangular shapes since the method involves the solution of three dimensional wave equation to obtain standing wave patterns and natural frequencies. For more complex geometries including furniture, machinery etc inside the enclosed space, the application of boundary conditions and definition of geometry become inconvenient and it is sometimes impossible to solve the equations due to lack of enough computing power and resources. Application of these techniques are mainly limited to low frequency acoustical analysis of enclosed spaces. On the other hand geometrical room acoustics methods like image source, ray tracing, beam tracing and radiosity has great advantage of satisfying a number of requirements and needs of acoustical analysis for enclosed spaces.

In geometrical room acoustics methods the concept of wave is replaced by the concept of sound ray. Sound ray is a small portion of a spherical wave which originates from a certain point. It has a well defined directional line of propagation as light ray. This analogy only holds for short wavelengths of sound, that is, the analysis is only good for mid-to-high frequency range. Methods can be viewed as convenient means to approximate reflections of sound waves from the internal surfaces.

The simulation of ray propagation explains the relation between shape of the enclosure and its sound decay characteristics. Although this technique has some restrictions like phase relationships between different sound sources are not considered and existence of standing waves are ignored, it still allows a meaningful numerical synthesis of echograms which may be used to determine reverberation time , clarity of sound and speech intelligibility.

2.2 Method of Image Sources

The method of images considers the sound energy received at a single point due to sources and their mirror images through different walls of the room. Sound waves reflected from walls more than once are represented by high order image sources. First order image source represents the first reflection from the boundaries. Order of image sources can be extended as desired. [1]

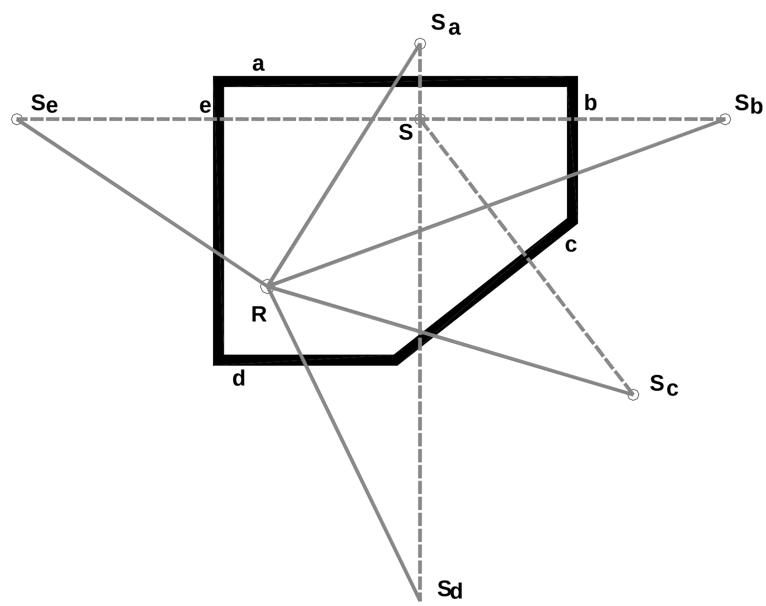

Figure 2.1 Image Source Method

The primary advantage of image source methods is their robustness. They guarantee that all specular paths up to a given order or reverberation time are found. However, image source methods model only specular reflection, and their expected computational complexity grows exponentially [3]. Although initially much faster than ray tracing the image method slows exponentially with increasing orders of reflection as the number of possible, though not necessarily, valid images increases.

Due to the computational demands of visibility checks from image source to receiver, image source methods are practical for modeling only a few specular reflections in simple environments [2].

Allen and Berkley applied the method of images to a small rectangular room. They compared the results of the applied theoretical analysis and the image modeling. They showed that image solution for a rectangular enclosure rapidly approached to the exact solution of wave equation [4].

Borish extended the method images to arbitrary room shapes. Fan-shaped concert halls were modeled by the extended image theory. Techniques were also developed to check the visibility and validity of characteristics of image sources [1].

Plomp, Steeneken and Houtgast applied the method images to rectangular rooms. They concluded that ray tracing technique would be much better suited for including diffusion of sound due to boundaries and objects in the hall. It was also revealed that treatment of directional sound sources and non perpendicular boundaries could pose problems when applying the method of images [6].

2.3 Ray Tracing

In ray tracing method, sound waves radiated from sound sources are represented by rays emitted in spherical directions. If these sound rays encounter a boundary surface of the enclosed space, the new direction of the reflected ray is calculated. The intensity of the ray is reduced upon reflection by a factor corresponding to the absorption coefficient of the surface it encounters. Each ray is traced until a specified total distance traveled or certain level of intensity is reached. Any ray that enters the receiver sphere is counted as a valid ray and it is contributed to built up an echogram in that receiver position. (Figure 2.2)

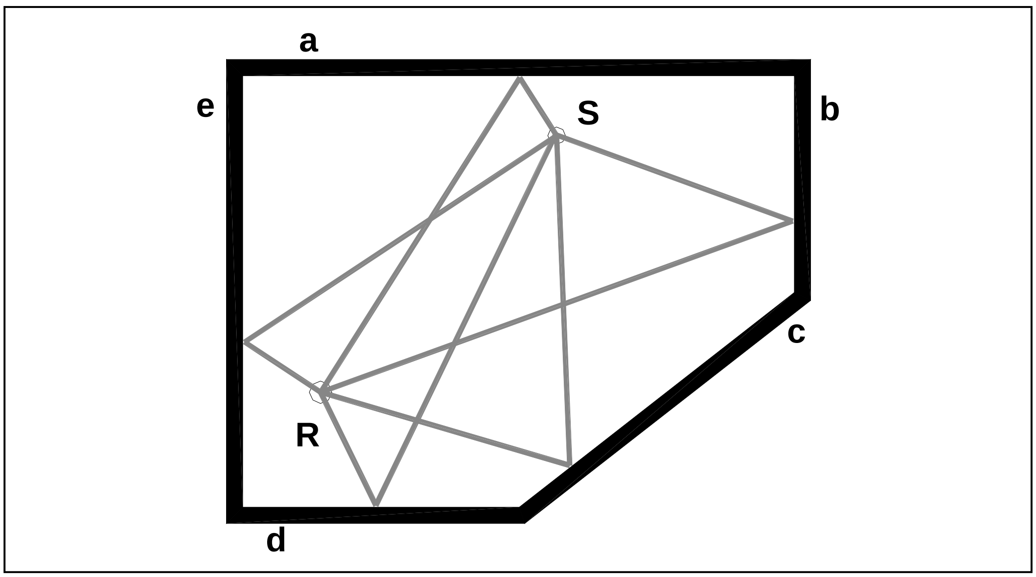

Figure 2.2 Ray Tracing Method

The primary advantage of this method is its simplicity. It depends only on ray-surface intersection calculations, which are relatively easy to implement and have computational complexity that grows sub linearly with the number of surfaces in the model. Another advantage is generality. As each ray-surface intersection is found, paths of specular reflection, diffuse reflection, diffraction, and refraction can be simulated. Even curved surfaces could be easily modeled with this method. The primary disadvantage of ray tracing method comes from their discrete sampling of rays, which may lead to under sampling errors in predicted room responses [7]. For instance, the receiver position is often approximated by volumes of space, like a sphere, in order to enable intersections with infinitely thin rays, which can lead to false hits and paths counted multiple times [7]. Moreover, important propagation paths may be missed by all samples. In order to minimize the likelihood of large errors, ray tracing systems often generate a large number of samples, which requires a large amount of computation. Another disadvantage of ray tracing is that the results are dependent on a particular receiver position, and thus these methods are not directly applicable in interactive applications where either the source or receiver can move.

Sound pressure contributions by valid rays are superimposed to obtain the sound pressure at a chosen receiver point. Phase differences among valid rays are ignored in the superposition. An echogram that represents the reflection pattern of sound waves inside the enclosure is obtained when superposition is performed along the time axis by recording the arrival times of valid rays at receiver locations. The acoustical impulse response in an octave band can be deduced by filtering the resulting echogram. The impulse response has been proven to be instrumental in determining the reverberation time and energy decay rate. Schoeder developed a method to obtain the reverberation time and energy decay curve by using data that comes from the impulse response. The method involved backward integration of the square of the impulse response [8].

Allen and Berkley used the modified form of the method termed integrated tone-burst method to incorporate the impulse response obtained by the method of images [2].

Energy criteria based upon the energy received during a certain interval in relation to the total energy are developed in order to characterize an enclosed space in terms of clarity and room response [8].

2.4 Beam Tracing

In beam tracing method, sets of rays are propagated from a source by recursively tracing pyramidal beams through the enclosed space boundaries (Figure 2.3). For each beam, polygons in the boundaries are considered for intersection with the beam in front-to-back visibility order. As intersecting polygons are detected, the original beam is clipped to remove the shadow region, a transmission beam is constructed matching the shadow region, and a reflection beam is constructed by mirroring the transmission beam over the polygon's plane. Since each beam represents an infinite number of potential ray paths originating from the source location. It does not suffer from the sampling problem of ray tracing, and there is no overlap problems like in cone tracing, since the entire space of directions leaving the source can be covered by beams exactly. The disadvantage is that the geometric operations, like intersection and clipping, required to trace beams through a three dimensional model are relatively complex, as each beam may be reflected and/or obstructed by several surfaces. Some systems avoid the geometric complexity of beam tracing by approximating each beam by its medial axis ray for intersection and mirror operations, possibly splitting rays as they diverge with distance. In this case, the beam representation is useful only for modeling the distribution of rays/energy with distance and for avoiding large tolerances in ray-receiver intersection calculations. If beams are not clipped or split when they intersect more than one surface, significant propagation paths can be missed, and the computed acoustical field can be grossly approximated [3].

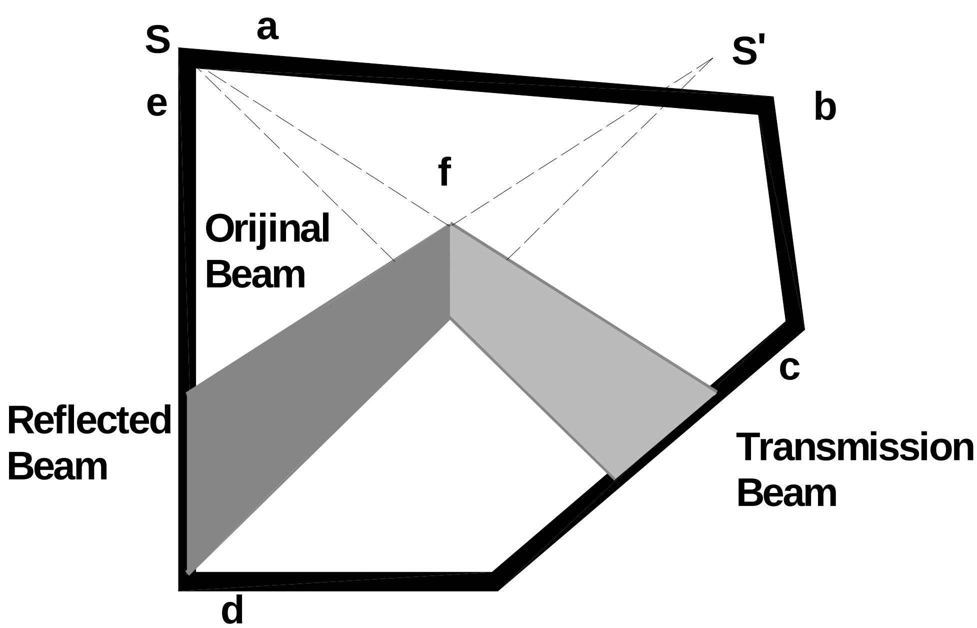

Figure 2.3 Beam Tracing Method

There are also conical [9] and triangular [10] beam tracing methods available. These algorithms provide the speed of ray tracing with the accuracy advantages of being able to use a point detector. However, since cones and triangles represent approximations of the propagating sound field, overlaps and missing reflections can happen and so have to be compensated for statistically.

Campo et al. used a variation of the Pyramid Tracing Method, which is also called Adaptive Pyramid Tracing. In that method energy carriers are three-sided pyramidal beams, which are adaptively split at each reflection according to impinged geometry. They have discretized the sound source as a user-defined number of pyramids so that it may have an arbitrary directivity pattern. Compared to a classical pyramid tracing the algorithm avoids receiver detection errors, energy losses, and consequently it does not require an (additive or multiplicative) correction factor to adjust the results. They have validated the simulation results with numerical tests in order to verify both stability and agreement with current analytical methods, and finally with data measured in a real environment. This method optimized the computation time and computer resource usage versus accuracy and stability of results.[29]

Xiangyang et al. developed a hybrid model method that combines ray tracing and image method to simulate the early reflected sound and use an improved ray tracing algorithm to simulate the reverberation sound. It was concluded, since the algorithm described in their paper is based on geometric acoustics, it is only accurate when the frequency is high enough [14].

2.5 Diffuse model

Diffuse model could be implemented as a combination of specular tracing and radiosity technique. Specular tracing could ray or beam trace for complex environments and could be image method for relatively simple spaces. Radiosity method is based upon a simple model of energy transfer. At each surface in a model the amount of energy that is given off is comprised of the energy that the surface emits internally, plus the amount of energy that is reflected off the surface. The amount of energy that is reflected off the surface can be further characterized by the product of the amount of energy incident on the surface and a reflectivity constant of the surface.

During the specular tracing process, time and plane dependant energy information passes to the diffuse system. Upon completion of the specular ray or beam tracing a separate diffuse sound profile is calculated using a radiant exchange process. For every time interval of every plane impulse response, the corresponding diffuse energy is re-radiated to all other planes. Hence each receiving plane has a proportion of this energy added to its plane impulse response at a time interval corresponding to an average distance between the radiating and receiving planes. These energy portions received will in turn be re-radiated to other planes later on during the exchange process, and so on. The exchange process cycles through successive time intervals redistributing energy until an arbitrary time that is much greater that the maximum selected order of ray reflection (Figure 2.4)

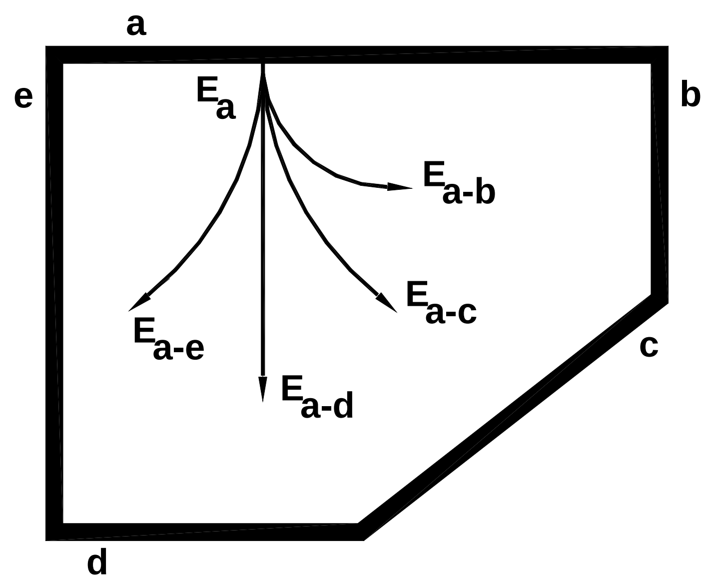

Figure 2.4 Diffuse Model

Drumm and Lam implemented diffuse model with radiosity and beam tracing. It was compared with the result obtained from image and ray tracing and it was concluded that the method has many advantages over existing methods. Although it is difficult to implement, it provides a logical and complete way to model sound propagation [11].

Korany et al. used the combination of extended radiosity method and geometrical room acoustics techniques i.e. ray tracing and mirror images in order to handle not only specular-specular and diffuse-diffuse reflections, but also diffuse-specular and specular-diffuse ones [12]. Their method allowed the calculation of wall responses independently from the receiving position, consequently, a certain receiving position room impulse response can be obtained.

Howarth and Lam showed the importance of considering the diffusion in simulation techniques. For spatially accurate predictions of sound fields, semi diffuse reflections may therefore need to be modeled using a ‘diffusion coefficient’ parameter to control the proportion of energy reflected non-specularly along with additional parameters to govern the directivity of non-specular energy. It was suggested for accurate prediction of many room acoustic parameters the modeling of surface reflections needs to be refined. Accounting for scattering in the modeling of all reflection orders assists in the prediction of reverberation time, early decay time, sound strength and clarity index [13].

2.6 Acoustics in Holy Spaces

Several studies have been made to evaluate acoustical properties of holy spaces such as churches and mosques. In general, relatively long reverberation times centering about 9 sec. are expected in such spaces. This is due firstly to the vast volume and very small absorption ratio of the audience, and secondly, to the high quality reflectors such as walls and vaults. This reverberation can be a thing of great beauty, as a listener in church is able to hear many notes of a musical solo layered on top of each other, enriching the sound beyond measure. Reverberation can also be disastrous, as the listener is subjected to different parts of a word or sentence overlapping of each other at the same instant, making it difficult to understand speech. Such long reverberation times greatly contribute to the divine atmosphere of the space. The speech intelligibility is known to be badly affected by an excessive reverberation time.

In case of church acoustics, there is much variation in the styles like Gothic or Baroque and volumes of the churches, and also in frequency dependant reverberation time due to the varying materials used to build it. It must be said that no space has the same sound, although it could be said that Gothic churches strongly emphasize the bass frequencies, Baroque the middle frequencies with less emphasis on the lower regions. Thus both the Gothic and the Baroque churches have their own sound characteristics.[30]

On the other hand the reverberation of the churches with large volumes are definitely higher then all the others. Evaluation of the relation between the reverberation time and the volume/floor seating area ratio (*V/F*) gives clues about acoustical behavior of these spaces. Magrini and Ricciardi have found that the reverberation time is directly related to the *V/S* ratio in churches. Thus, increasing values of *V/F* ratio correspond to increasing values of reverberation time. They have also concluded that value of clarity index C80 decreases with increasing V/F ratio [31].

Carvalho prepared a paper about relations between speech intelligibility and other acoustical and architectural measures in churches. It was found that the vast majority of churches tested have poor rating in the quality of speech intelligibility. It was also reported that different architectural styles have different speech intelligibility properties; for example, Renaissance appears as the style with the lowest speech intelligibility and the Visigothic and Baroque are the ones with the highest speech intelligibility values.[32]

Hamadah and Hamouda have examined the speech intelligibility within the main prayer hall of the Kuwait State Mosque and they have proposed a totally electronic approach to enhance existing poor speech intelligibility. [33]

In January 2000 a 3-years project as an international partnership called CAHRISMA was started with the main objective of innovation and implementation of the concept of “Hybrid Architectural Heritage” being a new way of identification that covers acoustical as well as visual features. Participants of the project are Yıldız Technical University (Turkey), UNIFE (Italy), INRETS (France), Technical University of Denmark, University of Malta, University of Malta, University of Geneva MIRALAB (Switzerland), EPFL-LIG (Switzerland) The main objective of the project being to be able to predict how the acoustics was and is and becomes after restorations. At the time this text was written, the results and conclusions obtained from the project had not yet been released.

CHAPTER 3

MOSQUE ARCHITECTURE

3.1 The Mosque

Mosques are public buildings that are used for prayers, sermons, teaching and social gatherings in Islamic communities. Their function has remained unchanged for the past fourteen centuries and some of these early mosques are still being used today. Activities within a mosque start early in the morning, approximately one hour before sunrise, and continue until midnight. *

The Islamic place of prayer demanded no particular building shape or form while the Christian church required buildings for the celebration of Mass. In Christian churches the apse or choir, for the priests and monks, was separated from the nave and trancepts for the lay people. The altar, always at the east end, was the focus of the service, and provision was made for processions and other rituals. In the Islamic religion there were no priests. Apart from readings from the Koran and Friday sermons on moral, political and social issues, the

* The following references are used in the writing of this chapter; [21], [22], [23], [24], [35], [36], [37], [38] and [39]

sole activity in the Mosque was personal prayer. This required a space protected from sun and rain where the faithful could pray together. The one other specific needs were a *mihrab*, a niche in the wall on the side facing towards Mecca to which the prayers were directed, the *mimber* or raised platform for the delivery of sermons, and a place for ablutions. The minaret, from which the muezzin calls the faithful to prayer five times a day, became an essential element of the mosque from early times. An important consideration in the design of mosques is the prohibition of images representing humans or animals, which was regarded as idolatry. While Christian churches were ornamented with sculpture, painting and stained glass on religious themes, Islamic religious buildings were enriched only with abstract decorations and calligraphy.

3.2 Pre-Ottoman Mosques

The oldest mosque within the borders of Turkey is the Ulu Cami (Great Mosque) of Diyarbakır, dating back to the seventh century, with several later restorations. Other early great mosques are in Urfa, Cizre, Silvan, Mardin, Kızıltepe, Bitlis, Harput, Niksar, and Kayseri. Probably the most important Seljuk work is the Old Mosque in Konya, constructed between 1155-1219. For several centuries, the Seljuk mosques were of the basilica type with the Great Mosque of Divriği providing a superb example. The first muslims had virtually no architectural traditions of their own, but the lands that they and their converts conquered were rich in art and architecture. They adopted various Roman and Christian building types and adapted them freely to serve their own purposes.

The longitudinal basilica, leading towards the altar in the apse had proved to be ideal for Christian worship. For Islamic mosques, similar aisled halls were built and further aisles were sometimes added to make a larger space. Columns from existing Roman buildings were often used. Large courtyards, providing a peaceful transition from the city streets or the openness of the desert, as well as extra space for worshippers, were often added. To provide shade, the courtyards were usually surrounded with arcades.

The plans of the mosques were longitudinal halls and in time the mosque architecture started to transform to centrally planned ones which were covered with a dome. Generally the aisled hall prevailed, but occasionally domes appeared, to emphasize the entrance or the area around the Mihrab. Eventually the dome was to emerge as an essential feature in Ottoman architecture.

3.3 The Ottoman Mosque Before Sinan

Generally, mosques were built by the Sultans and other high officials in Ottoman empire. It was a duty for them to build a mosque and by the fifteenth century they were making them part of larger complexes known as *külliyes*. These complexes typically included a mosque, religious schools (*medrese*), hospitals, hospices, and kitchens to feed the poor. The first Ottoman mosques were small square structures covered with hemispherical domes and surrounded by plain stone walls. No windows penetrated these domes; the only openings were small ones in the walls The Aladdin Mosque in Bursa, which is only 8.2 meters square, represents this type. But soon they were to build on a larger scale and to add further domes of the same size adjacent to each other. The Ulu Cami (Great Mosque) at Bursa (1396 - 1400) was planned on a four by five bay grid with twelve supporting piers and twenty equal domes on pendentives. The interior offers long vistas on horizontal axes, illuminated by the small openings in the domes. The concept of creating a more vertical and centralized space appears in the Üç Şerefeli Mosque at Edirne (1437 - 1447) A central dome is flanked by four smaller domes, arranged in pairs at both ends of a long interior. This design begins the transition towards the higher, single domed mosques that were to dominate Ottoman architecture in the time of Sinan. In a scheme somewhat similar to Hagia Sophia, the Sultan Beyazıt II Mosque in Istanbul (1500) carries the same theme further.

3.4. The Ottoman Mosque in the Age of Sinan

3.4.1 Biography of Sinan

Sinan was born in a village near Kayseri in Central Anatolia, in 1489. In about 1512 he was enrolled in the Janissary Corps, an elite wing of the Ottoman army whose members were all taken from Christian families converted to Islam and trained to fight for the Sultan. Sinan was taught the trade of carpentry, at which he clearly excelled. He participated in many military campaigns ranging from Central Europe to Iran and Iraq and received regular promotions. In his role as a military engineer he oversaw the building of fortifications, ships and bridges. During his extensive travels for military purposes he must have seen fine examples of the architecture of several civilizations, and taken note of their qualities. On the basis of his exceptional talents and flair for organization, he was appointed Chief Architect to the Sultan in 1538. From then until his death at the age of at least ninety he was responsible, with the assistance of a corps of architects, for the design and construction of over four hundred buildings. While he cannot personally have designed all of them or visited them during construction, there can be little doubt that he exercised full authority over a significant number of exceptional buildings.

3.4.2 The Ottoman Mosque

Sinan the Architect worked as a chief architect in the Ottoman Empire from year 1538 until his death. The society had approved a program of planning over the entire lands of Ottoman Empire, in which every act of refinement would be accumulation of organization and collaboration.

Sinan had signed more than three hundred works during his career. This was long, difficult and tiring position. Sinan’s works consisted of a wide variety of buildings from large and small mosques, tombs, schools, palaces, villas, caravanserais, baths, aqua ducts to bridges. The period he lived in was considered to be the golden age of the Ottoman Empire. Sinan’s works can be categorized into three main groups: religious architecture (mosques, tombs, etc.), civil architecture (caravanserais, baths, etc.) and military architecture (bridges, towers, etc.). Mimar Sinan’s first architectural experience was in the Ottoman army while he was a soldier. He witnessed in numerous wars and campaigns during which time he constructed bridges and worked on ship building and restoration works. He had a lot of experience on architecture during his military days especially during campaigns in which he had a chance to build some buildings like bridges and also he had chance to see different variety of buildings in different places and most important he had change to work with some experienced people in some repairement task. There is no doubt that these experiences have contributed to develop his architectural abilities. Sinan created a unity of style with his color schemes, decoration, and designs, reflecting a natural style. Beside his architectural ability he also showed his consideration in city planning by having his works built in the most appropriate places in the city. It is clear that there is nothing more natural than a monument which harmonizes with the environment. Sinan built huge mosques in the most suitable places so that they could be viewed in all their splendor. Sinan can be considered as one of the most forthcoming representatives of classical Ottoman architecture. He introduced an architectural concept similar to that of the Renaissance. Sinan created harmony between architecture and landscape by choosing such places, thus adding beauty to the overall appearance of the city.

Sinan experimented with domed structures and interior spaces in mosques. He observed the traditions in mosque architecture as a structure and religious space. His buildings differed in terms of structure, space, symbolism and ornament. If one can examine a selected group of his works, it would be seen that he did not only experimented with alternative schemes, but also continued to refine his designs. Although his early mosques built around 1540 show mastery of his profession, he was able to progress over the years towards a peak in the creation of the Selimiye Mosque in Edirne. He created masterpieces which were way ahead of his time.

3.4.3 Other Works of Sinan

Various sources state that Sinan built more than 300 structures. According to “*Tezkiret ul Bunyan*” which is one the document that list Sinan’s works he built 344 structures which included 81 mosques, 50 *mescit* (small mosque), 61 *medrese* (schools of theology), 7 *darülkurra* (schools for Koran reciters), 19 *türbe* (mausoleums), 16 *imaret* (Alm Houses), 3 *darüssifa* (hospitals), 14 aqua ducts and bridges, 17 caravansary (inns), 33 palaces, 6 vaults and 37 baths. Sinan held the position of chief architect of the Ottoman palace, which meant being the top manager of construction works of the Ottoman Empire, for nearly 50 years, worked with a large team of assistants consisting of architects and master builders.

Sinan’s works could be classified into three levels of experience: apprenticeship, qualification and mastery. The best samples for first two of these are in Istanbul - Sehzade Mosque which he calls his apprenticeship period work, Süleymaniye Mosque which is the work of his qualification stage, and Selimiye Mosque in Edirne the product of his master stage. Sehzade Mehmed Mosque is the first of the grand mosques that Sinan has created. Unexpected death of Sehzade Mehmed who was the son of Sultan Süleyman (Süleyman the Magnificent) was a kind opportunity for Sinan’s architectural carrier. He started to design and built the mosque by Sultan Süleyman’s order and finished it in 1548. Mihrimah Sultan Mosque in Uskudar was also completed in the same year and has an original design with its main dome supported by three half domes. When Sinan reached the age of 70, he had completed the Süleymaniye Mosque and the complex. This building, situated on one of the hills of Istanbul facing the Golden Horn, and built in the name of Süleyman the Magnificent, is one of the symbolic monuments of the period. The diameter of the dome which exceeds 31 meters at Selimiye Mosque which Sinan completed when he was 80, is the most significant example of the level of achievement Sinan reached in architecture. Mimar Sinan has reached his artistic summit with the design, architecture, tile decorations, land stone workmanship displayed at Selimiye.

Sinan also designed unique *türbe* (mausoleum) projects in his carrier. Mausoleum of Sehzade Mehmed gets attention with its exterior decorations and dome. Rüstem Pasa mausoleum is a very attractive structure in the classical style. The mausoleum of Süleyman the Magnificent which is one of his most interesting experimentations has an octagonal body and a rather flat dome. Selim II Mausoleum with has a square plan and is one of the best examples of Ottoman mausoleum architecture. Sinan's own mausoleum which is located at the north-east part of the Süleymaniye complex, on the other hand, is a very plain structure.

Sinan has masterfully combined art with functionalism in bridges. The largest of his work in this group is the nearly 635 m. long Büyükçekmece Bridge in Istanbul. He has also built arched aqueducts at several locations within the city in order to maintain and improve the water supply system of Istanbul.

CHAPTER 4

ACOUSTICAL MODELING: PRINCIPLES and IMPLEMENTATION

4.1 Introduction

The theory and its computer implementation used in BASS software is given in this chapter. BASS requires three-stage work flow. The first stage is associated with the graphical representation in terms of three dimensional modeling of the space. The second stage is to generate the form factors between pairs of planes used for modeling the diffuse sound energy transfer. The final phase involves execution of ray tracing to obtain specular sound reflections in the space. The energy decay curve for given sound receiver and source combination can be easily obtained afterwards. The energy decay curve will be used to determine acoustical properties like reverberation time, early decay time, clarity etc.

4.2 Room Geometry and Graphical Modeling

Room geometry definition is the first and most important stage of the geometrical acoustical analysis. All simulations and results associated with acoustical analysis depend on accurate representation of the room geometry. Basically, the geometry is defined by using one of the CAD software packages, which is AutoCAD in this thesis study. In fact, modern CAD technology is capable of creating very complicated three dimensional solid structures. All graphical models in case studies of this thesis are drawn in three dimensional technique by using solid modeling capability of the AutoCAD software. Solid modeling tools are very powerful in such a way that any complicated Boolean operation like union, subtract and intersect could be used to define the geometry as accurately as possible.

It is required to obtain architectural plans and sections in order to model the existing architectural buildings in three dimension. The models used in this study were developed by not only the existing drawings, but also by some field measurements carried to verify the accuracy of the final model. Theodilite-assisted measurements are performed inside the mosques for this purpose.

It should be also noted that photogrammetry technique can be used to measure space coordinates as precisely as possible. This technique is applied to one case study, namely, Cenabi Ahmet Pasa Mosque in Ankara. In photogrammetry, stereo photographs taken inside the space are digitized and stored in digital form with the use of sophisticated instruments. The computer controlled P3-Planicomp analytical plotting system by Zeiss, available in the Faculty of Architecture of the Middle East Technical University, is used to digitize the stereo photographs taken inside the mosque. The digitized coordinate data can be transformed into a three dimensional model of the mosque space. Further studies on acoustical analysis are based on this graphical model. Figure 4.1 shows a sample drawing of photogrammetric plotting of Cenabi Ahmet Pasa Mosque.

Figure 4.1 Photogrammetric Plotting of Cenabi Ahmet Pasa Mosque

4.3 Ray Tracing

In ray tracing technique, sound waves radiated from a sound source are represented by rays emitted in specified directions. Generation of rays are carried over a spherical surface around the source with its center coincident at the source center. These sound rays travels with the speed of sound and obey the laws of geometrical room acoustics or simply optics. If a ray hits a boundary surface of the enclosed space, the new direction of the reflected ray is calculated using the law of reflection in optical sense. The reflected ray must lie in the plane of incidence vector and the normal vector of the surface at the point of incidence. The angle between normal vector of the surface and incoming vector termed angle of incidence is the same with the angle of reflection, that is, the angle between normal vector of the surface and reflecting vector at the point of hit.

Each surface has certain amount of sound absorption coefficient which describes energy dissipation at the boundary. The intensity of the ray is reduced by a factor upon each reflection to that surface. Each ray is traced until its energy decreases below a specified value or until a specified number of total number reflection is reached. The receiver is represented by a sphere and any ray which intersects the receiver sphere is counted as a valid ray. Energy contributions by valid rays are superimposed to obtain the pattern and the energy decay curve at the receiver positions. Figure 4.2 shows reflections and energy curve relations.

4.3.1 Hitting the Receiver

In order to find the valid rays, each ray segment should be tested whether it hits the receiver sphere or not. The following analytical formulation is enough to check whether any hit occurs. The point of intersection can be found from the solutions to Equations (4.1) and (4.2) with the positive value of parameter l for which the ray tends towards the sphere.

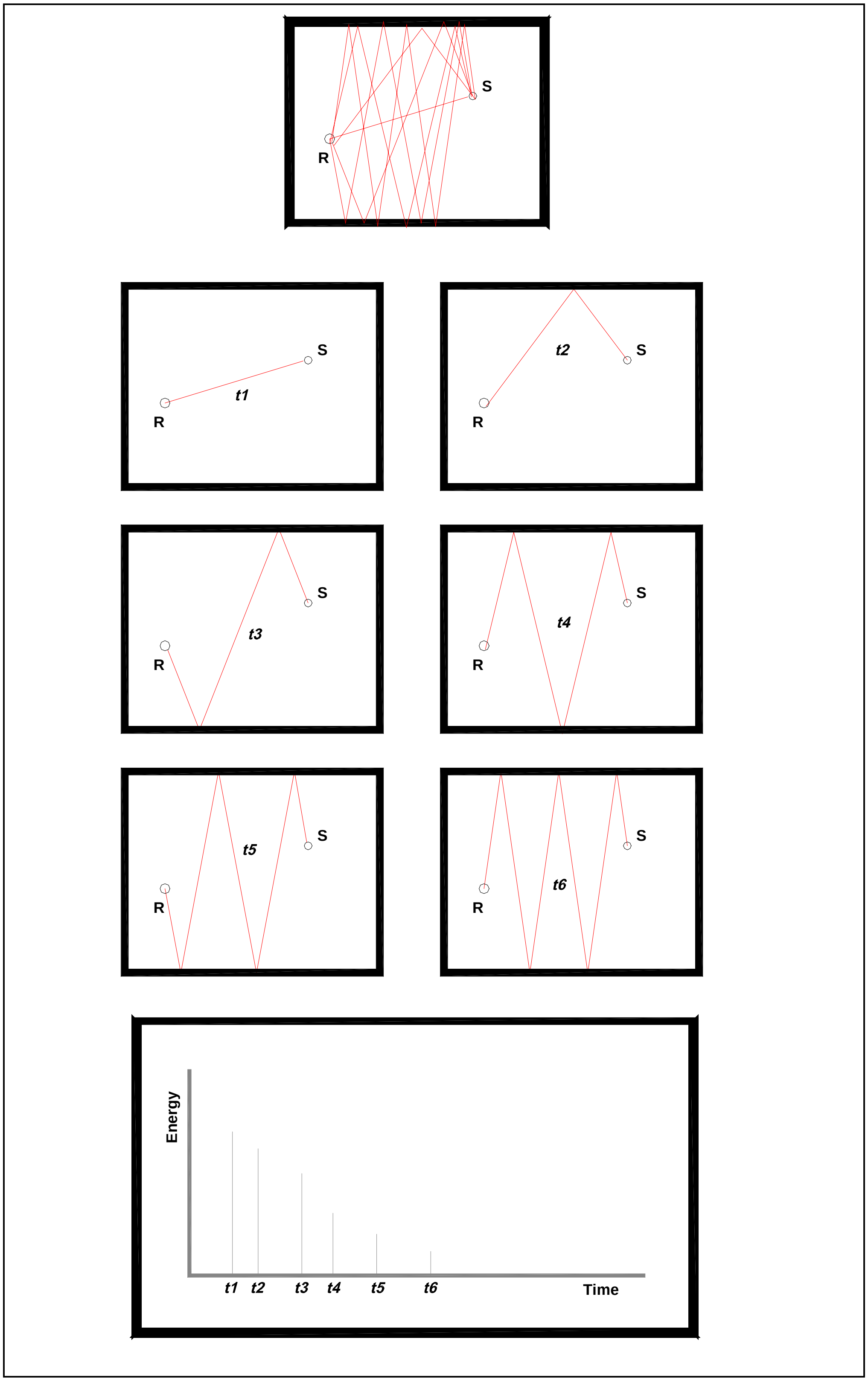

Figure 4.2 Ray Reflections and Energy Plot

$$(x-x_r)^2+(y-y_r)^2+(z-z_r)^2=R^2 \tag{4.1}$$

$$\begin{aligned} x &= x_s+v_x\cdot l \\ y &= y_s+v_y\cdot l \\ z &= z_s+v_z\cdot l \end{aligned} \tag{4.2}$$

where x, y, z are the coordinates of the intersection point of the sphere with the ray, x_r, y_r, z_r and R are the coordinates of and radius of receiver sphere, respectively; x_s, y_s, z_s are the coordinated of sound source, v_x, v_y, v_z are the directional cosines of the ray and l is the distance between the center of receiver and source.

The solution of Equations (4.1) and (4.2) has two roots given by

$$\begin{aligned} C_1 &= -A+\sqrt{A^2-B+R^2} \\ C_2 &= -A-\sqrt{A^2-B+R^2} \end{aligned} \tag{4.3}$$

where $A=v\bullet w$, $B=|w|^2$ and w is the vector between the point of incidence and the center of receiver sphere. The real roots should satisfy the requirement:

$$A^2-B+R^2\geq 0\,. \tag{4.4}$$

4.3.2 Ray Equation

There is some simplifications of acoustics phenomena such that sound energy travels in straight lines and wave phenomena are absent. Linear ray equation between points P and P_s after the assumptions simply becomes;

$$P(x, y, z) = P_s(x, y, z) + \bar{v} \cdot l \ P \tag{4.5}$$

where P_s is the coordinates of starting point of ray segment, P is the coordinates of running point, $\bar{v}$ is the direction vector of the ray and l is the distance between points P and P_s.

4.3.3 Room Surfaces

All surfaces in a enclosed space are represented by planes. Curved surfaces like dome or semi dome are approximated by planar patches. The number of planes in the model depends on the accuracy sought in the analysis. The equation of any surface plane is given by

$$Ax + By + Cz + D = 0 \tag{4.6}$$

with a normal vector N pointing inside enclosure expressed by

$$\overline{N} = Ai + Bj + Ck \tag{4.7}$$

Figure 4.3 shows a sample view of three dimensional plane approximation of Süleymaniye Mosque’s dome.

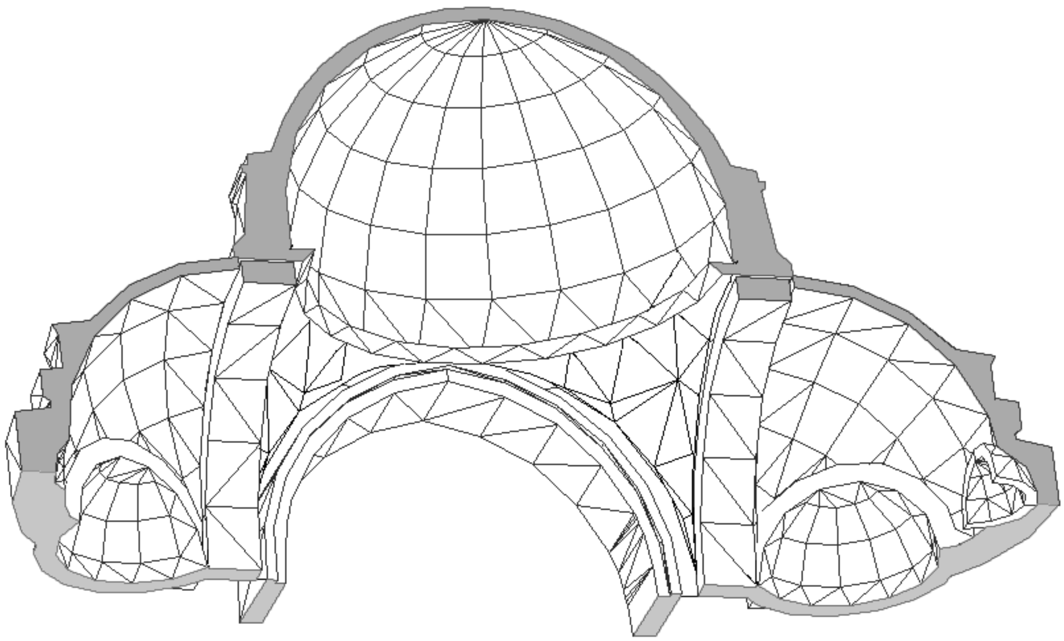

Figure 4.3 Plane Approximations of Süleymaniye Mosque's Dome.

4.3.4 Ray Reflections

Room geometry always generated as closed form, that is, there are no openings left so that rays are always within the space. In the environment for n number of planes there will be n intersection points for a given ray direction. If ray direction is parallel to any plane, then there won't exist any intersection point. Among the n intersection points only one of the solution is valid. In other words, any ray intersects only one plane in enclosed space at any time. The other possible intersection points of the planes fall outside the plane boundaries. The reason of existence of n intersection points is due to the fact that mathematical equation of plane defines an infinitely large planes. However, in room geometry, these planes are finite in size defined by edges. Therefore, the valid surface intersection occurs only where the intersection point falls inside the finite surface boundaries.

Finding a intersection point between a ray segment and a plane could be obtained simply by solving the Equation (4.8). In general the intersection point Q on a plane must satisfy the equation

$$\overline{N}_i \bullet P_i\overline{Q} = 0 \qquad (4.8)$$

where Pi is any point on i^{th} plane, P_iQ is the unit vector originating from P_i towards to intersection point Q. Figure 4.4 shows the point of intersection.

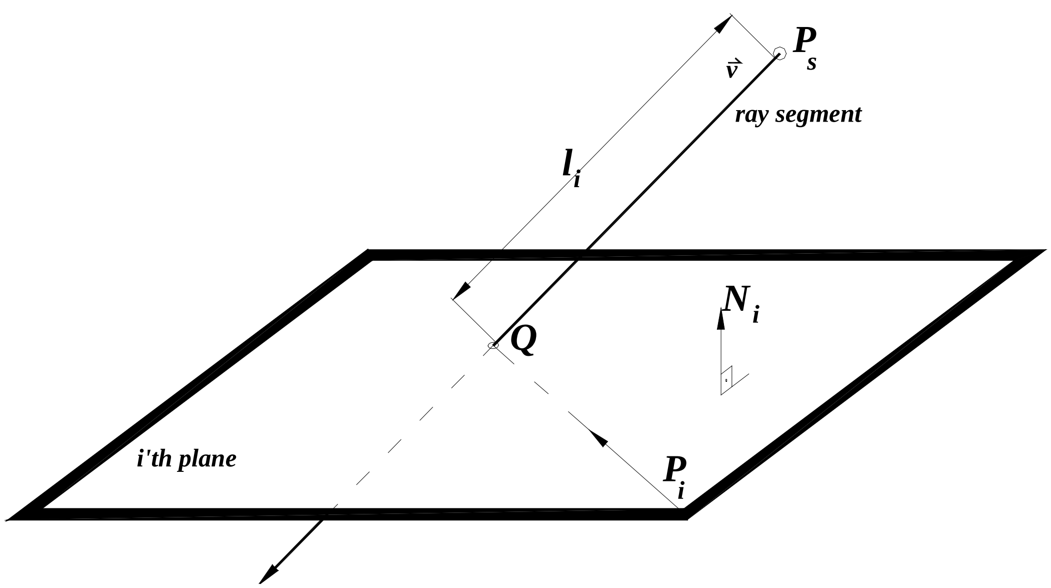

Figure 4.4 Intersection of a Ray Segment and a Plane.

The distance l_i between starting point, P_s and intersection point on the i^{th} plane can be calculated from

$$l_i = \frac{N_i \bullet P_iP_s}{v \bullet N_i} \qquad (4.9)$$

The dot product $v \bullet N_i$ yields negative number when a ray is directed to a plane since all normal vectors are selected to be oriented inwards to the room. So, the planes with positive value of this dot product can be skipped in order to speed up the computations for each ray segment direction. That is accomplished by introducing a constraint for the computations like

$$v \bullet N_i < 0 \tag{4.10}$$

The shortest distance designates the reflection point on the boundary plane involved in the reflection process, that is,

$$l_{\min} = \min(l_i) \tag{4.11}$$

then, the reflection point can be found from following linear line equation

$$Q(x, y, z) = P_s(x, y, z) + \bar{v} \cdot l_{\min} \tag{4.12}$$

The intersection point found using the Equation (4.12) requires additional test about whether the intersection point is within the plane boundaries. The point is not valid if it falls outside of the plane boundaries. The most efficient way to test this situation is shown in Figure 4.5. The method tests the point of intersection whether is inside or not by sending a rays in positive x and y directions and counting the intersection points on edges. If any number of count is odd number, then the point is inside or conversely, even number indicates that it is outside of the boundaries. For simplicity of calculations, plane corners are projected to one of the perpendicular coordinates system axis planes, such as xy, yz, xz.

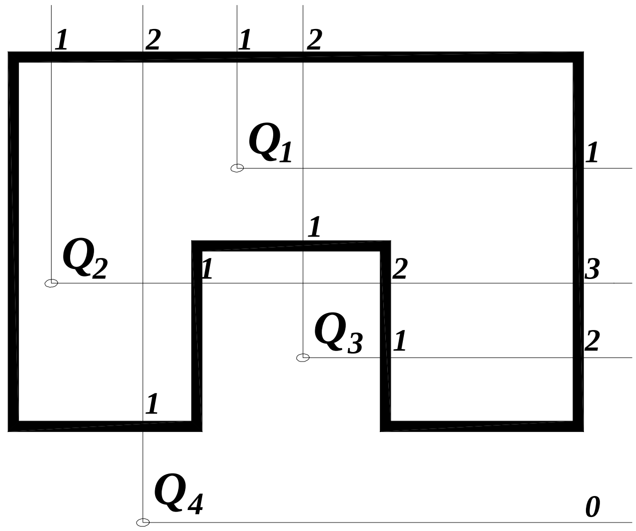

Figure 4.5 Intersection Point Check Whether It is Inside or Not.

In Figure 4.5, points Q_1 and Q_2 are inside the plane boundaries because of odd number of edge crossing occurs. On the other hand even number of edge crossing indicates that Q_3 and Q_4 are outside. Any point on an edge is taken as the inside point.

After determination of the valid point of intersection, the next step is to find the new direction of the reflected ray. This new direction is defined by a vector between intersection point Q and imaginary point P_i which is the mirror image of previous ray segment's starting point with respect to corresponding intersection plane. Figure 4.6 shows the this new direction determination parameters.

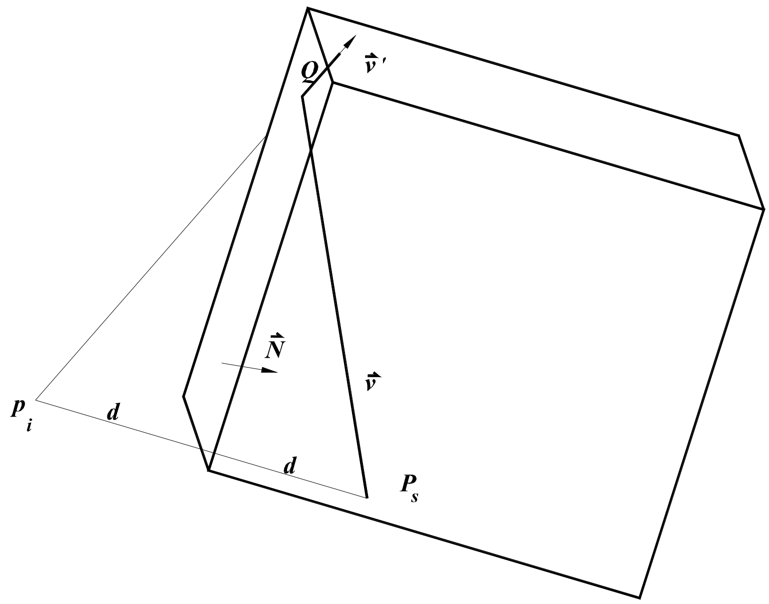

Figure 4.6 Reflection of a Ray in 3D.

The image point P_i can be calculated from following equation

$$P_i(x, y, z) = P_s(x, y, z) - N \cdot 2d \tag{4.13}$$

where P_s is coordinates of starting point of the ray segment. N is the normal vector of the plane and d is the perpendicular distance between the start pointing and the plane. The new ray direction can be calculated from

$$v' = Q(x, y, z) - P_i(x, y, z) \tag{4.14}$$

where Q is the intersection point.

4.4 Computer Implementation of Ray Tracing

Mathematical background of the ray tracing technique is given in previous sections in terms of ray propagation. The following pseudo code is used in the main ray tracing algorithm in BASS software as ray tracer. (Figure 4.7)

```
for i:=1 to NumberofRays
begin
        set V = RandomVector
        Set Ps = SourcePoint
        for j:=1 to NumberofReflections
        begin
                for each plane in planes
                if DotProduct(Normal, V) < 0 then
                begin
                        Set Q = FindIntersectionPoint(Plane, V)
                        If IsValidIntersection(Q,Plane) then
                        begin
                                StoreRaySegment(Ps,Q)
                                Set V = SetNewDirection(Plane,V,Ps)
                                Set Ps = Q
                        end
                end
        end
end
```

Figure 4.7 Pseudo Code for Ray Tracing Algorithm.

The outer loop counts for each ray, middle loop counts for each reflection of each ray and inner loop calculates the intersection point for each ray segment against each plane. The found intersection point for each plane is verified for its validity. Verified intersection point is then stored and new direction for new ray segment is calculated.

4.5 Energy Decay

It is assumed that any surface absorbs sound energy according to an energy absorption which is independent of angle of incidence. Sound is treated as an energy function not a pressure function. Thus, energies may be summed directly in the absence of phase effects. Rays carry energy and each time a ray hits a surface, some portion of the incoming energy is absorbed and some portion of its diffused and the remaining portion of energy travels in the new reflection direction. Upon reflection, specular ray energy is dissipated due to wall absorption and is diffused back into the space. Hence, given the incoming ray energy E_s, the wall absorption coefficient α, and diffusion coefficient δ, the reflected ray energy E is

$$E = E_s(1-\alpha)(1-\delta) \tag{4.15}$$

So the energy of a ray after j'th order reflection becomes

$$E_j = \frac{E_s}{N} \cdot \prod_{i=1}^{j} (1-\alpha_i) \cdot (1-\delta_i) \tag{4.16}$$

where Es is the energy of the primary source, N total number of rays traced α_i and δ_i are absorption and diffusion coefficients of i^{th} surface respectively.

It is important to note that each hit adds some energy to the surface later to be used as diffuse energy transfer between reflecting/diffusing surfaces and sound receiver. This energy can be expressed as

$$Ed \propto Es \cdot (1-\alpha) \cdot \delta \tag{4.17}$$

4.6 Radiosity

The diffuse energy fraction is accumulated in planes when a ray hits on a surface. These energy accumulations form impulse responses which consist of discrete energies at discrete time intervals for each surface. Diffuse sound energy transfer is calculated using a radiant exchange process after ray tracing is completed. The plane diffuse energy is re-radiated to all other planes in every time interval. Each receiving plane hence has a proportion of this energy added to its plane impulse response at a time interval corresponding to an average distance between the radiating and receiving planes. These energy portions received is in turn re-radiated to other planes later on during the exchange process and so on. The exchange process cycles through successive time intervals redistributing energy until an arbitrary time that is much greater that the maximum selected order of ray reflection. How much diffuse energy each plane receives is dependent on a form factor between the radiating and receiving planes. The plane form factor F_{ij} between two planes is the fraction of energy diffusely emitted from surface *i* that reaches surface *j* as given by Equation (4.18).

$$F_{ij} = \frac{1}{A_j} \int_{A_i} \int_{A_j} \frac{\cos\theta_i \cos\theta_j}{\pi r^2} dA_i A_j \qquad (4.18)$$

where A_i is the surface area of the emitting surface, r is the length of the line joining the two elemental areas and θ_i and θ_j are the angles formed between this line and the respective plane normal. The form factor is calculated as the average solid angle subtended by the receiving plane relative to grid of points on the radiating plane. When the radiant exchange process is completed diffuse energy at the receiver can be calculated. For each time interval of each plane impulse response, diffuse energy is re-radiated to the receiver. Hence, a diffuse impulse response at the receiver is built up allowing for the forms factors and distances between the receiver and radiating planes.

The radiosity method is based on the assumptions that surfaces are Lambertian and that radiative fluxes over a primitive are constant. This enables the approximation of the radiance equation as a system of linear equations. The radiosity equation expresses the radiant exitance over an oriented surface Ai as the reflection and the transmission of the incoming energy. The proportion of energy, scattered by a surface Aj and that reaches Ai , is a purely geometric term, called the form factor Fij.

4.7 Diffusion Model

Diffuse reflections are important and necessary to get uniform reverberation fields inside the enclosed spaces. Diffuse reflections reduce the risk of areas of poor acoustics within a space [15]. They create a softer sound and reduce the risk of undesirable echoes by improving the smoothness of the reverberant decay as well [16]. Hodgson noted that in rooms with only specularly reflecting surfaces sound decays were non-linear with slopes decreasing with time causing rates of sound decay to be less than that predicted by Eyring's theory, especially in disproportionate rooms [17]. However, in rooms with more diffuse surfaces, sound decays were found to be more linear.

Unfortunately, there is no standard method for measuring diffusion coefficients of surfaces. Surfaces in the model is classified either rough or smooth. This simplified approach has been tested in some previous studies comparing predictions with scale model measurements [18]. Surfaces like carpet, curtain are considered highly diffusing or rough and is assigned a high diffusion coefficient. On the other hand plaster or marble surface is considered smooth and is assigned a low diffusion coefficient. It is indicated that diffusion of 0.1 and 0.7 were best suited for smooth and rough surfaces, respectively. It should be also noted that a diffusion coefficient of 0.0 was not suitable for accurate predictions. In general for rough surfaces like carpet-covered floor a diffusion coefficient of 0.7 is used and for the smooth surfaces such as interior walls, a diffusion coefficient of 0.1 is used.

4.8 Form Factor Determination

Form factors are an essential component of the radiosity approach, just as geometrical rays are essential to ray tracing. Form factor is based on the geometry and geometric relation between the two surfaces. There are no surface properties involved. Form factor is a dimensionless constant representing the fraction of energy emitted by one surface and received by another and more. It takes into account the shape and the relative orientation of both surfaces and the presence of any obstructions, but is independent of any surface properties. Despite their apparent simplicity, form factors are notoriously difficult to solve using analytical methods. The problem of solving the Equation (4.18) can be simplified by considering the form factor from differential area dA_i to finite area A_j. Then the form factor $F_{dAi\text{-}Aj}$ is given by area integral equation [34]

$$F_{dAi-Aj} = \int_{A_j} dF_{dAi-dAj} = \int_{A_j} \frac{\cos\theta_i \cos\theta_j}{\pi r^2} dA_j \qquad (4.19)$$

The above equation cannot be solved directly for an arbitrary area A_i. However, there is a simple analytical solution for planar convex polygons. Figure 4.8 show the form factor geometry for differential area to polygon area. The equation could be approximated as

$$F_{dAi-Aj} = \frac{1}{2\pi} \sum_{k=0}^{n-1} \beta_k \cos\alpha_k \qquad (4.20)$$

where n is the number of polygon edges, B_k is the angle between vectors and α_k is the angle between the plane of dA_i and triangle formed by dA_i and k^{th} edge.

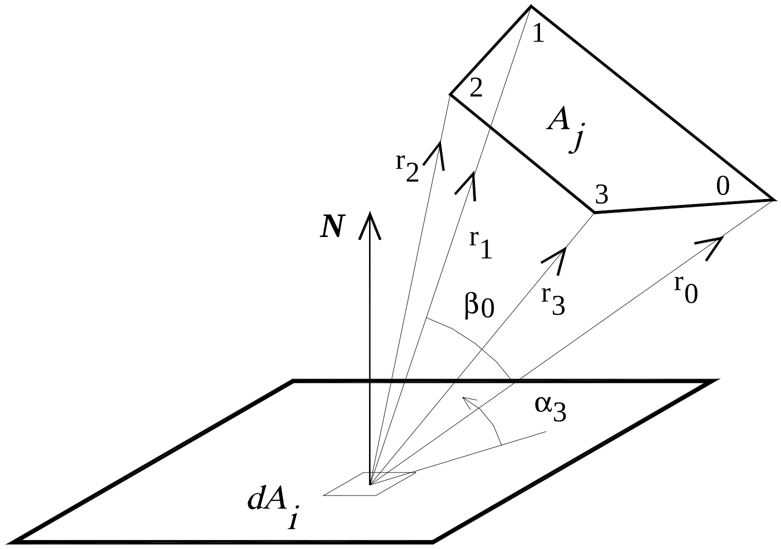

Figure 4.8 Differential Area *dAi* to Polygon *Aj* Form Factor Geometry

Nusselt's analogy could be used to solve geometrically the form factor determination. In Nusselt analogy approach a hemisphere is centered on the a differential area with unit radius and then an arbitrary area is projected first onto the surface of the hemisphere and then vertically projected to base of the hemisphere. The obtained projected area on the base of the hemisphere is proportional with the form factor of differential area to arbitrary area. The form factor for this situation is given by $F_{dEi-Ej} = \frac{A}{\pi}$ where A is projected area onto base. This equation is valid only dA_i is a differential area but it is a useful approximation for any two finite area if one of them is much smaller than the other. The configuration is given by Figure 4.9

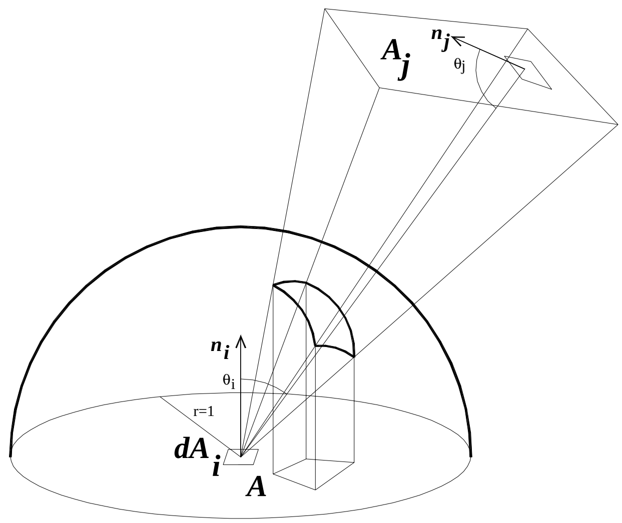

Figure 4.9 Nusselt's Analogy

Also, there is a relation between differential area and angles and distance in Nusselt's analogy which is given by

$$dA = \frac{\cos\theta_i \cos\theta_j dA_j}{r^2} \tag{4.21}$$

where dA is differential projected area on the hemisphere base

Despite the difficulties of projecting the areas on the spherical surface and then onto its base, hemicube which is half a cube approach could be much more easy to compute the area projections. In hemicube approach Nusselt's hemisphere is replaced with a hemicube. Figure 4.10 shows the projecting area onto the cells of hemicube.

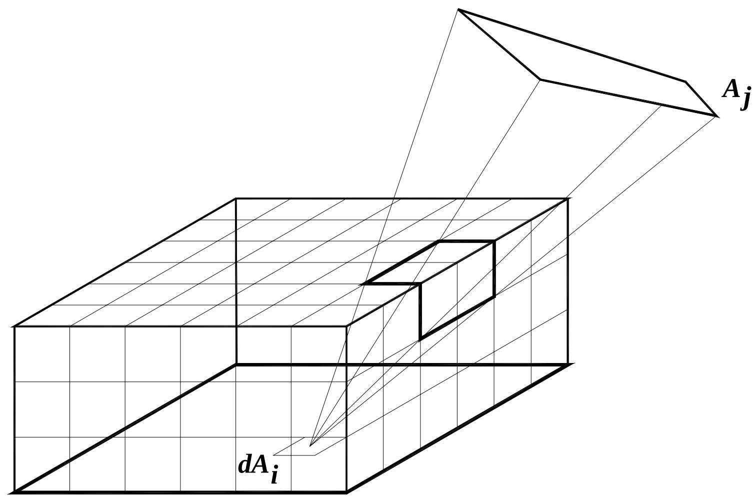

Figure 4.10 Projecting Area Aj onto the Cells of Hemicube

Each surface of the hemicube is divided in to grid of cells and for each grid cell their individual form factors determined which is called delta form factors and then summation of delta form factors gives the desired form factor which is given by

$$F_{dAi-Aj} \approx \sum \Delta F_{covered} \tag{4.22}$$

where $\Delta F_{covered}$ refers to the delta form factors of those cells covered by the projection of A_j onto one or more hemicube faces. This approximation is dependant on grid spacing of hemicube. This grid spacing have ranged from 32x32 to 1024x1024. It is clear that greater resolutions gives more accurate results but takes more computational time on computer.

By using Equation (4.21), it is obtained

$$\Delta F_{dAi-Aj} = \frac{\cos\theta_i \cos\theta_j}{\pi r^2} \Delta A_j \tag{4.23}$$

where A_j refers to a hemicube cell and and ΔAj is its area as a finite fraction of the entire face.

The major advantage of using the hemi cube is the easy in the calculation of delta form factors. Consider the top face cell given in Figure 4.11 then the following equations are easily derived:

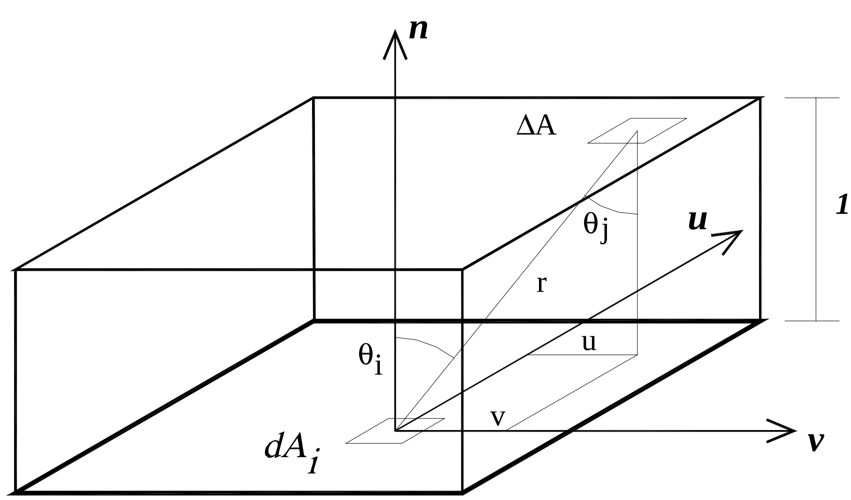

Figure 4.11 Top Face Hemicube Cell Form Factor

$$r = \sqrt{u^2 + v^2 + 1} \tag{4.24}$$

and

$$\cos\theta_i = \cos\theta_j = 1/r \tag{4.25}$$

from Equation (4.23) then

$$\Delta F_{top} = \frac{\cos\theta_i \cos\theta_j}{\pi r^2} \Delta A_{top} = \frac{\Delta A_{top}}{\pi (u^2 + v^2 + 1)^2} \tag{4.26}$$

where ΔA_{top} is the hemicube cell area a fraction of the top face area. For side face cells illustrated in Figure 4.12 where v=+/-1, the equations become

$$r = \sqrt{u^2 + n^2 + 1} \tag{4.27}$$

and

$$\begin{aligned} \cos\theta_i &= n / r \\ \cos\theta_j &= 1 / r \end{aligned} \tag{4.28}$$

Thus;

$$\Delta F_{side} = \frac{\cos\theta_i \cos\theta_j}{\pi r^2} \Delta A_{side} = \frac{n \Delta A_{side}}{\pi (u^2 + n^2 + 1)^2} \tag{4.29}$$

similarly for side face cells where u=+/-1 could be found by substituting v for u. The hemicube cell area ΔA_{side} is the fraction of the full side area, including the bottom half hidden below the hemicube base plane.

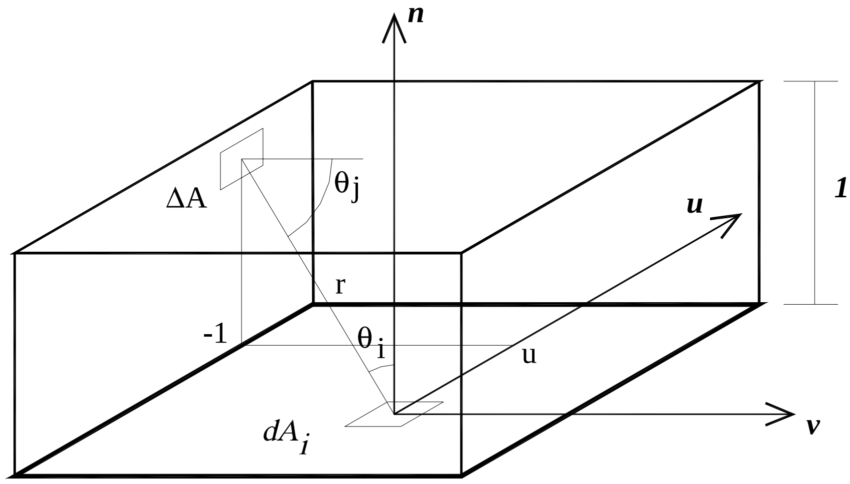

Figure 4.12 Side Face Hemicube Cell Form Factor

The hemicube algorithm is essentially a polygon scan conversion process. In order to find the form factor F_{ij} from polygon A_i to polygon A_j, the hemicube is placed over A_i and then performing perspective projection of A_j onto each of hemicube's faces. Delta form factors are then found by determination of which hemicube cells are covered by the projection. Once delta form factors are found, the approximate form factor F_{ij} is given by Equation 4.22. [34]

4.9 Computer Implementation of Form Factor Determination

Hemicube algorithm that calculates the form factors F_{ij} from A_i to all other polygons A_j in the environment is given if Figure 4.13 [19]

```
for each hemicube cell k
        Calculate delta form factor ΔF_k
endfor

for each hemicube face
      For each hemicube cell k
              set  cell_depth(k) = INFINITY
              set polygon_id(k) = NONE
      endfor
endfor
for each polygon Aij
      set Fij = 0
endfor
for each hemicube face
for each polygon Aj
      Transform Aj coordinates to Aj (hemicube) viewspace
      If Aj is visible
              Clip Aj to hemicube face view volume
              If clipped poyygon is inside view volume
                      Project polygon onto hemicube face
                      For each hemicube face cell k
                              If cell k is covered
                                      If depth of Aj at cell k < cell_depth(k)
                                              Set cell_depth(k) = depth of Aj at cell k
                                              Set poygon_id(k) = j
                                      end if
                              end if
                      end for
              end if
      end if
end for
for each hemicube face cell k
      m = polygon__id(k)
      Fim = Fim + ΔF_k
endfor
endfor
```

Figure 4.13 Pseudo Code for Hemicube Algorithm

In given pseudo code it is seen the first operation is to transform the hemicube face coordinates into local coordinates. Using this transformed coordinates, necessary visibility check are more easily performed to eliminate invisible and unwanted face grids for form factor calculation. Further calculation mainly is polygon clipping to identify which cell grids will contribute to overall form factor.

4.10 Determination of Acoustical Properties

The secular and diffuse impulse responses is combined to produce an accurate profile of the enclosed space acoustics. Clarity and Deutlichkeit can be calculated simply by integrating specular and diffuse energies with respect to time.

Clarity with a time window of 80 ms (C_{80}) is the ratio in dB between the energy received in the first 80 ms of the received signal and the energy received afterwards. C_{80} is suggested to be a measure of the sense of clarity.

$$C_{80} = 10\log_{10}\frac{\int_{0}^{80ms} E(t)dt}{\int_{80ms}^{\infty} E(t)dt} \tag{4.30}$$

Definition or Deutlichkeit with a time window of 50 ms (D) is the ratio between the energy received in the first 50 ms and the total energy received. It lies between 0 and 1. The duration of 50 ms was called the limit of perceptibility regarding speech. It is hypothesized to be a measure of how clear a sound appears to a listener - the higher the D, the clearer the sound.

$$D = \frac{E_{0-50}}{E_{0-\infty}} \tag{4.31}$$

In order to calculate Reverberation Time and Early Decay Time a profile of sound energy decay is needed. This is done combining specular and diffuse energy decay curves. A linear regression on the resultant curve can be used to determine RT and EDT. [20]

4.11 Acoustical Measurements

A real time frequency analyzer made by Brüel&Kjaer(Model 2143) was used in the measurements of reverberation time in conjunction with a sound source made by Brüel&Kjaer (Model 4224). A pressure response type ½ inch microphone (Brüel&Kjaer,model 4166) with a preamplifier (Brüel&Kjaer, model 2639) was mounted on a tripod at different heights corresponding to the ear to pick acoustical data. This height was 0.8 m for seated on floor listeners and 1.65 m for stand up listeners. The sound source was controlled remotely by the analyzer in the acquisition of sound decay data. Wide Band mode of excitation on the sound source was used in the experiments. Available software on the analyzer was exploited for the purpose in the measurements. A sound level calibrator made by Brüel&Kjaer(Model 4230) was used for calibration of the equipment. The calibration signal of 94 dB at 1 kHz was provided by the calibrator.

The collected data is then used to obtain sound energy decay curves for various sound and receiver positions. Linear regression technique is employed to determine reverberation time based on the measurement data. The data used for linear regression starts after first 5 dB drop and terminates further 20 or 30 dB drop. Extrapolation of this obtained linear regression to 60dB energy drop approximates the reverberation time.

Also, energy decays obtained from acoustical measuments are prepared as three dimensional surface graphics to give better representation of enegy decay within the space.

CHAPTER 5

CASE STUDIES

5.1 Introduction

Acoustical analysis are carried for four mosques in this thesis. They are Süleymaniye, Rüstem Pasa, Mihrimah Sultan Mosques in Istanbul and Cenabi Ahmet Pasa Mosque in Ankara. All these mosques were built in the XVI. century which is the period of classical Ottoman Architecture. All the mosques are presently in use.

The common appearance depicted to the mosque in XVI. century was once again provided by the domination of a great dome over a cubical body. For centuries the dome was known to constitute the important part of Ottoman Architecture. However, it always enriched but never dominated the structure such as in the classical XVI century architecture [x]. The mosque reflects the character of the century not only due to its usual profile of single dome placed on cubical body but also due to the three domes of last prayer section and decorations that reflect the common taste developed through the influential era of Mimar Sinan.

Each chosen mosque has different features and properties which they are important from the acoustical analysis point of view. For example, Süleymaniye has biggest inner space compared to others and it has two semi-domes. Rüstem Pasa is relatively small mosque with tile-covered inner surfaces. Mihrimah Sultan has a lot of windows on its walls and finally, Cenabi Ahmet Pasa has simply plaster covered surfaces.

5.2 Cenabi Ahmet Pasa Mosque

Cenabi Ahmet Pasa Mosque is located in the district of Ulucanlar in Ankara. This mosque is the only case study in thesis which is not located in Istanbul. According to the inscription panel above its entrance portal, the mosque of Cenabi Ahmet Pasa was built in 1565-1566. The donor Cenabi Ahmet Pasa was a well-known State official of the period and during the reign of Sultan Süleyman the Magnificent. Figure 5.1 show exterior view of mosque.

The architect of the mosque is unknown, however several architectural historians have seen the skill of Mimar Sinan in the method of design and structure, and have attributed the building to him. Related to this attribution, it is important to understand how impossible it is to erect more than 400 buildings within 50 years in the different regions of the Empire without collaboration. Only between 1561-1565 five mosques -at Northwest, East and at Central Anatolia- were built in far regions of Anatolia. Apparently, it was impractical to reach and get hold every constructional activity [24].

Figure 5.1 Cenabi Ahmet Pasa Mosque in Ankara

In fact another sign of such a belief is figured out by the defaults of the architecture of the mosque, such as : the portal rests on the right of the axis of the *mihrab*. Besides, the dome above the portal was built narrower than the width of the *revak* of the last prayer section thus, the void between the dome and base was filled by non-structural Turkish triangles [24].

The dome of Cenabi Ahmet Pasa mosque has a diameter of 14.40 m. The transition of the dome structure to square base is provided by squinches. At the skirts of the dome there is a small gallery. Windows around the gallery and on the walls supply a great extent of light so as to create space of transparency. Figure 5.2 shows the 3D computer model used in the analyses.

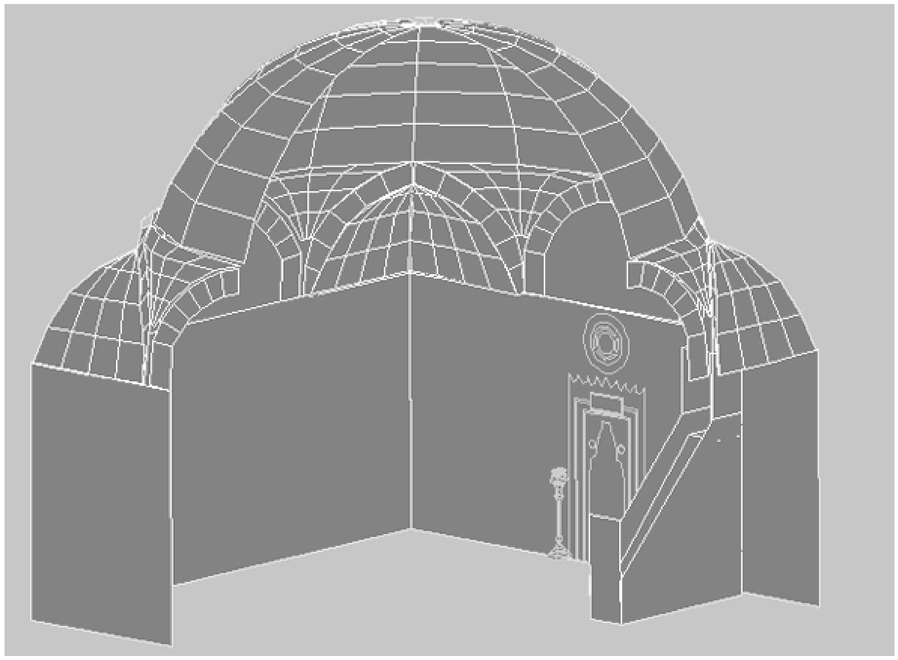

Figure 5.2 Three-Dimensional Model of Cenabi Ahmet Pasa Mosque

Again by referring to the inscriptions on the walls, it has been possible to learn the certain interventions to the building. In chronological order in 1802-1803, 1887-1888, 1940 and recently between 1959-1970 the mosque was repaired and it is still in use.

5.2.1 Acoustical Measurements in Cenabi Ahmet Pasa Mosque

In order to perform acoustical analysis and comparison with the simulation results several acoustical measurements performed in Cenabi Ahmet Pasa Mosque. These measurements are done on 6 January 1994 under the permission obtained from General Directorate of Foundations (Vakıflar Genel Müdürlügü). Stereo photogrammetry plotting has been used as an alterative coordinate measurement approach which is different than other cases. The main reason to use photogrammetry in this case is to test and see how it could be useful as a geometry generation method in acoustical simulation and analysis application. In photogrammetry, stereo photographs that were taken inside the space are digitized and stored in digital form. Computer controlled P3-Planicomp analytical plotting system by Zeiss is used to digitize the stereo photographs. Then, three dimensional model of the mosque space is generated by using he digitized coordinate data. The further studies on acoustical analysis are based on this model.

Two different sound sources located in front of the *mihrab* and at the *muezzin mahvili* (speaker corner). Receivers were located at 4 different positions corresponding to these sound sources. Layout diagram of these receiver and source locations are given in Figure 5.3.

Reverberation time results calculated from measurement data by linear regression of energy decay curve in different receiver positions at different frequency band are given in Table 5.1. All energy decay curves and data interval used in calculation of reverberation time are given in Appendix A. Three dimensional energy decay surface graphics for different source and receiver combinations are given through Figure 5.4 to 5.11.

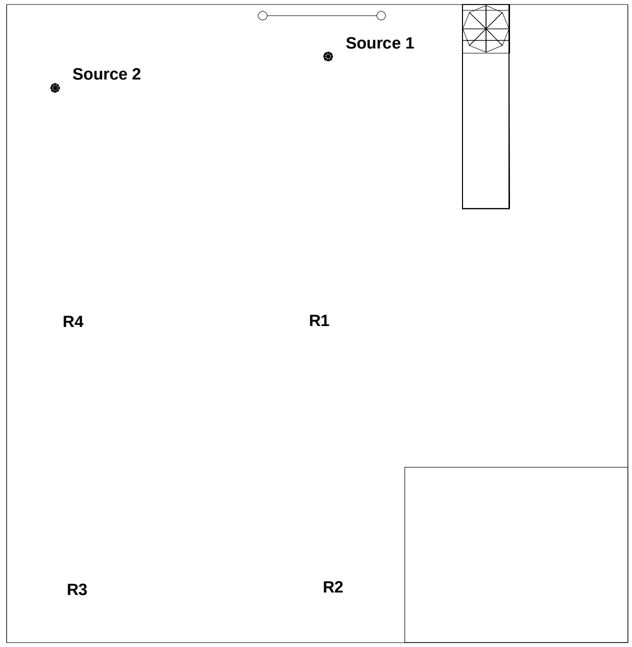

Figure 5.3 Source and Receiver Positions for Cenabi Ahmet Pasa Mosque

Table 5.1 Reverberation Time (T30) Results from Measurement Data at Different Source and Receiver Positions in Cenabi Ahmet Pasa Mosque

Receiver	125 Hz	250 Hz	500 Hz	1000 Hz	2000 Hz	4000 Hz
S1R1	4.4	4.5	3.7	3.5	2.5	1.5
S1R2	4.6	4.5	3.6	3.4	2.5	1.5
S1R3	4.7	3.9	3.5	3.5	2.5	1.6
S1R4	4.9	4.5	3.6	3.5	2.6	1.6
S2R1	4.5	4.8	3.6	3.5	2.5	1.5
S2R2	6.0	4.2	3.4	3.5	2.5	1.5
S2R3	5.2	4.6	3.8	3.5	2.5	1.5
S2R4	5.2	4.2	3.6	3.7	2.6	1.5

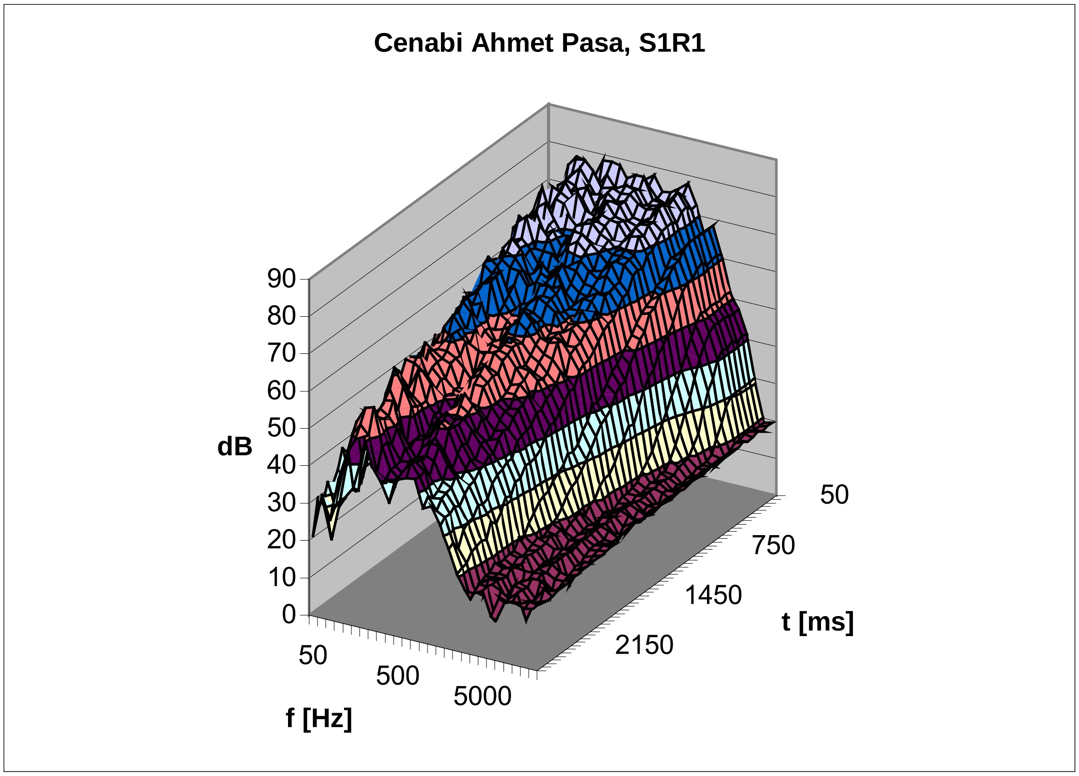

Figure 5.4 Energy Decay for Measurement Data in 3D at S1R1 in Cenabi Ahmet Pasa Mosque

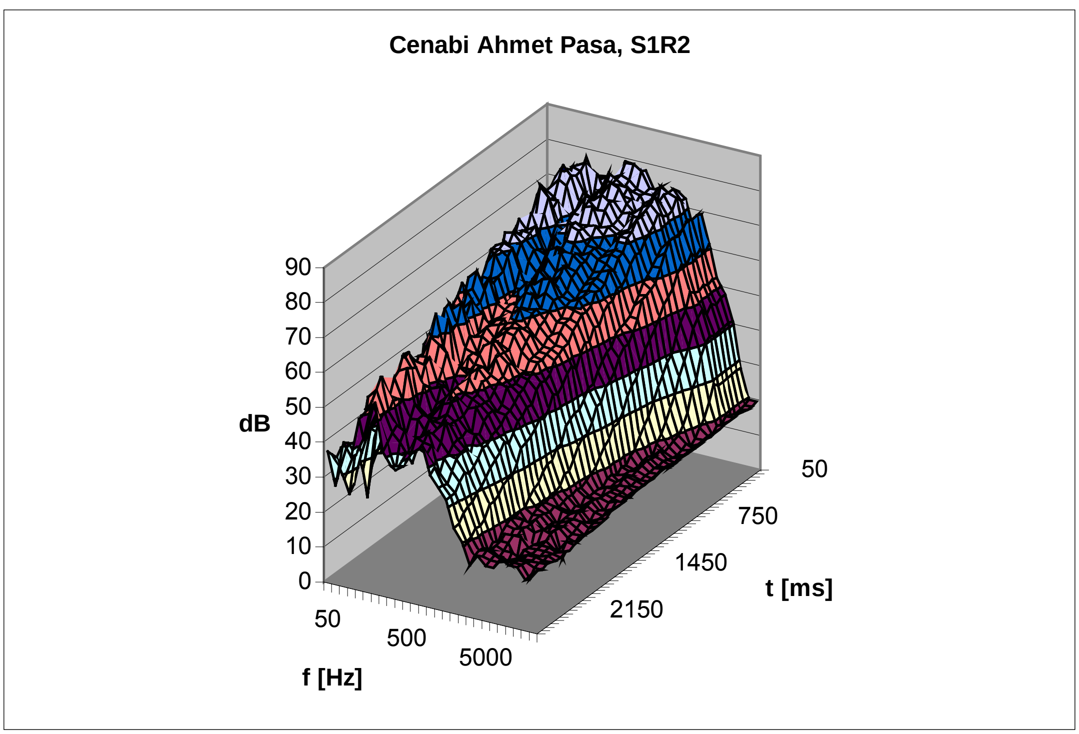

Figure 5.5 Energy Decay for Measurement Data in 3D at S1R2 in Cenabi Ahmet Pasa Mosque

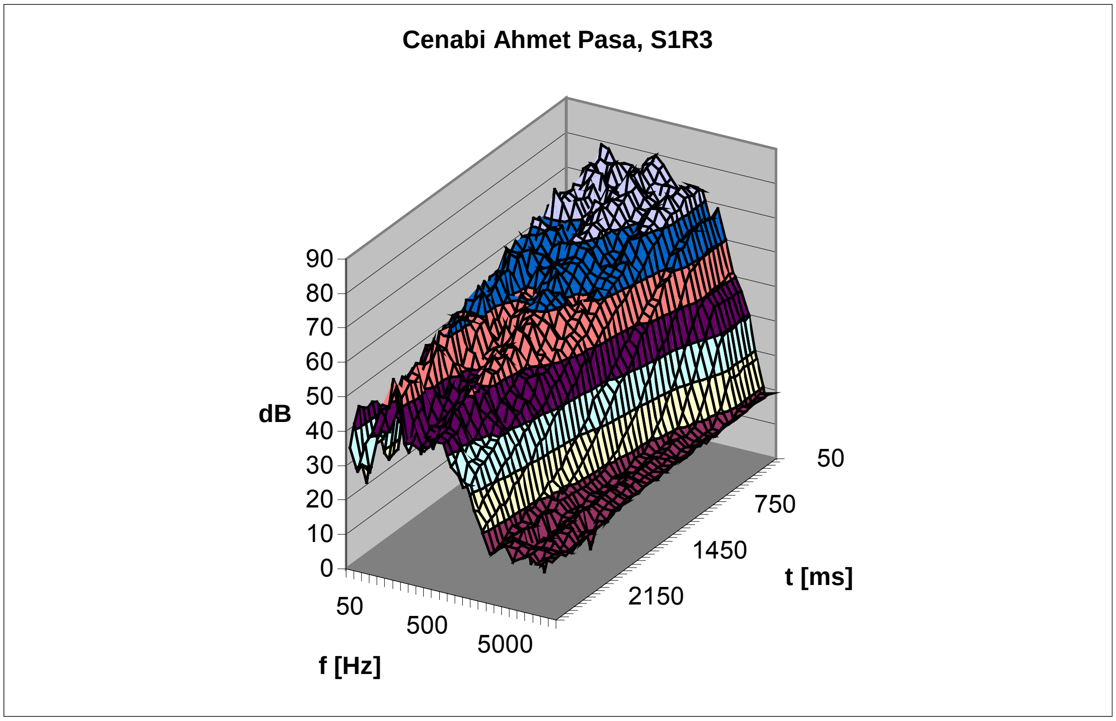

Figure 5.6 Energy Decay for Measurement Data in 3D at S1R3 in Cenabi Ahmet Pasa Mosque

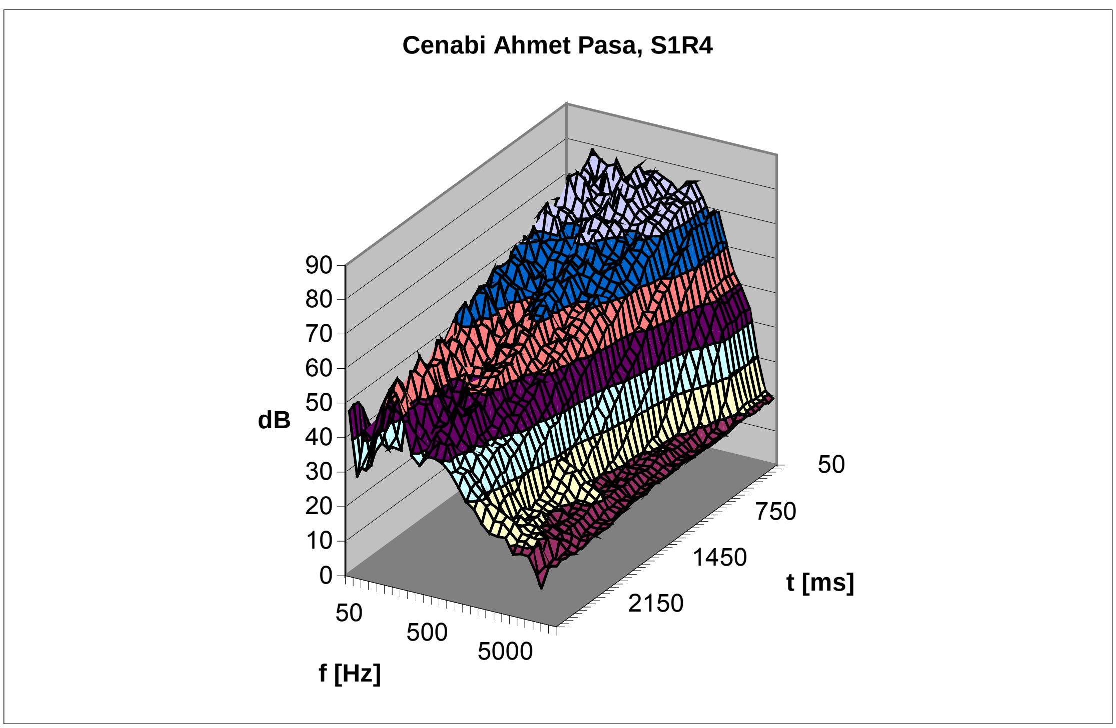

Figure 5.7 Energy Decay for Measurement Data in 3D at S1R4 in Cenabi Ahmet Pasa Mosque

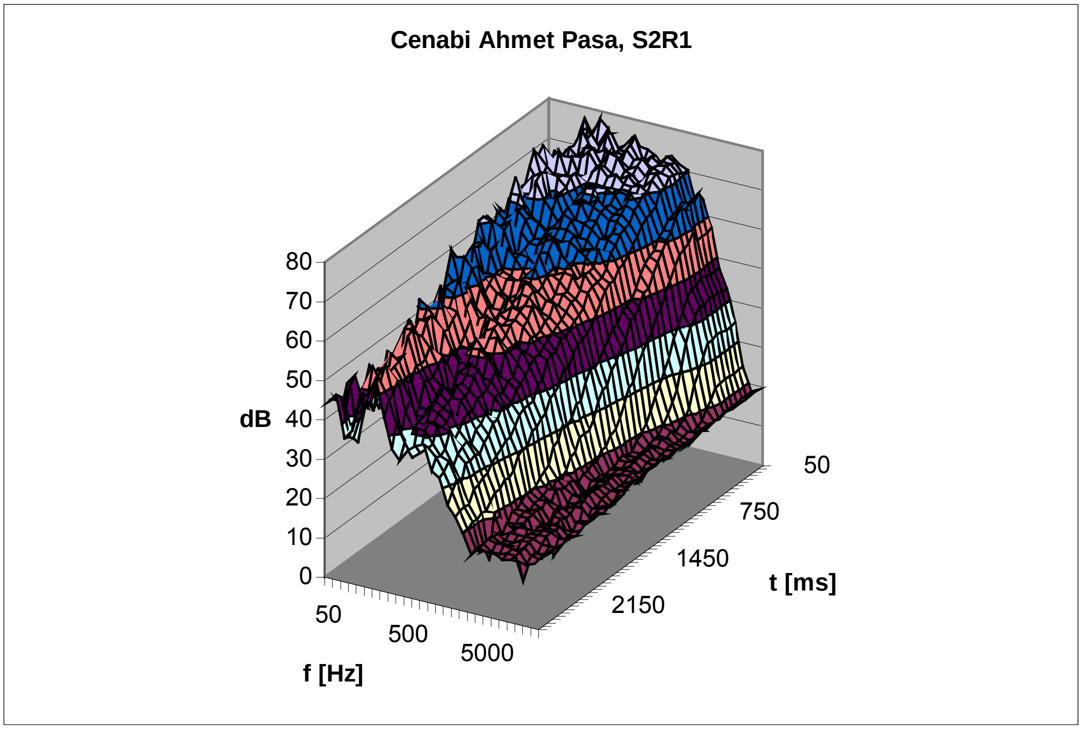

Figure 5.8 Energy Decay for Measurement Data in 3D at S2R1 in Cenabi Ahmet Pasa Mosque

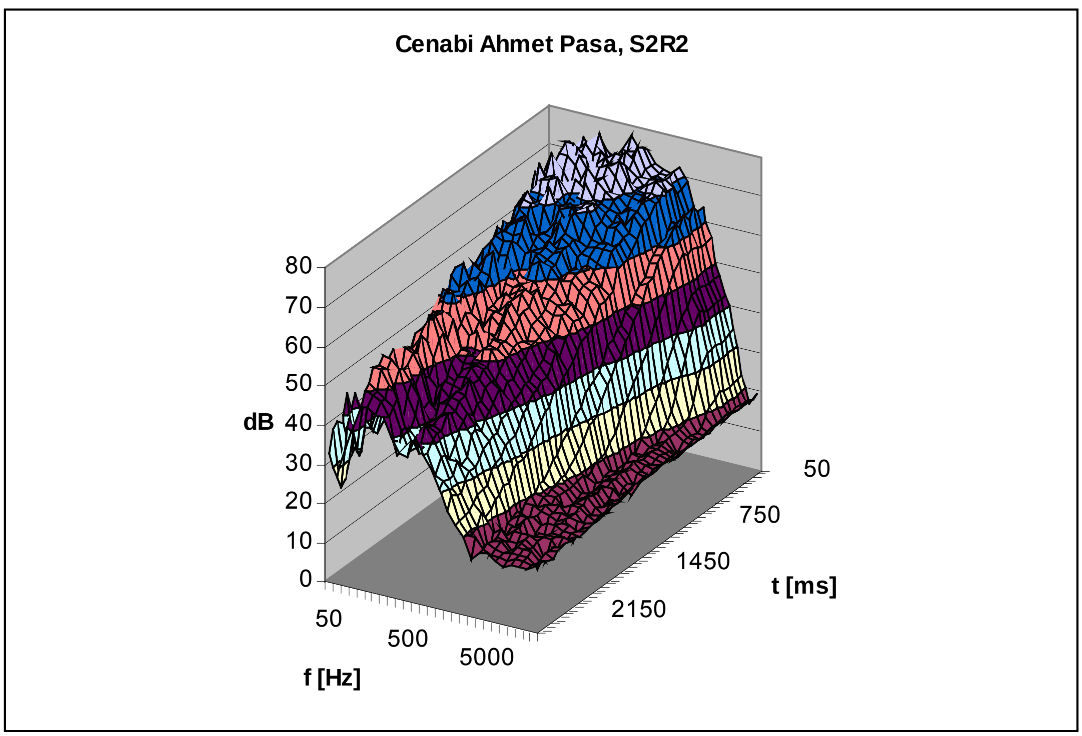

Figure 5.9 Energy Decay for Measurement Data in 3D at S2R2 in Cenabi Ahmet Pasa Mosque

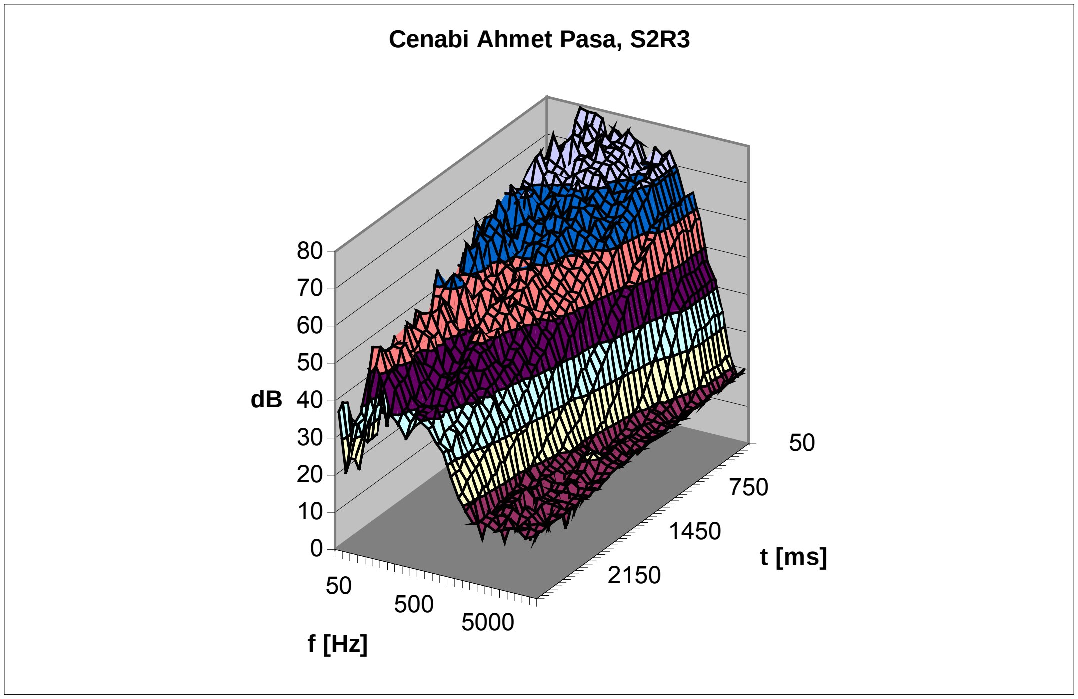

Figure 5.10 Energy Decay Measurement Data in 3D at R3S2 in Cenabi Ahmet Pasa Mosque

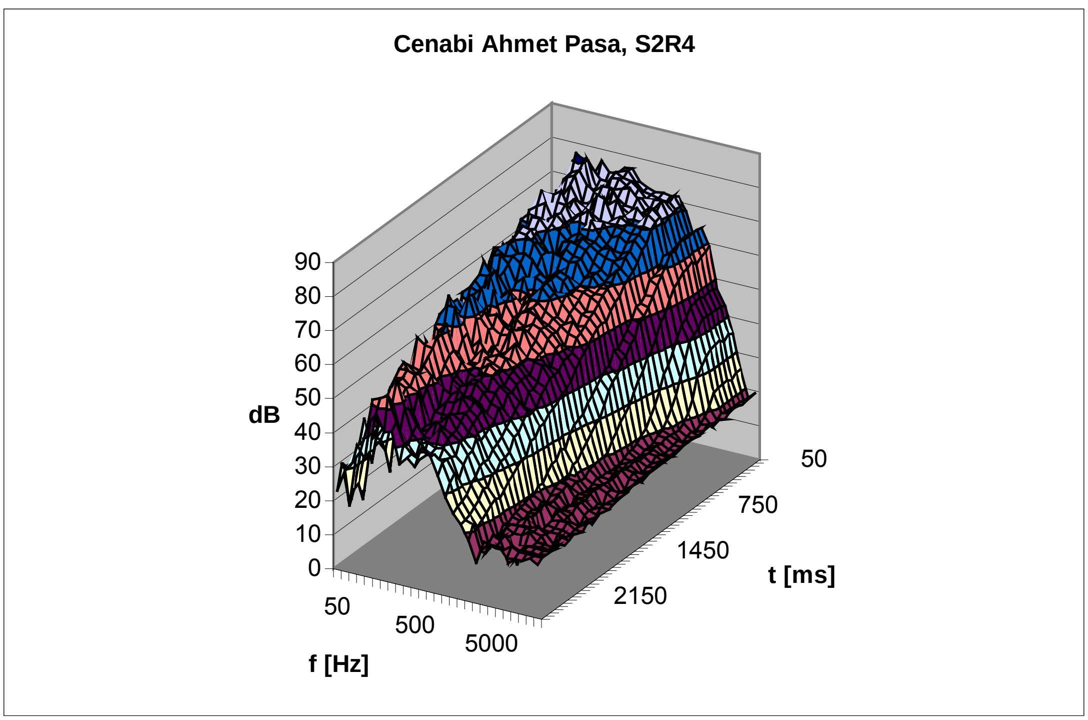

Figure 5.11 Energy Decay for Measurement Data in 3D at S2R4 in Cenabi Ahmet Pasa Mosque

5.2.2 Acoustical Simulations of Cenabi Ahmet Pasa Mosque

Acoustical simulations performed using combination of ray tracing and radiosity method. This hybrid model enables to obtain results very quickly since number of rays are reduced significantly. Cenabi Ahmet Pasa Mosque has plaster covered walls and floor is covered by thick carpet. Absorption coefficients used in simulation are given Table 5.2.

Table 5.2 Absorption Coefficients Used in Simulations

Surface	**125 Hz**	**250 Hz**	**500 Hz**	**1000 Hz**	**2000 Hz**	**4000 Hz**
Wood	0.15	0.20	0.10	0.10	0.10	0.10
Plaster	0.14	0.10	0.05	0.04	0.04	0.03
Carpet	0.02	0.06	0.14	0.37	0.60	0.65
Marble or Glazed tile	0.01	0.01	0.01	0.02	0.02	0.02
Stone	0.013	0.015	0.02	0.03	0.04	0.03
Glass	0.35	0.25	0.18	0.12	0.07	0.04

Cenabi Ahmet Pasa Mosque is modeled for simulation software by using 546 plane surfaces. Diffusion coefficient values are 0.7 for carpet covered surface and 0.1 for the plaster covered interior surfaced. Form factors are generated only once and values are used for different source and receiver combination. Form factor values generation is expensive operation in terms of computing time but since it is one time job for the entire simulation it is tolerable. In fact with the modern computer resources it is not a big and time consuming task. For example for Cenabi Ahmet Pasa Mosque model which has 546 planes it took less than 5 minutes to generate all form factors between planes by using a computer processor of Intel Pentium III 1 GHz speed and 256 Mbytes RAM. Form factor calculations produces the average plane to plane distances as well which approximates the mean free path inside the space.

Sound source and receivers are located at the same position as the measurements positions. Total number of generated rays is 1000 and each ray are traced up to 6 seconds of flight time within the space. Execution time for each sound and receiver pair simulation is less than 3 minutes on Pentium III 1 GHz processor computer.

Table 5.3 Reverberation time (T30), Clarity and Definition Results for 1000Hz from Simulation at Different Source and Receiver Positions in Cenabi Ahmet Pasa Mosque

	S1R1	**S1R2**	**S1R3**	**S1R4**	**S2R1**	**S2R2**	**S2R3**	**S2R4**
RT (s)	3.3	3.4	3.5	3.5	3.5	3.3	3.4	3.4
Clarity (dB)	-5.9	-5.7	-5.7	-5.9	-5.8	-5.9	-5.9	-5.7
Definition	0.10	0.10	0.11	0.11	0.11	0.10	0.11	0.11
RT difference between measurement and simulation	7%	1%	1%	0%	0%	6%	4%	9%

Reverberation time estimation, clarity and definition values for octave band of 1000 Hz are listed in Table 5.3. Reverberation times obtained from simulation are close to values obtained from measurements. This is actually expected result from such a simulation tool. Energy decay curves obtained from different set of source and receiver are given through Figure 5.12 to 5.19.

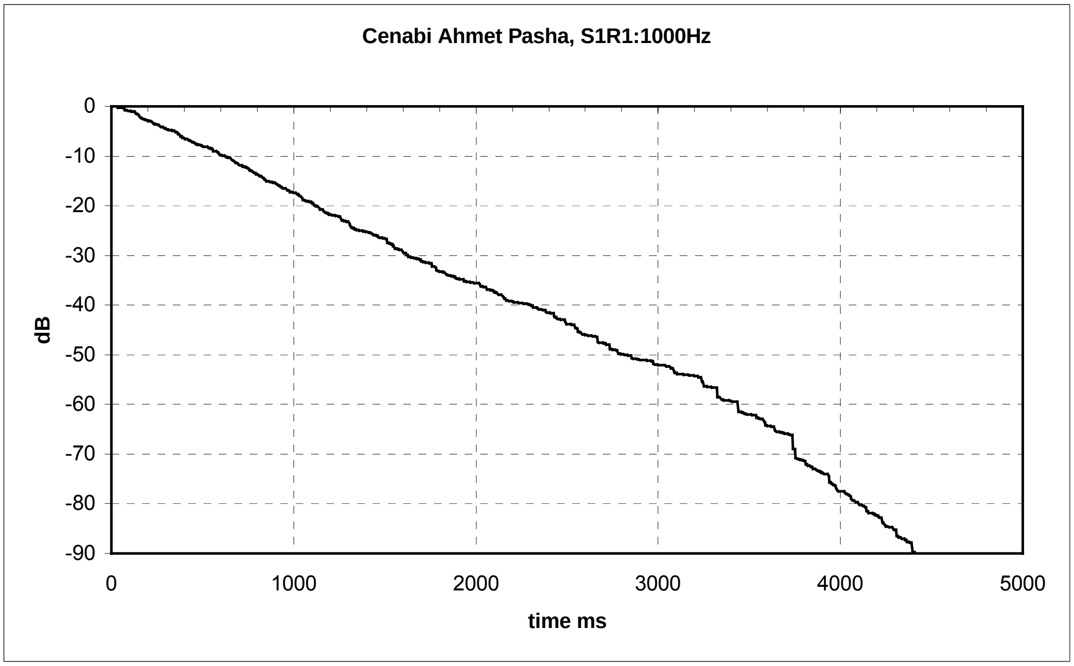

Figure 5.12 Energy Decay for Simulation Data for 1000 Hz at S1R1 in Cenabi Ahmet Pasa Mosque

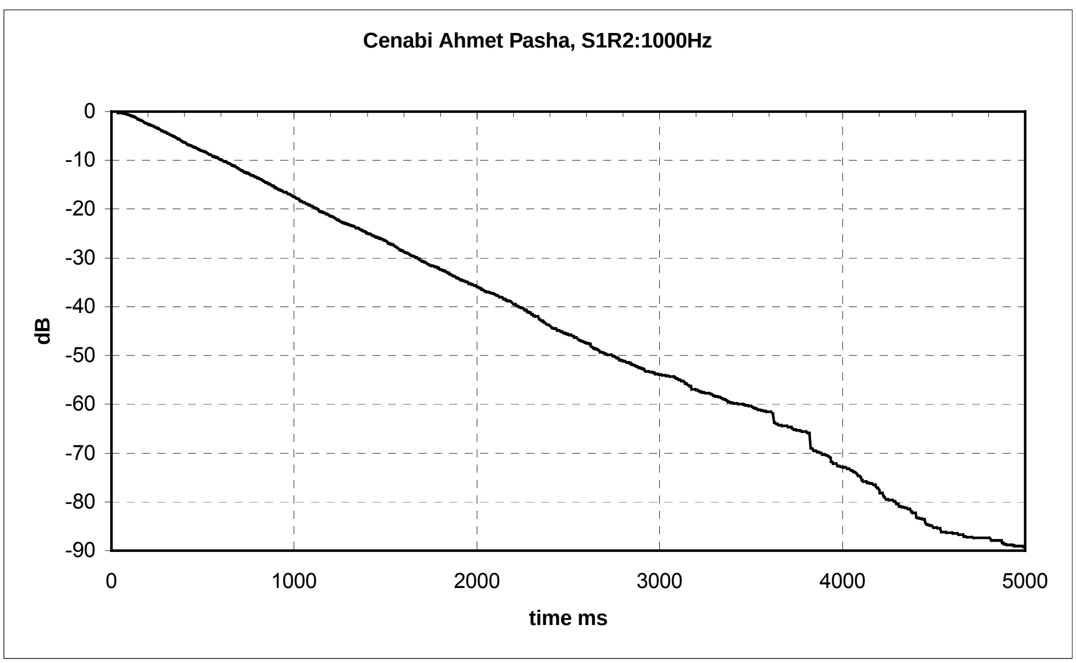

Figure 5.13 Energy Decay for Simulation Data for 1000 Hz at S1R2 in Cenabi Ahmet Pasa Mosque

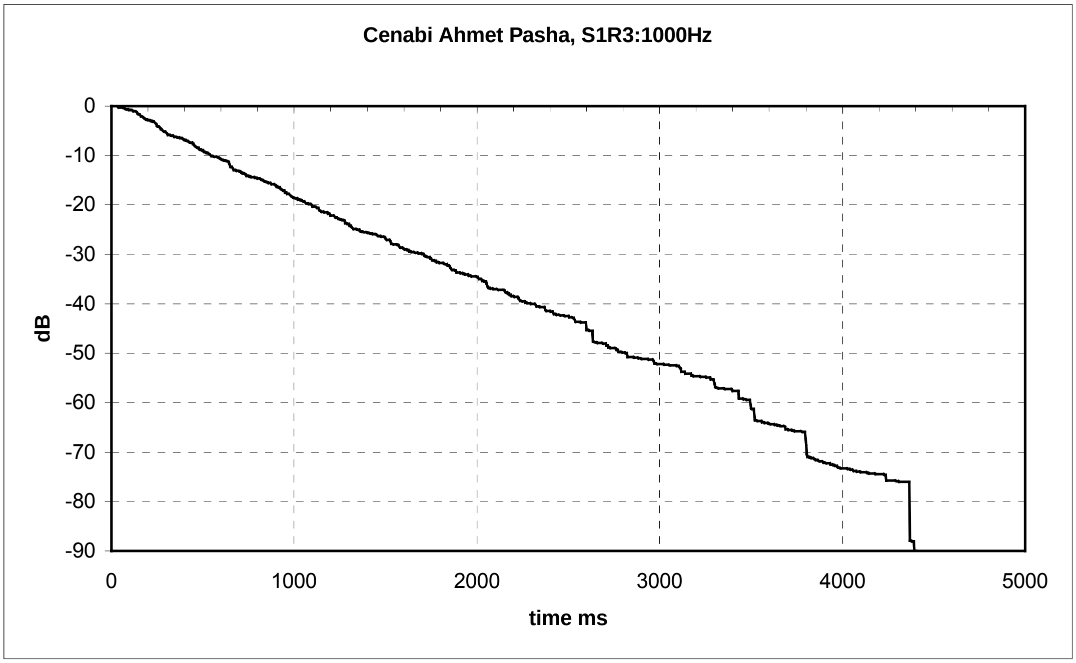

Figure 5.14 Energy Decay for Simulation Data for 1000 Hz at S1R3 in Cenabi Ahmet Pasa Mosque

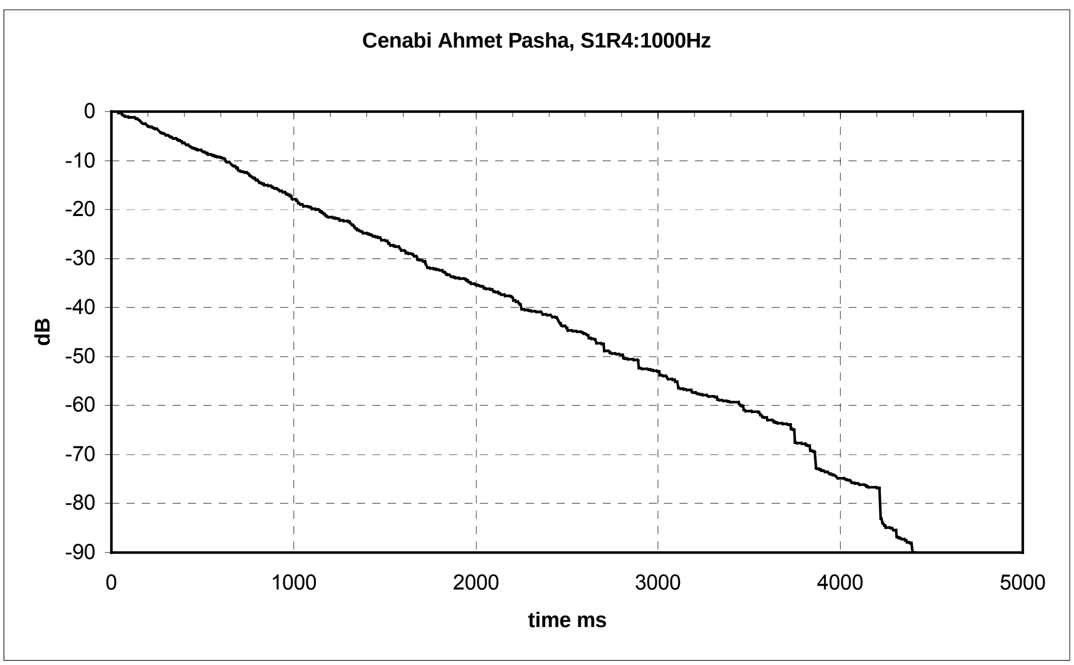

Figure 5.15 Energy Decay for Simulation Data for 1000 Hz at S1R4 in Cenabi Ahmet Pasa Mosque

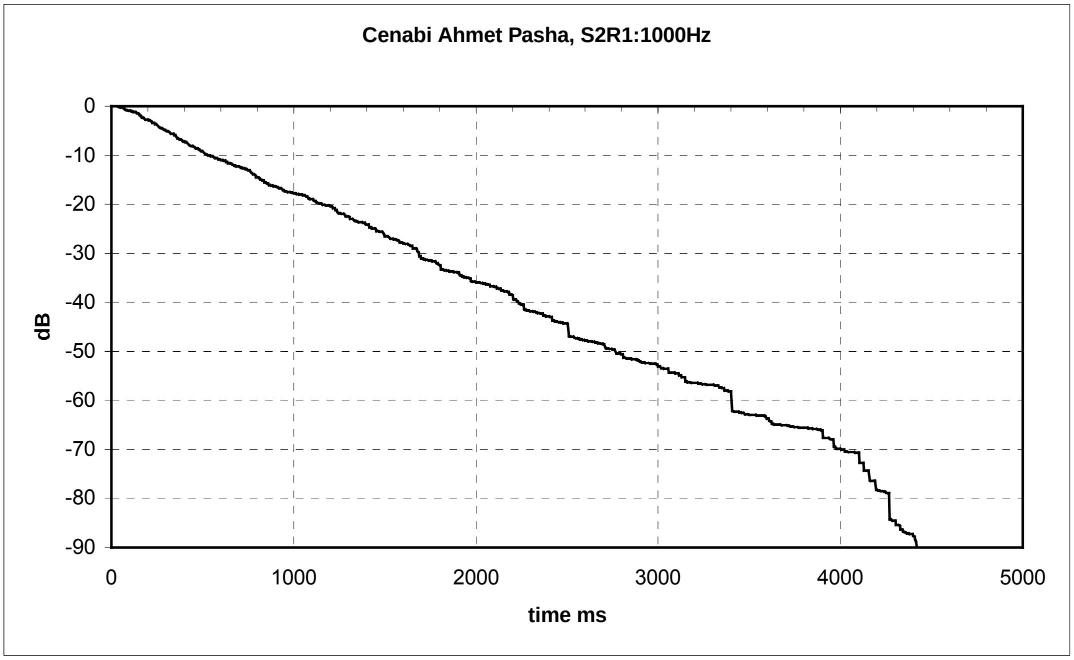

Figure 5.16 Energy Decay for Simulation Data for 1000 Hz at S2R1 in Cenabi Ahmet Pasa Mosque

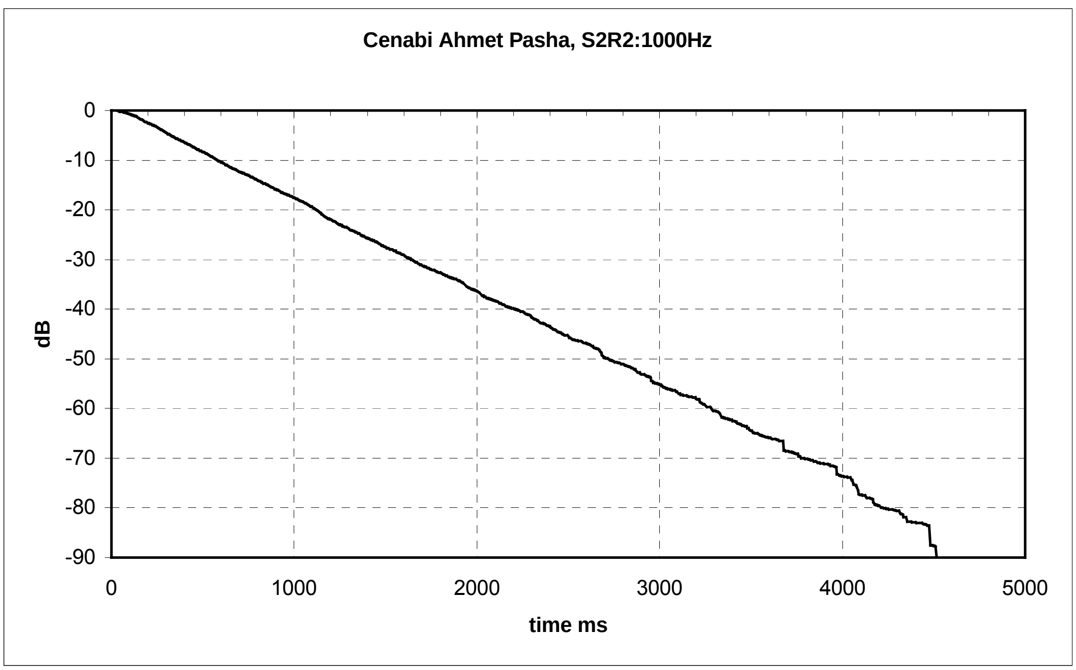

Figure 5.17 Energy Decay for Simulation Data for 1000 Hz at S2R2 in Cenabi Ahmet Pasa Mosque

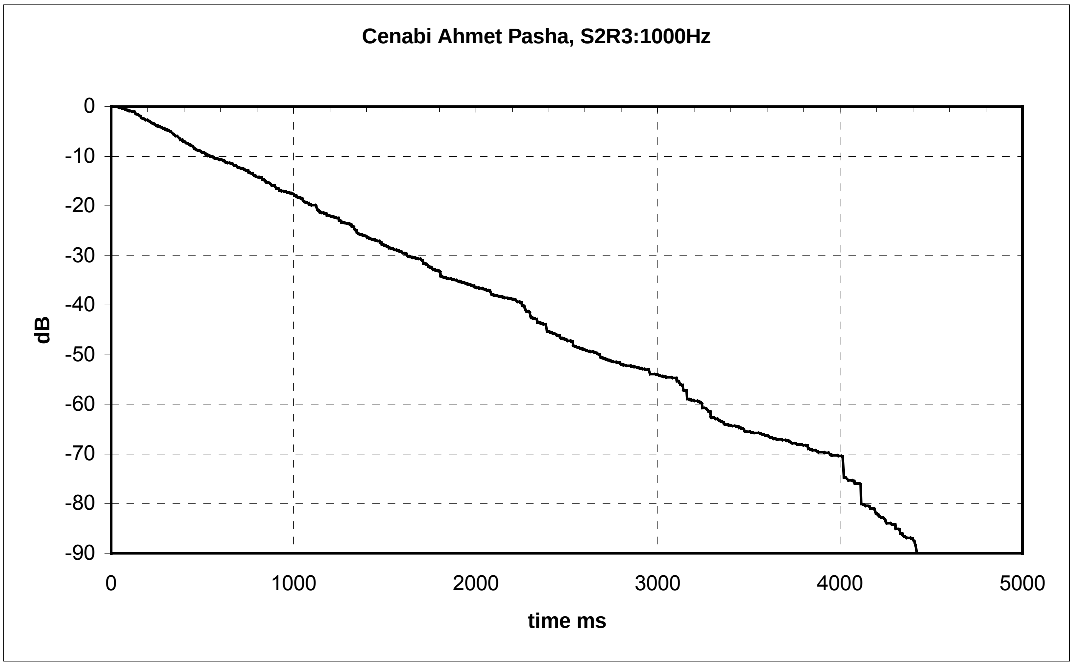

Figure 5.18 Energy Decay for Simulation Data for 1000 Hz at S2R3 in Cenabi Ahmet Pasa Mosque

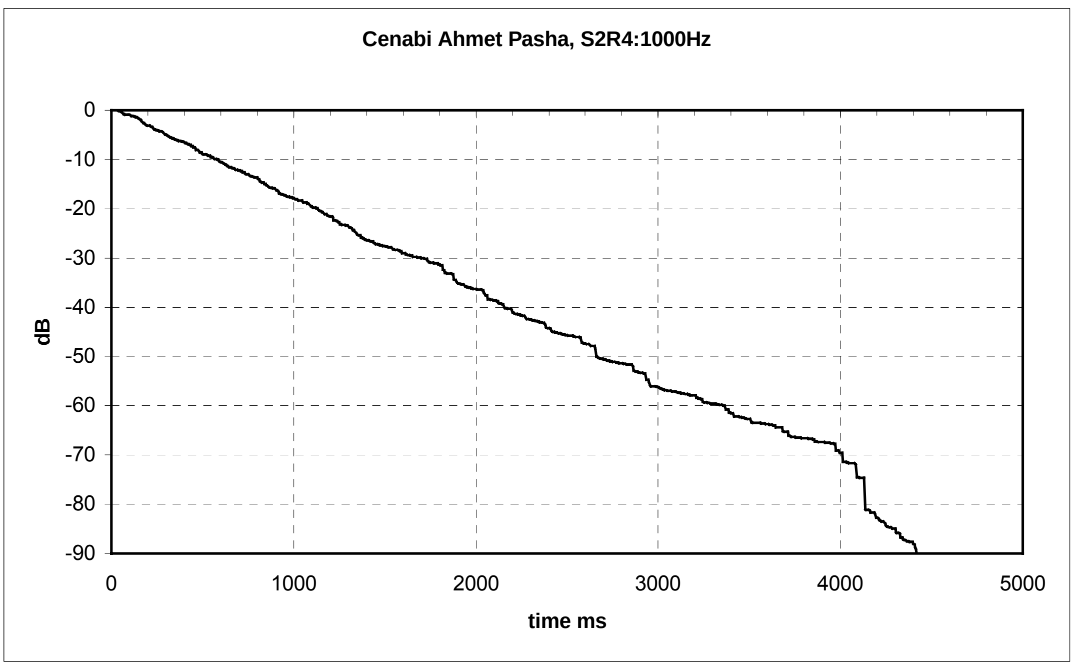

Figure 5.19 Energy Decay for Simulation Data for 1000 Hz at S2R4 in Cenabi Ahmet Pasa Mosque

5.3 Süleymaniye Mosque

Süleymaniye Mosque, the main central building of the Süleymaniye complex, is considered the most beautiful of all the imperial mosques in Istanbul. It was built between 1550 and 1557 by Mimar Sinan (Sinan the Architect). It is erected on the crest of a hill. The domes and four minarets dominate the sky and it has a spectacular view from different locations (Figure 5.20). Sultan Süleyman the Magnificent, who reigned in the Ottoman Empire, between 1520-1566, gave the order for its construction. The mosque also holds the tombs of the Sultan and his wife Hurrem (Roxelana, given name by birth), in the small cemetery behind the *mihrab* wall.

Figure 5.20 Süleymaniye Mosque, a View from Golden Horn

Inside the mosque the perfect unity of the whole could be felt easily. This mosque is an excellent example of the masterpiece of Sinan's architecture. It is pure, simple and unique. This mosque is the largest square based semi domed mosque which totals approximately 3100 m2. The two semi domes align with the direction of the *mihrab*. This layout is similar to Hagia Sophia and later it is used in Beyazid Mosque as well (1506).

Süleymaniye Mosque was opened for worship in Istanbul in August 1556. It was built on a plan of three adjacent squares: the mosque itself, the courtyard in which the Sultan and his wife Hurrem are buried, and the last prayer section. The building is covered centrally by a single dome which is supported on two sides by semi domes. The diameter of the dome is a uniform 27.25 meters. The height from the foundation to the impost is 33.70 meters. The inner rise of the dome is 14.05 meters, and thus the height of the dome from the ground to the keystone is 47.75 meters (Figures 5.21 and 5.22).

The *mihrab* and the *mimber* (pulpit) made of marvelously carved white marble and exquisite stained-glass windows coloring the incoming streams of light.

The inner plan of the mosque is a rectangle measuring 63 by 69 meters. There are four minarets, two of which have two galleries, while the other two have three.

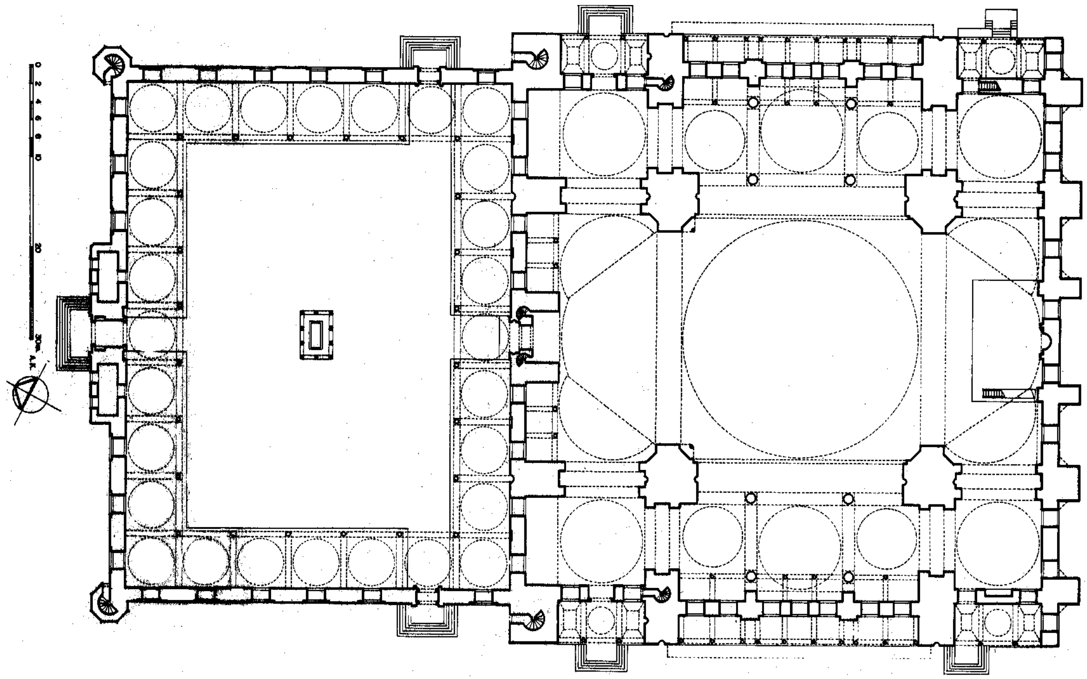

Figure 5.21 Plan of Süleymaniye Mosque

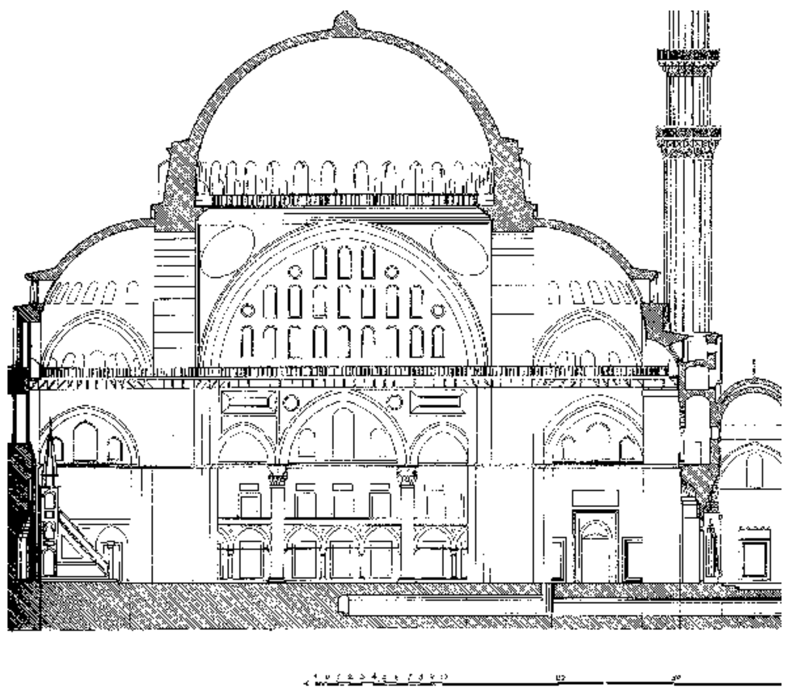

Figure 5.22 Longitudinal Section of Süleymaniye Mosque

The mosque complex also includes eleven social facilities consisting of a religious school, a *darül hadis* (school of Islamic traditions), a medical school, a lunatic asylum, a soup kitchen, a print shop, baths, and a children's school.

Figure 5.23 shows interior view from Süleymaniye Mosque in which dome and semi-dome structure can be seen.

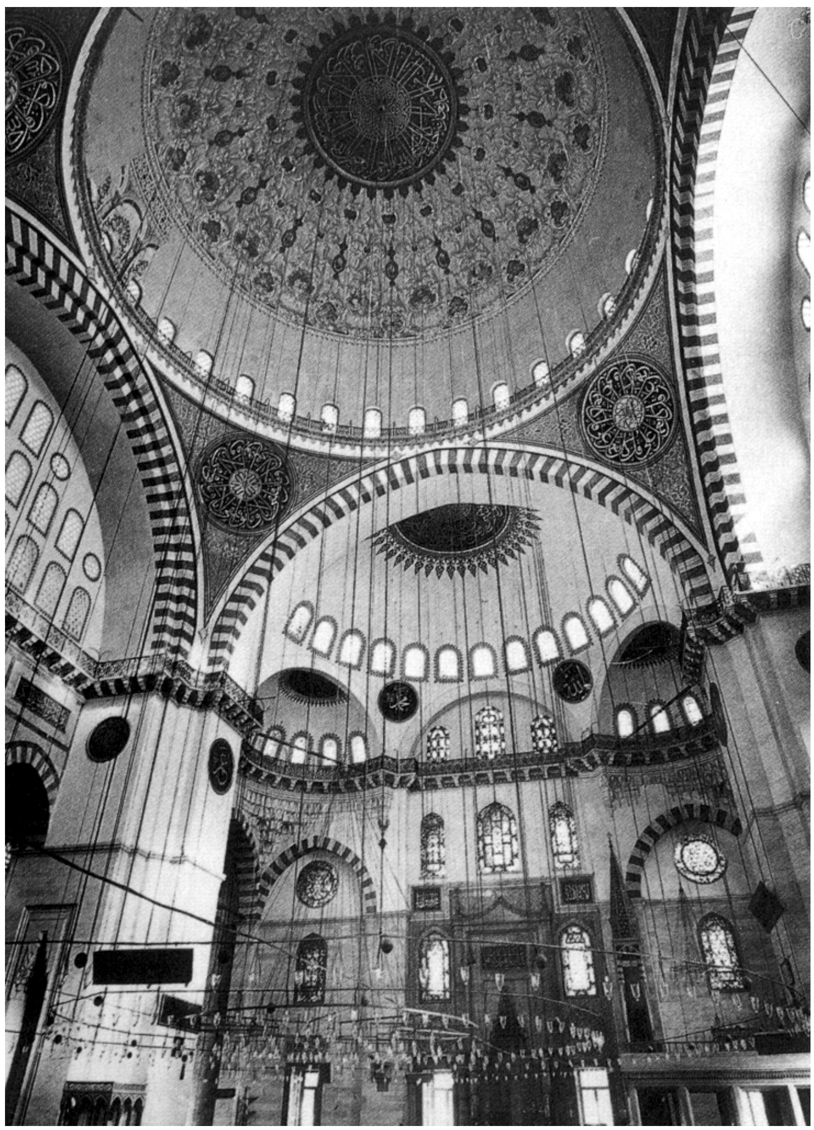

Figure 5.23 Interior View from Süleymaniye Mosque

5.3.1 Acoustical Measurements in Süleymaniye Mosque

Acoustical measurement have been performed for analysis and comparison with the simulation results purposes. These measurements are done on 21 December 1996 under the permission obtained from General Directorate of Foundations (Vakıflar Genel Müdürlügü). While performing acoustical measurements also three dimensional coordinates measurements has taken using optical measurement devices. These coordinate measurements were later used in generation of computer model.

Sound source located at two different places where in front of *mihrab* and at *müezzin mahvili* (speaker’s corner). These are the most common places inside the mosque where speaking and praying occur. Receiver positions are located 8 different positions against sound sources. Layout diagram of these receiver and source locations are given in Figure 5.24.

Reverberation time results calculated from measurement data by linear regression of energy decay curve at different receiver positions in different frequency bands are given in Table 5.4. All energy decay curves and data interval used in calculation of reverberation time are given in Appendix A.

Three dimensional energy decay surface graphics for different source and receiver combinations are given through Figure 5.25 to 5.32. These kinds of graphics are useful to see all decay in different frequency bands with respect to time in one graphic. Axes of the graphics are as follows decay in dB, frequency bands in Hz and time in milliseconds.

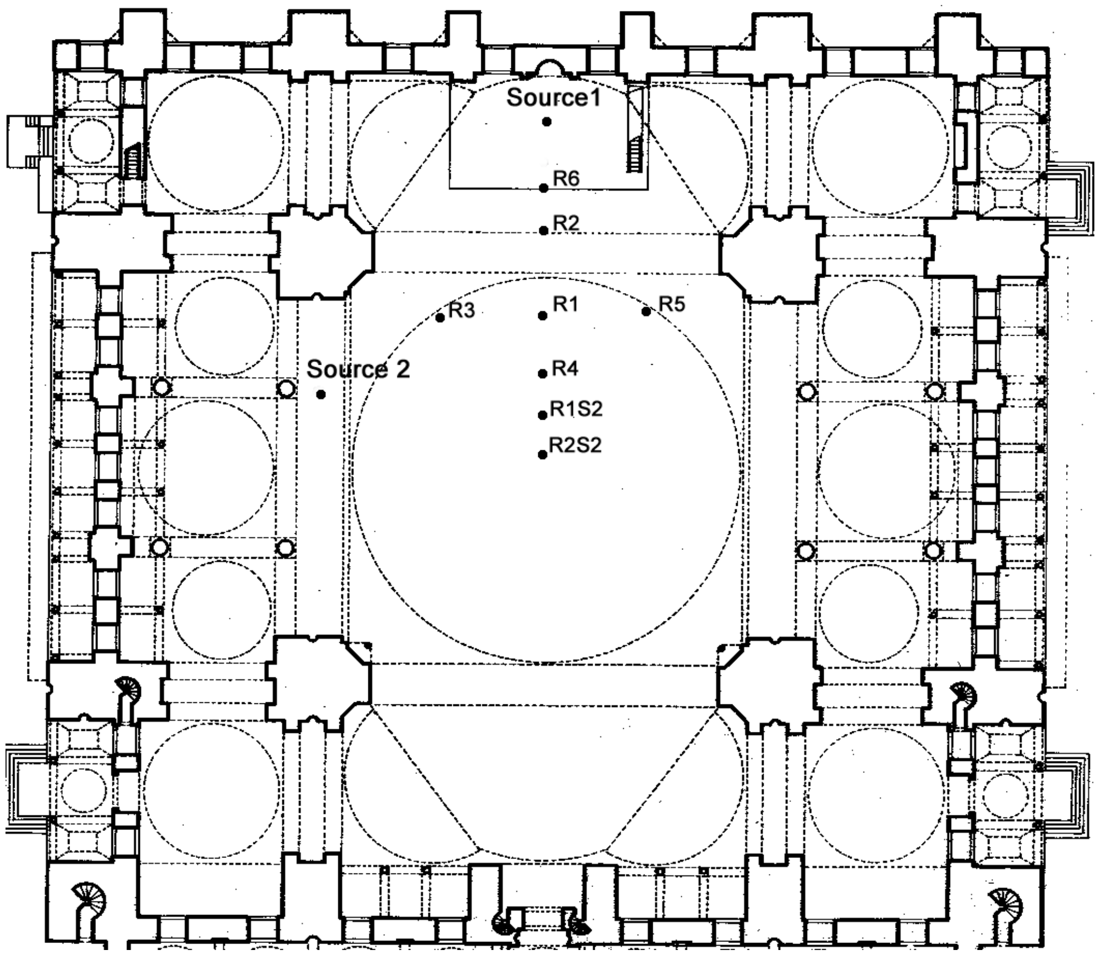

Figure 5.24 Source and Receiver Positions inside Süleymaniye Mosque

Table 5.4 Reverberation Time (T30) Results from Measurement Data at Different Receiver Positions in Süleymaniye Mosque

Receiver	125 Hz	250 Hz	500 Hz	1000 Hz	2000 Hz	4000 Hz
S1R1	7.3	8.0	7.1	6.6	4.3	2.6
S1R2	11.3	9.8	8.2	6.2	4.2	2.6
S1R3	8.8	9.4	9.0	6.1	4.4	2.5
S1R4	10.2	9.1	8.1	6.2	4.4	2.7
S1R5	8.1	7.6	7.9	6.1	4.5	2.6
S1R6	11.2	7.1	8.6	6.1	4.2	2.6
S2R1	12.5	9.8	9.0	5.8	4.5	2.8
S2R2	9.7	9.5	9.6	6.1	4.3	2.6

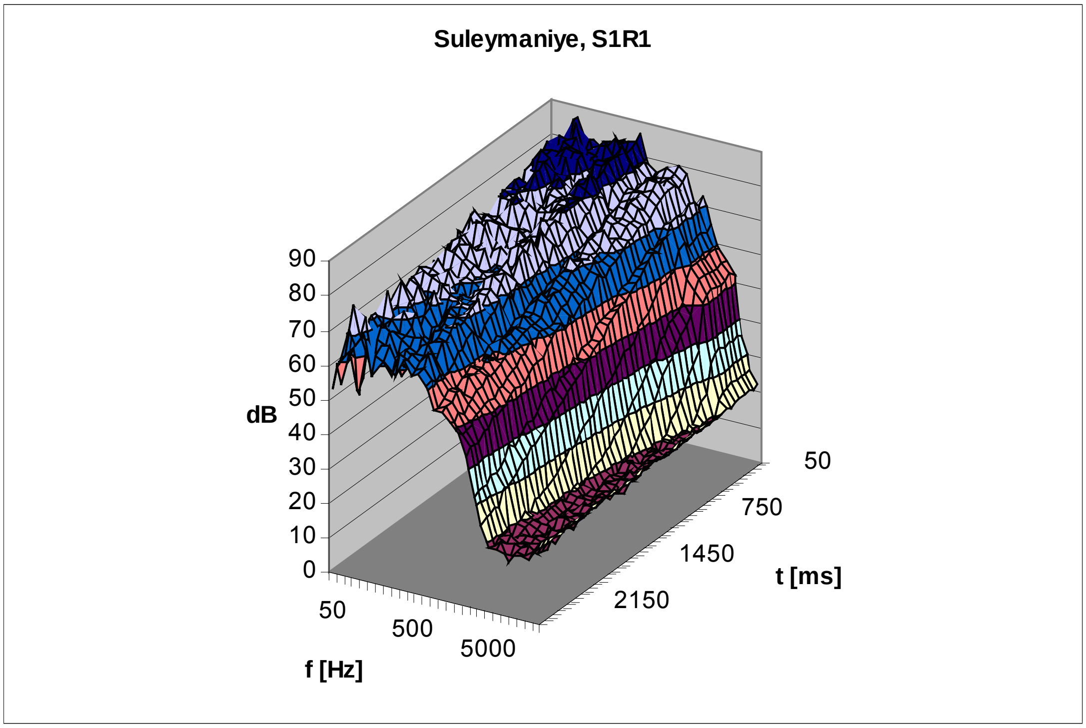

Figure 5.25 Energy Decay for Measurement Data in 3D at S1R1 in Süleymaniye Mosque

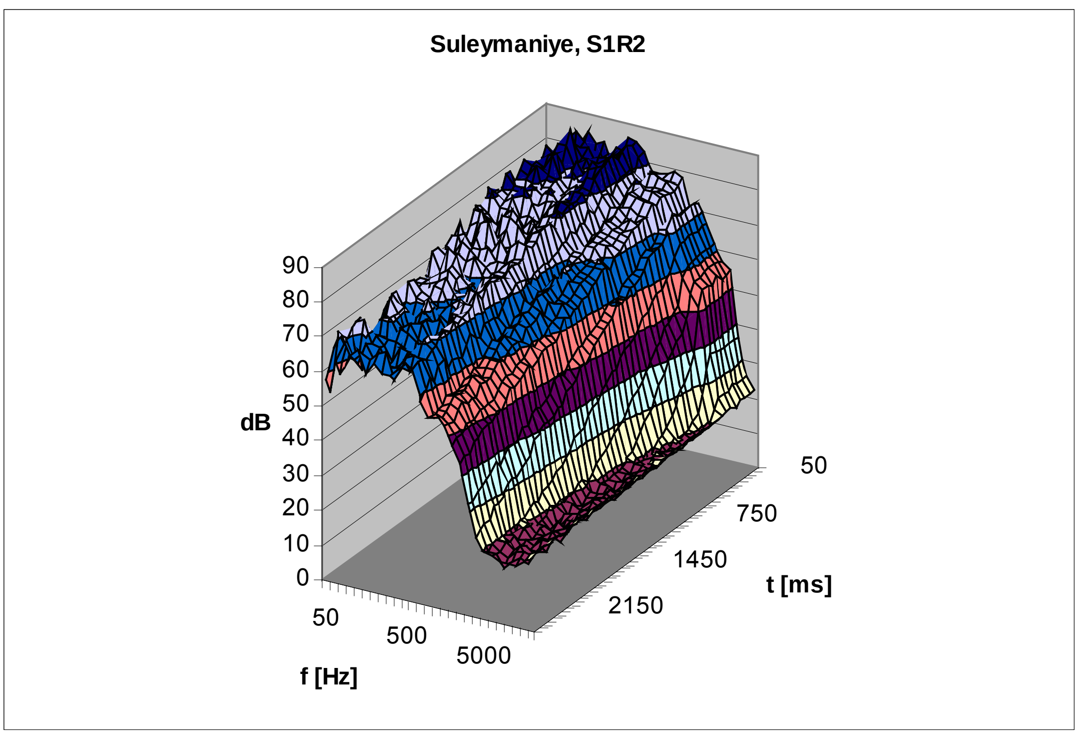

Figure 5.26 Energy Decay for Measurement Data in 3D at S1R2 in Süleymaniye Mosque

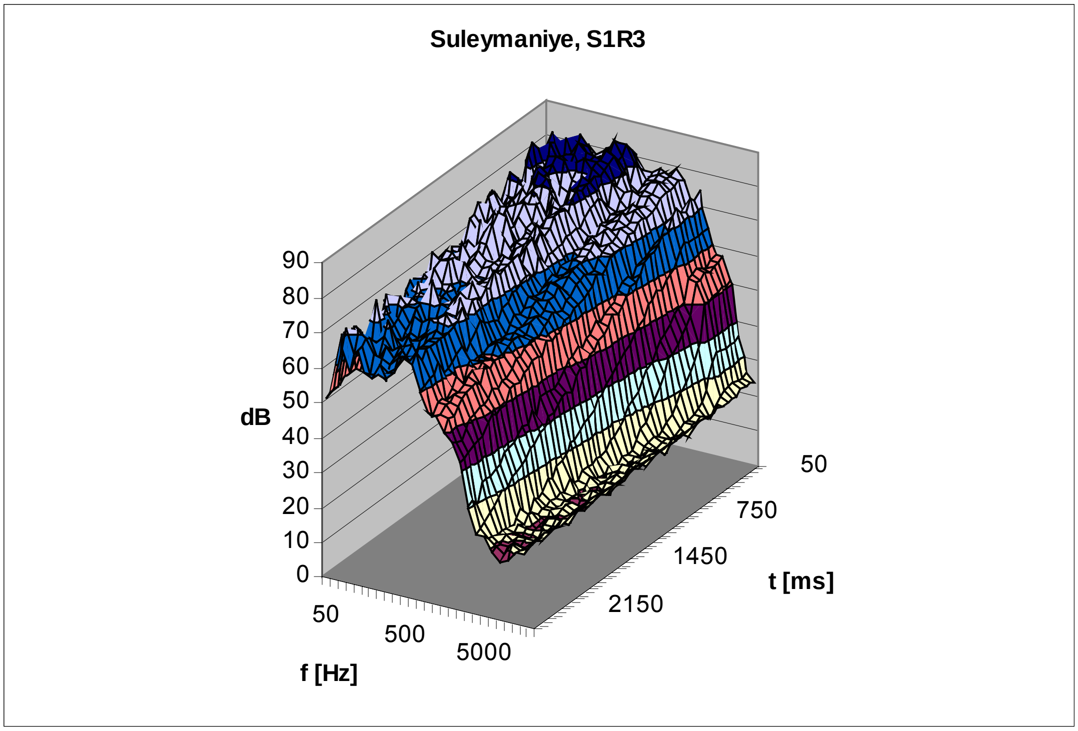

Figure 5.27 Energy Decay for Measurement Data in 3D at S1R3 in Süleymaniye Mosque

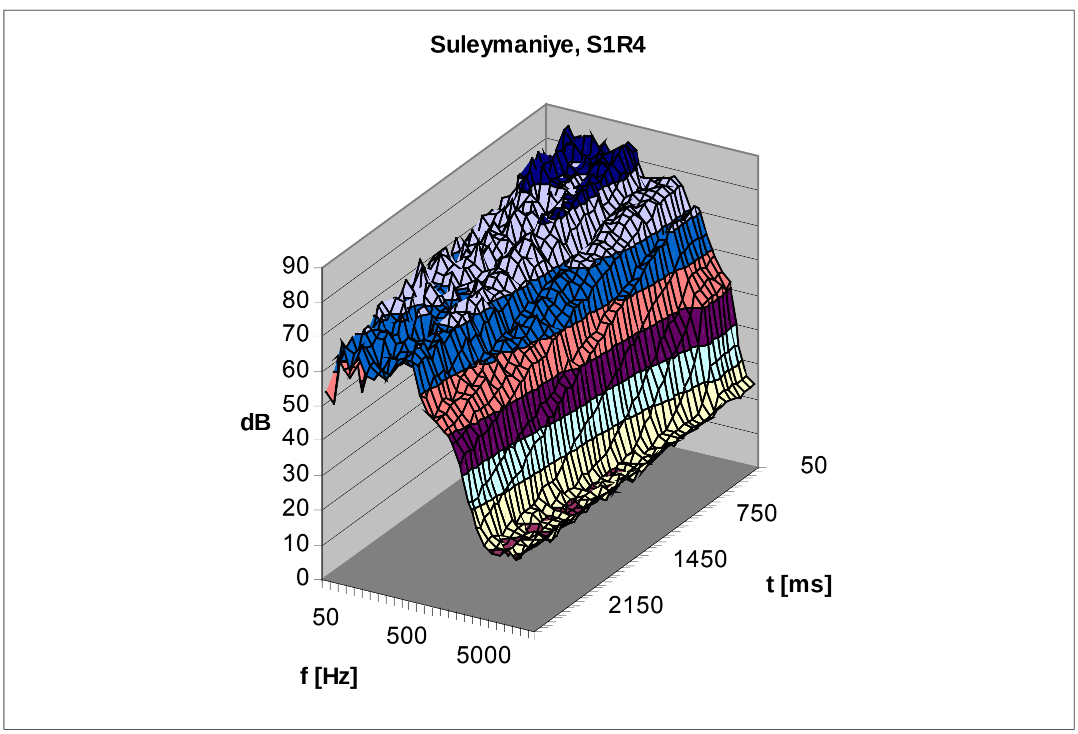

Figure 5.28 Energy Decay for Measurement Data in 3D at S1R4 in Süleymaniye Mosque

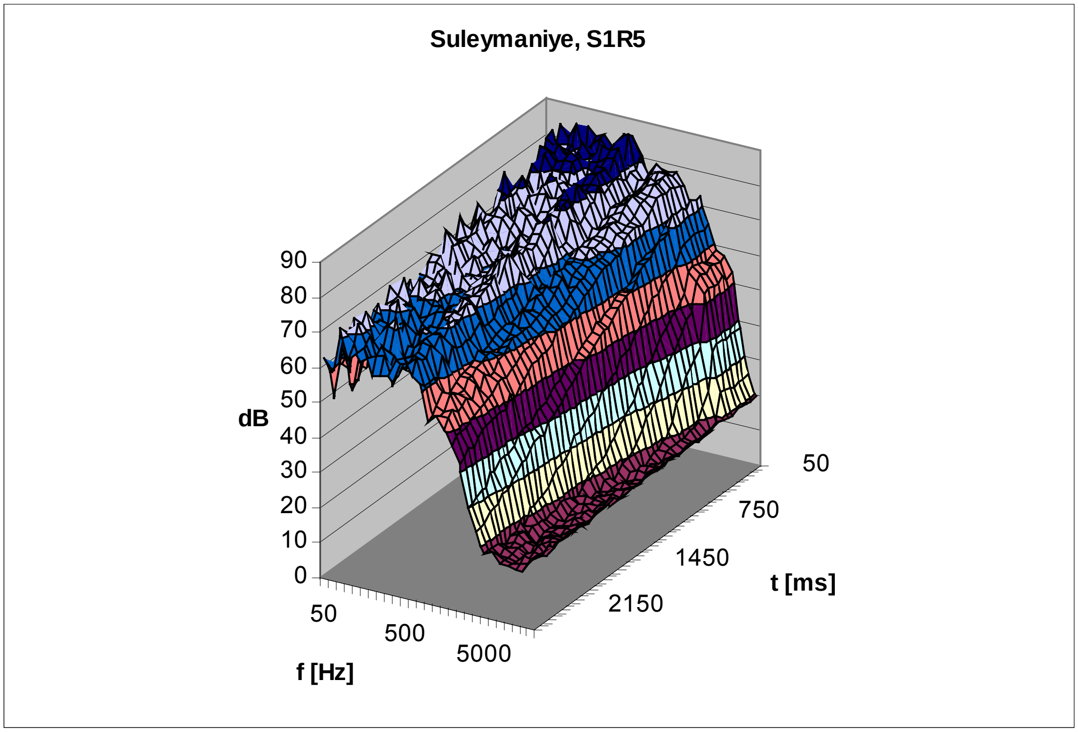

Figure 5.29 Energy Decay for Measurement Data in 3D at S1R5 in Süleymaniye Mosque

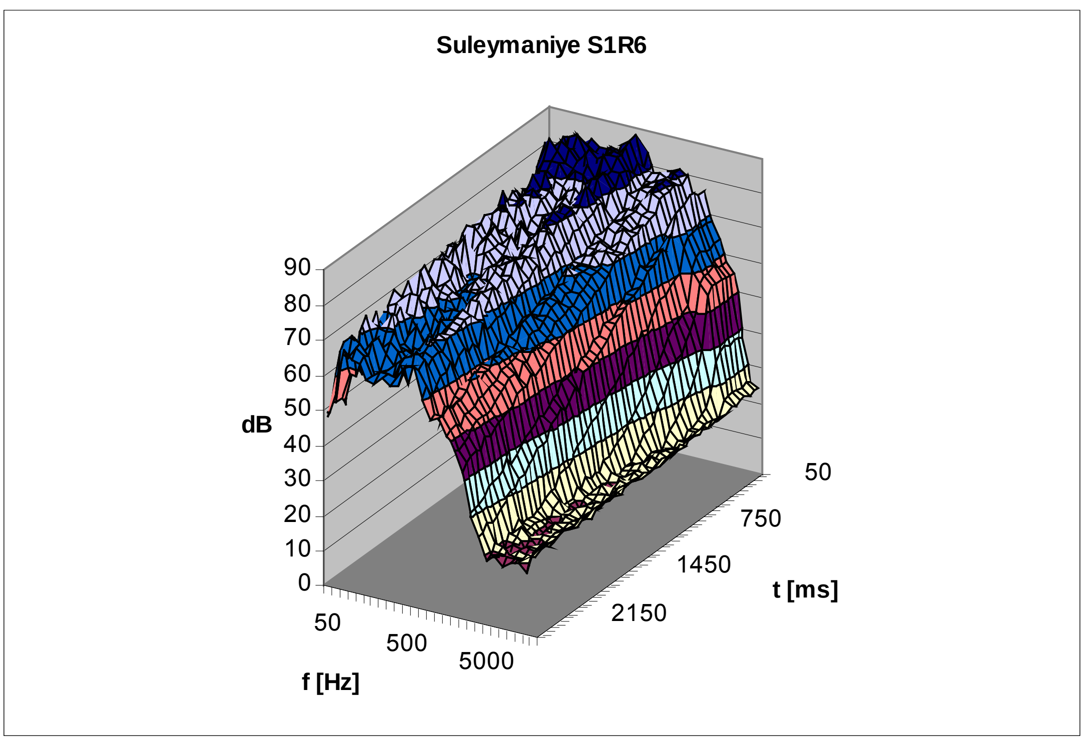

Figure 5.30 Energy Decay for Measurement Data in 3D at S1R6 in Süleymaniye Mosque

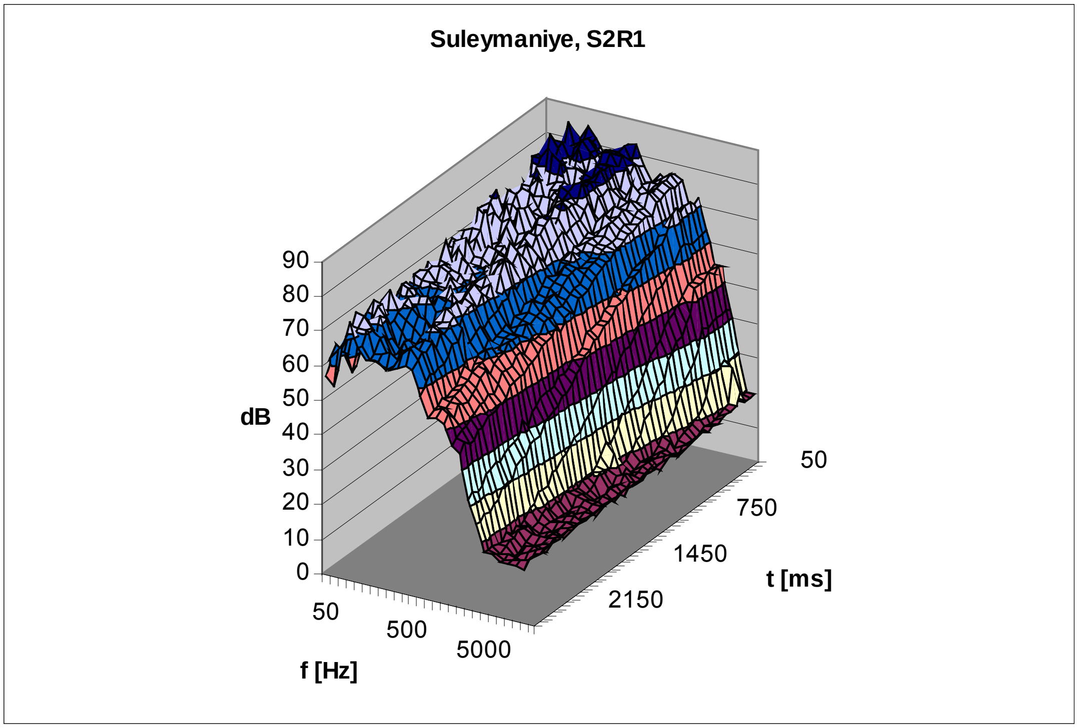

Figure 5.31 Energy Decay for Measurement Data in 3D at S2R1 in Süleymaniye Mosque

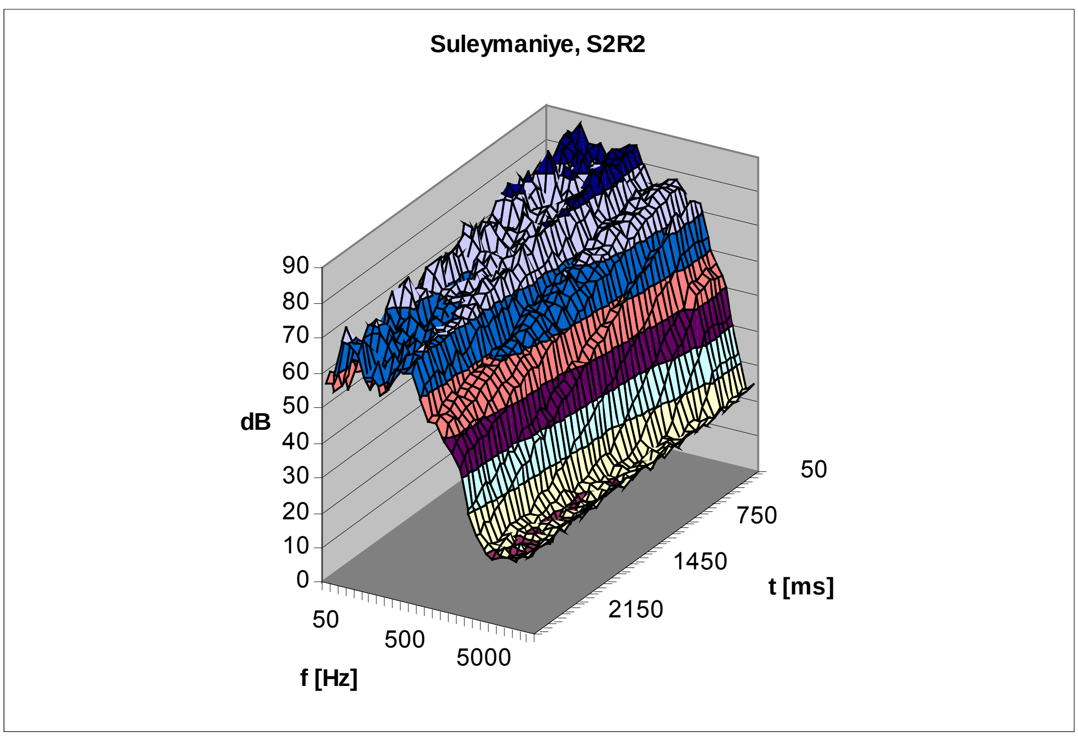

Figure 5.32 Energy Decay for Measurement Data in 3D at S2R2 in Süleymaniye Mosque

5.3.2 Acoustical Simulations of Süleymaniye Mosque

The combination of ray tracing and radiosity method again is performed in this case. Interior surfaces of Süleymaniye mosque is mainly plaster covered and stone. The floor is covered by thick carpet. Absorption coefficients used in simulation are given Table 5.2.

Simulation model of Süleymaniye Mosque consists of 2043 plane surface. Diffusion coefficient values used through out simulations are 0.7 for carpet covered surface and 0.1 for the plaster covered interior surfaced. Form factors are generated only once and values are used for different source and receiver combination. It took 15 minutes computing time with same computer used in all cases to generate all form factors between surface planes of the geometry. The mean free path inside the space is approximated 34 m in this mosque.

Sound source and receivers are located at the same position as the measurements positions. Total number of generated rays is 120000 and each ray is traced up to 10 seconds of flight time within the space. Since the volume and the mean free path ray inside Suleymaniye Mosque are much larger than the other cases, the total number of rays are kept much higher than the others. Execution time for each sound and receiver pair simulation in this case is around 1 hour on Pentium III 1 GHz processor computer.

Reverberation time estimation, clarity and definition values for octave band of 1000 Hz are listed in Table 5.5. Reverberation times obtained from simulation are close to values obtained from measurements. Maximum difference between measurement and simulation is 7%. This difference is an acceptable result from such a simulation tool. Energy decay curves obtained from different set of source and receiver are given through Figure 5.34 to 5.41.

Table 5.5 Reverberation time (T30), Clarity and Definition Results for 1000Hz from Simulation at Different Source and Receiver Positions in Süleymaniye Mosque

	S1R1	**S1R2**	**S1R3**	**S1R4**	**S1R5**	**S1R6**	**S2R1**	**S2R2**
RT (s)	6.3	6.1	6.1	6.6	6.2	6.5	6.2	6.2
Clarity (dB)	-6.7	-6.4	-6.4	-7.2	-6.6	-6.2	-6.8	-6.9
Definition	0.09	0.12	0.10	0.08	0.09	0.14	0.09	0.09
RT difference between measurement and simulation	5%	2%	0%	6%	2%	7%	7%	2%

It is observed two different slopes in energy decay curve in all receiver and source pairs. The first slope which approximately terminates around 3 seconds after 40 dB energy drop shows the contribution of central space and dome. The second slope corresponds the contribution of the side galleries of the mosque. This shape energy decay curve occurs when there is an acoustically coupled space. In this case the central space and the side galleries of the Süleymaniye Mosque forms a acoustically coupled space. Figure 5.33 shows the typical energy decay curve for such acoustically coupled spaces.

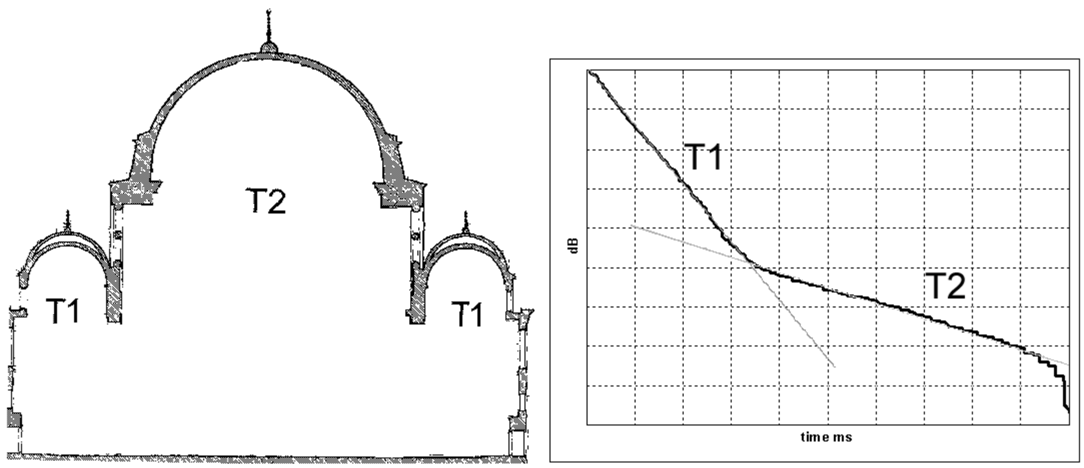

Figure 5.33 Form of Energy Decay Curve for Coupled Spaces

.

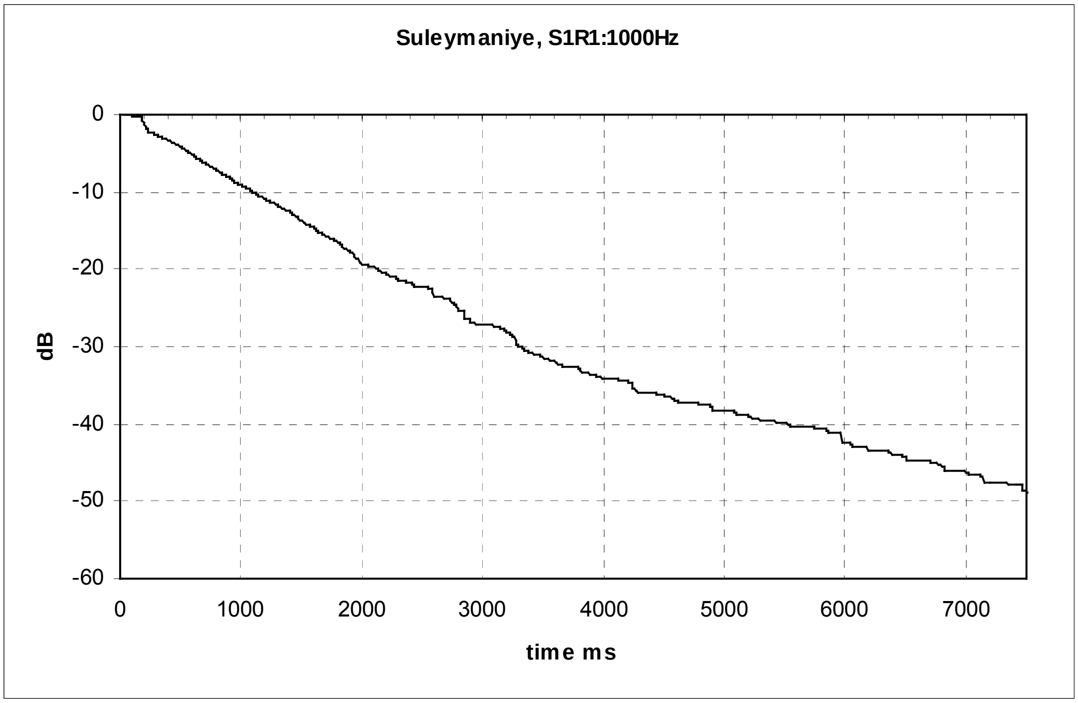

Figure 5.34 Energy Decay for Simulation Data for 1000 Hz at S1R1 in Süleymaniye Mosque

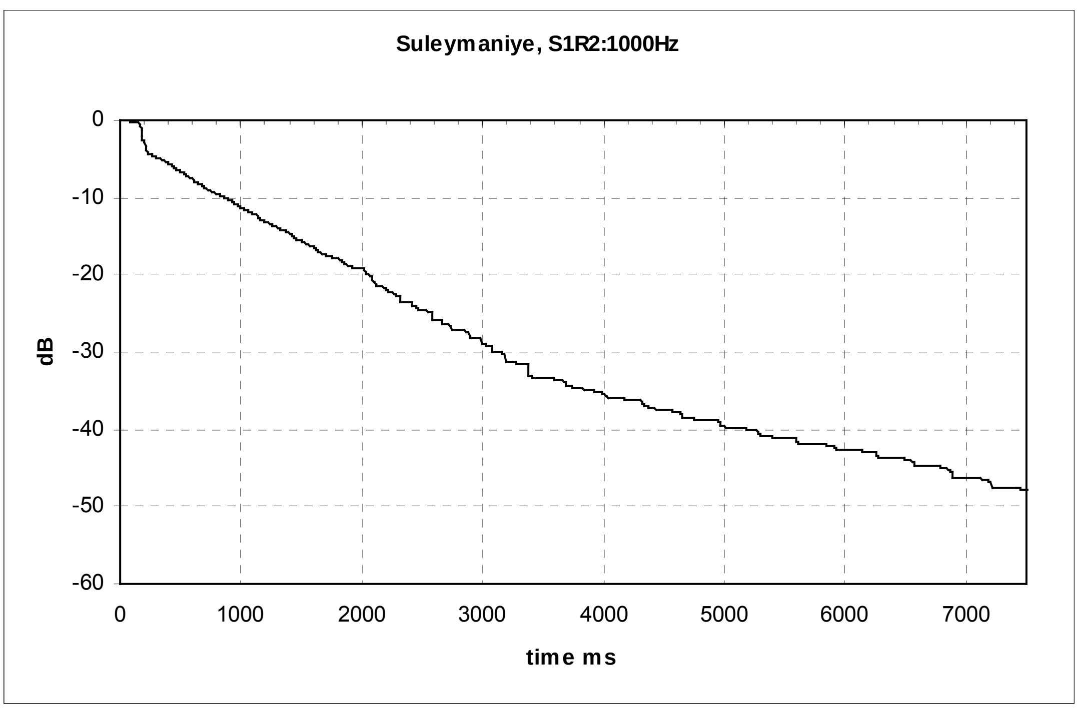

Figure 5.35 Energy Decay for Simulation Data for 1000 Hz at S1R2 in Süleymaniye Mosque

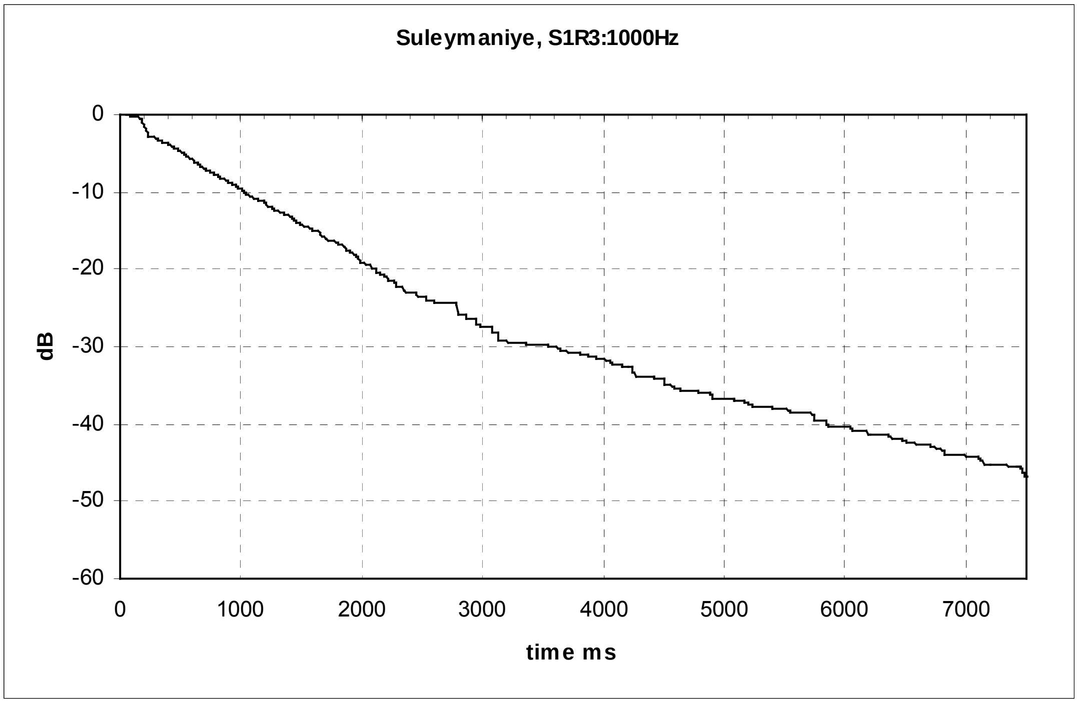

Figure 5.36 Energy Decay for Simulation Data for 1000 Hz at S1R3 in Süleymaniye Mosque

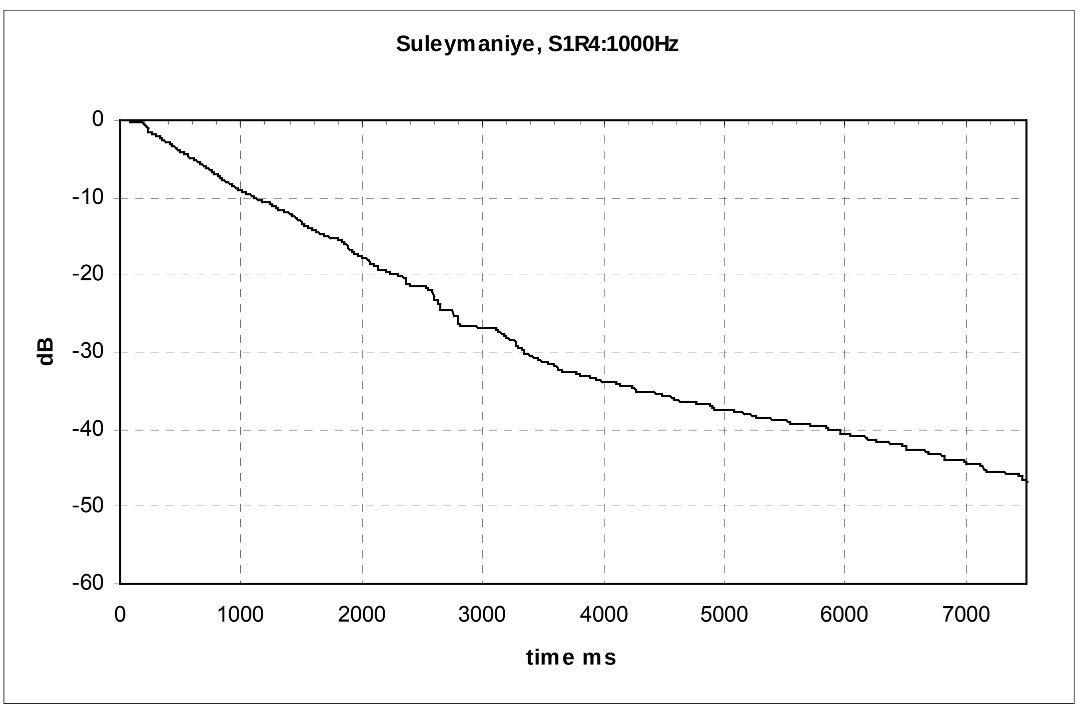

Figure 5.37 Energy Decay for Simulation Data for 1000 Hz at S1R4 in Süleymaniye Mosque

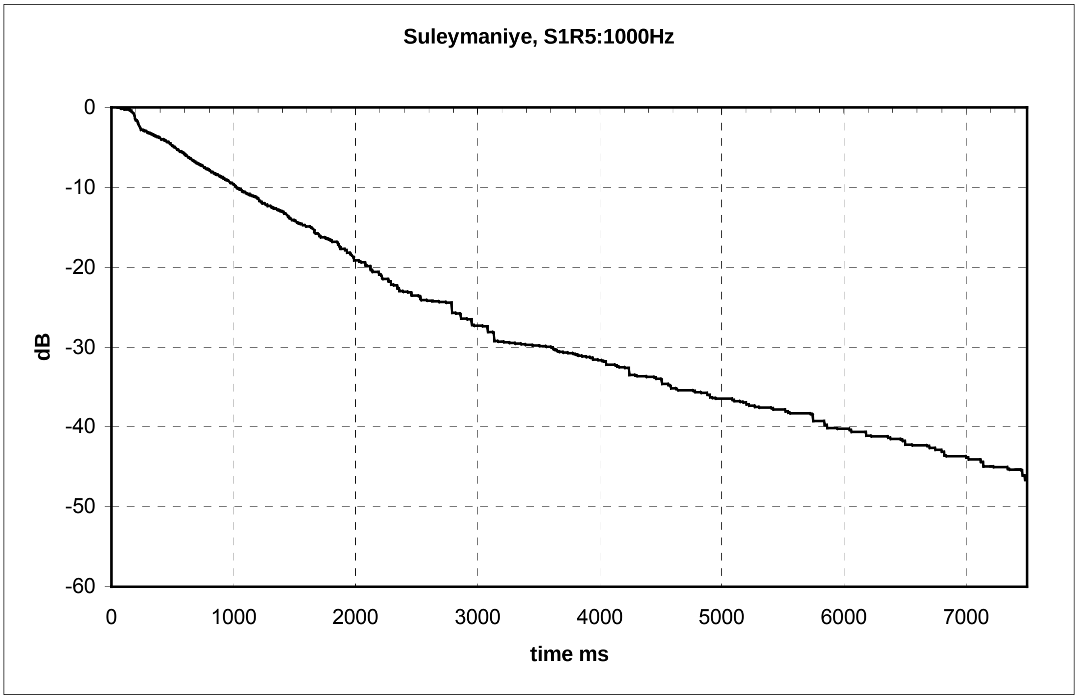

Figure 5.38 Energy Decay for Simulation Data for 1000 Hz at S1R5 in Süleymaniye Mosque

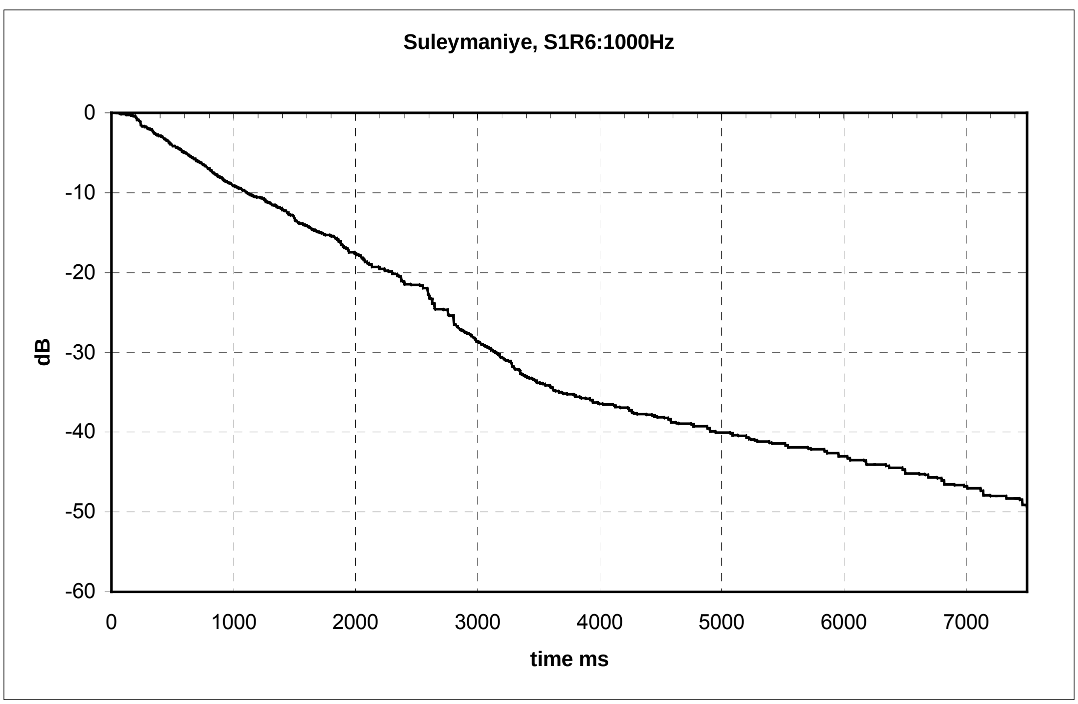

Figure 5.39 Energy Decay for Simulation Data for 1000 Hz at S1R6 in Süleymaniye Mosque

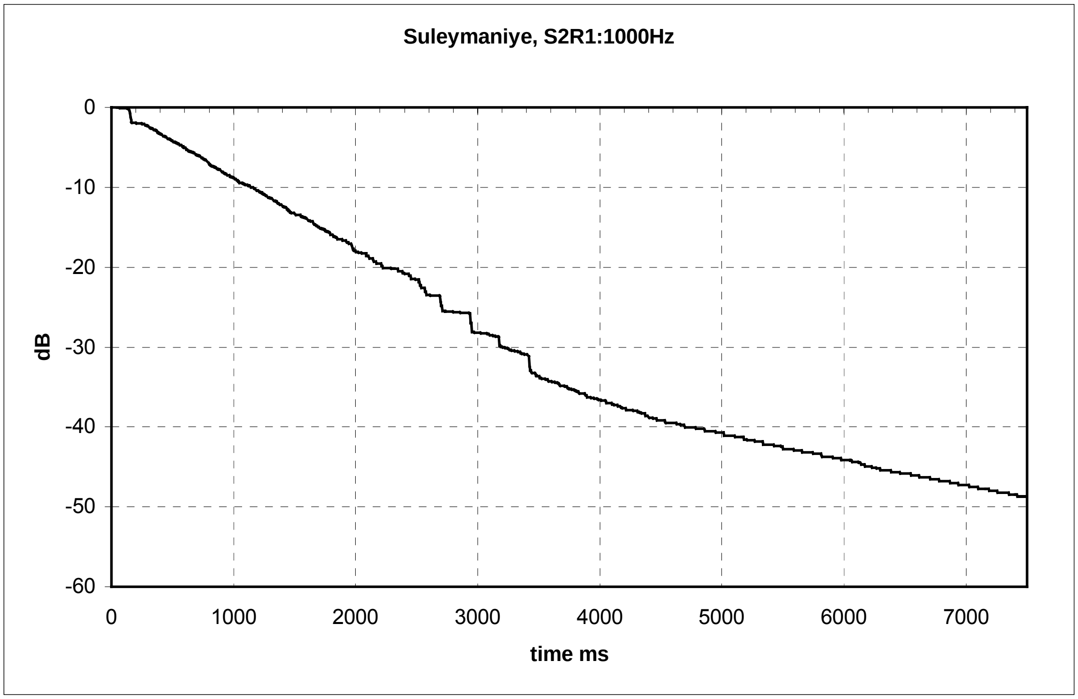

Figure 5.40 Energy Decay for Simulation Data for 1000 Hz at S2R1 in Süleymaniye Mosque

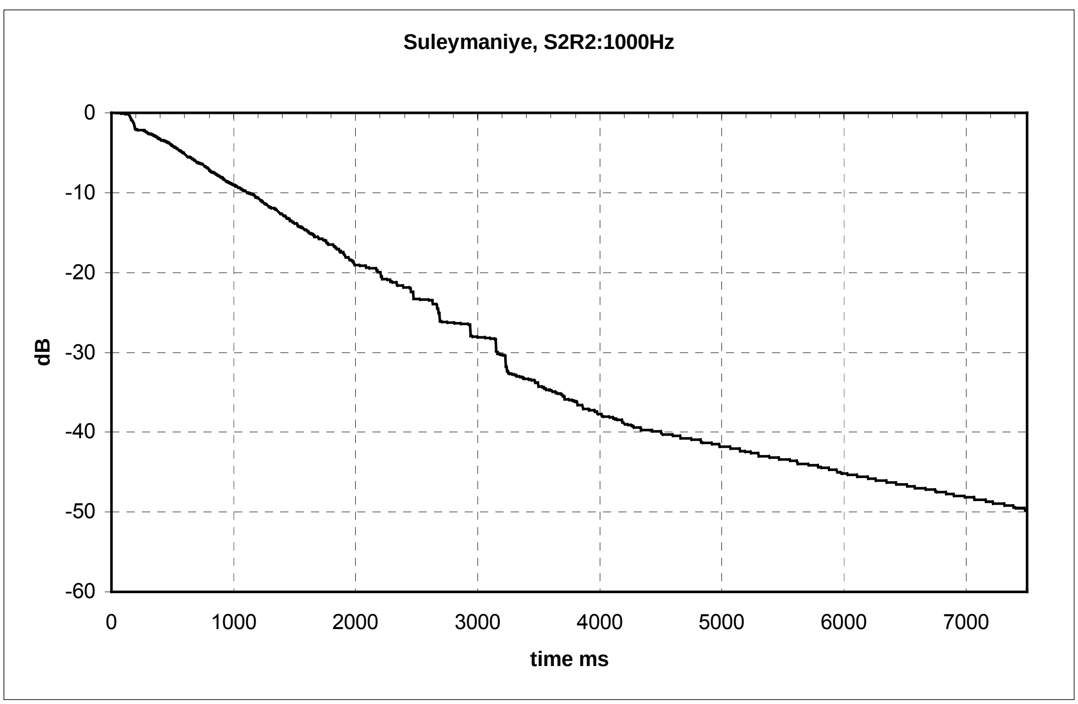

Figure 5.41 Energy Decay for Simulation Data for 1000 Hz at S2R2 in Süleymaniye Mosque

5.4 Rüstem Pasa Mosque

Rüstem Pasa mosque is one of the most beautiful of the smaller mosques by Sinan. This mosque was built in 1561 by Rüstem Pasa who was the Grand *Vezir* under Süleyman the Magnificent and the husband of the Sultan's most beloved daughter, Mihrimah Sultan. The mosque is built on a high platform over a complex of vaulted shops. There are two reasons to built this mosque in such a high platform; to generate invaluable space for shops beneath the mosque and to get better view from the Golden Horn. Today the shops around the mosque are still existing and daily trade is continuing for centuries (Figure 5.42)

Figure 5.42 Rüstem Pasa Mosque

Rüstem Pasa mosque is especially famous for its very fine tiles. The richest collection of tiles in Turkey is located within the interior of the mosque The tiles came from Iznik, famous with its tiles during period of 1555-1620. Almost entire interior surfaces, walls, *mihrab*, columns and *mimber* are covered by those beautiful floral and geometric design tiles. Since this thesis is analyzing the Sinan's mosque acoustics, the tile covered interior space in this mosque is excellent case study for acoustical purposes. The sound characteristics inside the mosque is expected to be different than the other mosques just because of sound absorption and reflection characteristics of tiled-surfaces (Figure 5.43).

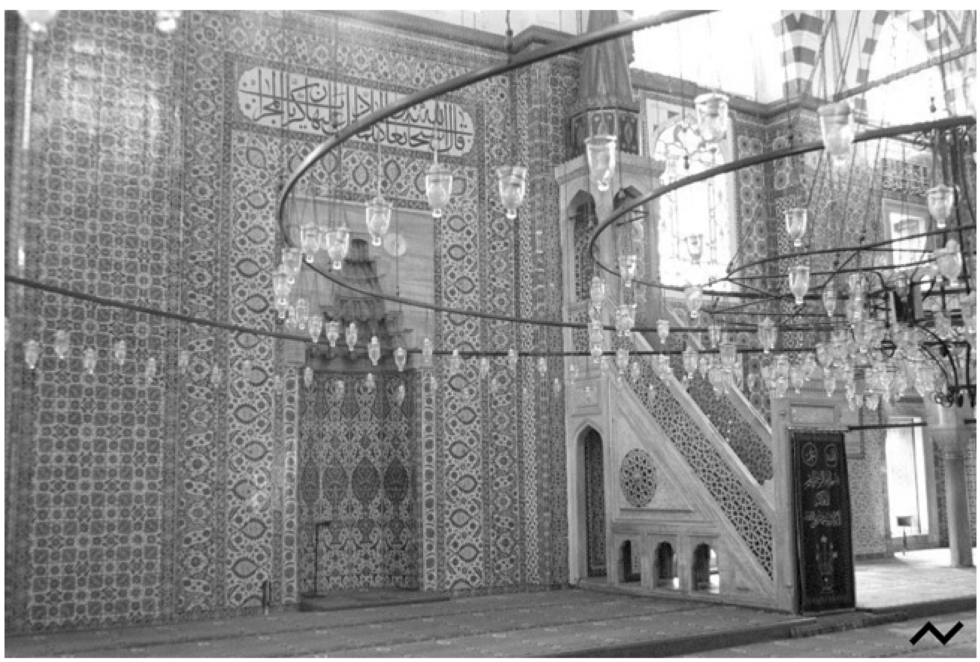

Figure 5.43 Interior View from Rüstem Pasa Mosque

The plan of the mosque consist of an octagon inscribed in a rectangle; the dome rest on four semi domes in the diagonals of the building. Four octagonal pillars carry the dome together with arches on top. The side galleries are supported by pillars and by small marble columns between them. The diameter of the dome is a uniform 15.20 meters. The height from the ground is 22.80 meters.(Figure 5.44).

The inner plan of the mosque is a rectangle measuring 26.8 by 19.6 meters. There is only one minaret with single gallery.

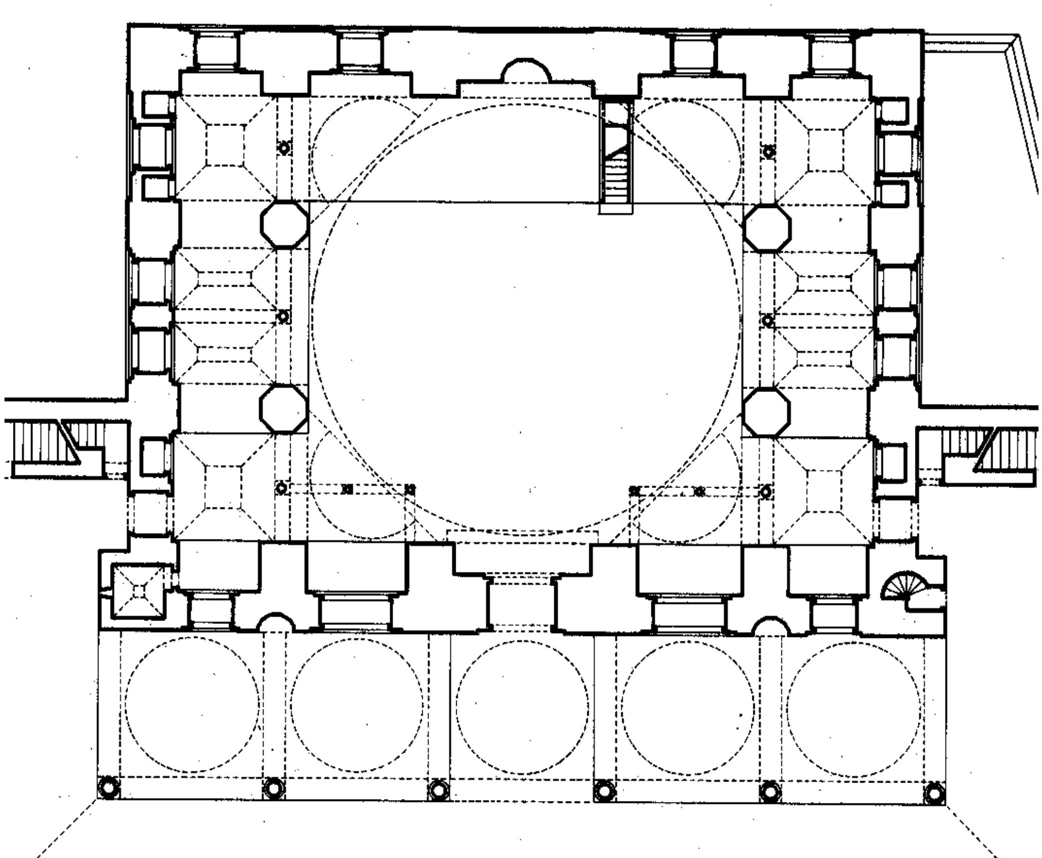

Figure 5.44 Plan View of Rüstem Pasa Mosque

5.4.1 Acoustical Measurements in Rüstem Pasa Mosque

Similar to other mosques several acoustical measurements were performed inside Rüstem Pasa Mosque. Three dimensional coordinate measurements were also taken using some optical measurement devices to generate computer model as well. All these measurements were carried on 22 December 1996 under the permission obtained from General Directorate of Foundations (Vakıflar Genel Müdürlügü).

There was only one sound source in this case. It was positioned in front of *mihrab* for the acoustical measurements. Receivers were located at 10 different positions. Layout diagram of these receiver and source locations are given in Figure 5.45.

Reverberation time results calculated from measurement data by linear regression of energy decay curve at different receiver positions in different frequency band are given in Table 5.6. All energy decay curves and data interval used in calculation of reverberation time are given in Appendix.

Three dimensional energy decay surface graphics for source and receiver combinations are given through Figure 5.46 to 5.55.

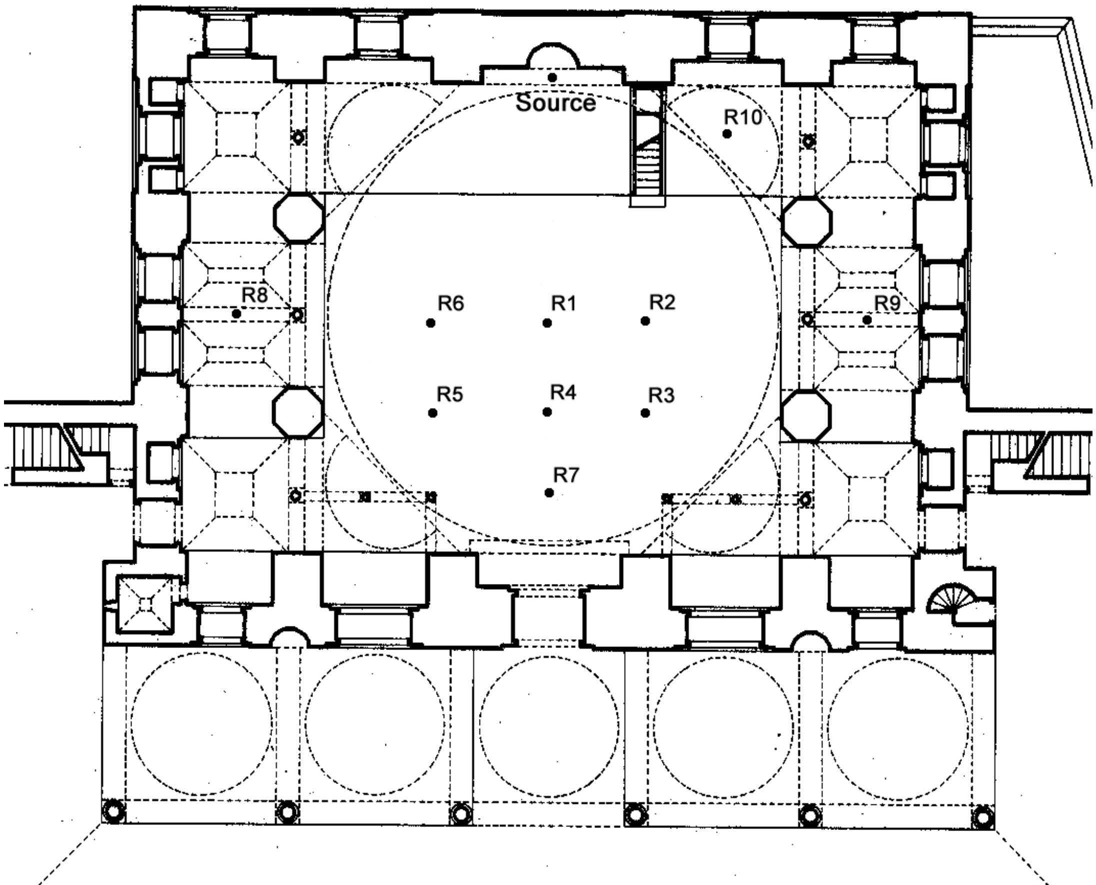

Figure 5.45 Receiver positions in Rüstem Pasa Mosque

Table 5.6 Reverberation time (T30) results from measurement data at different receiver positions in Rüstem Pasa Mosque

Receiver	125 Hz	250 Hz	500 Hz	1000 Hz	2000 Hz	4000 Hz
R1	5.6	5.8	4.7	3.5	2.9	1.9
R2	6.2	5.6	4.6	3.7	2.9	2.0
R3	5.4	5.7	4.7	3.8	2.9	2.0
R4	5.5	5.5	4.6	3.7	3.0	1.9
R5	6.2	7.3	4.9	3.7	3.0	2.0
R6	6.4	6.0	5.2	3.7	2.9	2.0
R7	5.0	6.9	4.6	3.6	3.0	2.0
R8	6.7	5.7	4.7	3.7	2.9	2.0
R9	5.6	5.8	4.5	3.8	2.9	2.0
R10	6.3	5.8	4.9	3.8	2.8	2.0

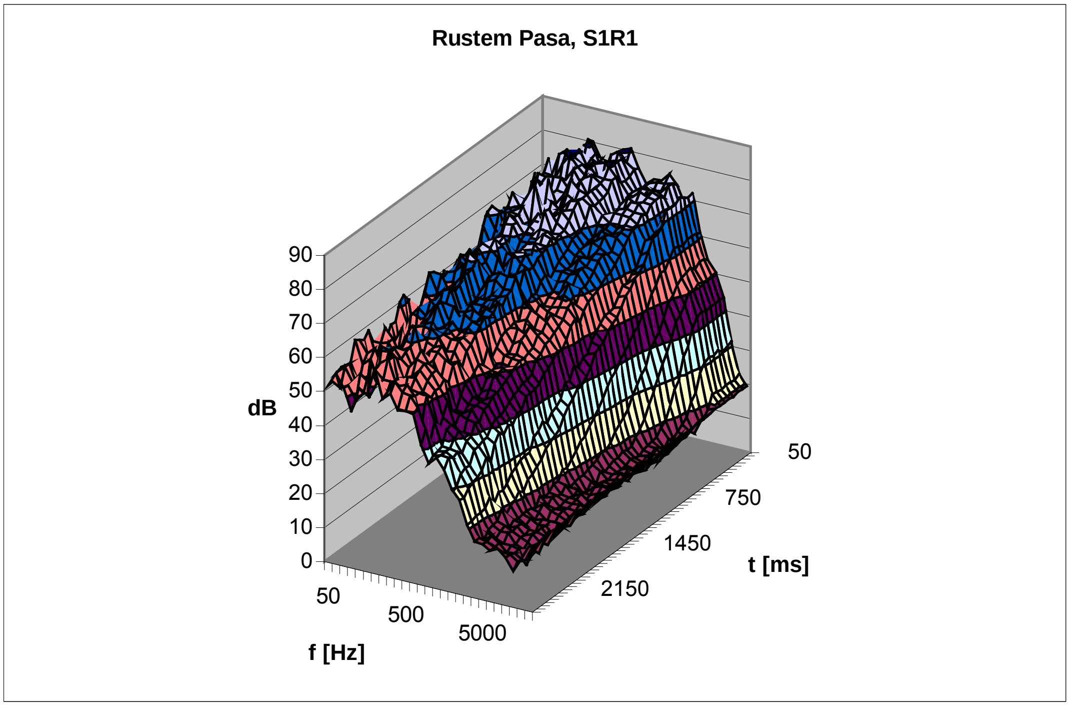

Figure 5.46 Energy Decay for Measurement Data in 3D at S1R1 in Rüstem Pasa Mosque

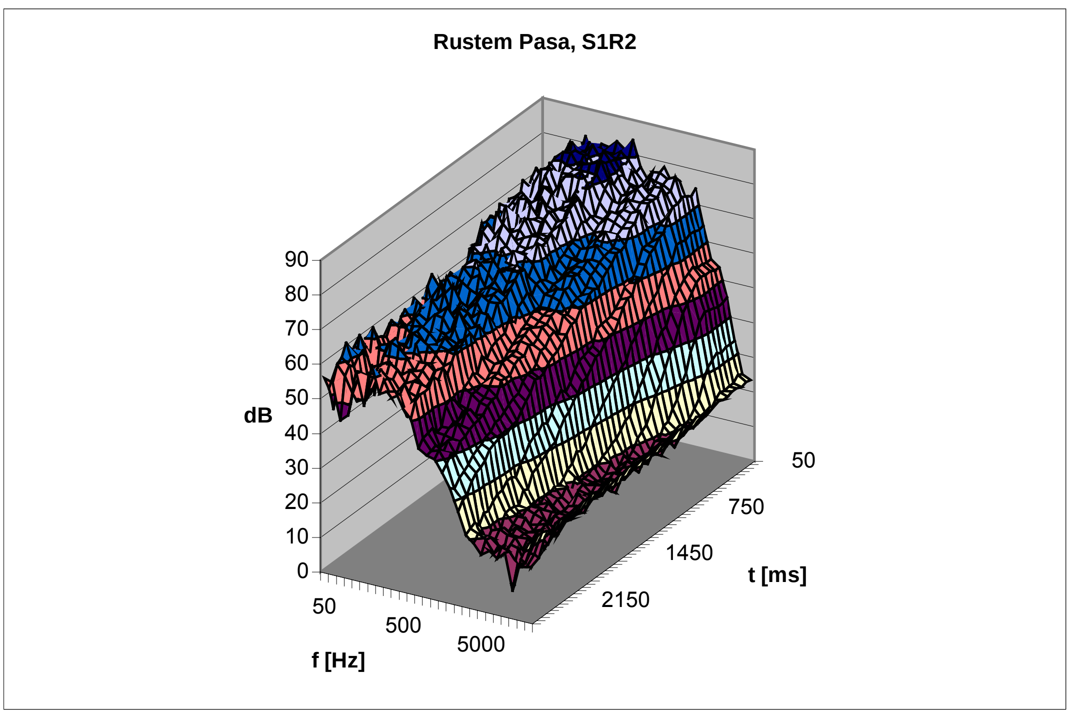

Figure 5.47 Energy Decay for Measurement Data in 3D at S1R2 in Rüstem Pasa Mosque

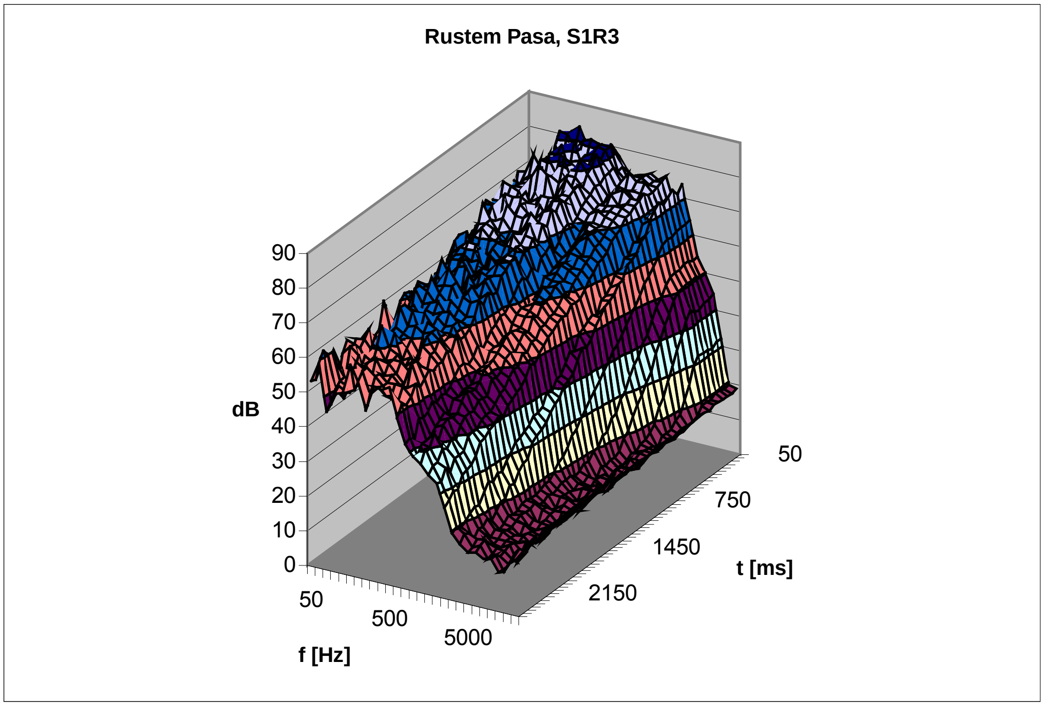

Figure 5.48 Energy Decay for Measurement Data in 3D at S1R3 in Rüstem Pasa Mosque

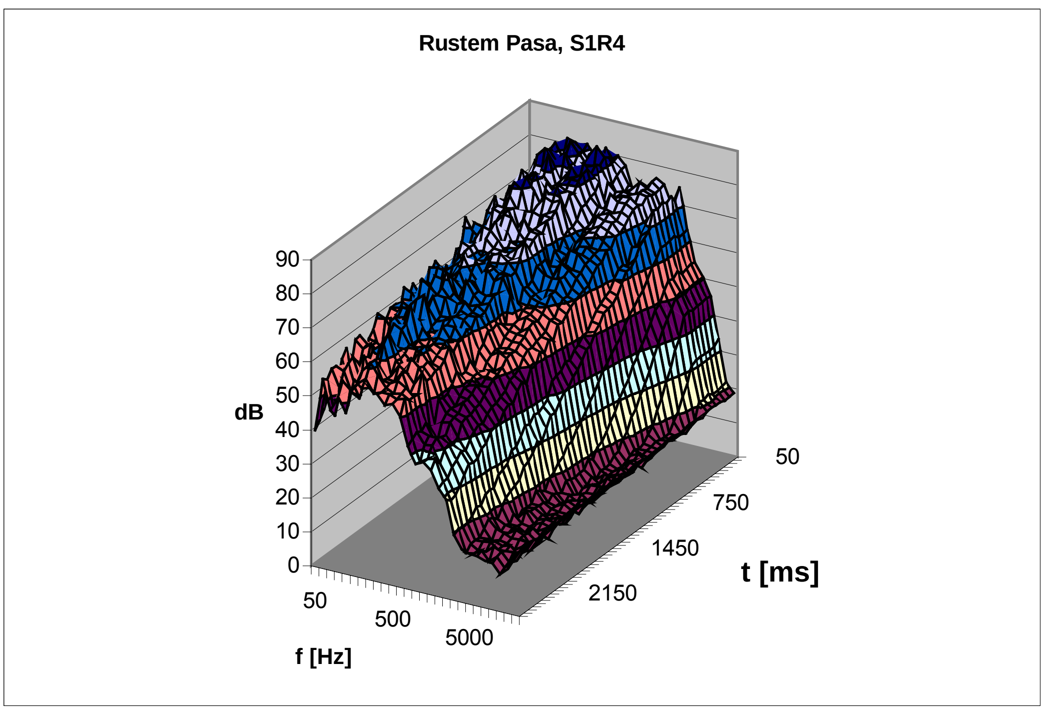

Figure 5.49 Energy Decay for Measurement Data in 3D at S1R4 in Rüstem Pasa Mosque

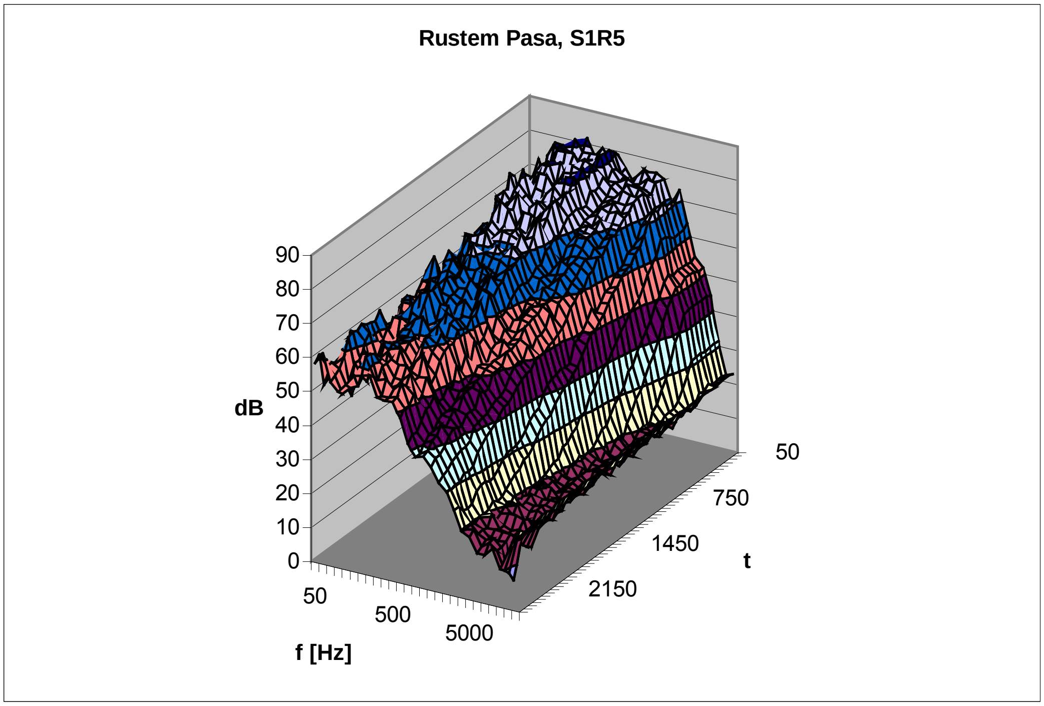

Figure 5.50 Energy Decay for Measurement Data in 3D at S1R5 in Rüstem Pasa Mosque

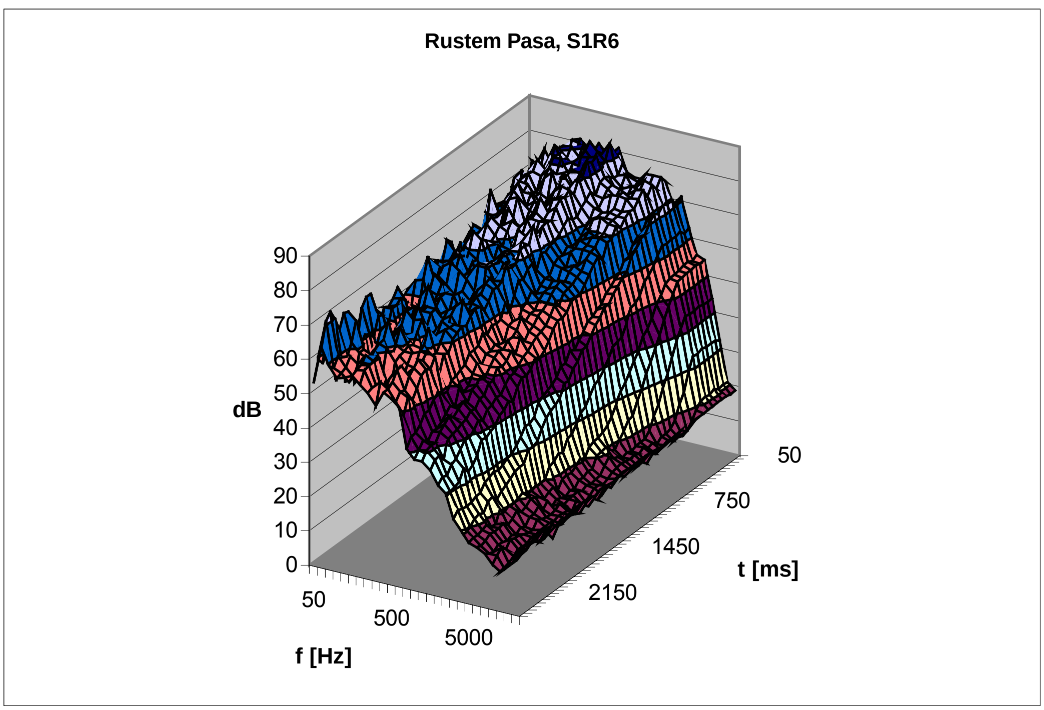

Figure 5.51 Energy Decay for Measurement Data in 3D at S1R6 in Rüstem Pasa Mosque

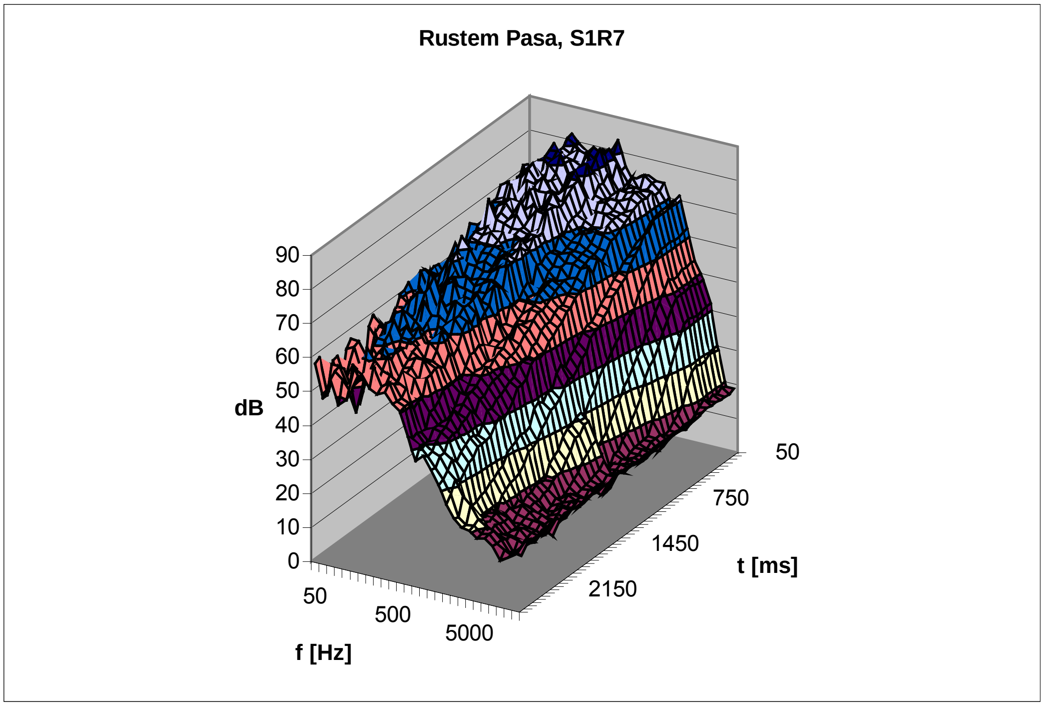

Figure 5.52 Energy Decay for Measurement Data in 3D at S1R7 in Rüstem Pasa Mosque

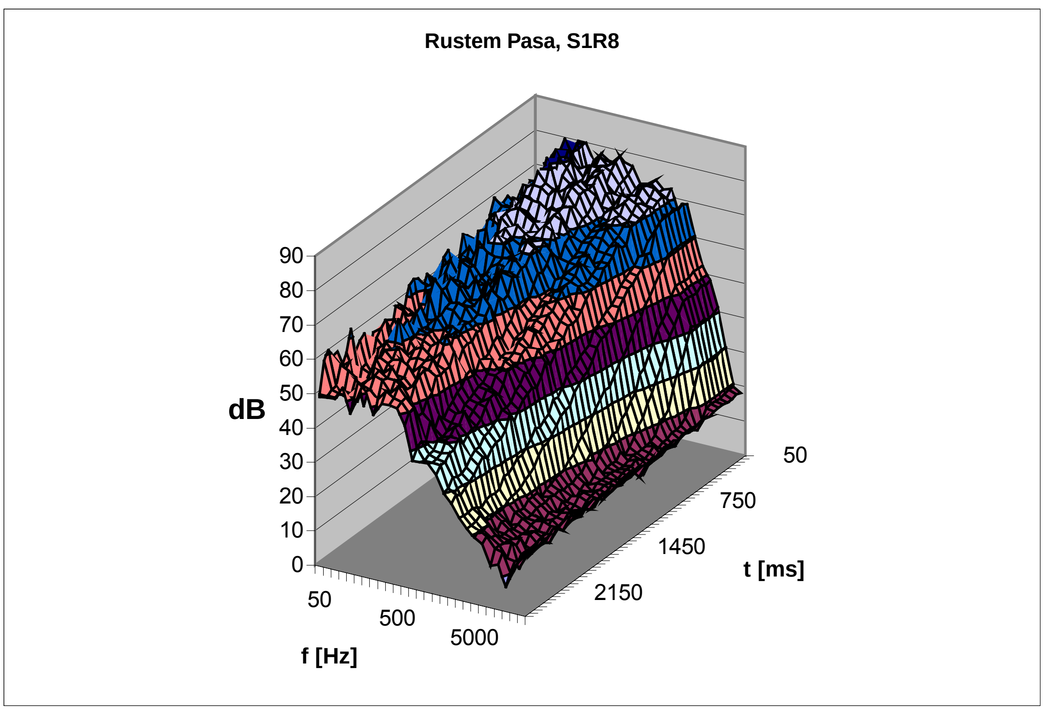

Figure 5.53 Energy Decay for Measurement Data in 3D at S1R8 in Rüstem Pasa Mosque

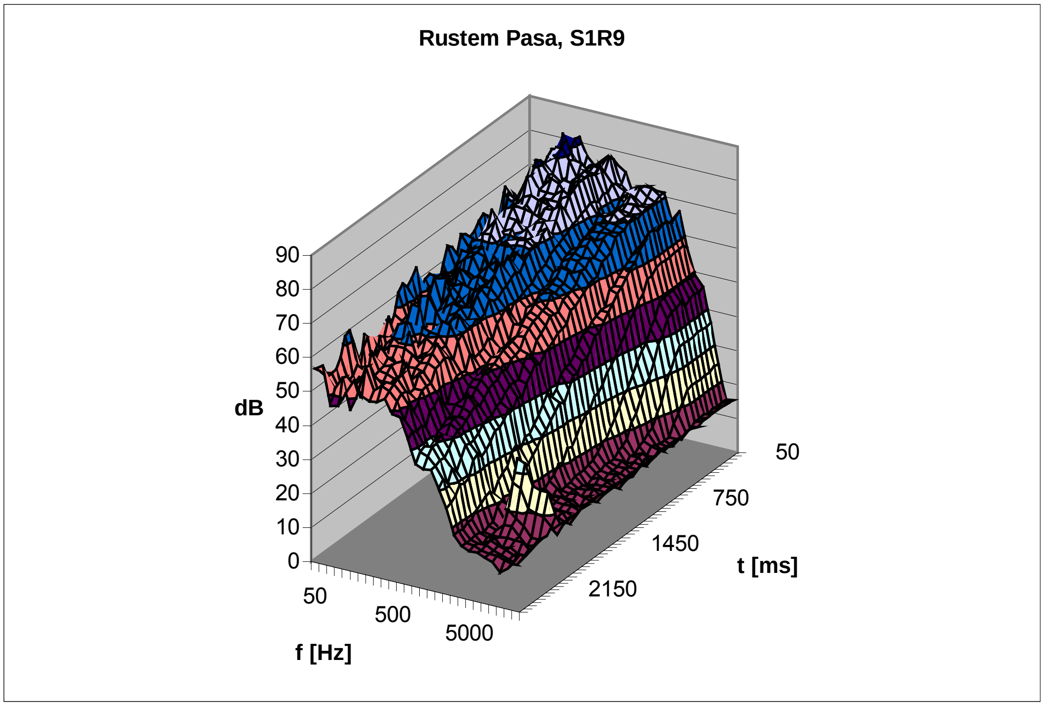

Figure 5.54 Energy Decay for Measurement Data in 3D at S1R9 in Rüstem Pasa Mosque

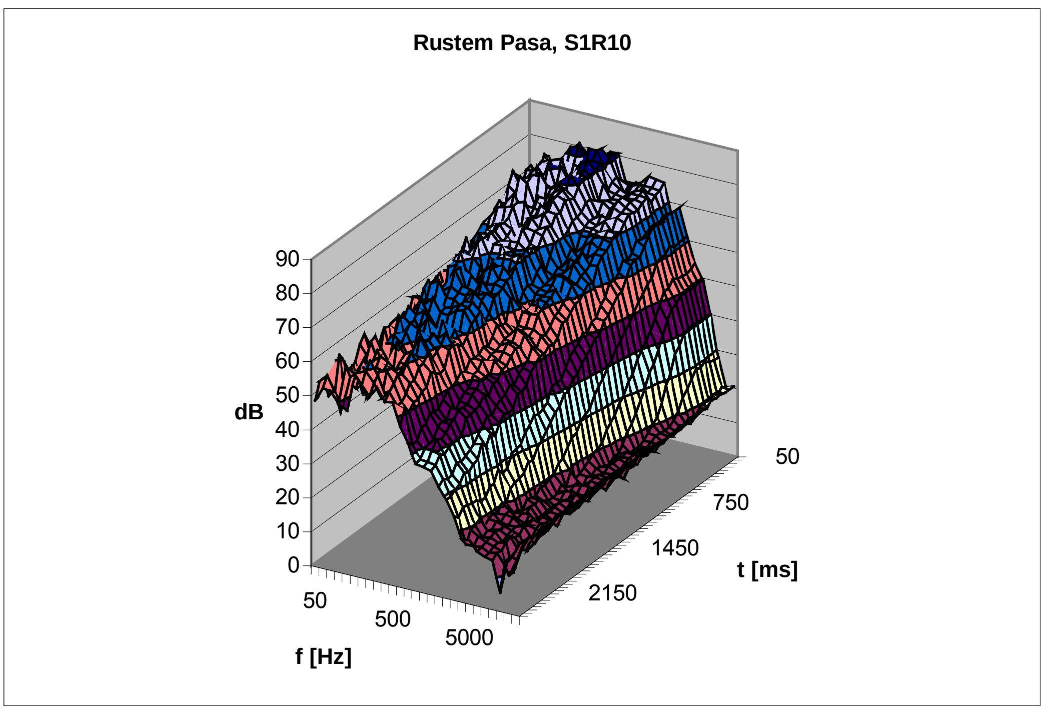

Figure 5.55 Energy Decay for Measurement Data in 3D at S1R10 in Rüstem Pasa Mosque

5.4.2 Acoustical Simulations of Rüstem Pasa Mosque

The combination of ray tracing and radiosity method again is used in Rustem Pasa Mosque simulations. Interior walls of the mosque is covered with ceramic tiles and the dome is plaster surface. The floor is covered by thick carpet. Absorption coefficients used in simulation are given Table 5.2.

Three dimensional geometry of this mosque is generated by using of 764 plane surface. Diffusion coefficient values used through out simulations are 0.7 for carpet covered surface and 0.1 for all other interior surfaces. Form factors are generated only once and values are used for different source and receiver combination. It took 5 minutes in computing time with same computer used in all cases to generate all form factors between surface planes of the geometry. The mean free path inside the space is approximated 14 m in this mosque.

Sound source and receivers are located to the same position with the measurements positions. Total number of generated rays is 10000 and each ray are traced up to 6 seconds of flight time within the space. Execution time for each sound and receiver pair simulation in this case is around 12 minutes on Pentium III 1 GHz processor computer.

Reverberation time estimation, clarity and definition values for octave band of 1000 Hz are listed in Table 5.7. Reverberation times obtained from simulation are close to values obtained from measurements. Maximum difference between measurement and simulation is 6%. This is actually expected result from such a simulation tool. Energy decay curves obtained from different set of source and receiver are given through Figure 5.56 to 5.65.

Table 5.7 Reverberation time (T30), Clarity and Definition Results for 1000Hz from Simulation at Different Source and Receiver Positions in Rüstem Pasa Mosque

	S1R1	**S1R2**	**S1R3**	**S1R4**	**S1R5**	**S1R6**	**S1R7**	**S1R8**	**S1R9**	**S1R10**
RT (s)	3.7	3.9	3.7	3.7	3.7	3.8	3.7	3.6	3.7	3.6
Clarity (dB)	-6.2	-5.8	-5.7	-5.7	-5.8	-5.3	-5.7	-5.7	-6.0	-6.1
Definition	0.10	0.12	0.11	0.11	0.11	0.13	0.11	0.12	0.11	0.11
RT difference between measurement and simulation	6%	5%	3%	0%	0%	3%	3%	3%	3%	5%

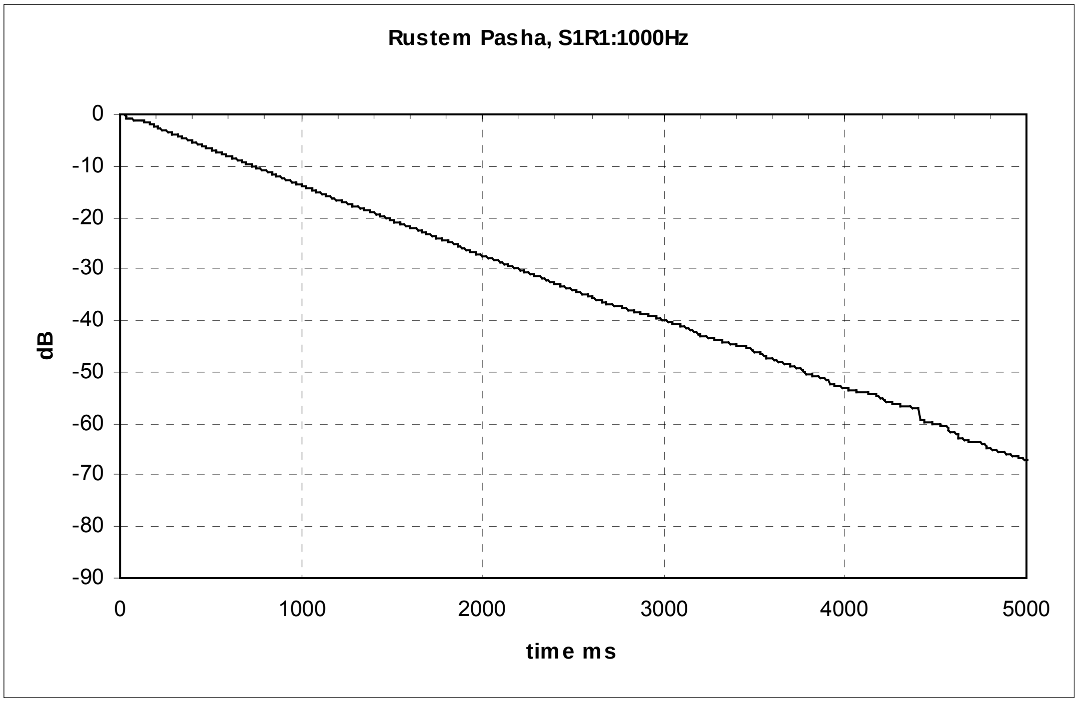

Figure 5.56 Energy Decay for Simulation Data for 1000 Hz at S1R1 in Rustem Pasa Mosque

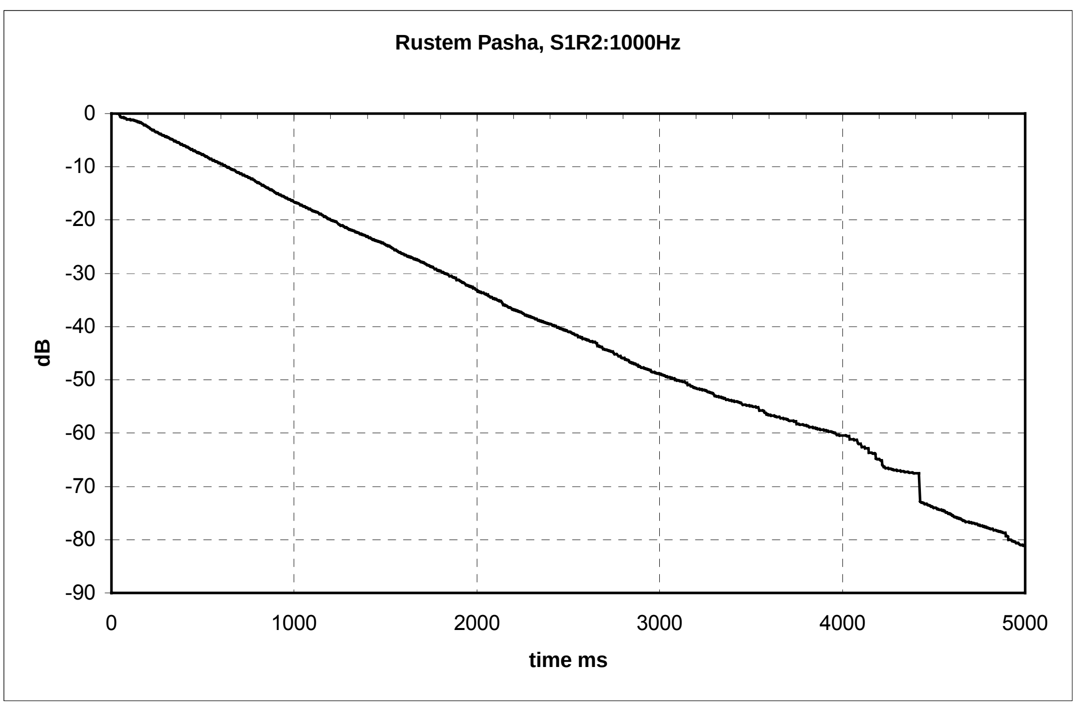

Figure 5.57 Energy Decay for Simulation Data for 1000 Hz at S1R2 in Rustem Pasa Mosque

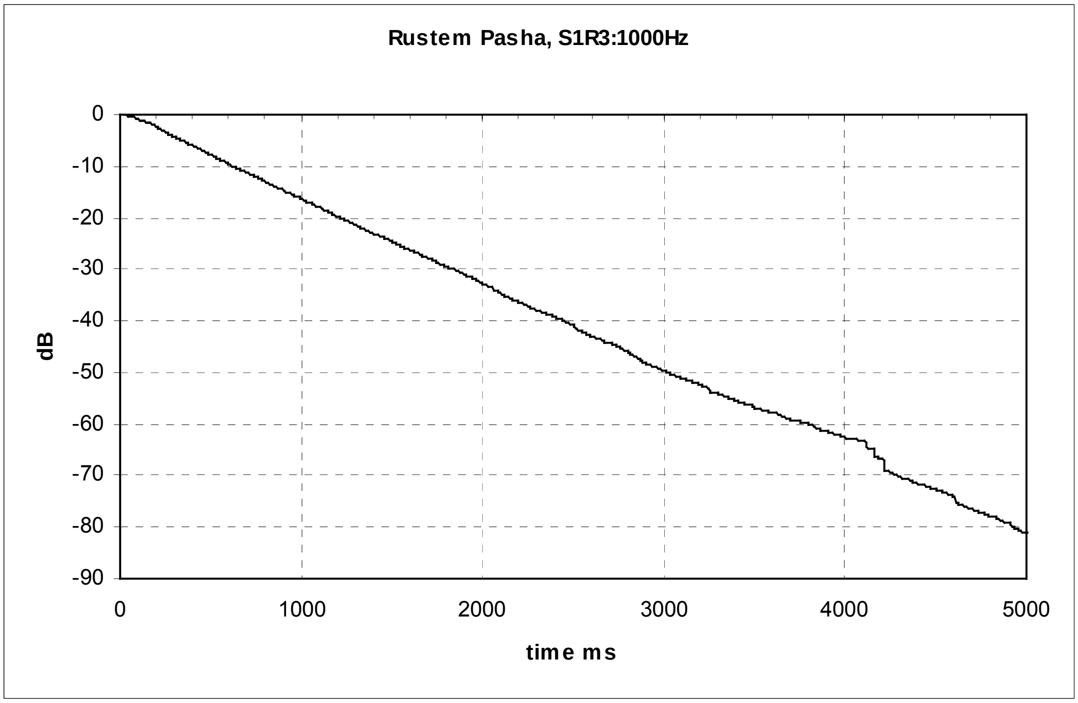

Figure 5.58 Energy Decay for Simulation Data for 1000 Hz at S1R3 in Rustem Pasa Mosque

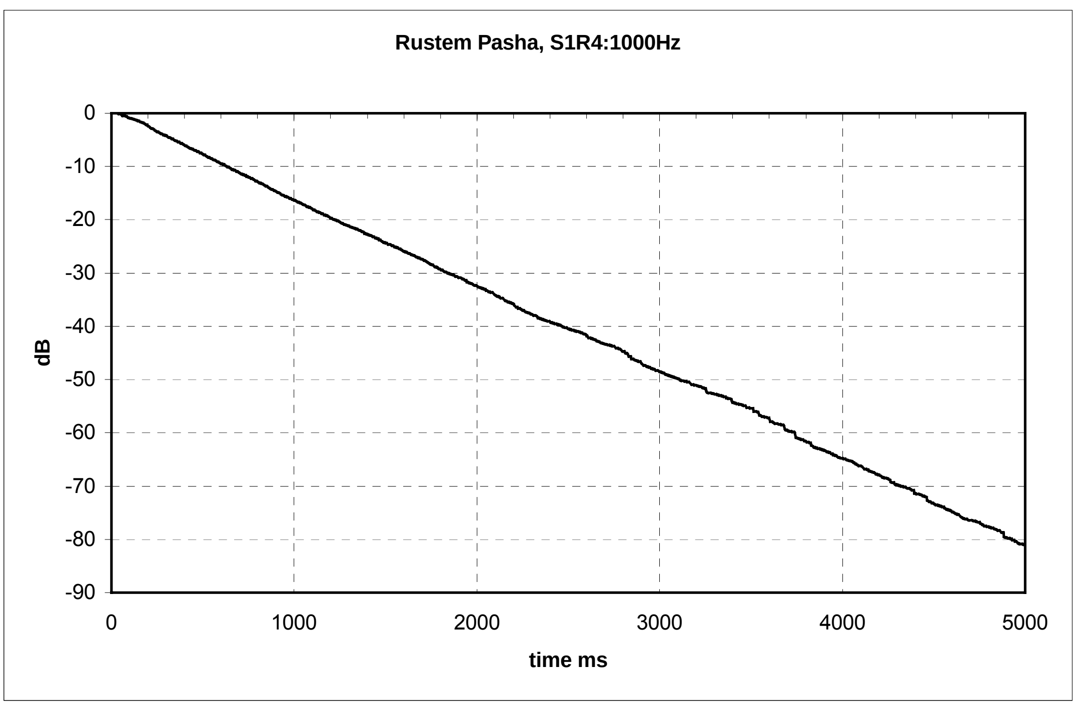

Figure 5.59 Energy Decay for Simulation Data for 1000 Hz at S1R4 in Rustem Pasa Mosque

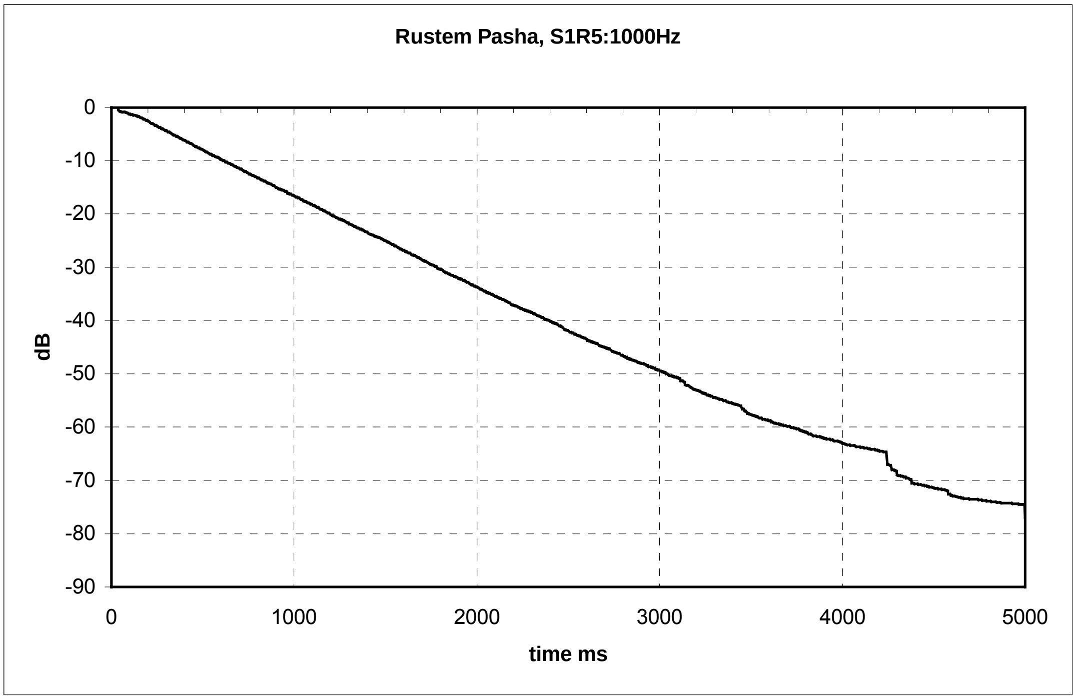

Figure 5.60 Energy Decay for Simulation Data for 1000 Hz at S1R5 in Rustem Pasa Mosque

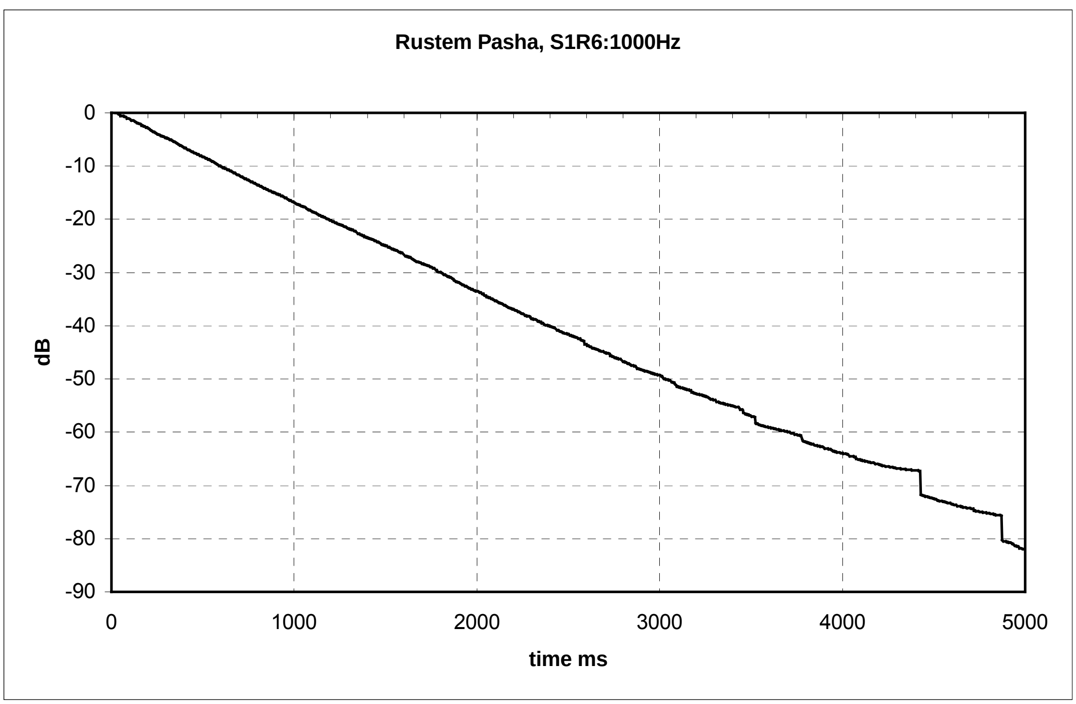

Figure 5.61 Energy Decay for Simulation Data for 1000 Hz at S1R6 in Rustem Pasa Mosque

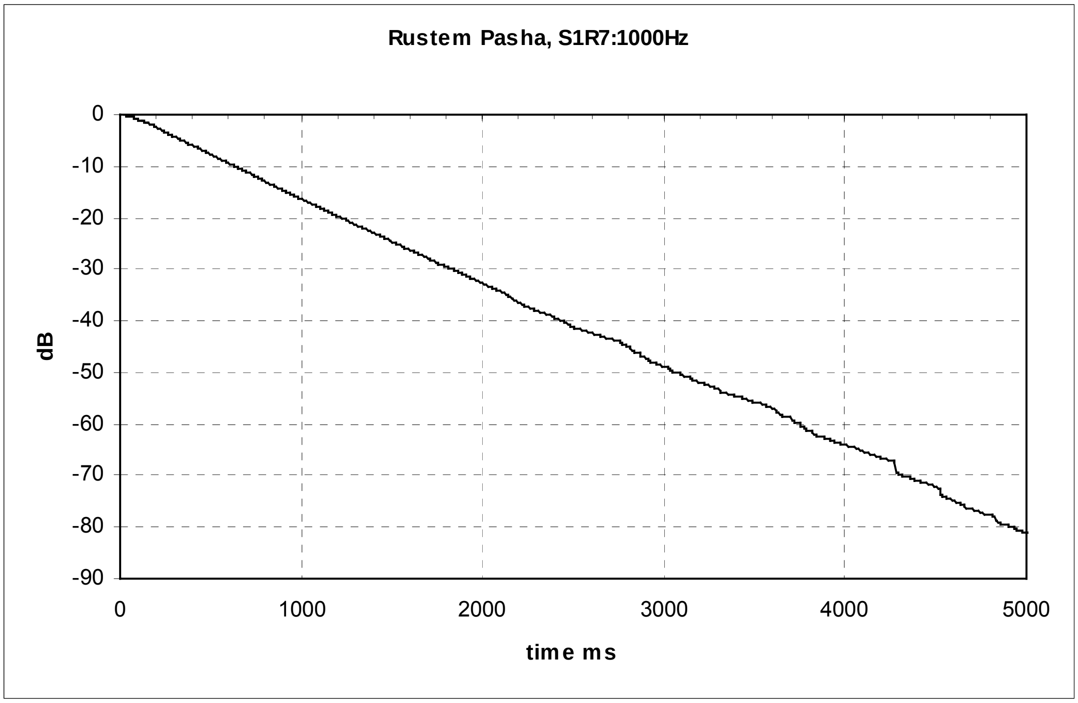

Figure 5.62 Energy Decay for Simulation Data for 1000 Hz at S1R7 in Rustem Pasa Mosque

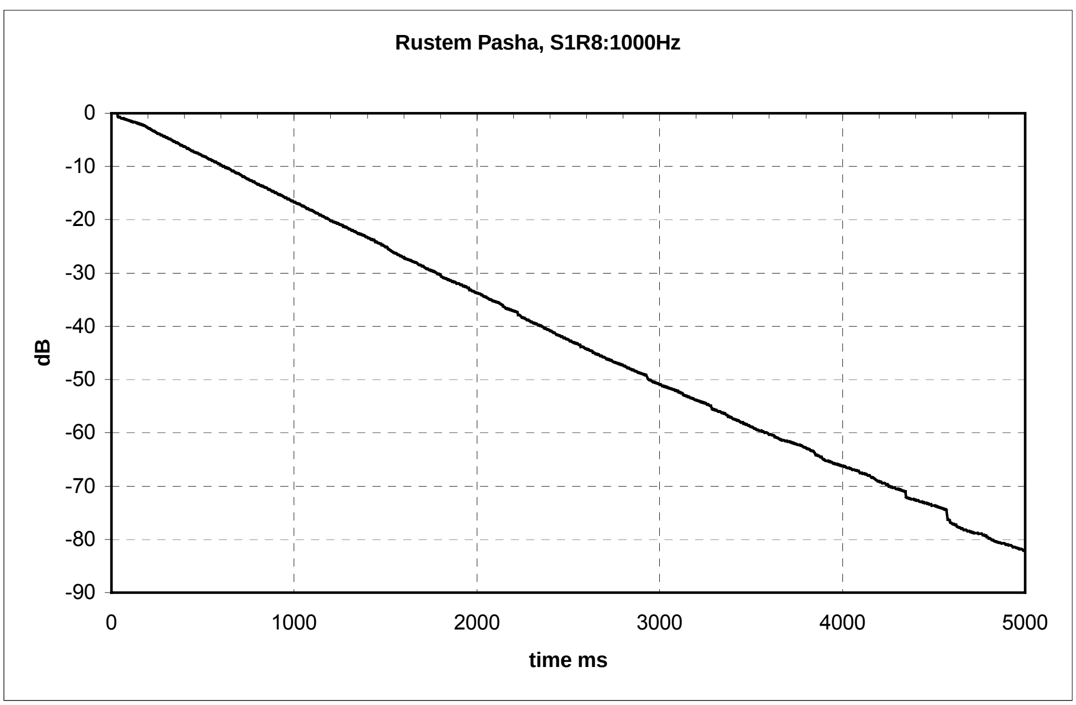

Figure 5.63 Energy Decay for Simulation Data for 1000 Hz at S1R8 in Rustem Pasa Mosque

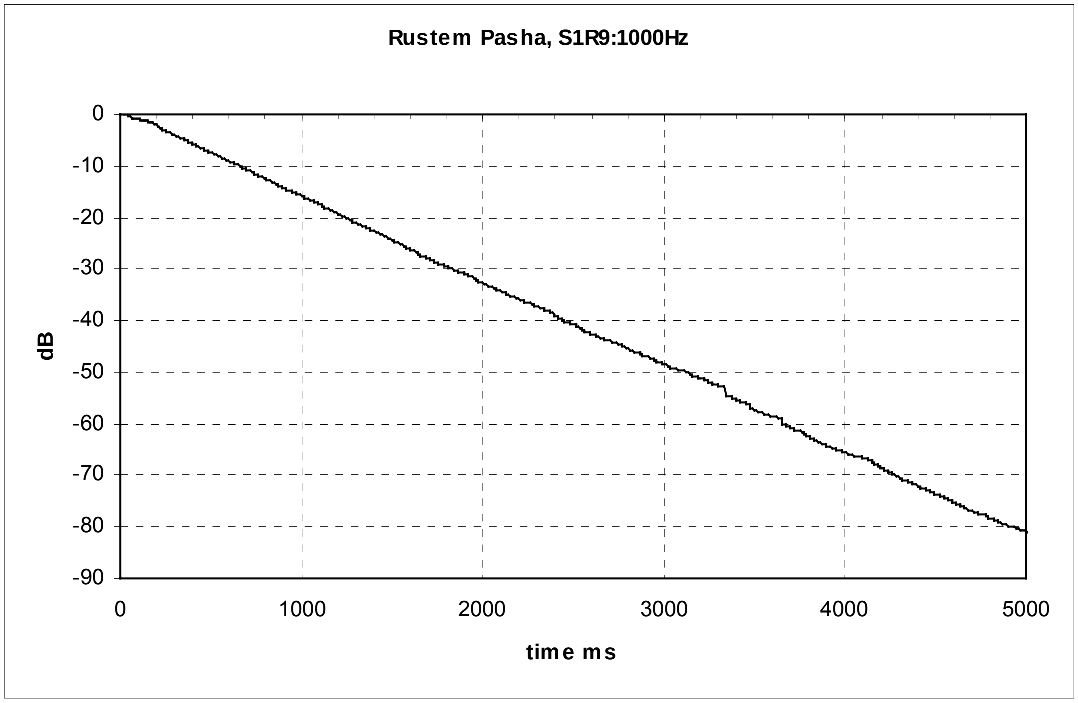

Figure 5.64 Energy Decay for Simulation Data for 1000 Hz at S1R9 in Rustem Pasa Mosque

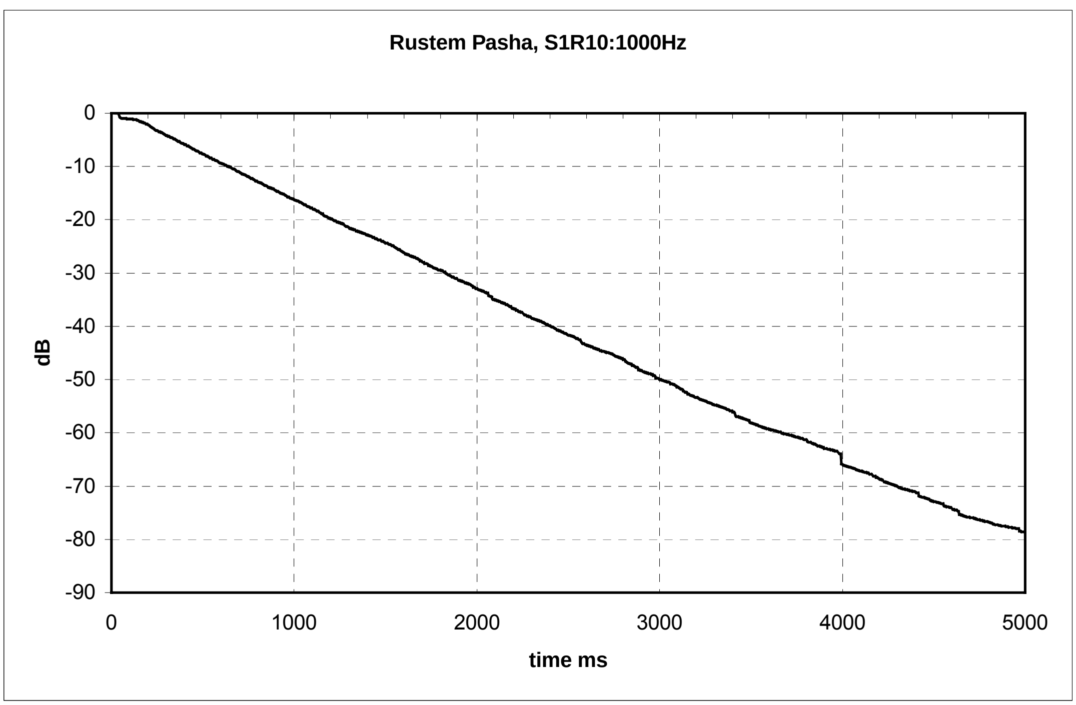

Figure 5.65 Energy Decay for Simulation Data for 1000 Hz at S1R10 in Rustem Pasa Mosque

5.5 Mihrimah Sultan Mosque

Mihrimah Sultan Mosque is located at the entrance to Edirnekapı by the old city walls. Mimar Sinan designed and built this beautiful mosque for princess Mihrimah who was the daughter of Süleyman, the Magnificent. It is believed that construction was completed in the 1560's. The whole structure was a complex of buildings composed of a mosque, *medrese*, double bath, *türbe*, market and primary school. Unfortunately many of them do not exist today (Figure 5.66).

Figure 5.66 Mihrimah Sultan Mosque, Edirnekapı

Mihrimah Sultan Mosque has more windows than any architect had ever dared before. There were some rumors that Sinan was in love with the Sultan's married daughter, Princess Mihrimah. To express his love, Sinan constructed a dome unlike any others built previously. The Mihrimah Mosque was the lightest structure Sinan had ever built, pierced all the way around with 204 windows. This mosque is fantastic mixture of art and engineering (Figure 5.67).

Figure 5.67 Interior View Showing the Windows, Mihrimah Sultan Mosque

These windows emphasize the transparency of such a divine space. They are also important for the scope of this thesis. They do possess definitely different acoustical characteristics in terms of reflection, absorption and diffusion stand points.

The height of the mosque is 37 meters from its foundations up to the center of the dome. The diameter of the dome is 20 meters. This mosque has single central dome and there are six domes (6m in diameter each) over side galleries. The dome is carried by four big arch on each side. The image of each massive arches has been lighten by weight by 19 beautiful window openings. Outside dimensions are 39.50m by 28.00m. (Figure 5.68).

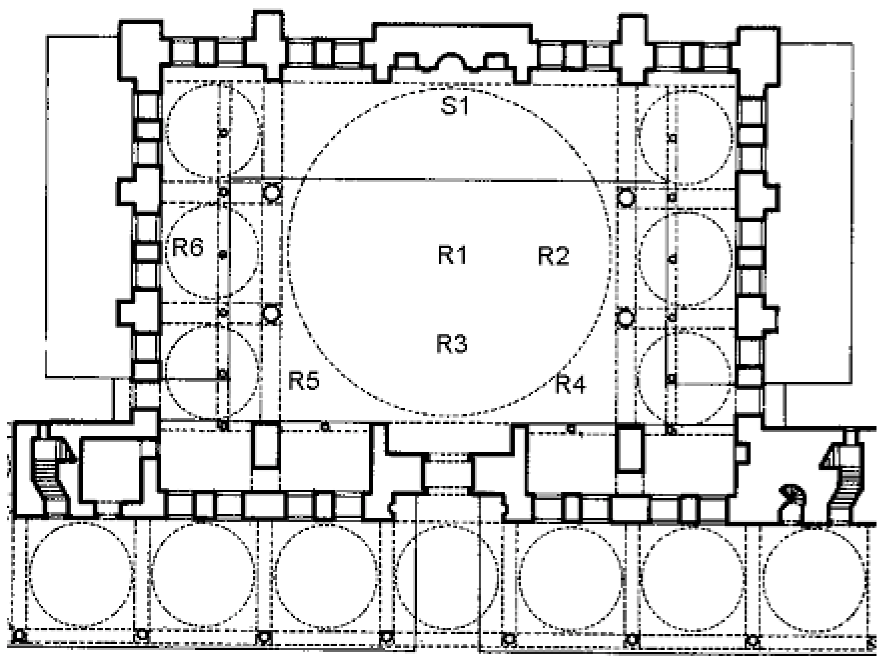

Figure 5.68 Plan View and Source/Receiver Locations of Mihrimah Sultan Mosque

There were certain damages to the building in 1648, 1690, 1719 and 1894.The latest repairement has made between 1956-1957 and it is still in use. The latest damage was caused by the Adapazarı earthquake in 1999.

5.5.1 Acoustical Simulations of Mihrimah Sultan Mosque

The same simulation technique is used for Mihrimah Sultan Mosque. There was no measurements in this case. Interior surfaces of this mosque are mainly covered by plaster. The floor is covered by thick carpet. The major difference is the number of windows used in this mosque. There exists 204 windows. Absorption coefficients used in simulation are given Table 5.2.

Total number of 651 plane surface are used to generate three dimensional geometry of Mihrimah Sultan Mosque. Diffusion coefficient values used through out simulations are 0.7 for carpet covered surface and 0.1 for all other interior surfaces. Like all other cases, form factors are generated only once and values are used for different source and receiver combination. It took 10 minutes in computing time with same computer used in all cases to generate all form factors between surface planes of the geometry. The mean free path inside the space is approximated 19 m in this mosque.

Sound source and receivers locations for simulations are shown in Figure 6.68. Total number of generated rays is 50000 and each ray are traced up to 6 seconds of flight time within the space. Execution time for each sound and receiver pair simulation in this case is around 18 minutes on Pentium III 1 GHz processor computer.

Reverberation time estimation, clarity and definition values for octave band of 1000 Hz are listed in Table 5.8. Energy decay curves obtained from different set of source and receiver are given through Figure 5.69 to 5.75.

Table 5.8 Reverberation time (T30), Clarity and Definition Results for 1000Hz from Simulation at Different Source and Receiver Positions in Mihrimah Sultan Mosque

	S1R1	**S1R2**	**S1R3**	**S1R4**	**S1R5**	**S1R6**
RT (s)	3.9	3.7	3.9	4.0	3.9	4.0
Clarity (dB)	-6.2	-6.2	-6.4	-6.5	-5.9	-5.8
Definition	0.10	0.10	0.10	0.10	0.11	0.11

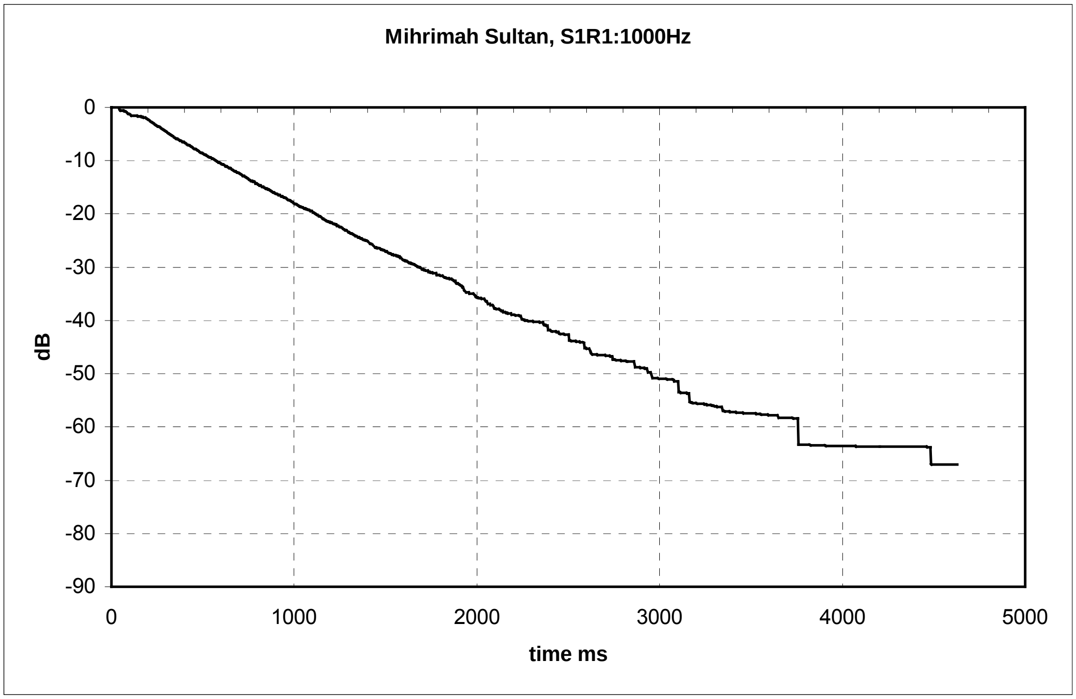

Figure 5.69 Energy Decay for Simulation Data for 1000 Hz at S1R1 in Mihrimah Sultan Mosque

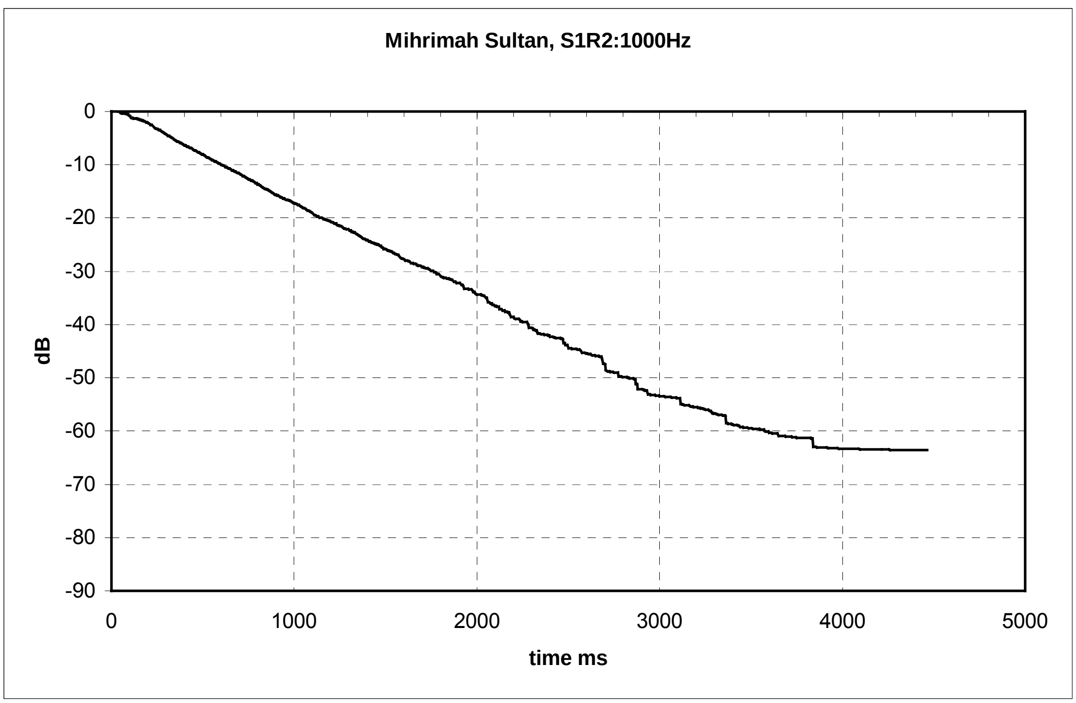

Figure 5.70 Energy Decay for Simulation Data for 1000 Hz at S1R2 in Mihrimah Sultan Mosque

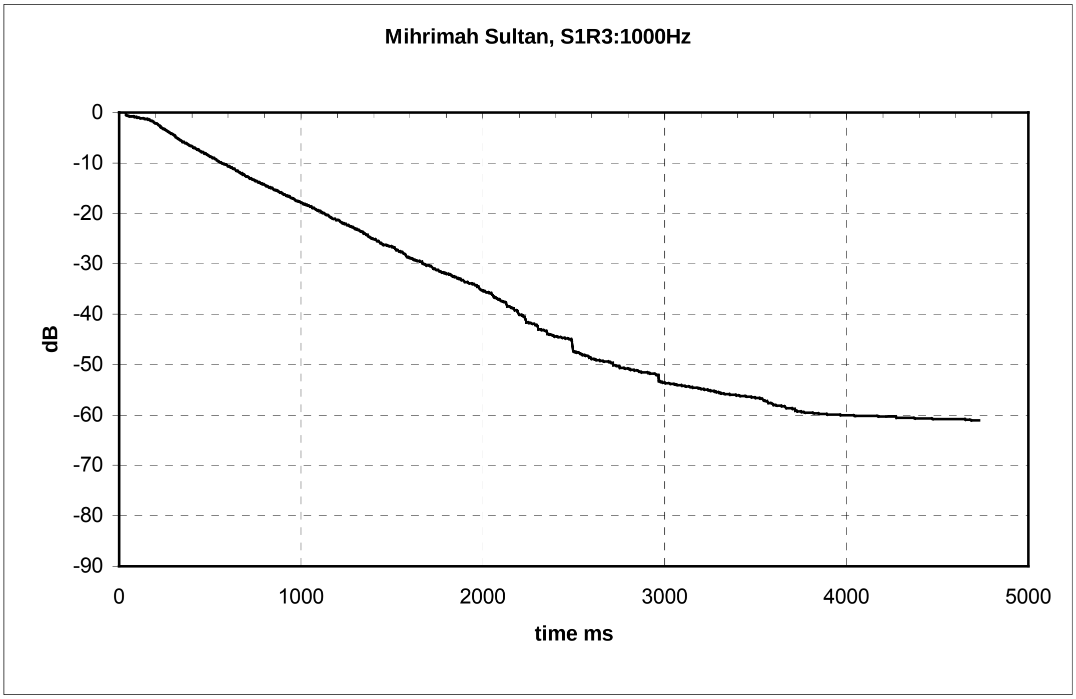

Figure 5.71 Energy Decay for Simulation Data for 1000 Hz at S1R3 in Mihrimah Sultan Mosque

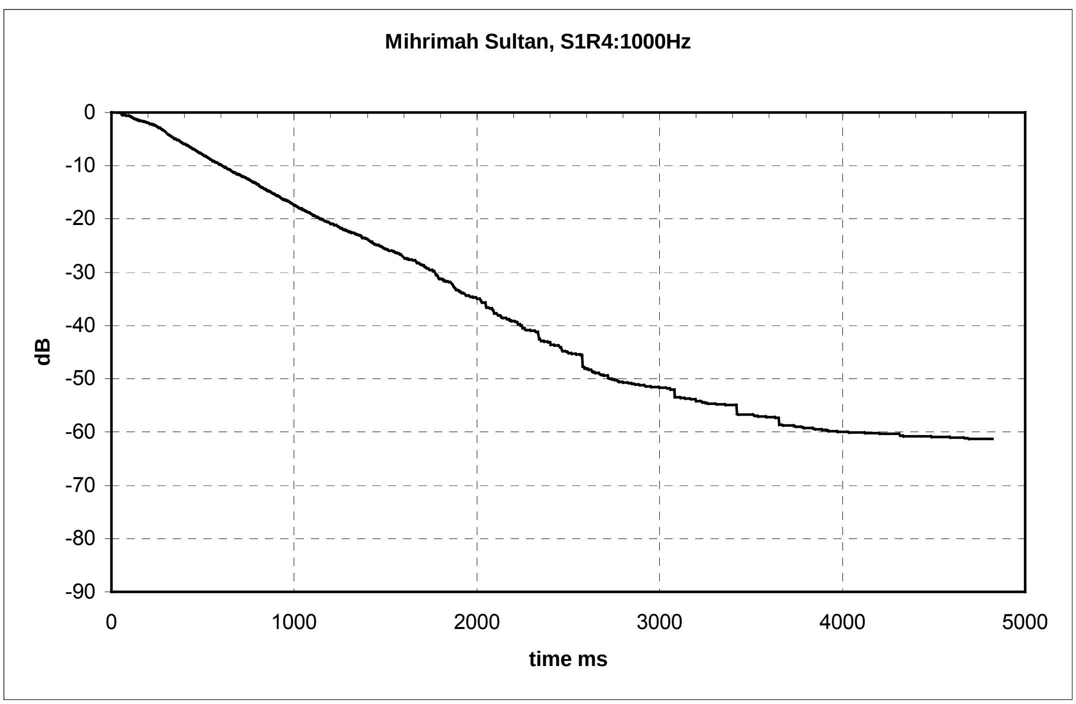

Figure 5.72 Energy Decay for Simulation Data for 1000 Hz at S1R4 in Mihrimah Sultan Mosque

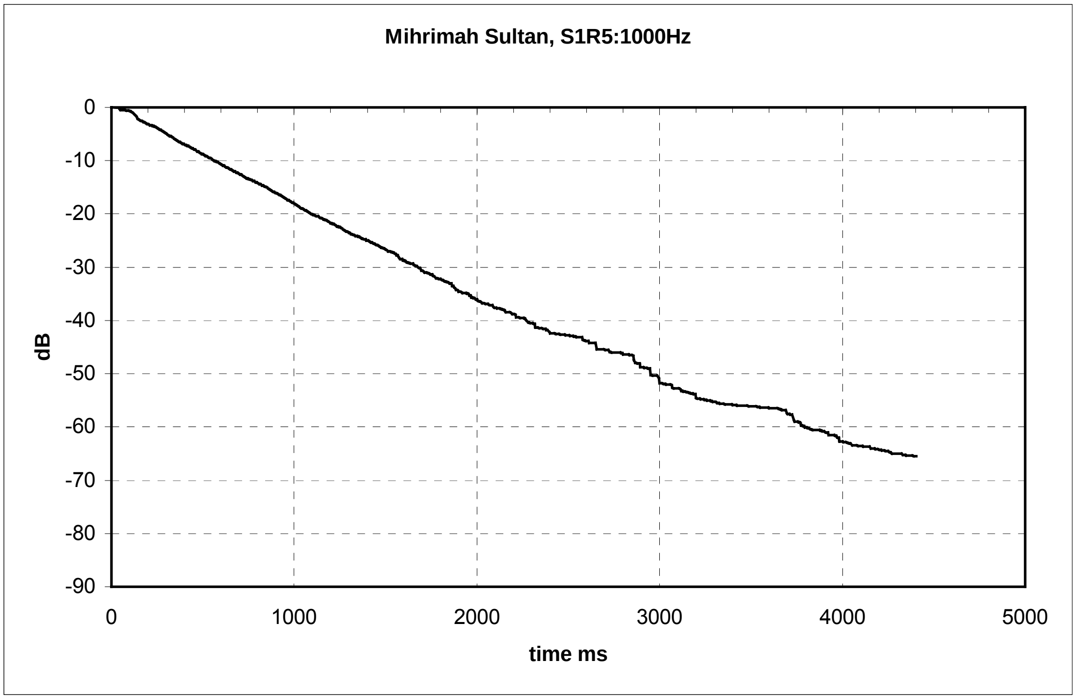

Figure 5.73 Energy Decay for Simulation Data for 1000 Hz at S1R5 in Mihrimah Sultan Mosque

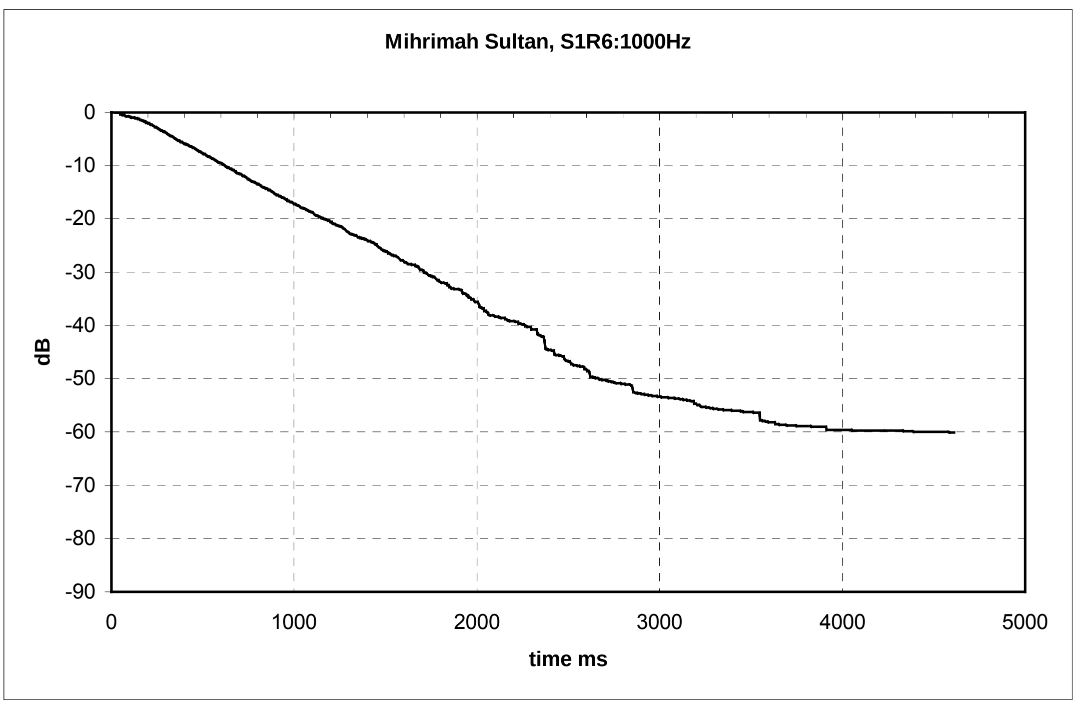

Figure 5.74 Energy Decay for Simulation Data for 1000 Hz at S1R6 in Mihrimah Sultan Mosque

CHAPTER 6

CONCLUSIONS

6.1 Introduction

The main purpose of this study is to investigate and understand the acoustical characteristics of classical Ottoman mosques by conducting acoustical measurements and computer simulations. A computer simulation software has been developed by using a combined geometrical room acoustics and radiosity approach for analyzing their acoustical characteristics of the mosques. Results obtained from simulations are verified by real time measurements so that the simulation model could be used to investigate the acoustics of other mosques or spaces. It is projected to show that simulation model could serve a viable tool to predict acoustical properties in such spaces.

As a result of this study it is possible to draw out main acoustical design principles through analyses on acoustics of historical mosques. Additionally, the study aims to provide detailed knowledge to researchers striving to reach a consensus on mosque acoustics. The results of this study may serve as a reference for future studies. Another purpose of such a study is to document the acoustical characteristics of the selected mosques through measurements. These mosques are important historical buildings which represent a period of Ottoman architecture and the mastery of their architect, Sinan. All acoustical data captured during measurements are given in Appendices for follow up studies in future.

The reason for choosing Sinan's mosques for the study is based on the belief in his superiority in mosque design. The selected and acoustically evaluated mosques belong to a period, referred to as the golden period of mosque architecture in Ottoman history and all designed and built by Sinan the Architect. Süleymaniye, Rüstem Pasa, Mihrimah Sultan (Edirnekapı) in Istanbul and Cenabi Ahmet Pasa in Ankara have been selected for measurements and acoustical simulation. Each chosen mosque has different features and properties important from the acoustical characteristics stand point.

6.2 Comparative Evaluation of Results

In holy spaces reverberation times in the order of 2.5 - 6 seconds are quite common. Churches are reported to exhibit such long reverberation characteristics. Mosques are also found to have comparably long reverberation times [30,31,33].

In the study, Cenabi Ahmet Pasa Mosque was discovered to possess reverberation times in the order of 3.5 seconds through measurements conducted at four different locations. Measured early decay times at these locations were shown to be in harmony with their simulated counterparts. These figures were found to coincide with the ones obtained by ray tracing simulations based on photogrammetric measured drawings. However, due to geometrical/acoustical deficiency of dome structure, echoes and focusing were observed in the measurements. Such acoustical defects were also revealed by simulation studies.

Süleymaniye Mosque was both measured and simulated to have the longest mid frequency reverberation times (average of T30 in 500Hz and 1000 Hz bands) of 7.3 seconds than any other mosque. This result is expected since it has the largest volume. Experimental studies and computer simulations have revealed that Rüstem Pasa Mosque possesses slightly longer reverberation times than Cenabi Ahmet Pasa due to mainly tile interior surfaces. On the other hand, Mihrimah Sultan Mosque has reverberation times around 4.5 seconds through acoustical simulations.

In the previous chapter, It is shown that experimental and simulation results are consistent. The following study for design parameters for such spaces is carried on the simulation results.

Together with simulated reverberation times, different design parameters such as volume/person, functional floor area, estimated capacity audience (maximum number of people inside) are summarized in Table 6.1. The capacity of audience for each mosque is estimated by the assumption that each person uses an area of 0.6 m x 1.2m. Functional floor area is the usable floor area for praying.

Table 6.1 Simulated Empty Mid frequency Reverberation Time, Volume, Functional Area of Case Studies

Mosque	**Volume,V** m^3	**Funct. Area,F** m^2	**V/F** m	**Audience,N** (full)	**V/N** m^3/person	**RT** s
Cenabi Ahmet	2,900	195	14.9	250	11.6	3.6
Süleymaniye	85,300	3,100	27.5	4300	19.8	7.3
Rüstem Pasa	5,950	385	15.5	550	10.8	4.2
Mihrimah Sultan	13,600	675	20.1	950	14.3	4.5

In order to study the acoustical behavior of the spaces considered and to obtain practical design parameters the relation between the reverberation time (T30) and the volume/functional floor area ratio (*V/F*) was evaluated. The Figure 6.1 shows a plot of the reverberation time versus *V/F* ratio for the mosques considered in the study. It can be easily concluded that the T30 is directly related to the V/F ratio in mosques. Thus, linearly increasing values of *V/F* ratio are found to correspond to increasing values of T30.

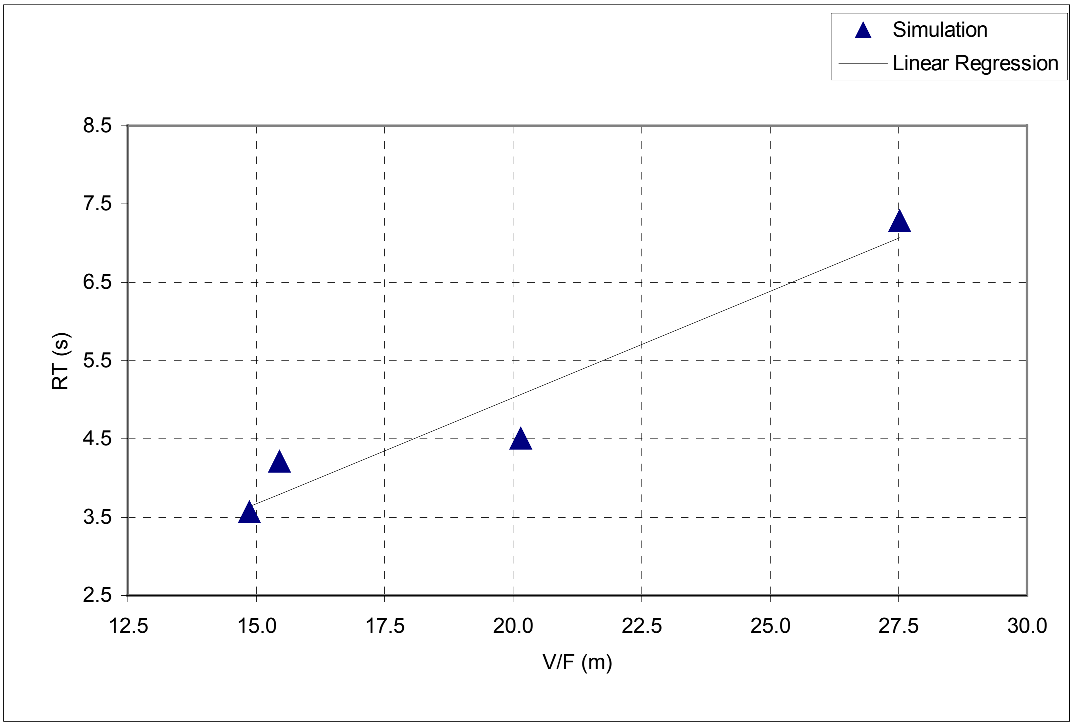

Figure 6.1 Plot of the Mid Frequency Reverberation Time versus *V/F* Ratio (ratio of the volume to the floor functioning area) of the Measured and Simulated Mosques Compared to the Linear Regression Line

Figure 6.2 shows the plot of the clarity index versus the *V/F* ratio for the mosques studied. It can be observed that clarity index C80 is inversely proportional to the *V/F* ratio in mosques. Thus, increasing values of *V/F* ratio corresponds to the decreasing values of clarity index, already low for such spaces. The *V/F* ratio can be interpreted as effective height, also evaluated by other authors and termed as the total average height [31].

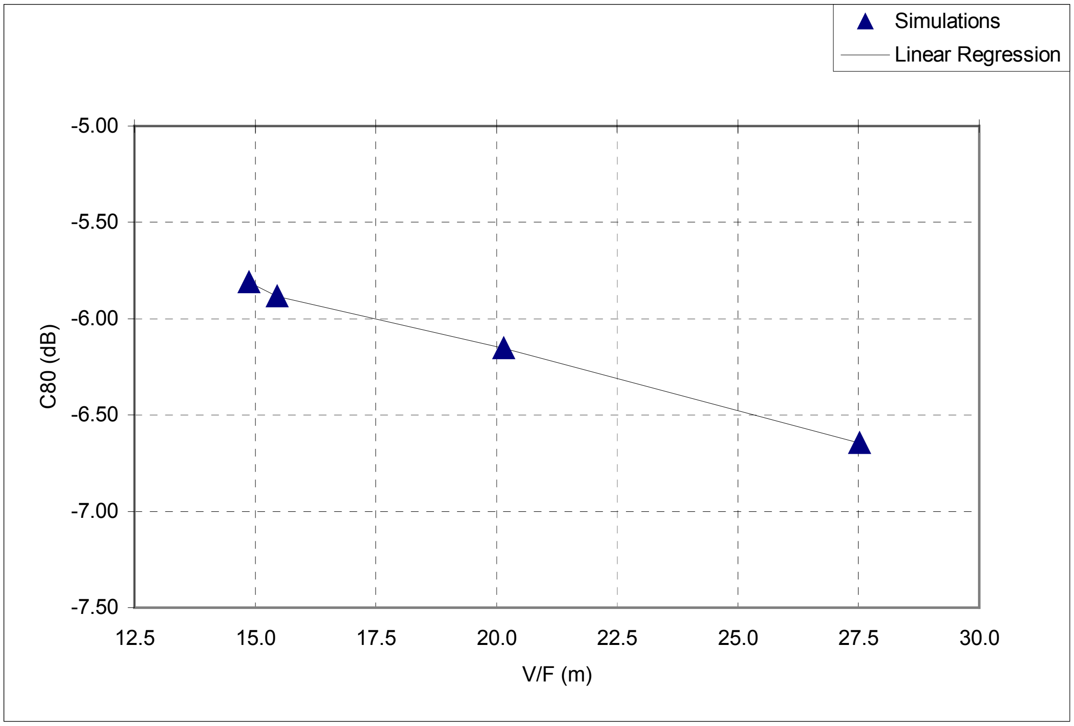

Figure 6.2 Plot of the Clarity Index versus *V/F* Ratio (ratio of the volume to the floor functioning area) of the Simulated Mosques Compared to the Linear Regression Line (linear dependence between C80 and *V/F*)

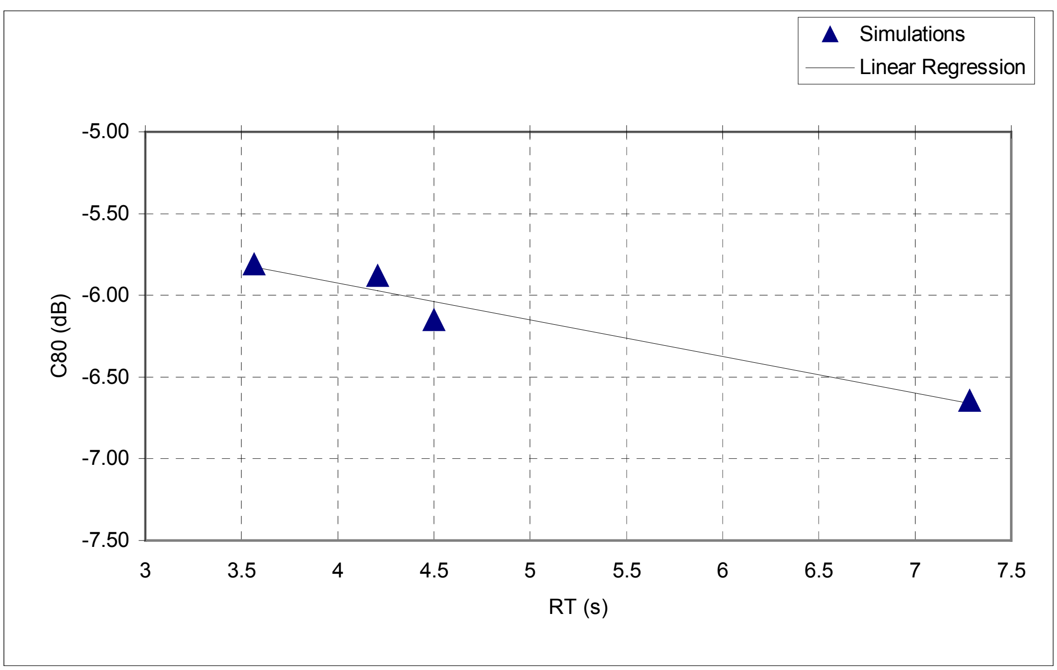

Figure 6.3 Plot of Simulated Values of C80 versus RT and Comparison with the Linear Regression Line

Figure 6.3 presents a inverse linear relation between the average values of the already low clarity index for frequencies of 500 and 1000 Hz and the reverberation time. Thus, increasing values of reverberation time ratio are found to correspond to the decreasing values of clarity index.

The results of both measurements and simulation show a dependence on volume. Highest spatial averaged values of reverberation time and lowest spatial averaged clarity index are reached by Süleymaniye mosque. Definition (D50) values for all four case are in the same order of magnitude around 0.10.

Reverberation time and clarity index values show a dependency on the ratio of the volume to floor functioning area (*V/F*). In particular, reverberation time is found to be linearly proportional to *V/F* and clarity index is certified to be inversely proportional to *V/F*. It is also observed that V/F has no significant effect on D50 definition values.

Table 6.2 gives suggested space volume values for optimum acoustical performance for different functional usage [40]. The estimated volume per person values for each case study were already given in Table 6.1. It's observed that volume per person values in Cenabi Ahmet Pasa, Rüstem Pasa Mosque and Mihrimah Sultan Mosque volume per person value close to in concert hall upper range. The value for Süleymaniye Mosque does not fit any range in the table at all.

Table 6.2 Optimum Volumes/Person for Functional Use of Spaces

Function	**Volume (m3/person)**			
	Doelle			Maekawa
	Minimum	Suggested	Maximum	Suggested range
Speech	2.3	3.1	4.3	4-6
Movie theater	2.8	3.5	5.1	4-6
Opera	4.5	5.7	7.4	6-8
Multi purpose	5.1	7.1	8.5	6-8
Concert hall	6.2	7.8	10.8	8-10

Due to the fact that floor in all cases being covered with highly sound absorptive material, i.e., thick carpet, the measurements and simulation results at unoccupied and empty spaces are not anticipated to show great differences when comparing with the occupied ones.

In Islam religion practice of music inside the mosque while praying is rather rare. However, musical function is more emphasized when there is a special session known as '*mevlid'* held on religious days like '*kandil'* and on occasions after deceased. Speech intelligibility is important when there is a speech in the mosque. In this study the low values of clarity and long reverberation times obtained from simulation and measurements from the mosques indicate that speech intelligibility is not good at all. This result concludes that the studied mosques are not suitable for natural speech environment.

The data gathered through out the measurements and simulations are also used to calculate the bass ratio, which is suggested as objective measure for warmth of sound. If a sound field is more than warm, the enclosed space can be undesirably *dark*.

$$BR = \frac{RT_{125Hz} + RT_{250Hz}}{RT_{500Hz} + RT_{1000Hz}} \tag{6.1}$$

where the numerator is an average of RT's in the 125 Hz and 250 Hz octave bands, and the denominator is an average of RT's in the 500 Hz and 1000 Hz octave bands.

The spatial average of measured RT’s for Cenabi Ahmet Pasa, Rustem Pasa and Suleymaniye mosques and simulation RT for Mihrimah Sultan mosque are used to form Table 6.3. The values in $\mathbf{T_{2000/}\,T_{Mid}}$ column are calculated by dividing RT in 2000Hz to the average of RT's in the 500 Hz and 1000 Hz octave bands. Similarly, the values in $\mathbf{T_{4000/}\,T_{Mid}}$ column are calculated by dividing RT in 4000Hz to the average of RT's in the 500 Hz and 1000 Hz octave bands. These ratios represent brilliance value of the sound.

Table 6.3 Bass Ratio and Other Ratios for the Case Studies

Mosques	**Bass Ratio**	**Ratio1 ($T_{2000/}\,T_{Mid}$)**	**Ratio2 ($T_{4000/}\,T_{Mid}$)**
Cenabi Ahmet Pasa	1.34	0.70	0.43
Rustem Pasa	1.41	0.69	0.47
Suleymaniye	1.28	0.60	0.36
Mihrimah Sultan	1.32	0.68	0.42

A bass ratio between 1.1 and 1.25 is desirable in spaces with a high RT, and a bass ratio between 1.1 and 1.45 is recommended for any space with an RT of 1.8 sec or less [41]. So bass ratios obtained from case studies are close but not in the ranges as recommended above. Average values for $T_{2000/}$ T_{Mid} and $T_{4000/}$ T_{Mid} are given as 0.93 and 0.84 respectively [41]. It is observed that brilliance values obtained are lower than values above, which concludes that brilliance of the sound is less then expected in these case studies.

It is known that, to reduce the acoustical problems due to dome's geometrical deficiency, Sinan has used some ceramic containers (Helmholtz resonators) in the forms of pots. However, sealing the openings of the ceramic containers and changing the original material during the restoration studies over the years, longer reverberation time values than original ones have resulted. Unfortunately, these containers cannot be modeled in computer the simulations because of missing information on their quantity and locations.

REFERENCES

[1] Borish J., Extension of the image model to arbitrary polyhedra. *J. of the Acoustical Society of Americ*a, 75(6), (1984).

[2] Kristiansen U.R., Krokstad A., and Follestad T., Extending the image method to higher-order reflections. *Applied Acoustic*s, 38(2–4):195–206, (1993).

[3] Funkhouser T.,et all., A Beam tracing method for interactive architectural acoustics. *J. of the Acoustical Society of Americ*a,99(3), (1996)

[4] Allen J.B., Berkley D.A., Image method for efficiently simulating small room acoustics. *J. of the Acoustical Society of Americ*a, 65(4), (1979)

[5] Lam Y.M., Dependence of diffusion parameters in room acoustics prediction model on auditorium sizes and shapes. *J. of the Acoustical Society of Americ*a, 100(4), (1996).

[6] Plomp,R., Steeneken,H.J.M. and Houtgast, T., Predicting speech intelligibility in rooms from the modulation transfer function II: Mirror Image computer model applied to rectangular rooms. *Acustica,46:73-81, (1980).*

[7] Lehnert H., Systematic errors of the ray-tracing algorithm. *Applied Acoustics*, 38, (1993).

[8] Schoeder M.R., Digital simulation of sound transmission in Reverberant space. *J. of the Acoustical Society of Americ*a, 47, 424-431,(1970).

[9] Maercke D. Van, Martin J., The Prediction of Echograms and Impulse Responses within the Epiduare Software, *Applied Acoustics* 38, 93-114, (1993)

[10] Lewers T. A., Combined Beam Tracing and Radiant Exchange Computer Model of Room Acoustics, *Applied Acoustics*, 38, 161–178, (1993)

[11] Drumm I.A., Lam, Y.W., The Adaptive Beam Tracing Algorithm, *J. of the Acoustical Society of Americ*a,107:1405 –12, (2000).

[12] Korany N., Blauert J., Abdel Alim O., Acoustic simulation of rooms with boundaries of partially specular reflectivity, *Applied Acoustics, 62, 875-887, (2001).*

[13] Howarth M.J., Lam Y.W., An assessment of the accuracy of a hybrid room acoustics model with surface diffusion facility, *Applied Acoustics* 60, 237-251, (2000).

[14] Xiangyang Z., Ke-an C., Jincai S., Development of a hybrid computer model for simulating the complicated virtual sound field in enclosures, *Applied Acoustics* 63, 481–491, (2002).

[15] Kuttruf H., Room Acoustics. 2nd ed. London: Applied Science Publishers Ltd, (1979).

[16] Schroeder MR., Binaural dissimilarity and optimum ceilings for concert halls: more lateral sound diffusion. *J. of the Acoustical Society of America*,65:958, (1979).

[17] Hodgson M., Evidence of diffuse surface reflections in rooms. *J. of the Acoustical Society of America*,89:765, (1991).

[18] Howarth MJ, Lin K, Lam YW., Predicting the acoustic influence of scale model modifications using a hybrid model. Proceedings of the 15th International Congress on Acoustics, Volume II, (1995).

[19] Rushmeir, H., D. R. Baum, and D.E. Hall, Accelerating the Hemi-Cube Algorithm for Calculating Radiation Form Factors, *Journal of Heat Transfer* 113:1044-1047, (1991).

[20] M. R. Schroeder, New Method for Measuring Reverberation Time, *J. of the Acoustical Society of America* 37, 409-412, (1965).

[21] Kuran,A., Mimar Sinan, *Hürriyet Vakfı Yayınları (Publications of Hürriyet Foundation)*, Turkish, (1986).

[22] Erzen,J., Sinan Camilerinde Uslup Değişmeleri (Style Changes in Sinan's Mosques), *Mimarlık (Architecture),* Vol 27, Turkish, (1981).

[23] Erzen,J., Mimar Sinan Estetik Bir Analiz (Mimar Sinan An Esthetical Analysis), *Mimarlık (Publications of Şevki Vanlı Foundation)*, Turkish, (1996).

[24] Baskan,S., Ankara Cenabi Ahmet Pasa Camii, Kültür Bakanlığı Tanıtma Eserleri (Ministry of Culture Publications), Turkish, (1992).

[25] Jordan,V.L., Acoustical Design of Concert Halls and Theaters, Applied Science Publishers Ltd. Essex, (1980).

[26] Topaktaş, L., Analysis of Acoustical Field Inside Enclosed Spaces by Ray Tracing Techique, Master Thesis, Middle East Technical University, (1990).

[27] Topaktaş L. and Çalışkan M., Analysis of Acoustic Field Inside Enclosed Spaces by Ray Tracing Technique and Comparative Evaluation with Method of Images Proceedings of 7th Seminar and Exhibition on Noise Control, pp.344-349, Eger,Hungary, (1992).

[28] Topaktaş L. and Çalışkan M., Bakırer Ö., Evaluation of Acoustical Characteristics of Cenabi Ahmet Pasha Mosque: Simulation and Measurements 17th International Congress on Acoustics 2001, Rome,Italy, (2001).

[29] Campo N.,Rissone P.,Toderi M., Adaptive pyramid tracing:a new technique for room acoustics *Applied Acoustics* 61, 199–221, (2000).

[30] Fearn R.W., Reverberation in Spanish, English and French Churches, *J.Sound and Vibration*, 43, 562-567,(1975).

[31] Magrini A., Ricciardi P., An Experimental Study of Acoustical Parameters in Churches, Int. *J. of Acoustics and Vibration*, Vol. 7, No. 3, 177-183, (2002).

[32] Carvalho A.P.O., Relations between rapid speech transmission index (RASTI) and other acoustical and architectural measures in churches *Applied Acoustics,* 58, 33-49, (1999).

[33] Hamadah H. A., Hamouda H. M., Assessment of speech intelligibility in large auditoria case study: Kuwait state mosque *Applied Acoustics* 54,273-289, (1998).

[34] Ian A., Radiosity, A programmer's Perspective, John Wiley, (1994)

[35] Akurgal E., The Art and Architecture of Turks, Rizzoli International Publications, NY, (1980).

[36] Goodwin G., A History of Ottoman Architecture, Thames and Hudson Ltd., London, (1971).

[37] Kozlich, J., http://w3.tyenet.com/kozlich/mimar.htm

[38] Akin G. Asya Merkezi Mekan Geleneği, Kültür Bakanlığı Yayınları 1220, Tanıtma Eserleri Dizisi 38, Ankara, (1990).

[39] Erzen J., Mimar Sinan Cami ve Külliyeleri, Tasarim Süreci Üzerine Bir İnceleme, ODTÜ Mimarlık Fakültesi, Ankara, (1991).

[40] Doelle L.L., Acoustics in Architectural Design, Bibliography 29, National Research Council, Ottawa, (1965), 543 pp.

[41] Bearnek L., How They Sound Concert and Opera Houses,Acoustical Society of America, New York, (1996).

APPENDIX A

Table A.1 Measurements at R1 in C.A.P.

time	dB					
ms	125	250	500	1000	2000	4000
50	76.55	78.69	75.33	73.94	77.87	68.23
100	71.99	76.22	74.25	72.98	75.54	68.32
150	80.36	73.68	77.80	73.63	77.37	68.11
200	76.41	71.78	75.23	73.05	76.69	68.41
250	75.92	73.82	77.16	74.22	75.45	68.41
300	74.25	76.65	78.06	75.52	77.00	68.30
350	74.25	74.41	77.66	72.86	76.95	67.31
400	77.02	77.16	76.03	72.76	74.20	65.71
450	70.60	69.82	72.91	74.01	74.34	65.26
500	78.83	73.16	73.33	74.15	72.22	63.36
550	74.41	68.67	74.34	70.18	73.16	60.37
600	72.15	67.47	74.06	71.54	68.98	59.95
650	71.85	71.80	70.22	70.53	68.98	57.74
700	72.65	70.98	74.11	69.97	68.32	57.13
750	74.43	68.11	71.40	66.20	64.89	53.20
800	70.27	65.59	65.92	67.14	64.67	52.14
850	66.77	64.30	67.36	64.65	63.99	49.46
900	70.15	64.60	66.27	63.26	64.06	47.39
950	64.91	66.70	66.06	61.12	59.74	43.88
1000	61.43	67.54	65.57	60.89	61.50	43.53
1050	70.60	64.77	66.30	61.08	58.96	42.19
1100	69.52	63.10	63.76	61.48	57.92	38.92
1150	62.60	61.78	63.64	62.82	56.18	37.68
1200	64.06	60.06	63.17	57.97	56.02	36.92
1250	63.99	56.68	61.41	57.15	54.87	34.62
1300	64.65	58.04	60.72	58.77	50.14	32.20
1350	62.70	58.40	61.05	57.90	52.30	30.36
1400	58.32	56.77	58.72	55.97	49.88	28.22
1450	58.56	60.23	56.96	54.33	48.45	26.58
1500	60.72	57.64	54.89	54.54	47.95	25.85
1550	54.96	59.15	57.60	55.60	45.88	24.32
1600	58.30	56.37	58.98	51.83	45.98	22.27
1650	57.29	56.82	57.03	50.87	43.81	20.51
1700	60.09	56.18	55.57	50.07	43.30	20.04
1750	53.55	53.17	54.75	49.83	42.69	18.88
1800	51.22	54.00	49.41	49.86	42.10	18.01
1850	54.73	52.16	52.26	47.44	38.66	18.98
1900	59.59	54.59	49.46	48.78	38.62	18.30
1950	56.02	50.94	48.56	45.84	37.70	17.50
2000	56.56	51.01	50.54	47.44	37.11	16.98
2050	55.48	51.41	47.48	44.64	35.58	17.57
2100	54.33	52.33	49.91	45.77	32.67	16.32
2150	49.67	42.66	47.15	43.98	32.08	16.51
2200	45.27	47.22	45.79	40.94	32.81	17.57
2250	51.03	49.34	46.10	42.92	30.39	17.14
2300	52.92	46.10	44.07	39.44	30.10	17.05
2350	41.93	47.48	44.47	37.82	29.04	17.57
2400	52.23	47.27	43.72	36.85	24.95	14.04
2450	49.55	41.58	43.27	38.43	27.54	18.01
2500	45.67	43.65	42.12	36.05	26.79	16.58

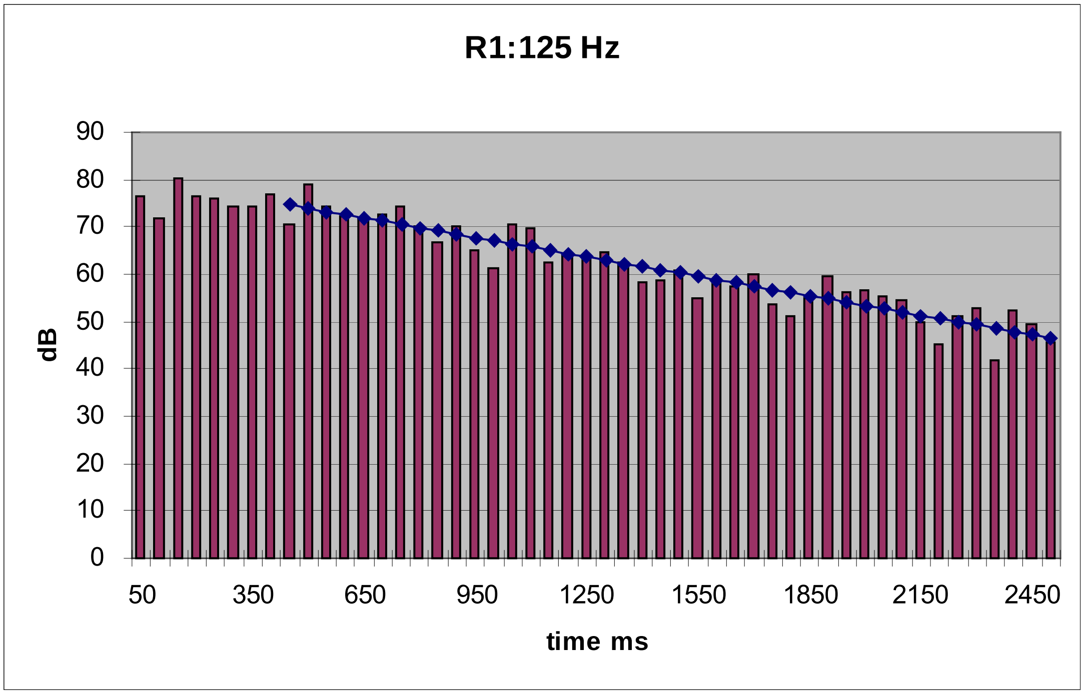

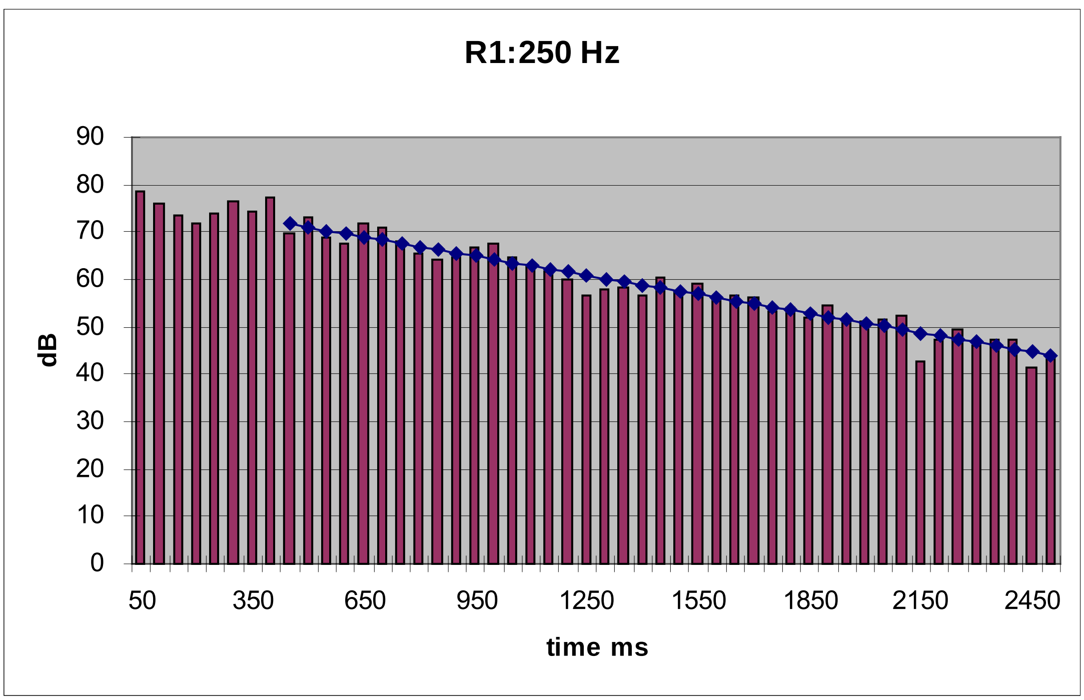

Figure A.1 Decay and Fit for T30 for 125 and 250 Hz at R1 in C.A.P.

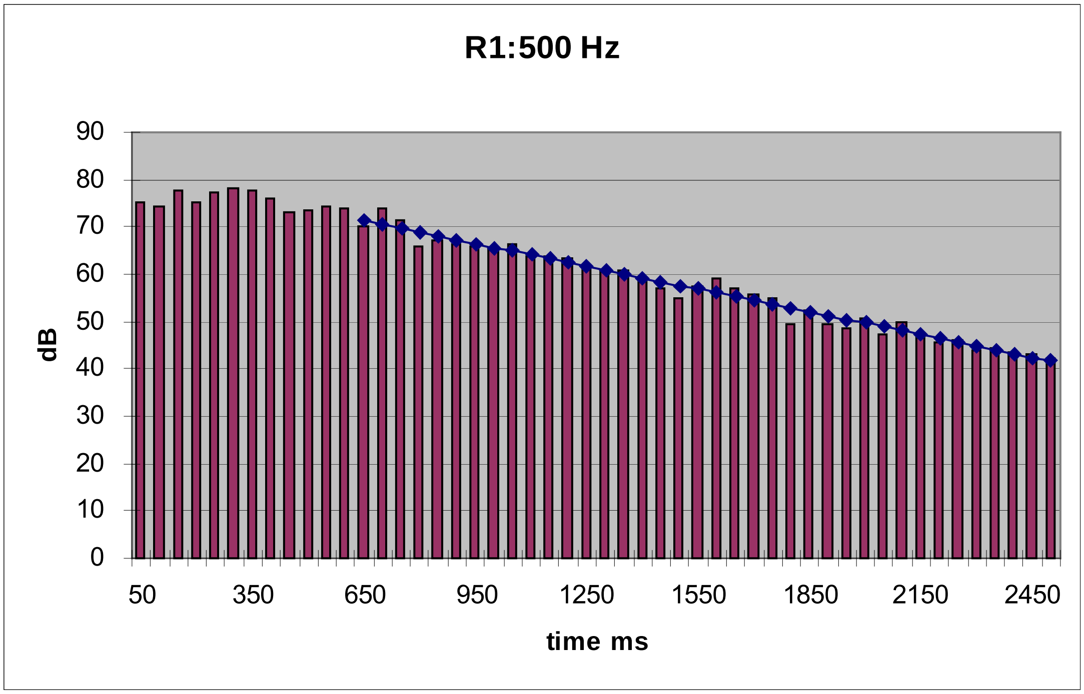

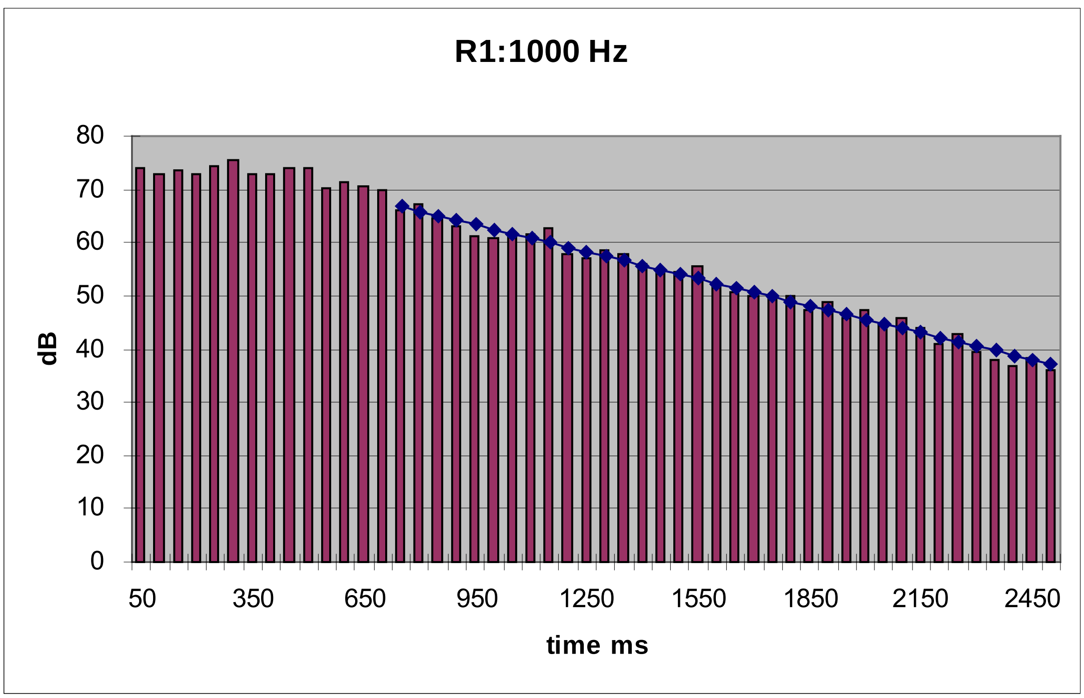

Figure A.2 Decay and Fit for T30 for 500 and 1000 Hz at R1 in C.A.P.

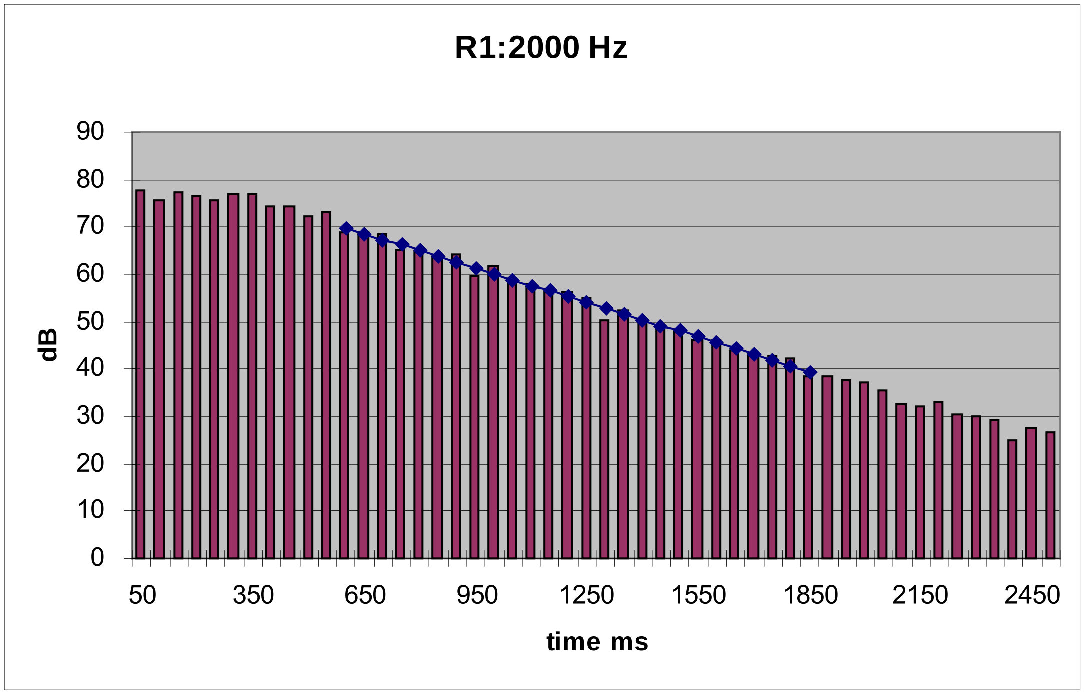

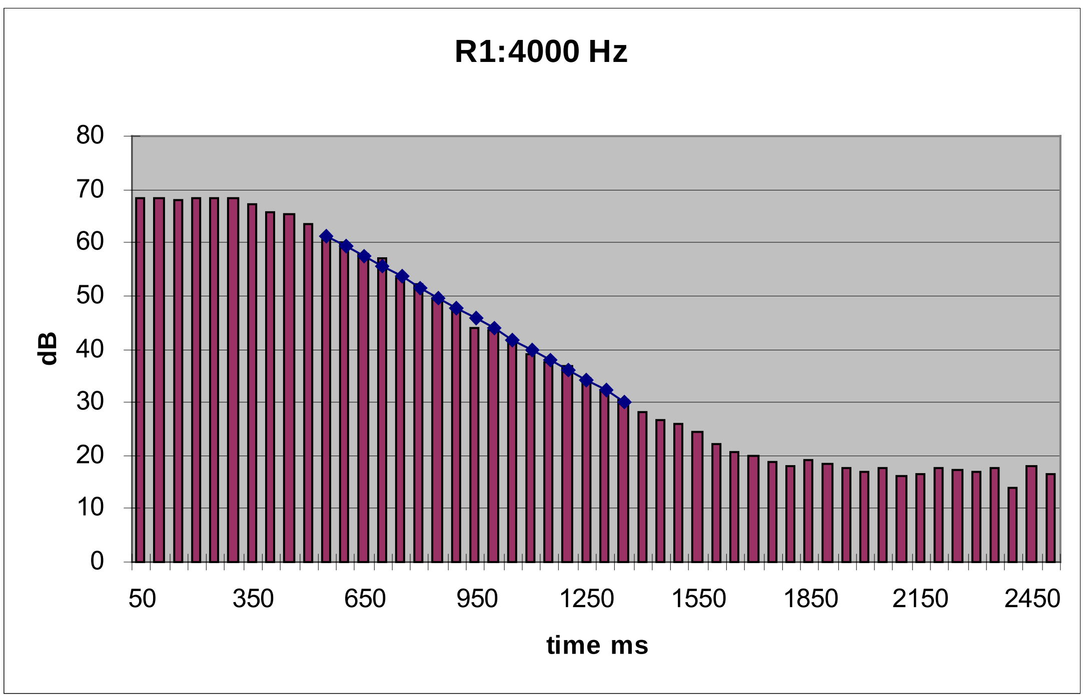

Figure A.3 Decay and Fit for T30 for 2 and 4 kHz at R1 in C.A.P.

Table A.2 Measurements at R2 in C.A.P.

time	dB					
ms	125	250	500	1000	2000	4000
50	74.22	73.47	74.48	72.84	74.27	69.19
100	71.47	73.61	80.34	74.18	75.68	69.92
150	74.90	75.87	77.40	73.63	75.52	69.52
200	74.95	68.98	76.95	74.06	75.99	70.53
250	75.47	70.08	76.76	72.62	75.07	68.86
300	75.87	73.59	78.50	75.00	77.35	67.54
350	77.37	71.61	76.08	74.53	76.15	68.27
400	75.47	69.07	77.52	72.86	75.45	68.25
450	75.33	69.73	75.89	71.94	74.58	65.69
500	77.59	64.82	76.72	71.28	74.48	62.42
550	75.80	67.33	75.82	71.82	71.99	59.08
600	71.96	70.18	71.75	70.25	71.12	58.09
650	70.01	67.10	73.40	67.78	68.08	57.41
700	64.53	63.90	73.21	68.60	67.38	57.08
750	72.86	66.09	70.15	68.34	64.70	52.61
800	68.23	66.67	68.88	66.74	65.76	49.67
850	64.09	67.61	70.04	66.91	62.96	47.37
900	71.99	65.29	66.44	65.73	61.97	47.39
950	66.49	60.89	68.46	64.89	62.39	45.15
1000	70.22	64.49	66.30	62.11	59.38	42.05
1050	70.01	60.39	67.21	61.48	58.58	40.57
1100	67.28	58.28	64.13	61.99	58.87	39.58
1150	64.09	58.32	65.45	62.23	57.34	36.26
1200	58.42	56.42	63.80	60.02	56.02	36.05
1250	63.57	60.02	60.44	58.54	53.57	32.43
1300	66.65	56.18	59.45	57.60	53.24	30.15
1350	61.88	56.16	55.06	55.53	52.19	30.10
1400	58.77	59.10	58.75	57.48	51.43	28.29
1450	59.05	55.17	58.04	56.07	48.35	25.66
1500	58.72	55.24	56.84	54.33	47.48	23.33
1550	62.21	56.47	57.27	49.69	48.14	23.47
1600	57.13	53.83	54.63	52.42	46.80	21.03
1650	56.80	48.59	57.13	53.67	43.60	20.32
1700	55.29	47.32	55.69	50.85	43.79	20.60
1750	55.90	52.19	53.69	50.52	42.14	19.03
1800	54.26	56.30	52.19	48.61	41.70	19.59
1850	54.68	52.33	48.12	47.01	39.27	19.21
1900	51.41	49.51	51.13	47.46	37.25	18.51
1950	54.70	43.84	51.18	47.39	38.62	16.84
2000	50.42	50.35	50.78	47.84	36.55	18.88
2050	52.40	51.50	48.28	41.04	35.49	17.43
2100	53.41	46.50	48.99	43.25	34.05	18.25
2150	52.82	48.35	45.86	42.07	32.27	16.51
2200	45.30	45.04	46.02	42.52	30.55	18.67
2250	56.23	41.42	47.60	41.98	29.73	17.57
2300	47.62	43.58	44.54	40.17	28.10	17.29
2350	49.72	46.19	44.24	39.82	27.87	17.05
2400	53.53	44.92	45.34	36.62	26.79	18.01
2450	42.47	42.83	41.37	39.25	24.79	17.14
2500	49.08	41.23	42.73	38.03	24.48	18.18

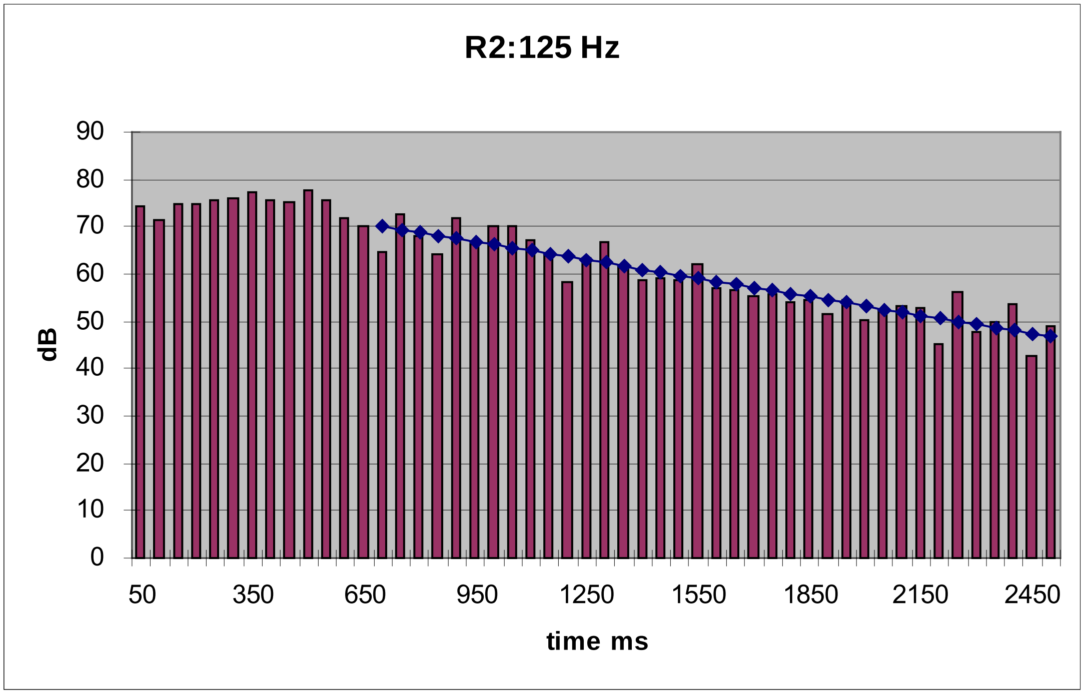

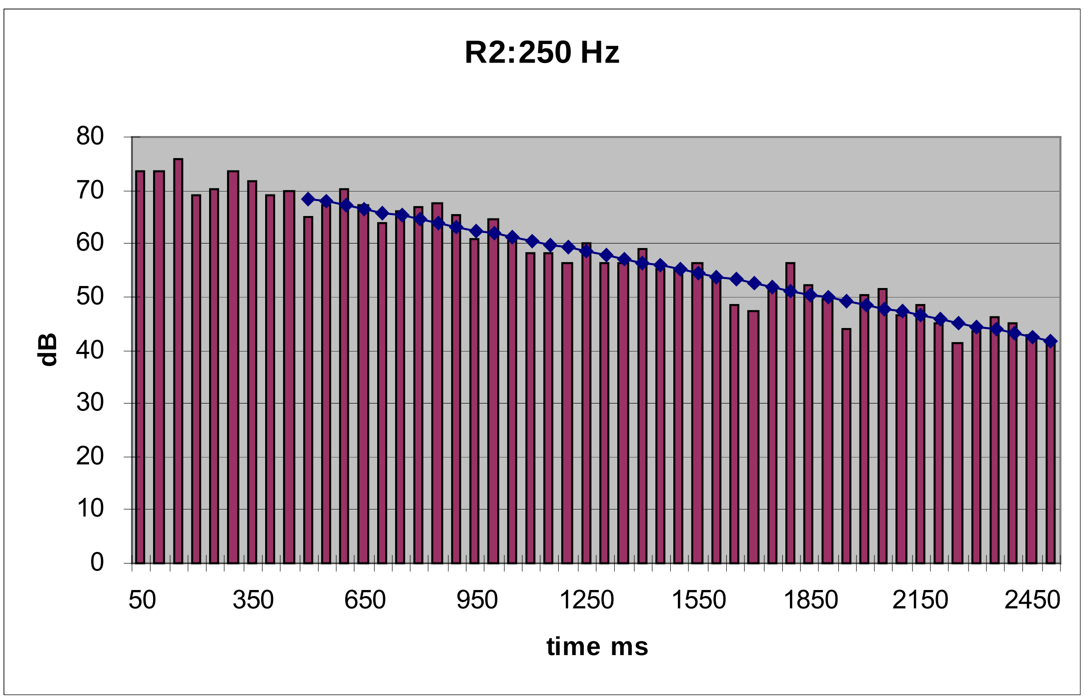

Figure A.4 Decay and Fit for T30 for 125 and 250 Hz at R2 in C.A.P.

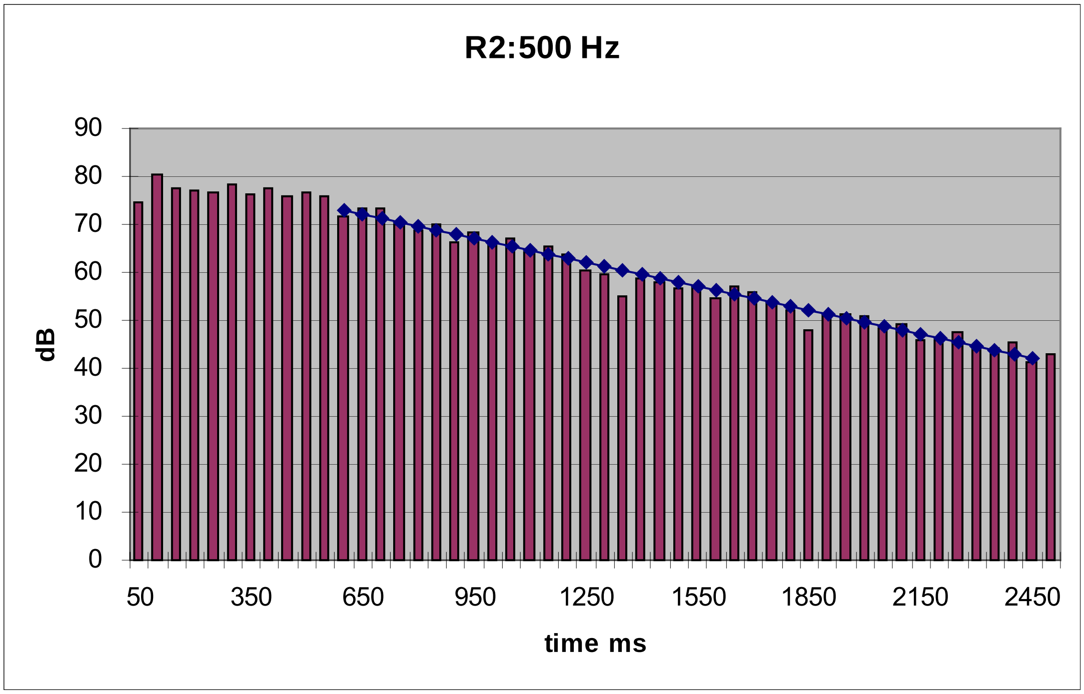

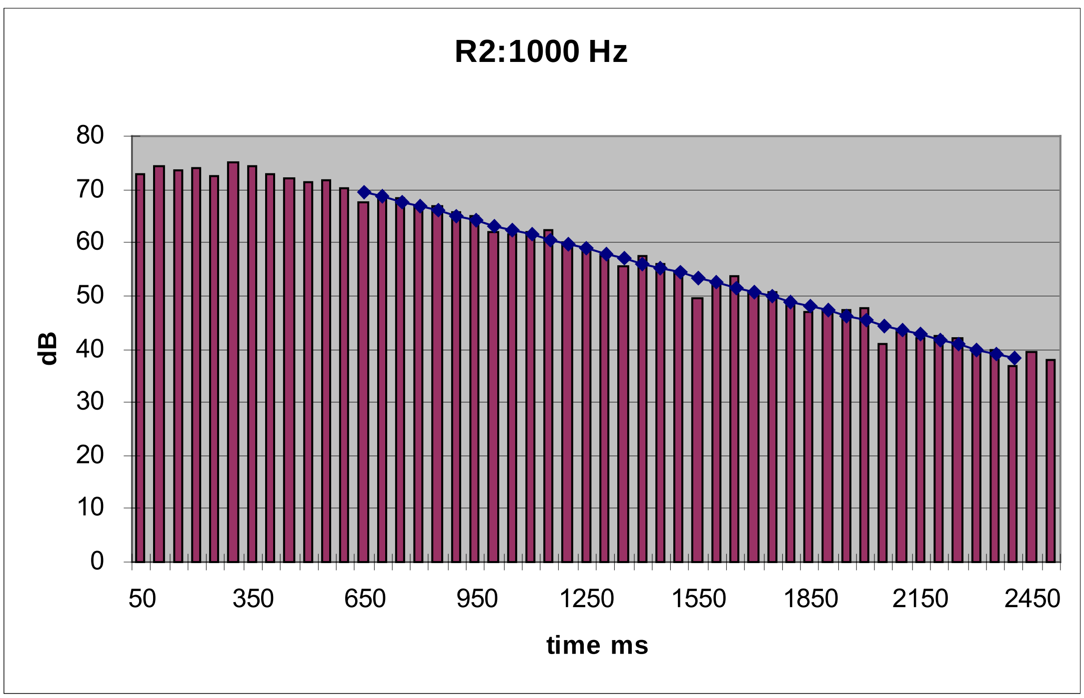

Figure A.5 Decay and Fit for T30 for 500 and 1000 Hz at R2 in C.A.P.

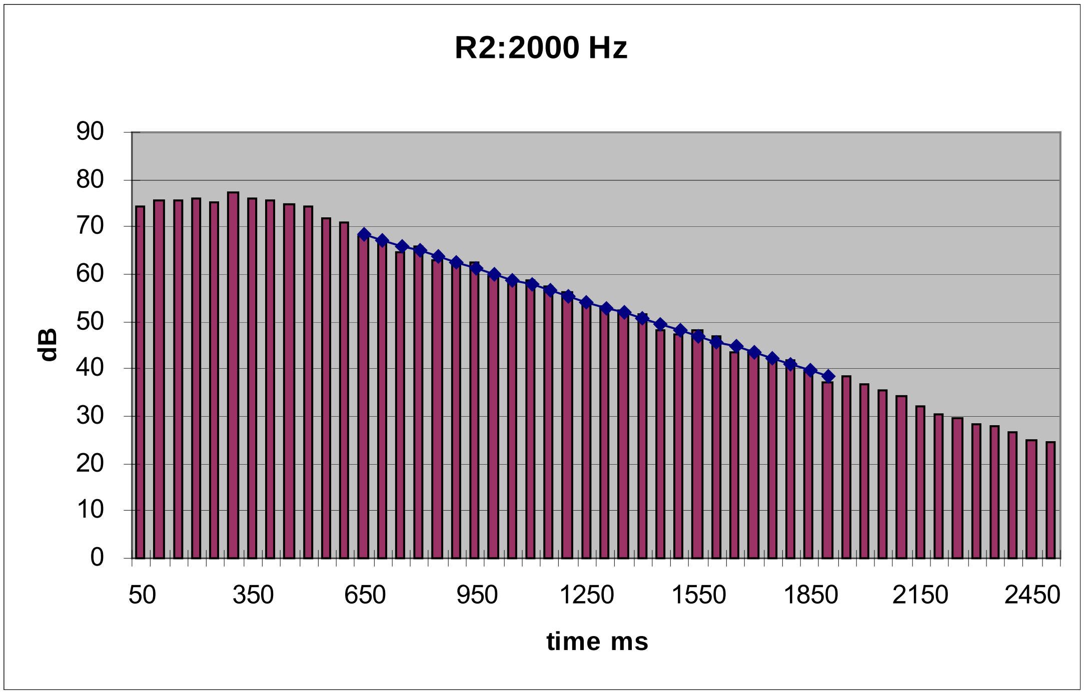

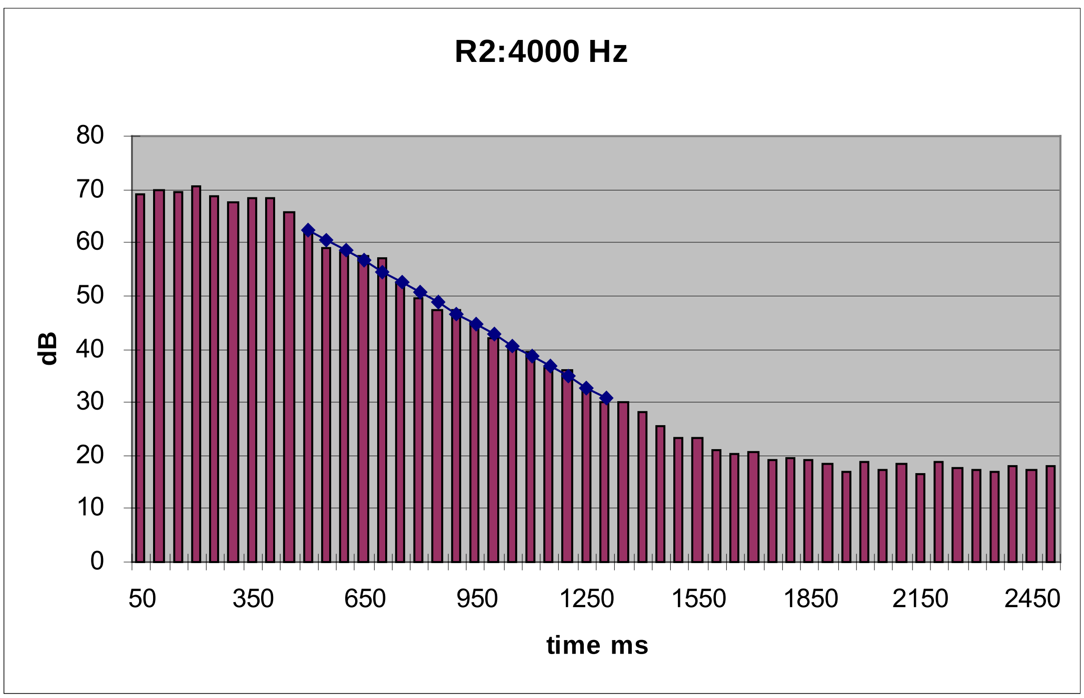

Figure A.6 Decay and Fit for T30 for 2 and 4 kHz at R2 in C.A.P.

Table A.3 Measurements at R3 in C.A.P.

Time	dB					
Ms	**125**	**250**	**500**	**1000**	**2000**	**4000**
50	79.00	75.09	77.96	73.96	73.33	68.53
100	70.46	75.85	77.16	73.56	74.60	66.60
150	73.92	77.19	74.18	73.85	74.72	67.68
200	68.18	76.46	73.56	69.71	76.10	67.50
250	75.68	72.41	77.84	73.78	75.33	68.39
300	65.83	76.76	75.75	73.23	74.93	66.86
350	73.05	68.55	75.45	74.18	76.60	68.06
400	69.94	75.54	75.26	71.94	73.71	65.33
450	72.34	72.91	76.29	72.98	74.34	64.60
500	73.42	73.33	73.14	70.37	71.31	64.63
550	70.18	74.15	74.25	71.12	71.19	60.84
600	69.17	74.65	72.06	70.08	70.18	58.87
650	64.91	69.80	73.59	68.79	69.97	58.25
700	68.08	67.21	70.30	65.43	65.76	54.11
750	67.64	70.27	72.18	65.62	63.71	53.24
800	71.92	69.80	70.30	66.01	65.62	51.18
850	68.04	66.18	71.28	63.55	63.43	48.35
900	68.58	64.27	70.51	66.84	62.77	48.16
950	66.16	65.54	66.16	63.90	61.95	45.15
1000	69.03	63.66	65.38	64.06	61.12	42.78
1050	66.89	60.91	66.56	61.78	59.64	40.73
1100	68.67	61.19	66.98	57.03	58.91	39.60
1150	63.36	58.49	63.22	57.92	57.20	38.71
1200	63.80	59.29	58.70	59.29	55.69	36.62
1250	59.81	55.41	62.06	59.99	53.24	34.27
1300	58.77	56.51	61.26	59.27	53.15	32.13
1350	63.99	61.55	59.81	54.98	52.82	30.43
1400	56.02	59.59	60.42	57.24	51.32	28.64
1450	59.15	56.42	57.85	54.30	49.36	26.72
1500	55.13	57.57	55.38	52.19	48.16	25.23
1550	62.32	54.73	54.63	51.62	46.17	23.82
1600	56.84	59.15	54.70	54.68	45.72	22.32
1650	46.97	58.77	54.42	50.96	44.90	21.52
1700	52.14	57.29	53.17	49.22	42.47	20.37
1750	58.14	52.87	55.38	49.41	41.44	18.77
1800	58.68	54.63	54.07	47.65	40.87	20.77
1850	58.77	50.38	52.66	46.99	40.66	17.50
1900	50.07	52.00	50.09	45.86	38.52	19.47
1950	51.86	53.29	49.76	45.62	38.43	17.29
2000	54.47	48.61	47.95	43.13	35.94	17.43
2050	51.03	45.77	50.38	44.75	36.03	17.29
2100	54.54	46.35	47.69	44.35	33.98	15.45
2150	52.21	48.56	44.78	43.37	33.80	17.22
2200	47.25	44.97	48.07	41.53	32.69	15.87
2250	45.34	40.78	44.54	39.49	31.11	17.22
2300	49.13	47.27	43.41	40.38	29.16	17.05
2350	48.66	46.07	44.24	37.86	28.08	17.43
2400	40.36	44.59	41.44	40.92	27.23	16.25
2450	45.32	36.92	41.13	37.91	24.93	16.32
2500	48.80	40.73	43.25	37.09	26.08	16.25

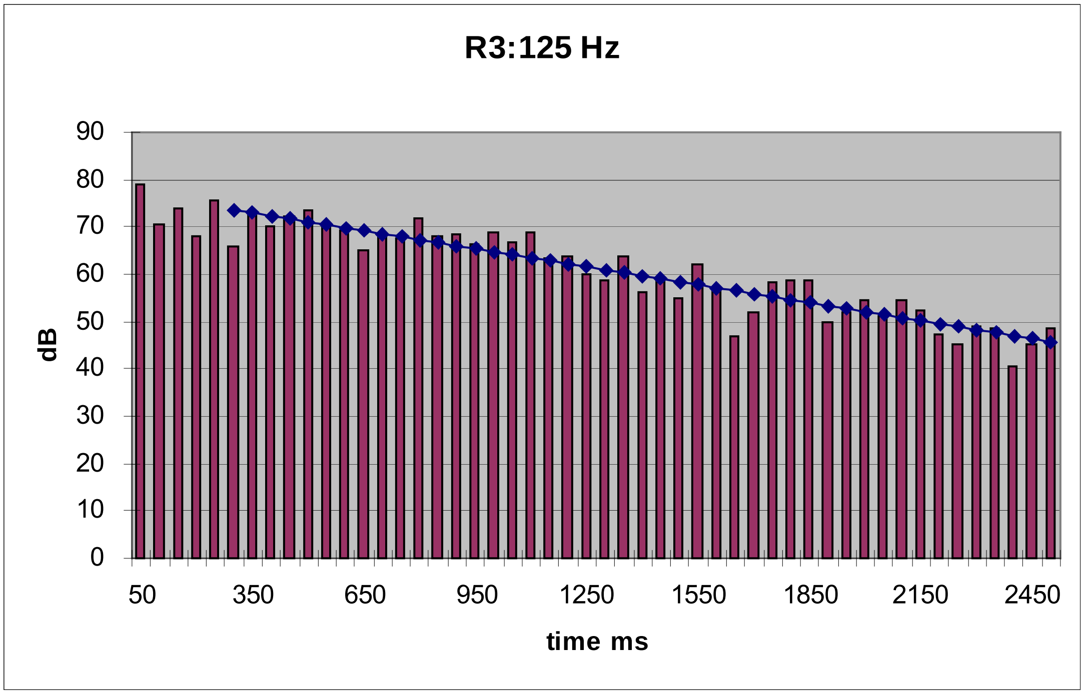

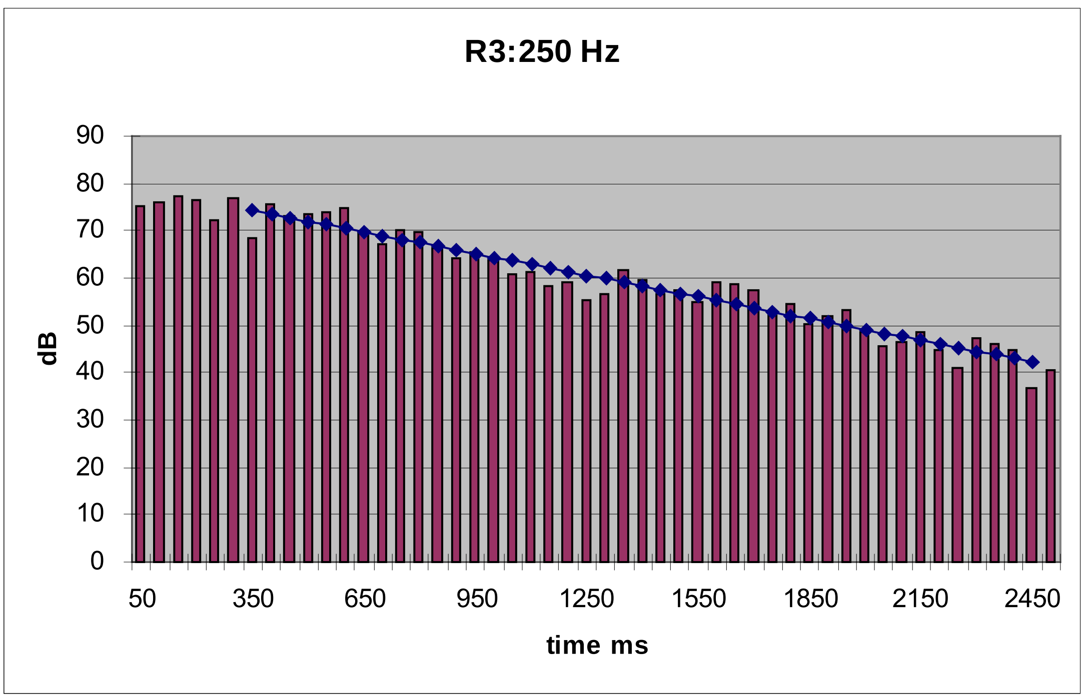

Figure A.7 Decay and Fit for T30 for 125 and 250 Hz at R3 in C.A.P.

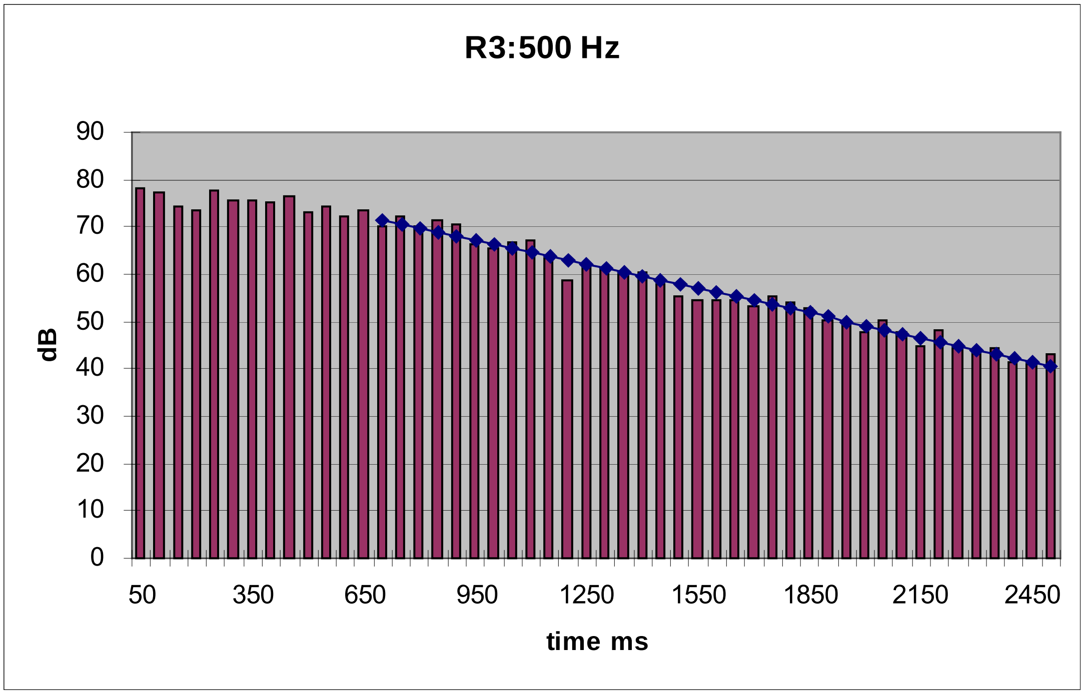

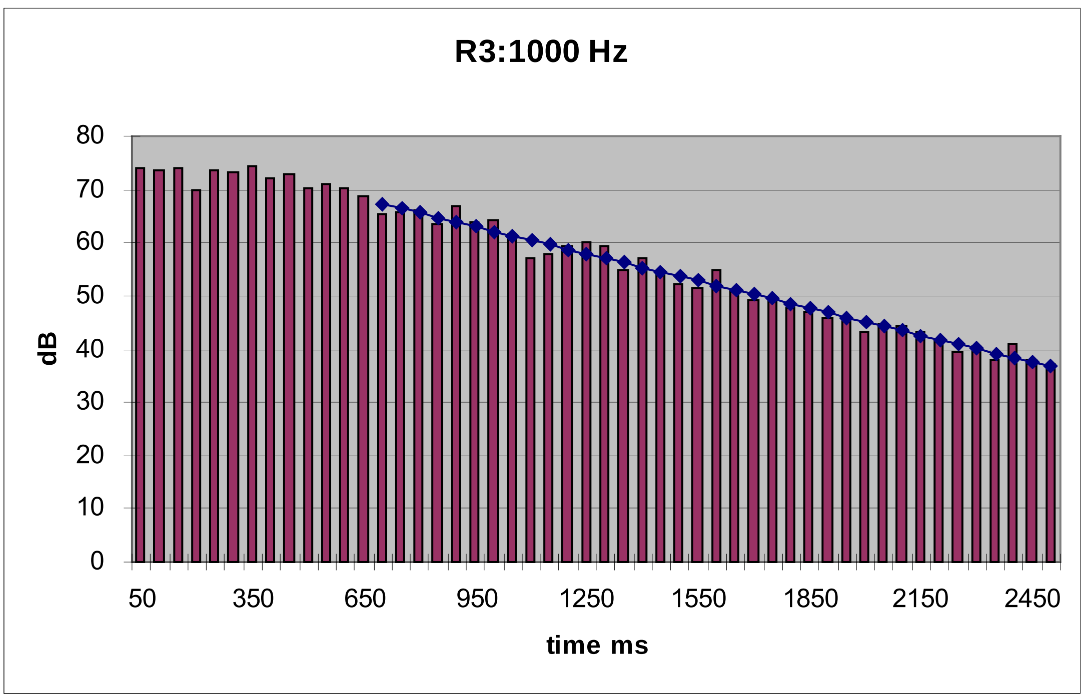

Figure A.8 Decay and Fit for T30 for 500 and 1000 Hz at R3 in C.A.P.

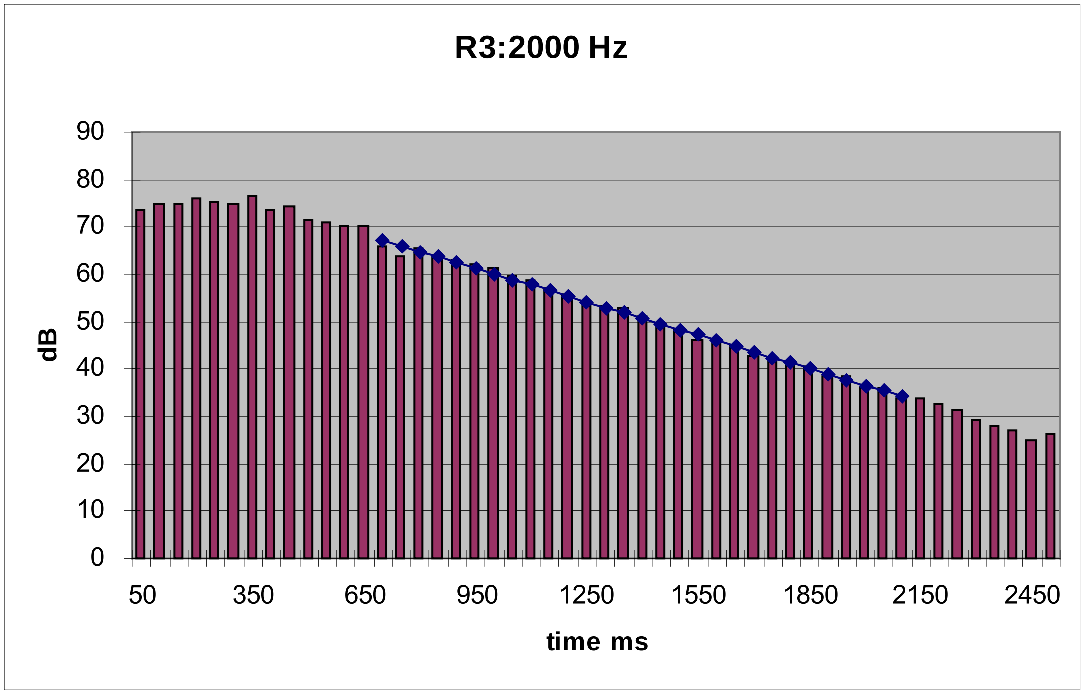

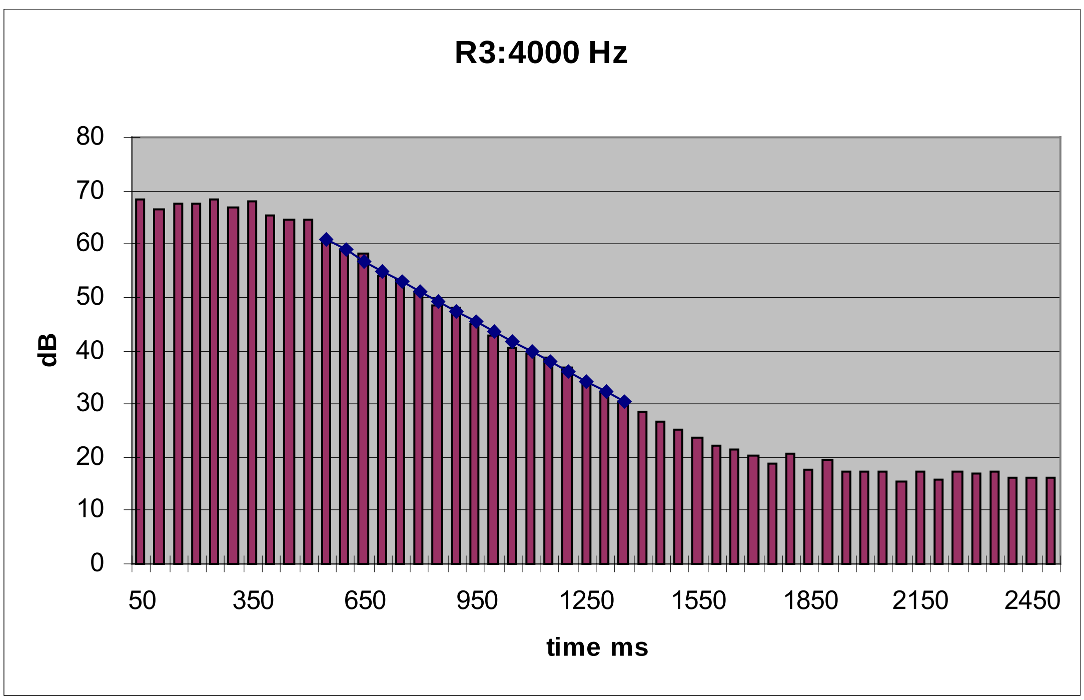

Figure A.9 Decay and Fit for T30 for 2 and 4 kHz at R3 in C.A.P.

Table A.4 Measurements at R4 in C.A.P.

time	dB					
ms	125	250	500	1000	2000	4000
50	76.36	72.95	76.08	74.41	76.50	69.21
100	75.21	74.83	76.81	72.39	76.81	70.55
150	80.97	78.41	79.80	70.84	74.22	70.74
200	78.57	71.38	79.70	75.19	73.33	68.67
250	77.56	77.42	78.57	73.00	74.90	69.66
300	75.12	73.21	76.39	72.74	75.14	69.64
350	76.93	73.42	80.01	72.79	74.03	69.92
400	78.06	72.55	78.55	73.31	73.23	65.69
450	72.34	74.06	73.02	72.51	72.11	65.33
500	66.30	73.42	75.94	70.84	72.39	63.36
550	71.82	68.88	71.80	69.03	69.59	61.59
600	70.32	69.97	74.15	71.68	70.18	57.50
650	75.09	65.54	74.79	69.14	67.92	57.29
700	70.91	66.41	71.40	66.77	66.20	54.98
750	68.63	67.10	67.97	66.11	65.36	53.50
800	71.12	68.77	72.79	65.05	62.60	51.41
850	65.43	66.63	67.57	63.57	62.30	49.74
900	70.20	65.14	66.51	64.91	63.26	46.02
950	63.64	63.10	65.59	63.99	61.08	44.61
1000	69.28	62.91	64.09	60.77	60.65	42.92
1050	68.11	62.44	64.72	61.90	57.24	41.37
1100	62.35	64.72	63.85	59.71	58.58	39.35
1150	66.41	61.24	65.69	58.91	57.52	37.30
1200	67.24	62.46	65.92	57.67	55.60	35.72
1250	67.00	63.08	63.24	54.91	54.75	33.56
1300	61.48	56.98	62.30	56.28	52.84	32.95
1350	58.63	58.79	60.02	56.37	50.45	29.40
1400	65.19	56.23	56.42	53.43	49.67	27.33
1450	62.96	58.54	58.02	54.30	50.21	27.52
1500	59.29	54.89	59.71	54.30	47.67	25.02
1550	59.90	57.41	53.95	52.05	46.71	23.96
1600	54.40	51.01	55.36	52.92	47.67	21.90
1650	62.09	55.22	55.83	51.36	43.58	23.35
1700	49.25	54.73	56.33	49.03	42.33	27.75
1750	55.03	49.79	52.45	50.47	41.30	26.03
1800	55.53	50.28	52.37	46.85	39.79	24.76
1850	54.19	52.16	52.68	45.60	40.22	22.39
1900	55.57	50.09	51.53	47.22	39.30	21.17
1950	51.57	47.08	49.18	46.00	38.31	21.40
2000	52.77	49.53	50.07	45.55	36.69	20.74
2050	55.55	47.69	50.87	42.64	35.68	20.18
2100	53.88	49.91	46.21	42.07	35.28	21.97
2150	53.76	52.26	48.56	41.79	32.50	21.03
2200	52.61	48.21	48.16	42.07	33.07	21.12
2250	43.70	48.89	43.44	38.52	32.29	23.14
2300	51.62	41.89	39.53	40.90	30.64	21.57
2350	48.16	46.02	45.25	39.35	29.16	21.52
2400	54.35	39.32	44.99	36.95	31.07	26.03
2450	52.42	48.07	41.25	36.76	30.60	25.23
2500	45.98	48.56	40.17	36.99	28.08	21.99

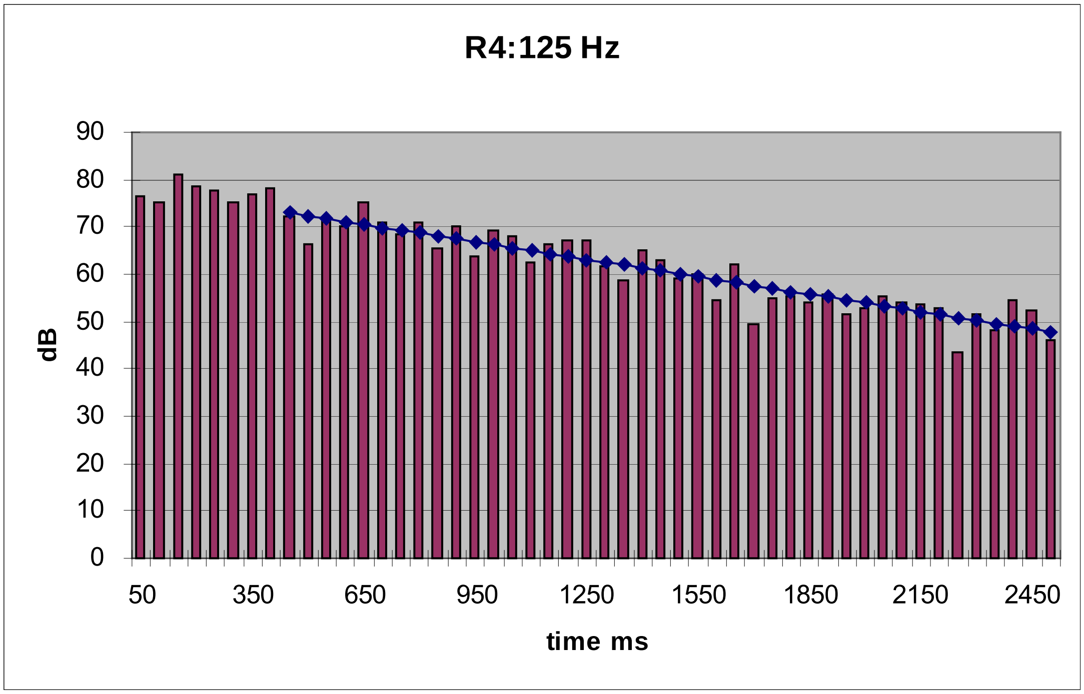

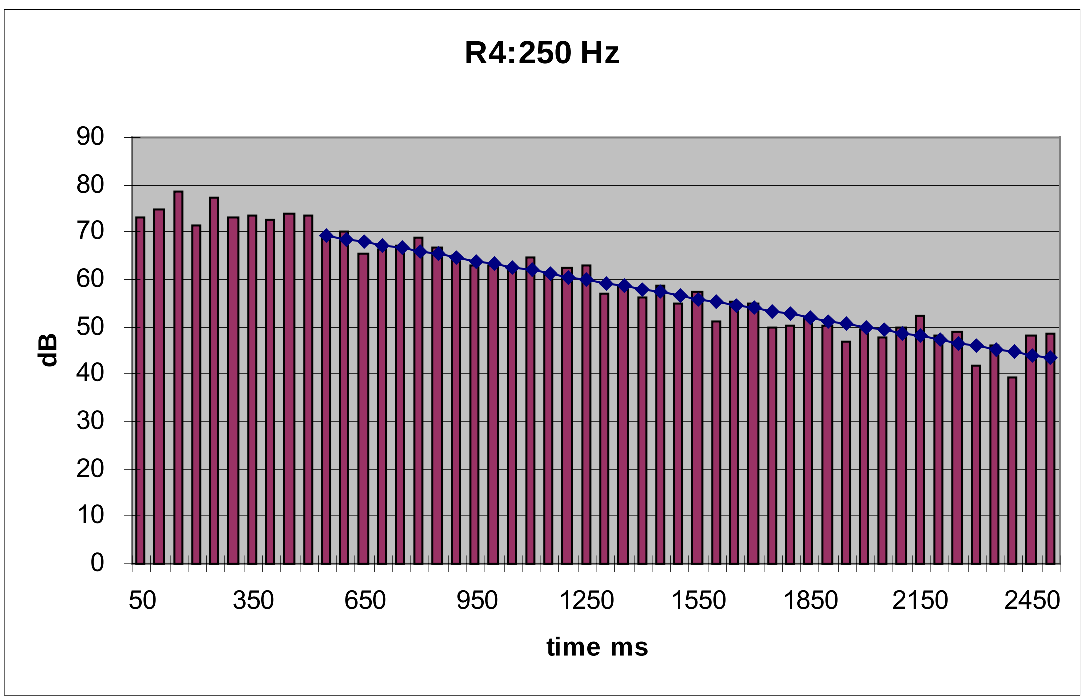

Figure A.10 Decay and Fit for T30 for 125 and 250 Hz at R4 in C.A.P.

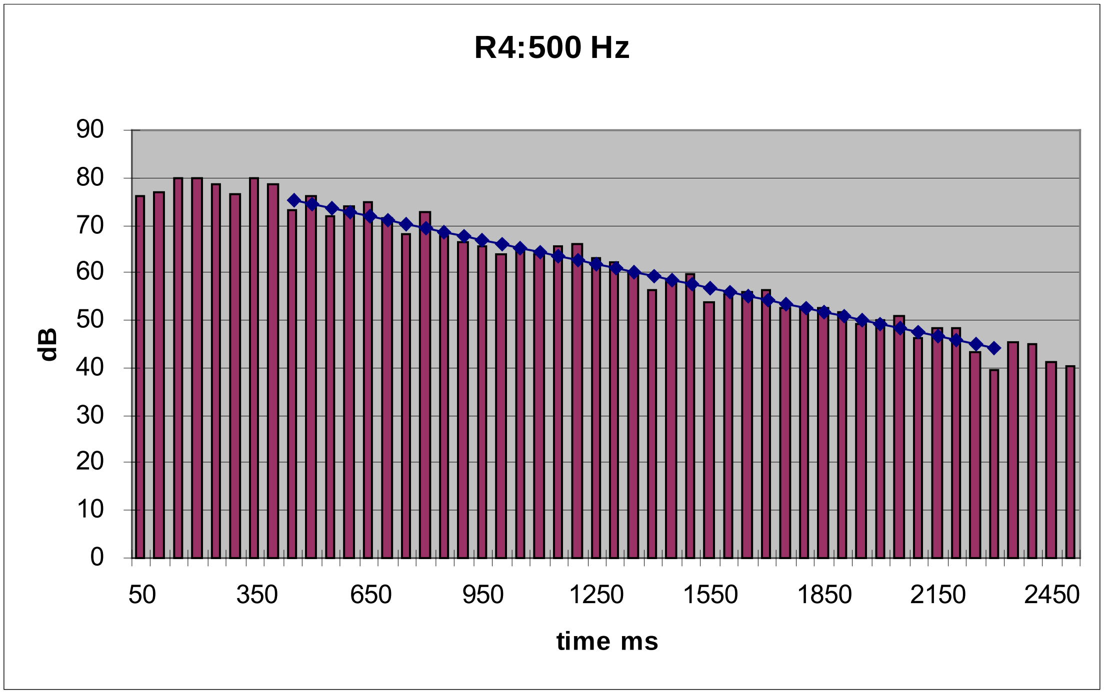

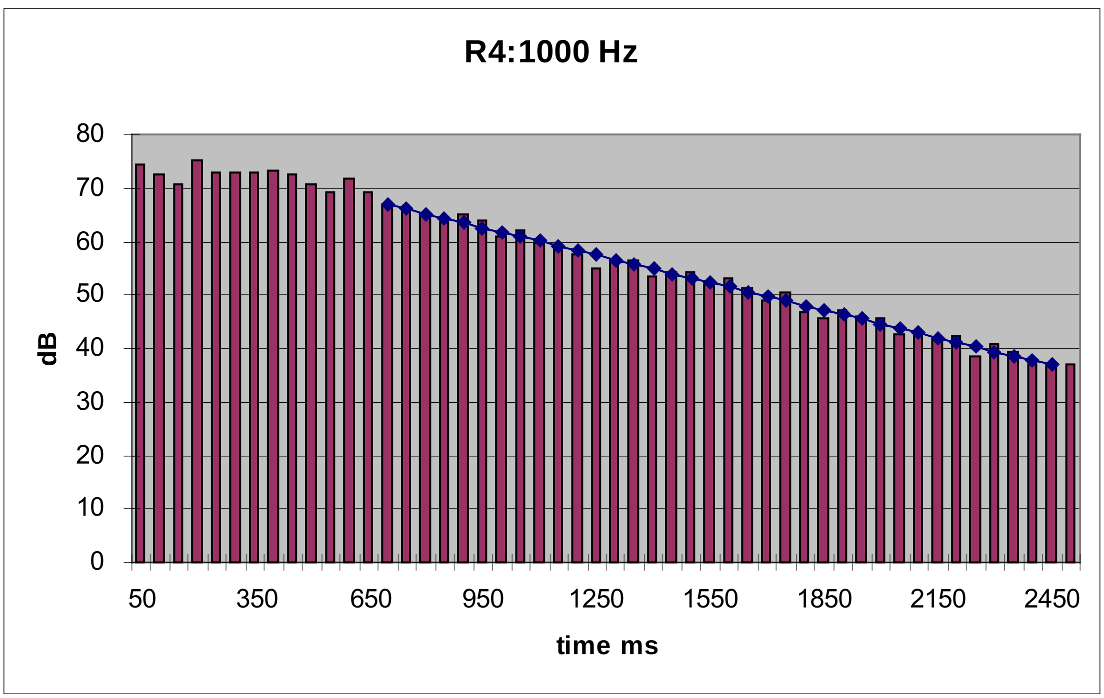

Figure A.11 Decay and Fit for T30 for 500 and 1000 Hz at R4 in C.A.P.

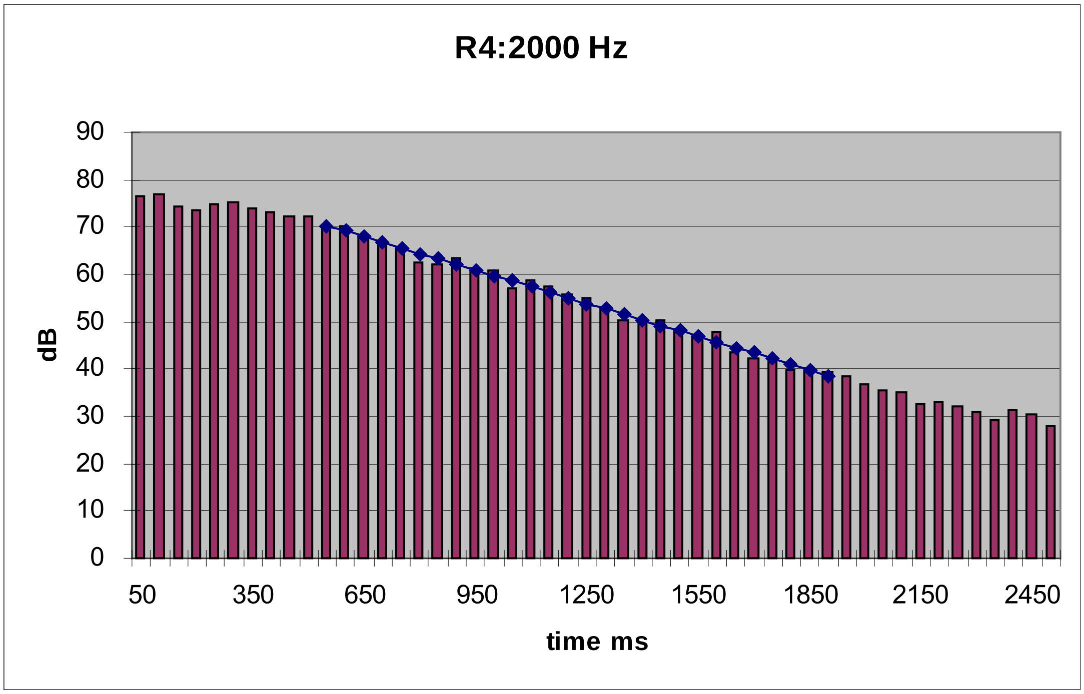

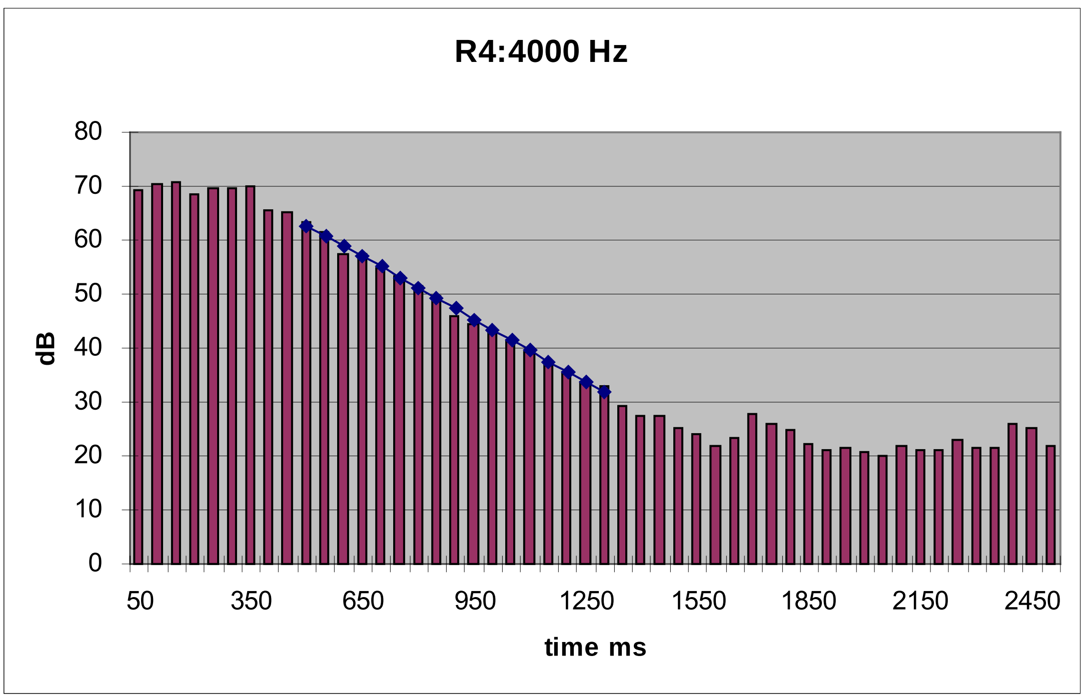

Figure A.12 Decay and Fit for T30 for 2 and 4 kHz at R4 in C.A.P.

Table A.5 Measurements at R1S2 in C.A.P.

time	dB					
ms	125	250	500	1000	2000	4000
50	77.09	76.06	75.14	71.99	71.42	63.92
100	74.79	75.00	72.58	72.72	72.67	66.39
150	71.12	72.95	72.74	71.73	73.07	64.86
200	69.10	70.72	72.04	73.89	73.52	65.50
250	72.44	75.07	70.72	72.84	72.48	64.70
300	71.47	75.38	75.54	71.38	73.38	65.83
350	69.45	73.68	73.07	72.06	72.46	64.39
400	70.72	67.83	73.92	70.81	70.13	61.78
450	75.19	75.61	69.35	69.64	70.60	60.32
500	77.82	71.12	70.25	69.66	68.81	58.42
550	76.46	72.67	70.86	68.20	67.92	56.51
600	78.31	72.86	68.91	68.11	65.59	54.21
650	74.95	65.71	68.98	67.87	65.07	51.57
700	71.40	68.53	68.60	66.49	64.49	51.18
750	70.69	69.75	69.43	65.17	62.68	48.42
800	74.74	64.65	68.55	63.43	61.76	46.89
850	71.57	65.85	65.69	61.38	58.42	46.59
900	66.44	67.97	64.04	62.53	57.08	42.69
950	66.30	68.06	65.80	60.35	56.68	41.53
1000	69.59	65.83	65.07	60.70	56.51	38.97
1050	66.06	59.99	63.03	59.43	55.69	37.46
1100	69.90	62.25	60.39	57.92	52.56	34.41
1150	70.91	64.35	56.70	55.57	51.62	34.15
1200	70.72	59.34	59.83	54.56	51.08	31.96
1250	65.83	58.75	59.43	55.67	49.86	28.43
1300	65.17	60.14	56.73	53.57	48.66	26.48
1350	64.06	58.61	55.34	55.50	49.13	26.43
1400	62.37	57.27	57.45	56.58	46.57	26.43
1450	65.76	59.19	54.68	54.07	46.82	23.45
1500	68.34	55.41	55.01	53.29	46.17	23.09
1550	63.33	57.97	52.96	48.05	42.14	20.55
1600	59.19	56.73	55.60	49.74	41.86	18.63
1650	56.02	49.01	53.36	49.41	38.50	20.23
1700	51.67	57.48	48.73	50.26	38.24	18.30
1750	54.87	56.40	52.99	45.01	38.17	19.12
1800	53.93	54.73	51.36	47.18	37.35	18.46
1850	61.78	55.15	48.09	45.58	35.28	18.25
1900	54.61	47.65	47.74	44.19	33.58	18.06
1950	46.99	50.78	47.95	43.51	33.42	17.14
2000	55.41	53.53	44.33	43.53	32.36	17.83
2050	55.08	51.43	42.64	41.09	31.30	17.36
2100	54.11	50.87	46.73	41.67	30.36	16.32
2150	52.68	51.55	45.88	41.02	28.50	16.16
2200	54.51	48.14	44.85	38.76	28.22	18.13
2250	49.48	49.20	43.74	37.42	27.37	16.16
2300	51.83	50.28	40.38	40.07	27.12	17.22
2350	51.76	50.99	39.86	36.69	24.04	17.36
2400	54.37	48.49	41.16	35.72	24.32	17.50
2450	50.21	47.91	34.81	36.24	24.04	17.22
2500	49.08	44.19	37.46	33.63	23.52	16.98

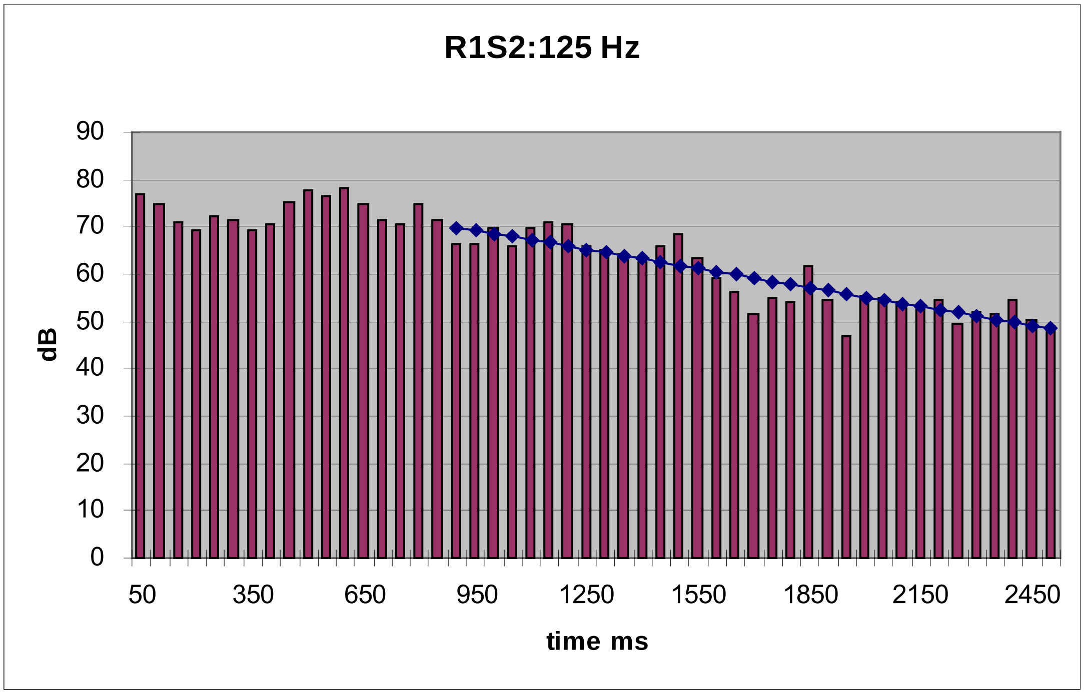

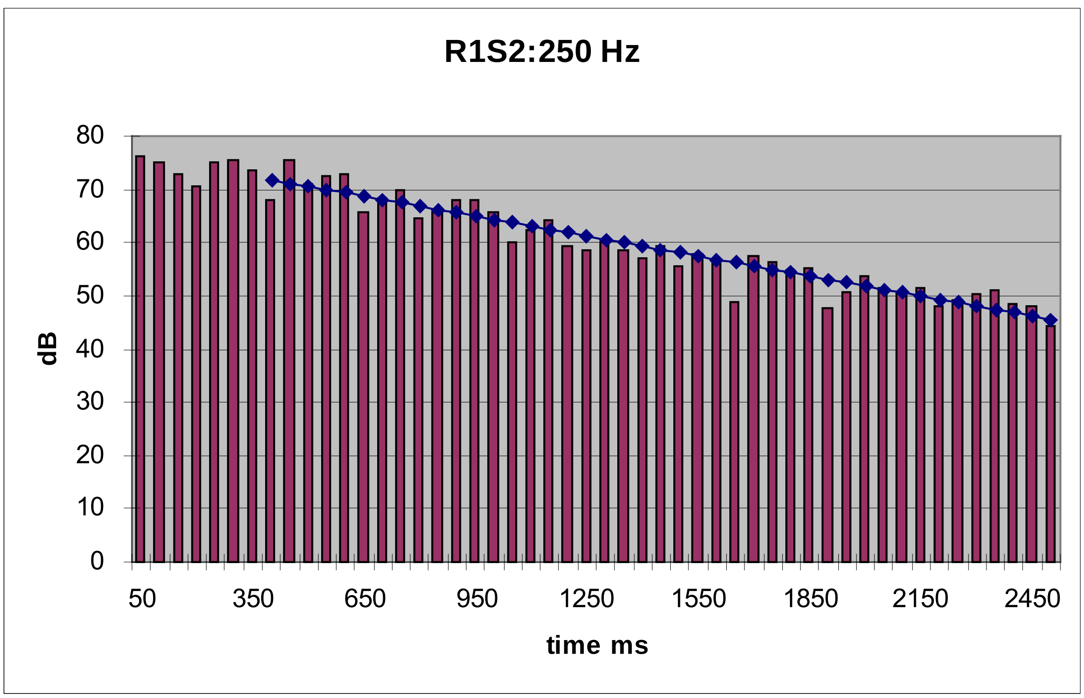

Figure A.13 Decay and Fit for T30 for 125 and 250 Hz at R1S2 in C.A.P.

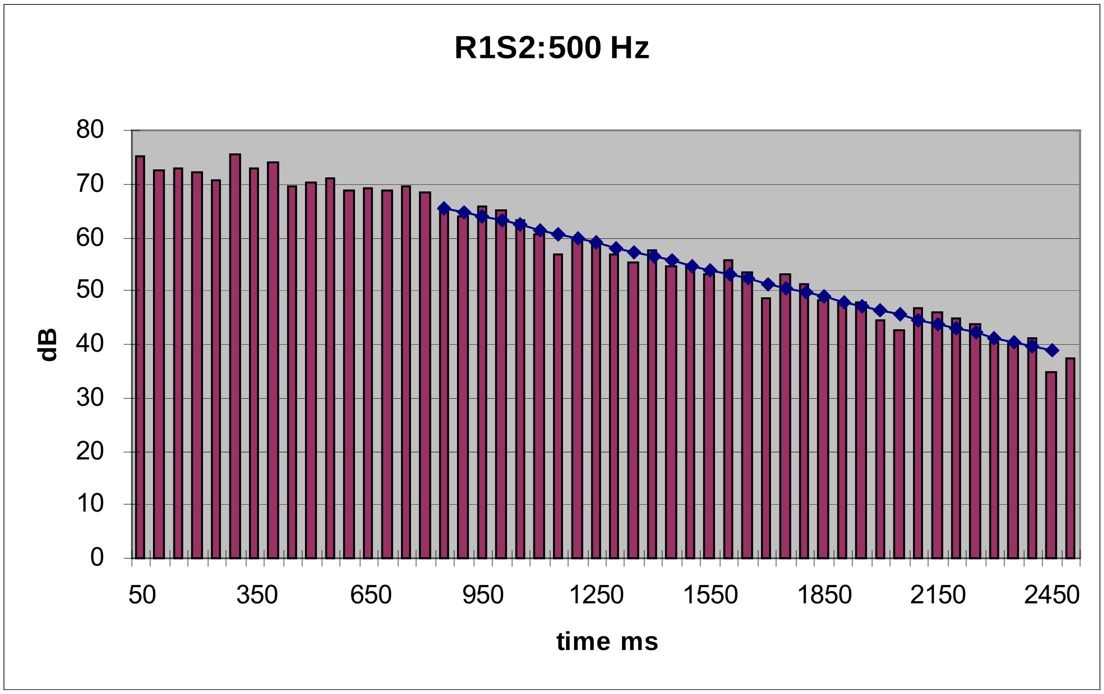

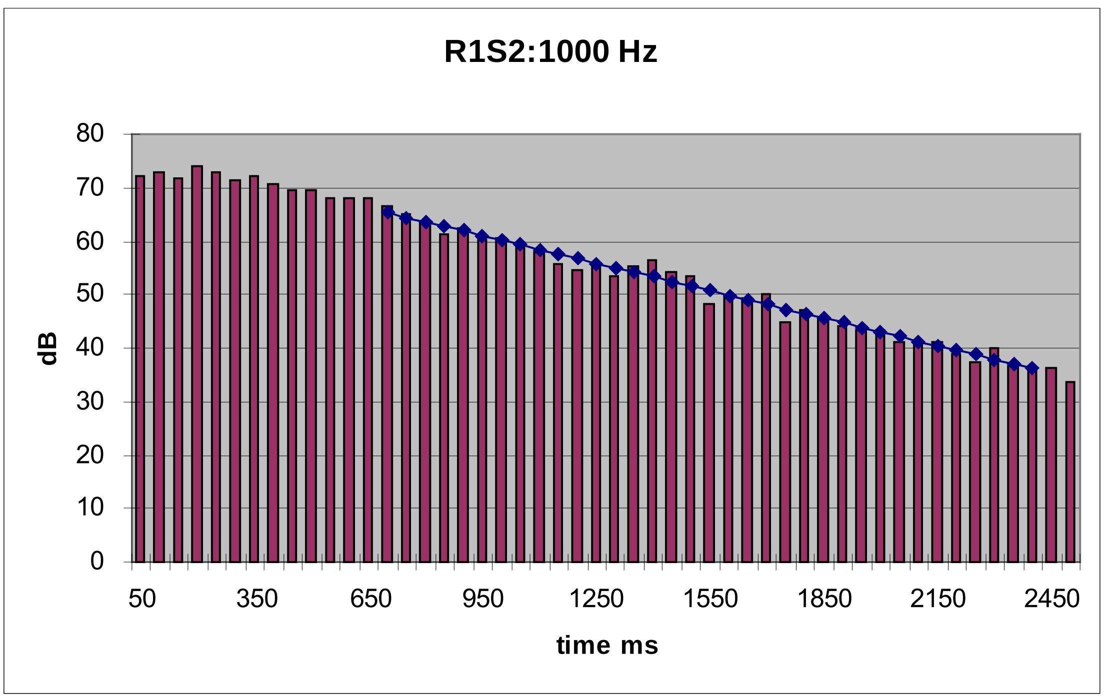

Figure A.14 Decay and Fit for T30 for 500 and 1000 Hz at R1S2 in C.A.P.

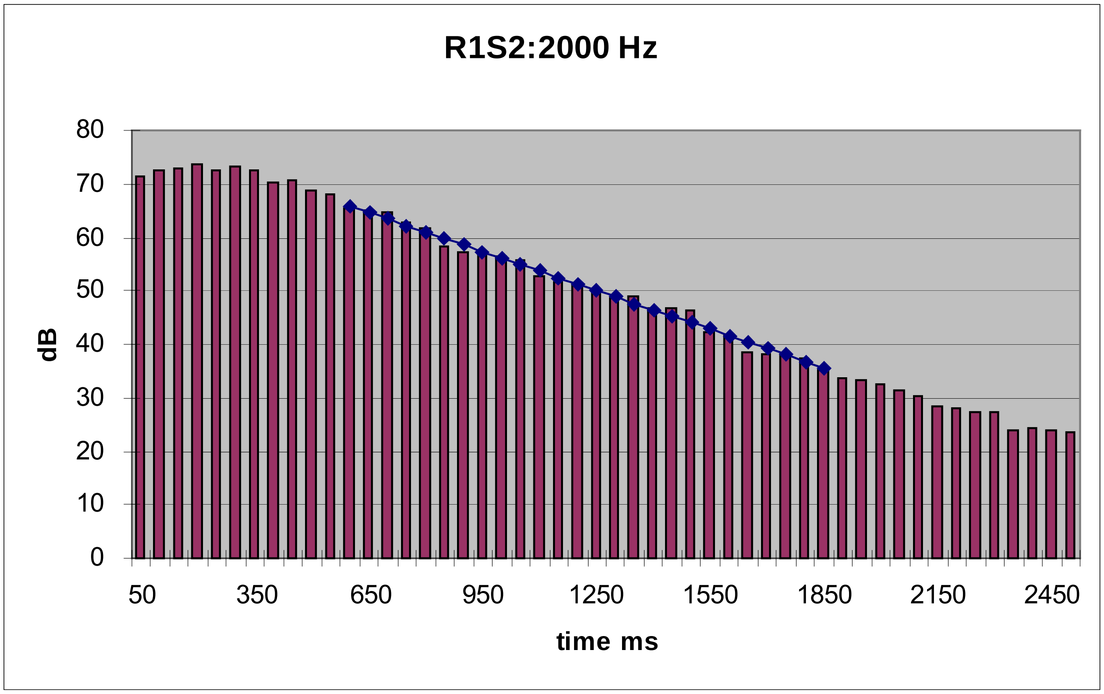

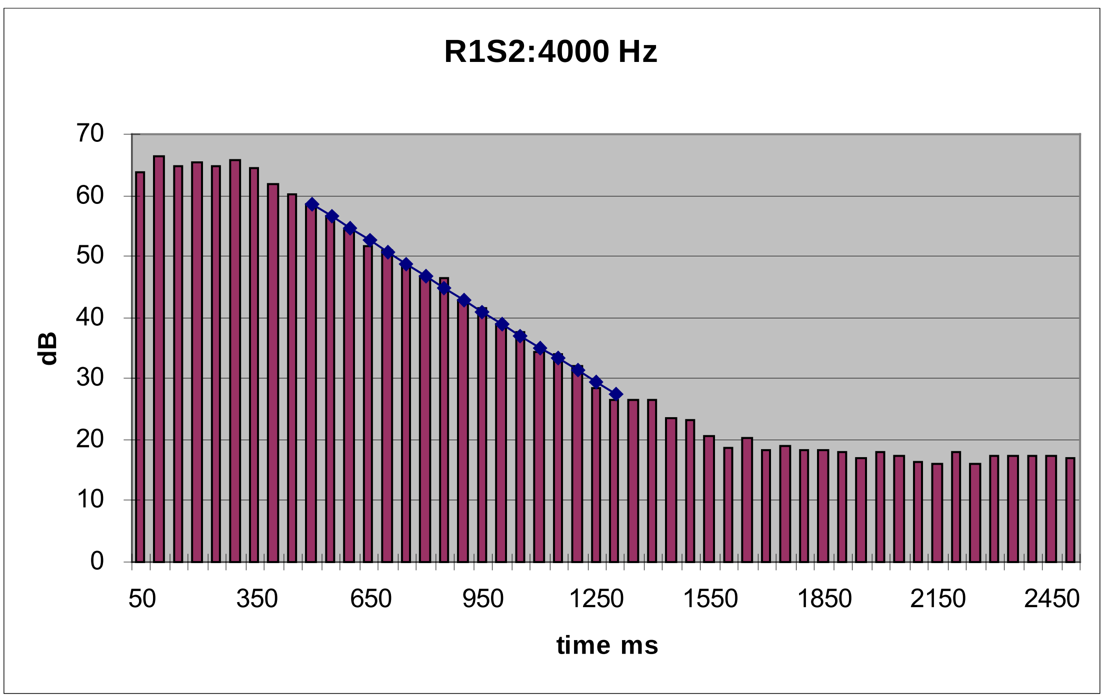

Figure A.15 Decay and Fit for T30 for 2 and 4 kHz at R1S2 in C.A.P.

Table A.6 Measurements at R2S2 in C.A.P.

time	dB					
ms	125	250	500	1000	2000	4000
50	73.68	71.61	77.35	71.68	72.22	63.50
100	70.39	74.15	73.82	71.89	72.08	63.31
150	71.96	78.24	73.75	71.80	71.05	65.24
200	75.16	73.07	72.55	70.44	71.68	62.65
250	76.06	68.44	70.41	71.42	72.04	64.77
300	73.05	74.53	74.48	70.48	72.81	62.30
350	70.30	75.61	73.87	72.58	70.74	63.83
400	68.79	73.96	75.02	69.85	70.44	62.91
450	70.98	68.84	72.76	70.11	70.15	60.49
500	72.46	70.55	70.86	69.59	68.27	58.91
550	75.61	72.06	73.38	68.27	68.46	57.36
600	67.85	74.25	68.93	68.39	64.56	54.91
650	69.45	70.34	69.10	67.05	64.70	54.02
700	70.44	73.42	69.92	66.13	63.71	50.87
750	69.28	69.40	66.65	64.35	63.62	49.46
800	68.55	63.64	66.23	62.96	63.66	47.01
850	64.96	63.40	68.88	62.09	59.52	44.38
900	66.49	65.38	63.90	61.95	56.18	43.65
950	62.84	69.92	65.52	58.63	57.15	40.92
1000	67.00	67.17	64.74	60.49	56.87	39.42
1050	57.27	65.05	64.32	58.82	54.94	36.90
1100	60.58	66.89	64.70	59.81	52.23	35.82
1150	64.18	63.92	62.89	57.71	52.19	32.64
1200	54.40	59.92	59.31	56.73	52.42	30.24
1250	60.28	62.21	59.57	55.08	50.21	29.12
1300	60.58	67.64	58.98	54.40	49.32	29.23
1350	58.89	62.44	57.71	53.88	45.95	26.03
1400	61.52	59.99	57.29	53.50	47.81	24.58
1450	64.44	62.58	55.29	50.33	45.23	23.40
1500	63.43	58.51	53.67	51.08	43.11	21.94
1550	54.33	55.97	51.76	51.10	42.94	20.46
1600	61.26	56.98	53.01	51.08	42.14	20.86
1650	56.75	55.08	48.02	49.93	41.72	19.85
1700	57.41	53.97	49.36	50.05	39.06	19.52
1750	56.49	57.95	49.48	47.76	38.29	18.98
1800	45.37	53.86	48.73	45.67	36.05	19.52
1850	54.89	55.76	47.74	46.50	34.57	17.71
1900	55.48	55.38	49.13	46.28	33.77	19.17
1950	52.09	51.10	48.12	43.20	33.40	16.25
2000	52.28	47.11	46.73	43.56	31.61	17.57
2050	46.64	48.21	44.73	41.53	30.83	18.88
2100	54.19	51.25	44.35	42.64	29.44	16.74
2150	55.57	47.93	44.83	41.53	27.07	17.57
2200	53.24	49.22	41.49	39.42	26.81	16.42
2250	55.53	47.06	41.93	37.77	25.82	18.63
2300	54.19	41.74	41.89	34.76	24.95	17.64
2350	54.23	47.91	41.30	36.22	23.56	17.43
2400	51.32	46.26	37.58	36.57	23.45	17.71
2450	50.21	44.85	40.24	33.23	22.98	16.98
2500	46.75	45.48	37.09	35.51	22.37	16.98

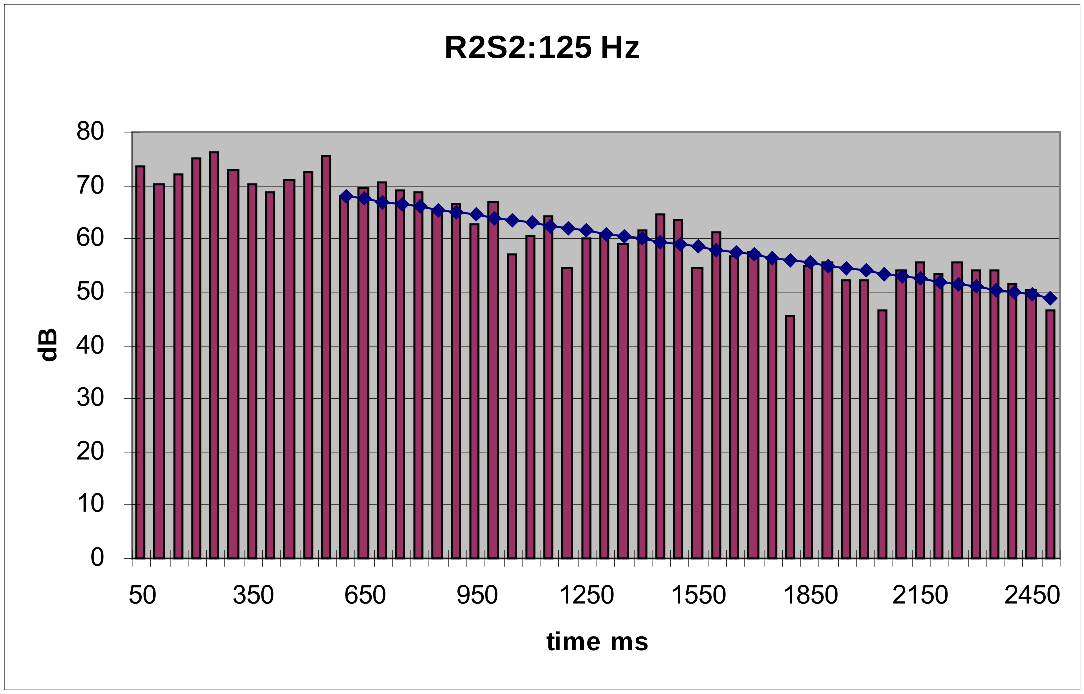

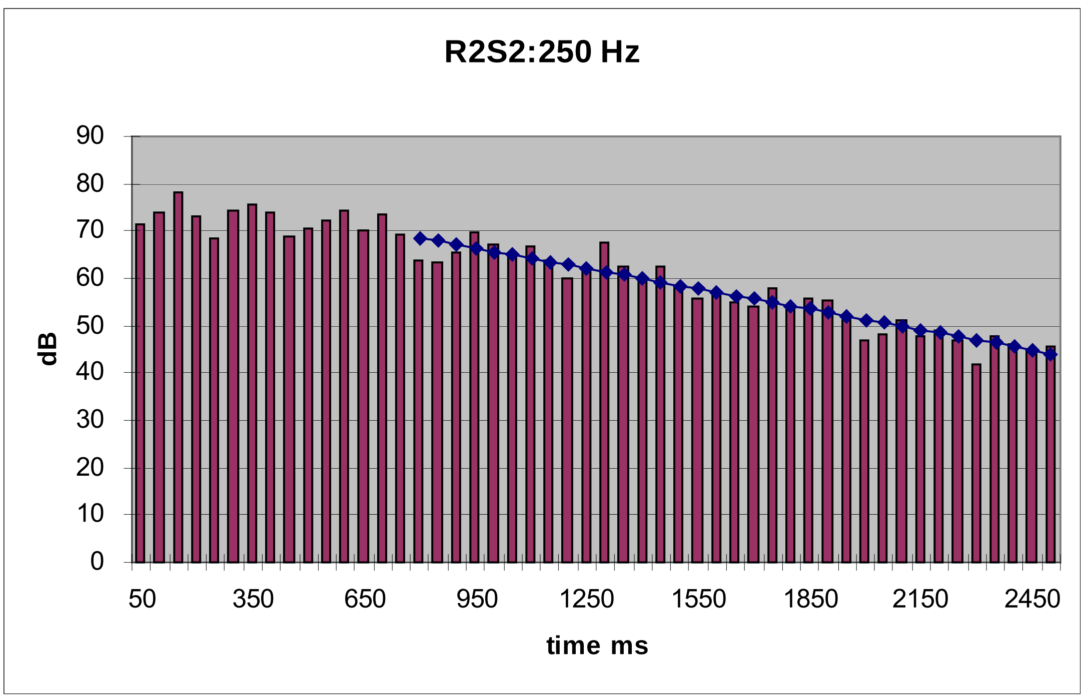

Figure A.16 Decay and Fit for T30 for 125 and 250 Hz at R2S2 in C.A.P.

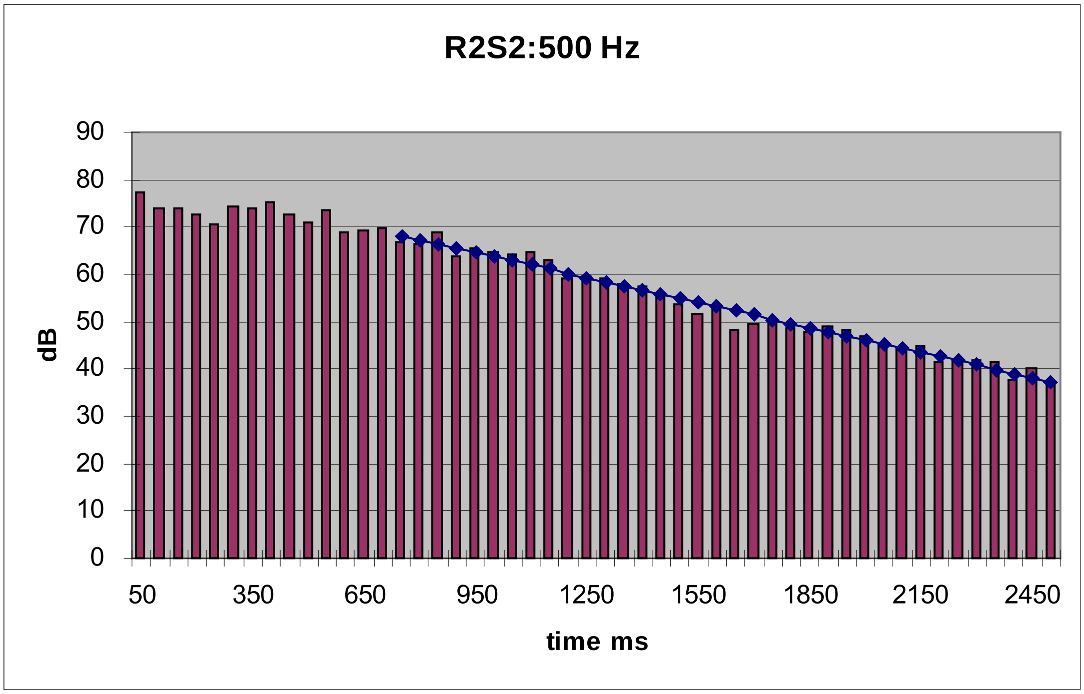

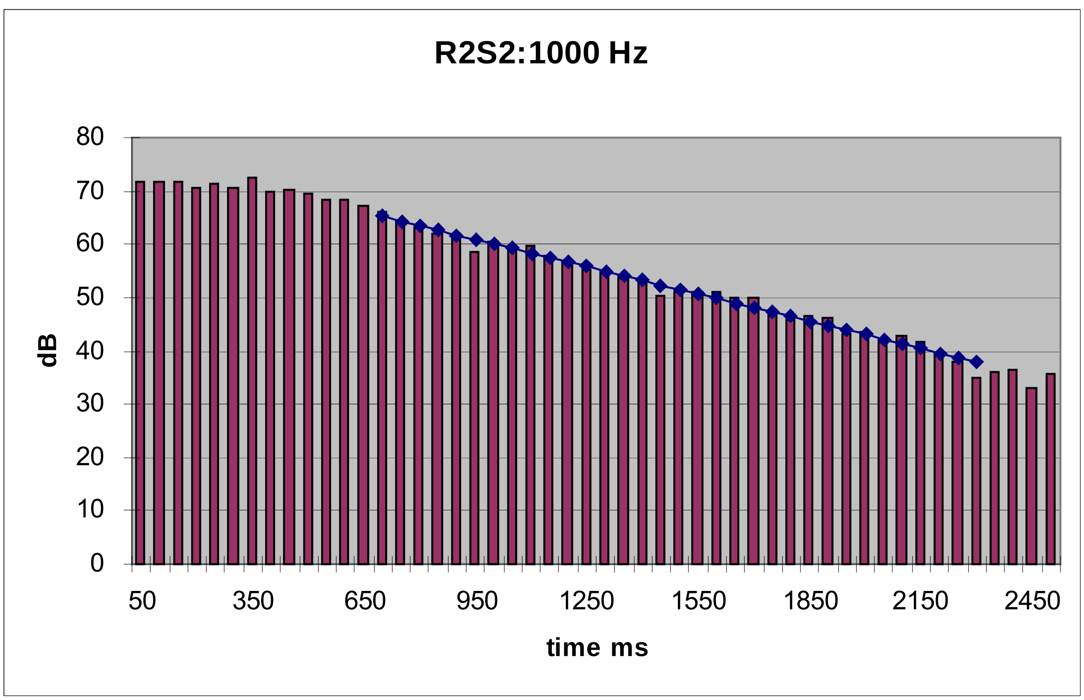

Figure A.17 Decay and Fit for T30 for 500 and 1000 Hz at R2S2 in C.A.P.

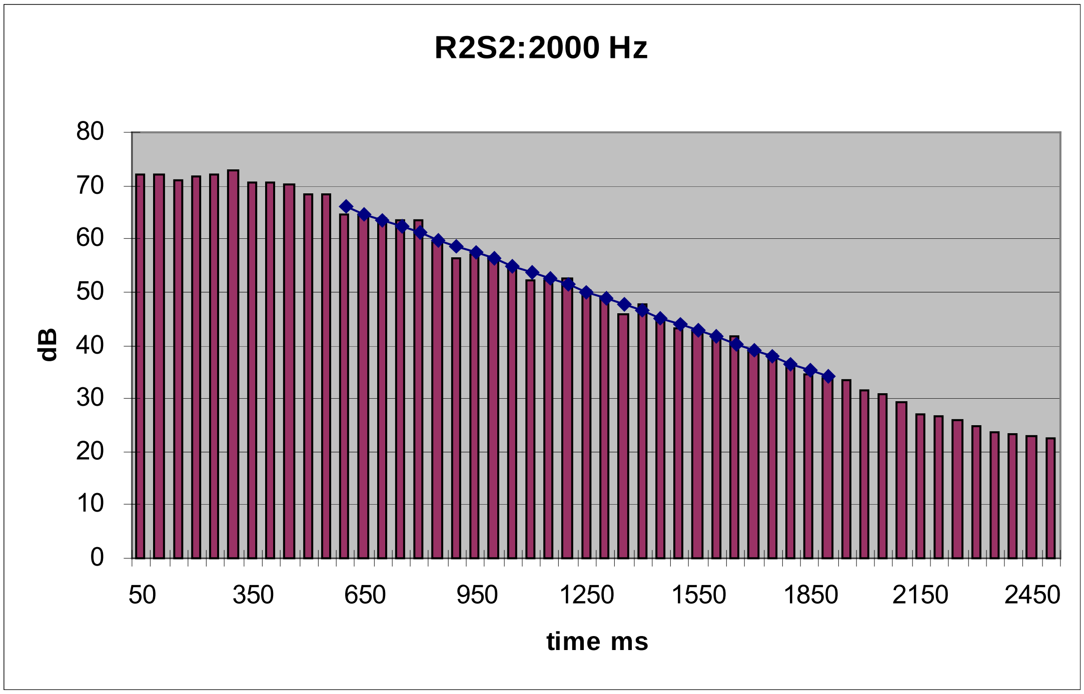

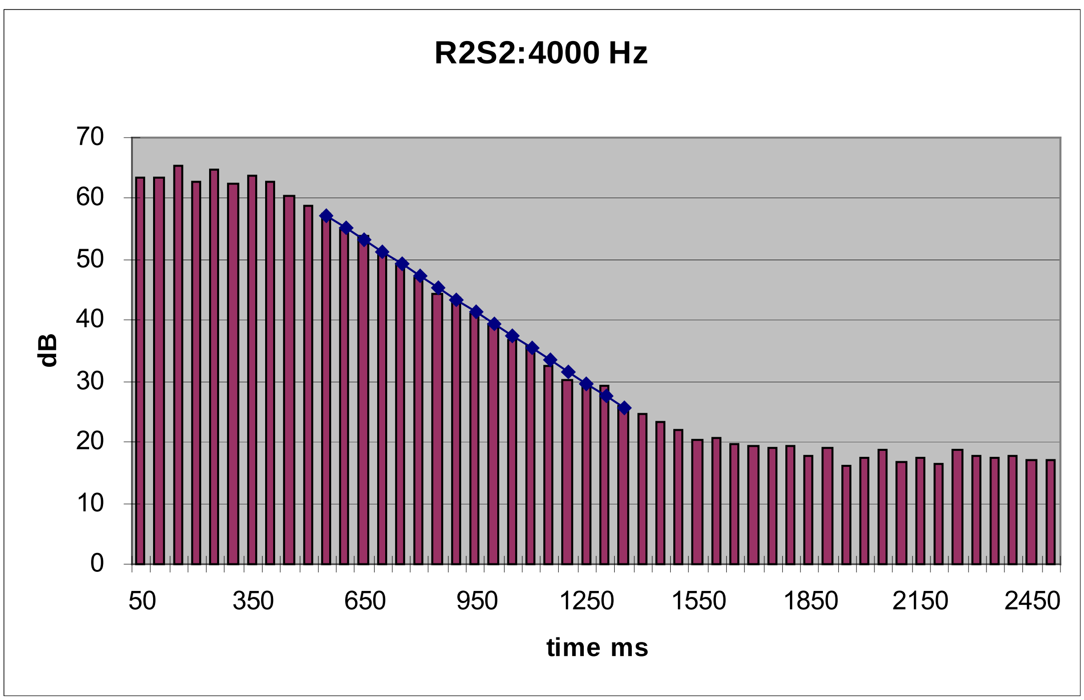

Figure A.18 Decay and Fit for T30 for 2 and 4 kHz at R2S2 in C.A.P.

Table A.7 Measurements at R3S2 in C.A.P.

time	dB					
ms	**125**	**250**	**500**	**1000**	**2000**	**4000**
50	79.30	77.75	73.63	68.48	73.47	63.78
100	76.69	74.43	75.00	69.57	72.84	63.99
150	72.34	73.35	74.74	69.75	71.94	64.16
200	72.98	73.80	75.23	72.22	71.94	63.12
250	71.21	73.52	74.98	69.19	72.39	63.47
300	70.67	76.95	75.00	71.87	70.74	63.55
350	73.33	73.75	78.20	71.28	70.67	62.44
400	72.48	78.71	73.68	69.97	71.31	62.98
450	72.06	69.00	73.02	67.19	70.62	60.84
500	73.35	71.73	73.31	69.35	69.28	58.61
550	71.45	70.62	70.46	67.40	66.30	58.14
600	71.14	72.36	71.75	65.97	65.57	56.02
650	72.60	68.44	68.98	67.47	64.32	52.56
700	70.74	67.43	66.25	65.54	64.96	50.21
750	68.84	67.00	62.06	60.42	62.82	49.15
800	70.06	67.38	63.57	63.76	61.78	48.31
850	71.92	63.62	66.77	63.64	57.69	44.10
900	60.25	65.90	59.36	59.83	57.74	43.39
950	65.85	65.14	60.94	60.77	56.58	39.96
1000	70.51	65.38	63.62	60.21	55.74	39.20
1050	62.46	61.43	63.05	58.40	54.70	37.18
1100	64.77	63.50	63.71	59.52	53.20	34.97
1150	68.32	61.33	58.14	57.38	51.79	33.30
1200	62.89	65.26	56.98	55.43	52.35	30.74
1250	68.95	60.70	58.35	55.76	50.68	29.84
1300	62.46	54.28	60.28	55.71	48.94	27.77
1350	60.56	57.74	57.27	51.22	48.73	25.00
1400	62.96	58.00	56.84	52.42	46.66	24.41
1450	57.50	56.49	54.47	53.83	46.28	23.75
1500	51.74	60.94	52.16	50.75	44.03	23.31
1550	54.96	54.96	55.03	51.20	43.53	20.95
1600	58.25	56.73	55.38	47.41	42.19	19.97
1650	57.08	60.42	54.30	46.26	40.78	19.57
1700	63.45	57.13	53.69	44.14	37.49	18.46
1750	57.57	51.95	52.23	43.06	37.37	18.63
1800	48.87	53.24	51.06	45.37	34.81	17.57
1850	45.93	53.29	49.48	45.23	35.91	16.42
1900	53.48	49.67	48.49	45.27	34.45	18.01
1950	56.96	53.08	45.60	45.25	33.04	16.58
2000	50.78	52.37	44.40	41.49	33.89	16.84
2050	55.48	52.82	43.25	41.06	32.41	17.83
2100	49.55	46.75	44.47	41.67	30.46	17.76
2150	51.95	47.55	40.80	40.50	29.47	17.50
2200	54.21	48.85	40.45	38.85	28.64	17.14
2250	50.40	50.45	44.19	37.13	27.30	17.36
2300	52.14	47.55	40.10	36.76	26.46	16.42
2350	49.08	46.66	41.20	36.57	25.68	14.75
2400	51.86	46.80	40.64	36.48	24.60	17.83
2450	55.78	45.84	40.71	34.36	22.62	17.43
2500	48.85	39.79	38.05	35.25	21.85	16.98

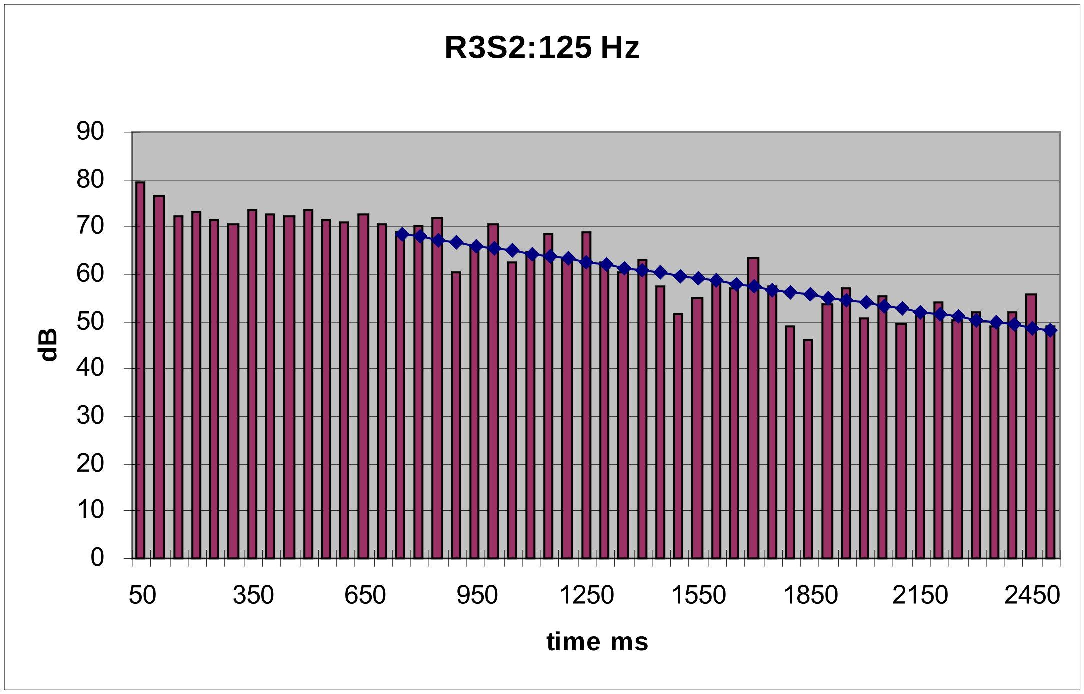

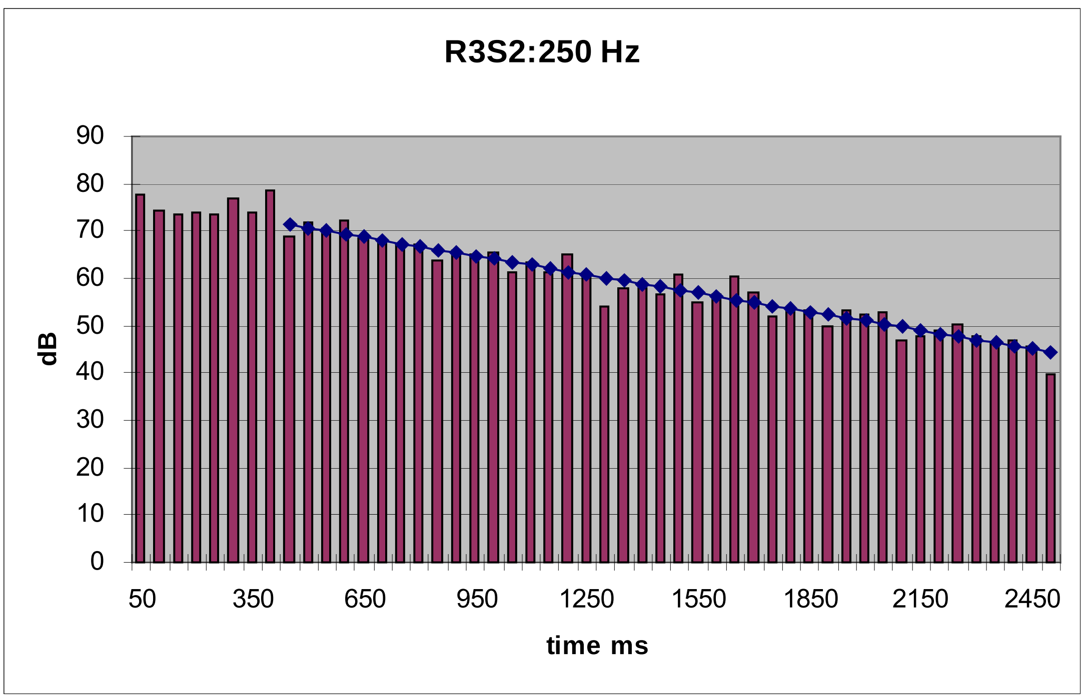

Figure A.19 Decay and Fit for T30 for 125 and 250 Hz at R3S2 in C.A.P.

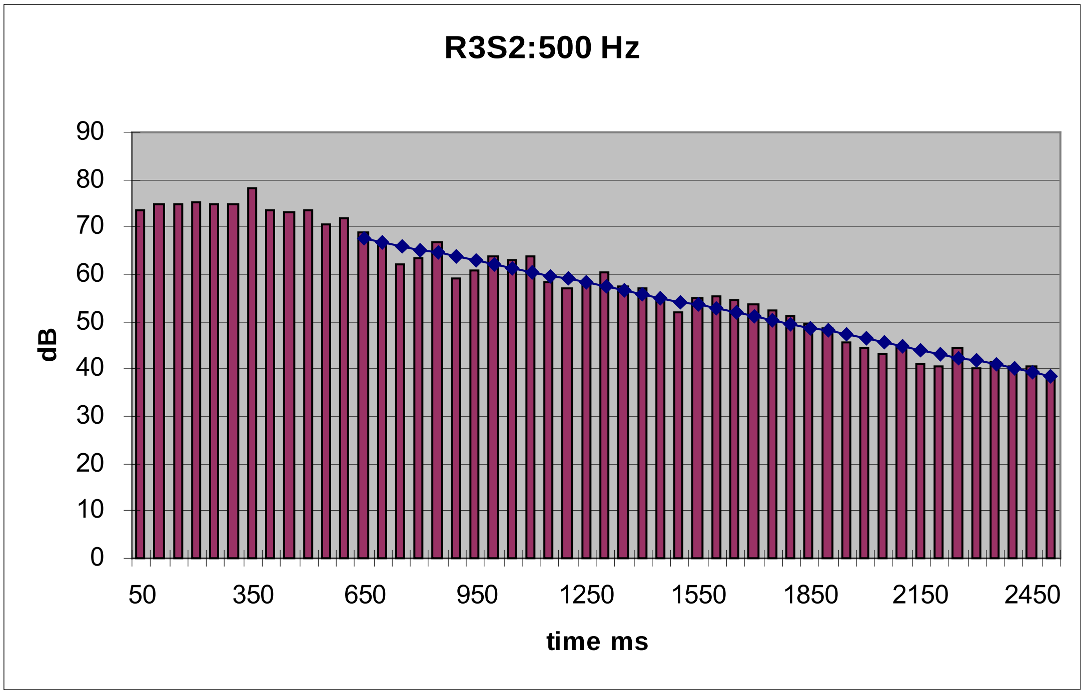

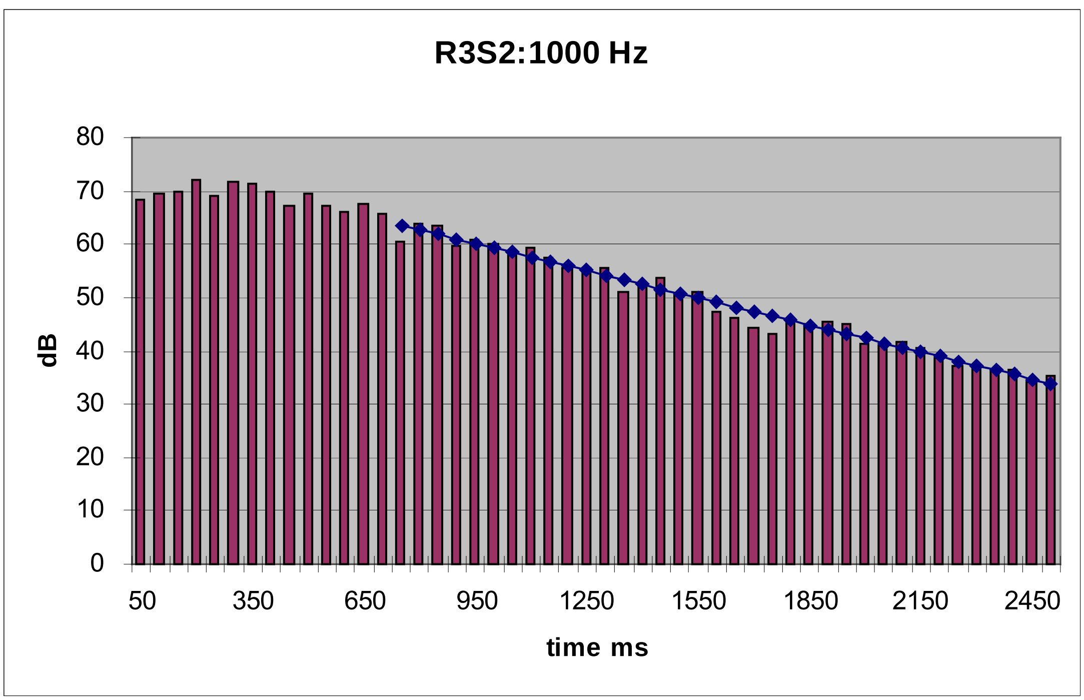

Figure A.20 Decay and Fit for T30 for 500 and 1000 Hz at R3S2 in C.A.P.

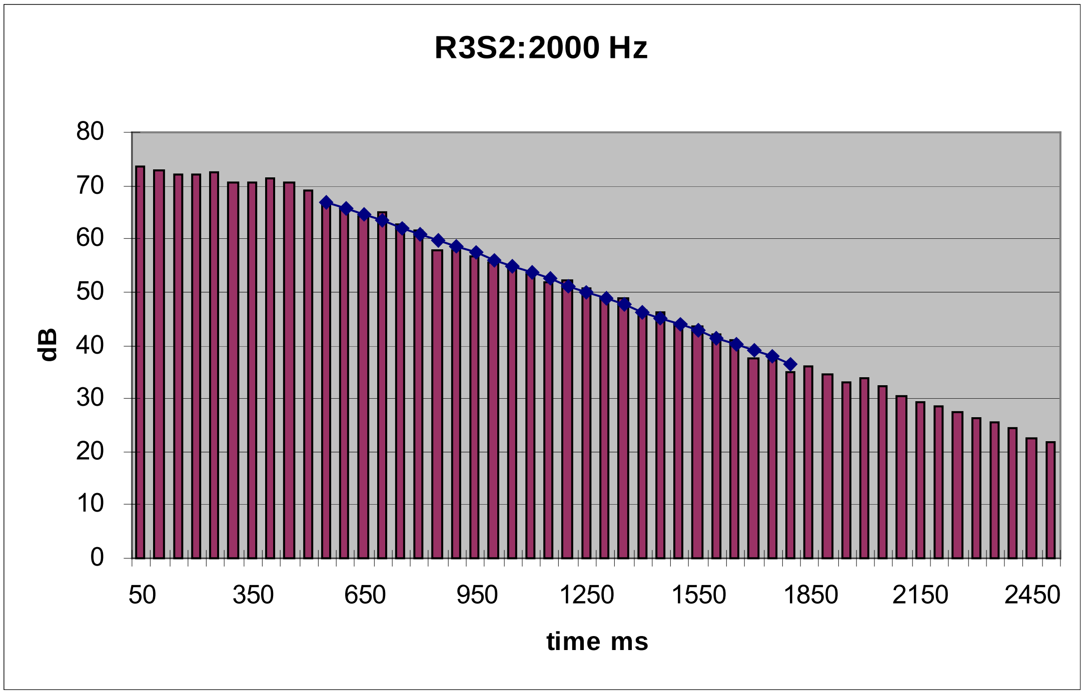

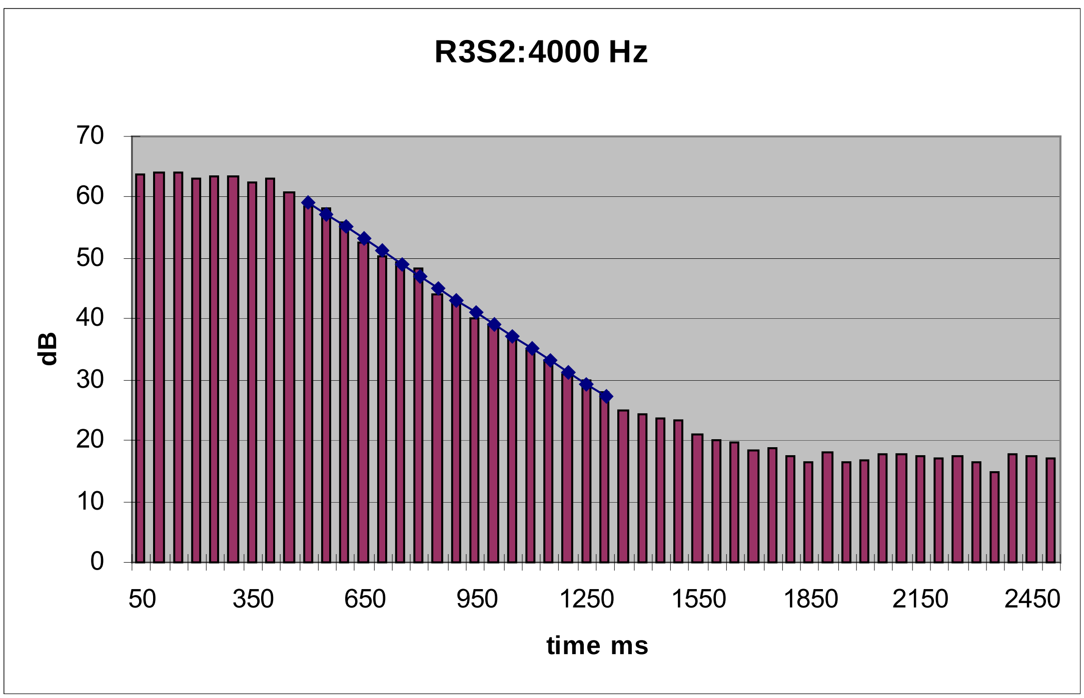

Figure A.21 Decay and Fit for T30 for 2 and 4 kHz at R3S2 in C.A.P.

Table A.8 Measurements at R3S2 in C.A.P.

time	dB					
ms	125	250	500	1000	2000	4000
50	76.29	73.73	76.50	71.14	71.61	64.09
100	73.89	71.49	76.83	71.40	72.65	64.46
150	70.98	73.56	75.68	71.07	71.87	64.67
200	76.08	71.85	76.32	72.22	72.86	64.20
250	72.62	71.92	74.18	73.16	73.89	64.37
300	74.79	74.79	75.61	71.38	72.04	64.58
350	68.27	70.37	72.11	70.65	73.68	62.70
400	71.64	71.94	74.29	70.74	72.91	63.33
450	72.25	73.38	76.39	71.61	70.46	60.84
500	74.46	71.42	71.68	69.68	69.05	58.96
550	76.22	73.78	73.68	67.50	68.41	56.73
600	72.62	72.13	66.23	66.30	66.18	54.37
650	65.78	72.76	69.07	65.92	65.22	52.16
700	72.25	70.88	67.12	66.06	62.77	50.56
750	62.98	70.20	68.51	63.87	63.22	50.54
800	66.93	67.17	67.17	61.71	60.63	46.07
850	65.76	68.25	65.71	61.10	59.76	44.99
900	62.32	69.24	62.56	59.95	58.94	42.66
950	68.06	65.83	62.35	59.69	57.38	42.19
1000	68.27	68.01	61.92	59.36	55.93	38.88
1050	68.72	66.11	61.88	60.35	54.89	37.89
1100	67.73	61.24	59.31	58.49	53.57	36.08
1150	60.51	59.10	60.75	55.55	52.54	33.00
1200	67.87	60.89	60.21	56.21	52.02	29.94
1250	64.96	60.37	57.67	55.13	48.56	29.12
1300	64.27	59.69	58.02	55.41	48.35	27.33
1350	63.33	63.87	56.96	55.86	48.16	25.61
1400	58.56	57.34	53.97	53.36	46.31	24.22
1450	55.57	59.59	54.44	52.37	45.81	22.32
1500	62.46	58.58	52.19	50.23	45.86	22.18
1550	62.60	59.29	50.28	49.36	44.19	19.21
1600	65.36	52.05	53.67	49.81	42.80	19.33
1650	57.13	56.89	51.86	49.36	39.86	19.92
1700	61.92	56.35	52.35	48.59	40.33	19.12
1750	59.29	53.29	50.16	46.78	40.92	17.90
1800	50.35	55.01	48.49	47.74	38.85	16.32
1850	56.94	54.30	48.92	46.68	36.62	18.18
1900	53.69	52.66	48.42	44.54	36.17	16.42
1950	59.85	49.95	45.62	42.61	32.85	17.50
2000	52.21	49.36	48.64	44.43	32.20	17.57
2050	53.67	52.12	45.95	43.30	31.87	16.32
2100	55.48	49.62	43.23	42.31	29.70	17.22
2150	54.47	47.20	43.60	40.83	30.10	16.58
2200	52.63	50.23	43.23	39.63	27.35	18.06
2250	51.06	44.75	44.05	40.19	27.96	18.06
2300	48.24	47.15	40.00	36.85	25.47	16.74
2350	47.65	48.52	40.17	37.42	24.27	16.74
2400	50.16	42.43	37.16	37.82	23.07	18.63
2450	51.13	46.28	36.83	37.56	22.48	16.91
2500	45.01	44.52	35.77	34.74	22.22	18.67

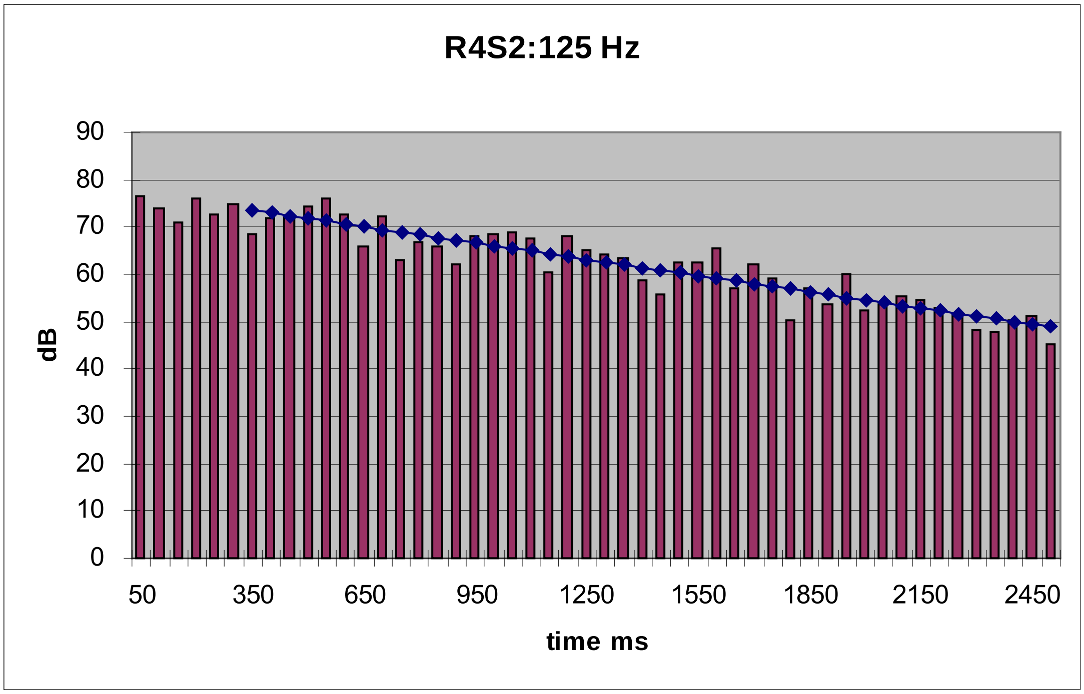

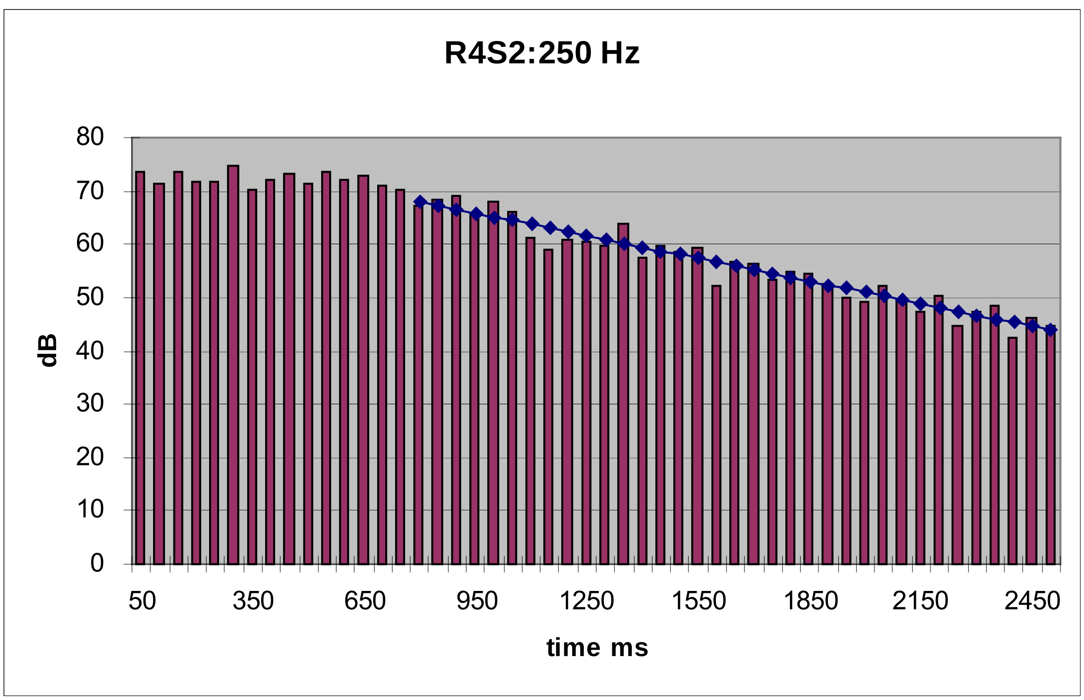

Figure A.22 Decay and Fit for T30 for 125 and 250 Hz at R4S2 in C.A.P.

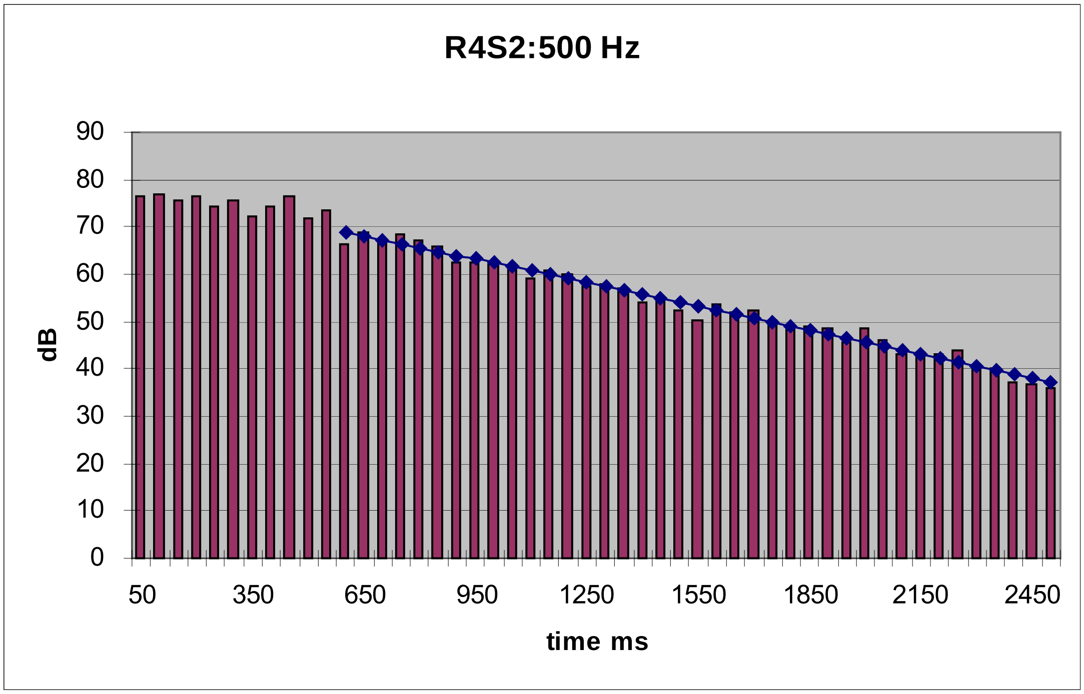

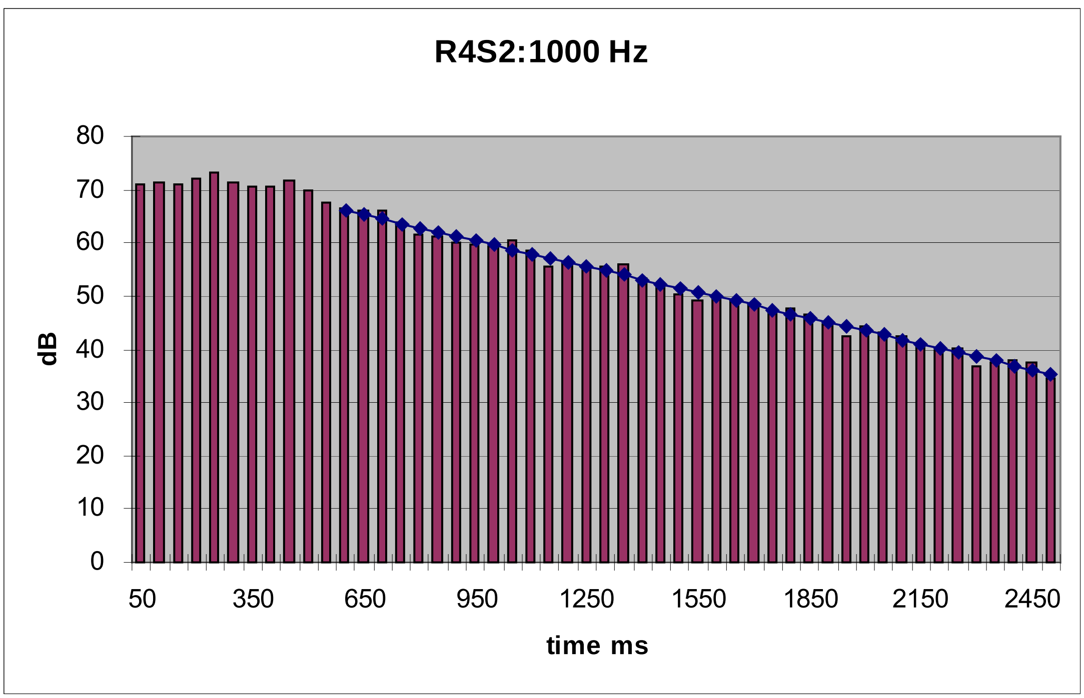

Figure A.23 Decay and Fit for T30 for 250 and 500 Hz at R4S2 in C.A.P.

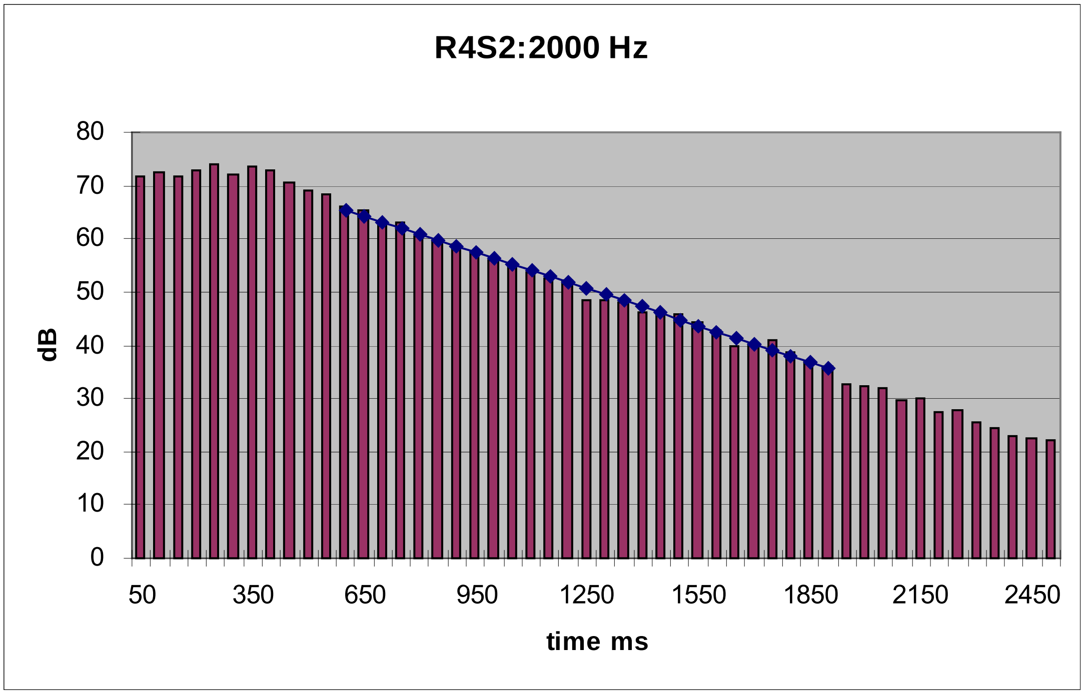

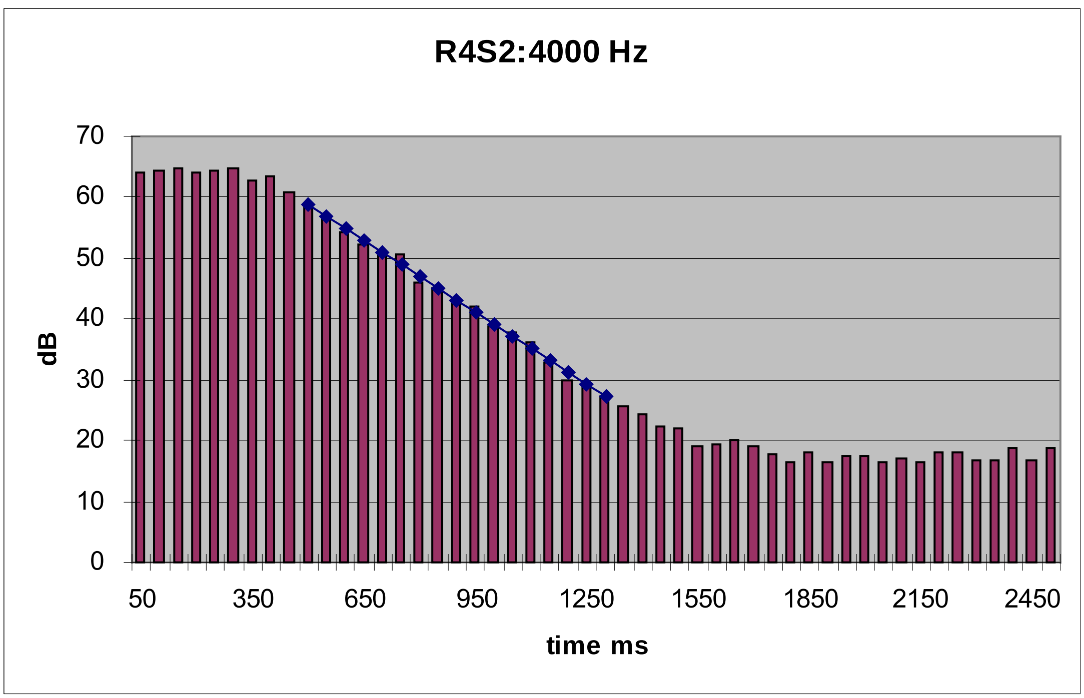

Figure A.24 Decay and Fit for T30 for 2 and 4 kHz at R4S2 in C.A.P.

Table A.9 Measurements at R1 in Süleymaniye

time	dB					
ms	125	250	500	1000	2000	4000
50	80.85	81.61	81.44	76.55	80.01	72.72
100	80.60	82.64	84.71	75.75	78.46	70.72
150	87.63	82.48	80.31	76.67	78.39	72.91
200	83.11	80.83	83.02	75.07	78.46	73.35
250	84.92	80.85	82.55	76.76	77.47	71.14
300	85.02	78.60	83.42	75.16	80.22	71.61
350	83.21	84.15	83.21	77.47	78.74	72.84
400	81.40	83.25	83.51	76.62	77.49	71.68
450	82.97	77.09	76.95	75.23	74.50	68.72
500	83.02	80.31	78.81	73.40	76.20	68.46
550	82.31	79.91	82.52	73.78	73.47	65.73
600	77.47	82.01	81.65	73.92	73.75	67.10
650	78.43	80.17	83.02	72.13	73.94	65.71
700	80.17	79.14	79.58	71.52	71.49	64.16
750	79.14	75.85	80.53	72.44	72.51	62.89
800	80.62	77.82	79.14	71.35	71.61	61.83
850	78.90	76.72	79.63	70.22	69.24	59.88
900	79.35	70.67	78.46	70.60	68.39	58.49
950	77.07	73.49	77.42	68.20	69.07	59.12
1000	76.57	73.75	77.63	68.81	70.32	58.30
1050	76.65	75.16	80.41	67.73	68.48	56.56
1100	77.70	66.72	76.03	68.34	66.23	55.57
1150	78.55	64.13	72.76	66.56	67.24	52.82
1200	74.93	68.39	76.97	66.77	65.87	52.75
1250	80.62	74.62	76.17	66.77	65.99	51.57
1300	73.47	69.57	77.42	64.79	64.20	50.09
1350	74.58	69.00	72.32	64.89	63.76	49.15
1400	76.48	69.21	72.25	65.29	62.25	48.00
1450	77.04	70.72	76.13	64.77	60.94	46.66
1500	75.80	68.72	74.79	64.13	60.86	45.39
1550	72.22	70.51	73.71	62.72	61.36	44.92
1600	71.94	64.79	74.86	63.47	61.50	43.56
1650	72.32	68.16	70.15	61.99	57.50	42.19
1700	73.45	68.81	72.51	61.50	60.16	41.51
1750	73.82	64.51	71.99	61.05	58.14	39.93
1800	67.52	71.05	65.83	62.65	58.35	39.18
1850	72.01	68.04	70.93	61.50	56.44	38.01
1900	74.20	66.13	68.70	61.50	56.40	36.45
1950	70.84	64.70	69.45	59.88	55.10	36.90
2000	71.19	65.43	70.01	58.21	53.67	34.62
2050	61.12	60.86	67.43	58.77	54.09	34.36
2100	62.09	65.03	67.97	59.69	51.88	32.20
2150	69.07	61.48	69.66	58.42	52.28	31.30
2200	69.90	66.56	68.04	58.23	52.16	29.82
2250	67.33	64.63	67.87	56.33	51.01	30.48
2300	70.53	64.93	68.44	57.15	50.89	26.13
2350	66.89	58.23	65.38	57.20	49.39	27.00
2400	59.31	63.59	65.14	56.00	48.49	26.13
2450	62.37	60.28	63.43	54.26	48.38	25.87
2500	71.49	63.92	62.65	54.16	49.48	24.60

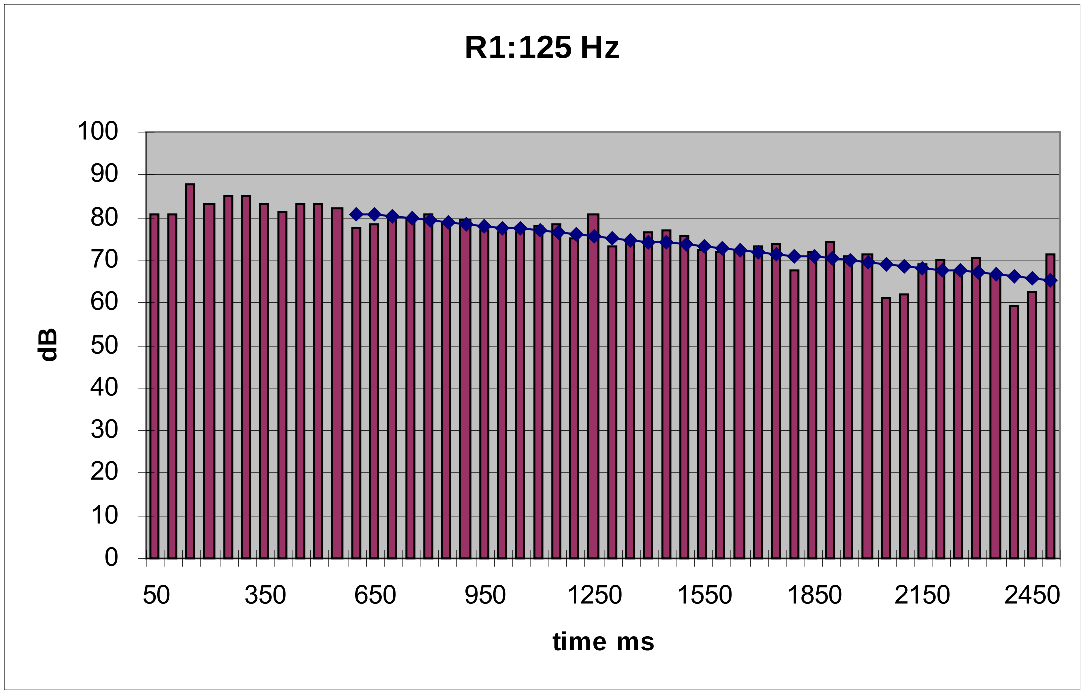

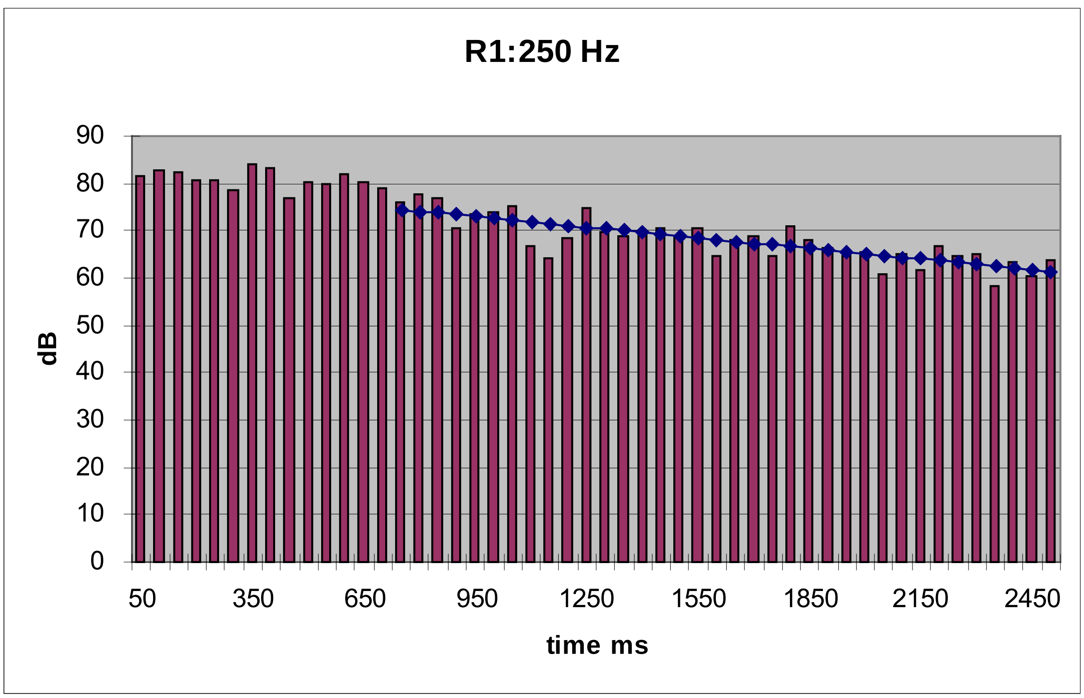

Figure A.25 Decay and Fit for T30 for 125 and 250 Hz at R1S1 in Süleymaniye.

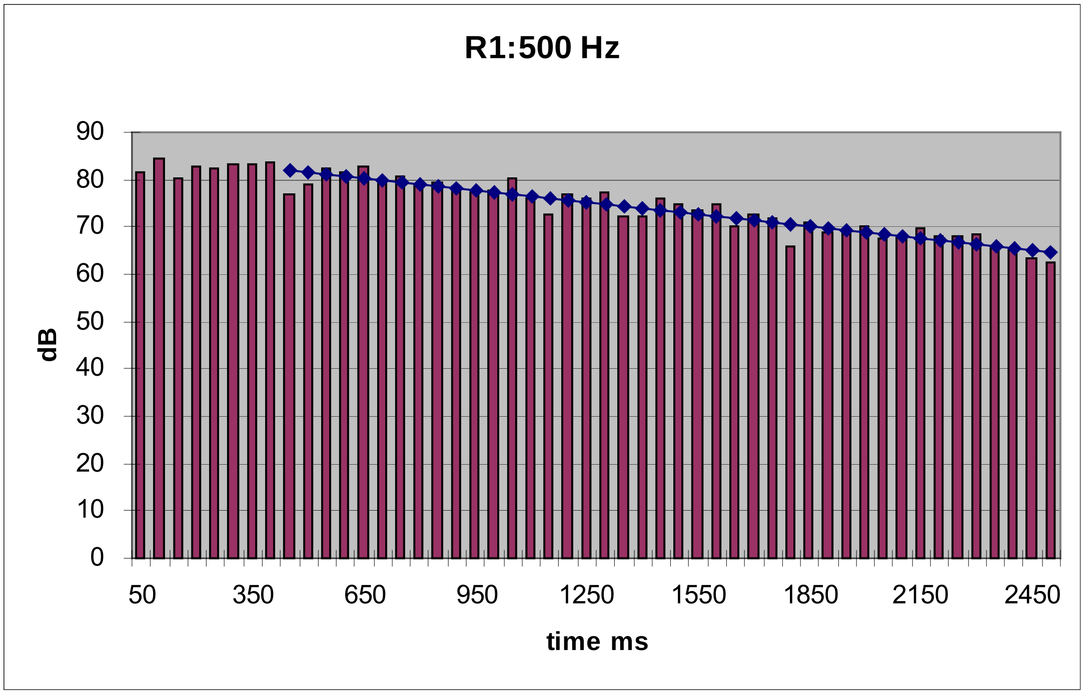

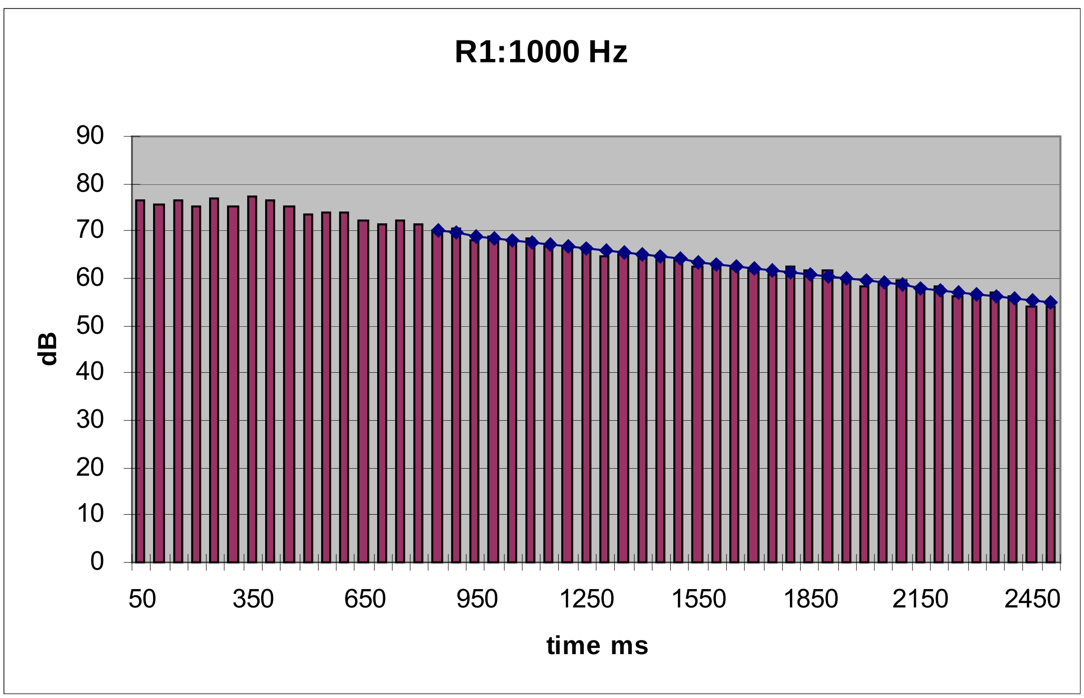

Figure A.26 Decay and Fit for T30 for 500 and 1000 Hz at R1S1 in Süleymaniye.

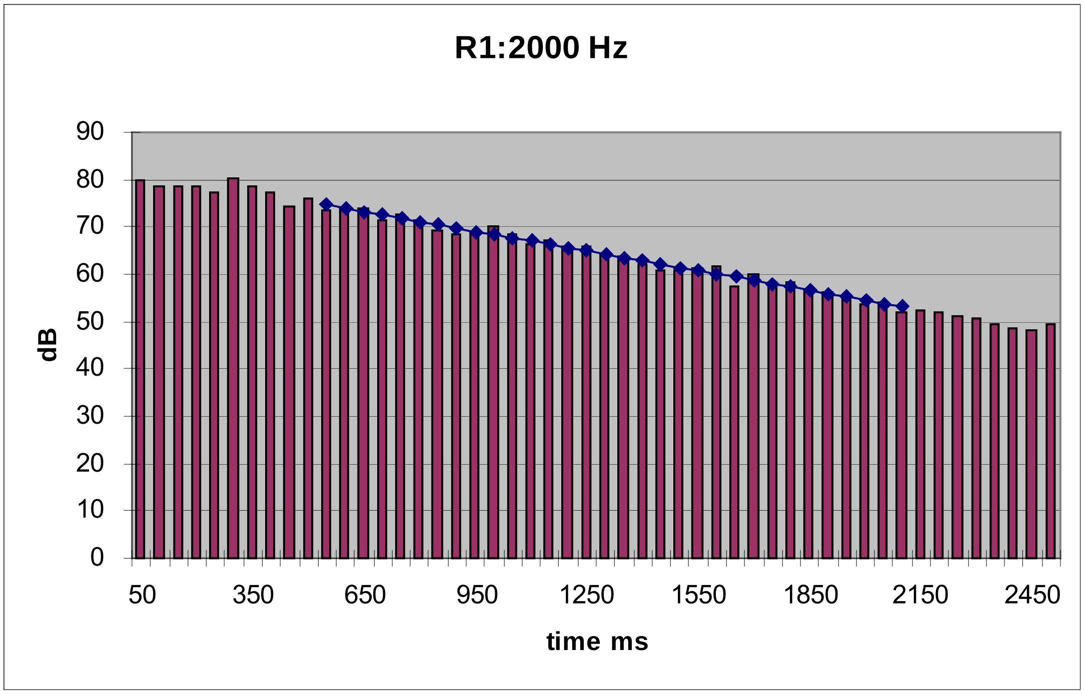

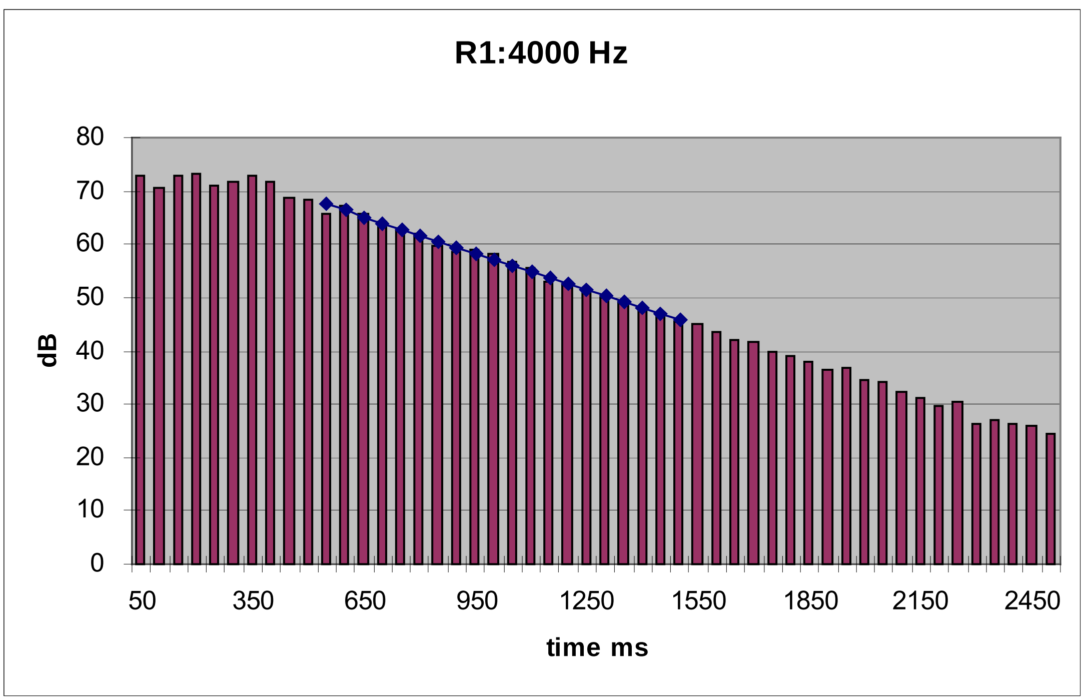

Figure A.27 Decay and Fit for T30 for 2 and 4 kHz at R1S1 in Süleymaniye.

Table A.10 Measurements at R2 in Süleymaniye

time	dB					
ms	**125**	**250**	**500**	**1000**	**2000**	**4000**
50	80.81	83.21	86.24	77.63	79.54	72.25
100	85.30	80.69	83.09	75.21	77.70	72.91
150	73.33	79.47	83.16	77.00	78.53	73.54
200	77.52	81.02	81.82	76.55	77.23	72.79
250	75.68	82.05	81.61	76.29	77.70	72.15
300	85.65	79.47	84.41	77.37	78.53	73.12
350	84.34	83.16	82.69	76.41	76.95	74.06
400	84.34	81.18	84.19	74.79	77.89	71.02
450	81.98	77.00	81.58	74.88	74.41	68.32
500	82.50	77.14	83.25	76.39	73.38	67.99
550	84.05	76.83	80.95	73.26	75.07	67.71
600	79.42	76.36	81.16	70.18	72.72	67.03
650	79.07	81.18	81.72	70.27	73.19	64.30
700	80.53	78.60	79.21	72.01	72.58	63.12
750	77.23	73.38	81.28	70.62	71.80	62.09
800	80.22	74.32	81.82	70.55	72.91	61.97
850	77.07	75.87	79.35	69.50	68.98	60.18
900	76.72	71.75	79.96	71.28	70.65	59.48
950	74.74	74.62	78.17	71.07	69.21	61.01
1000	71.47	76.97	75.59	68.18	68.04	57.52
1050	72.58	68.58	78.17	66.60	67.38	56.77
1100	68.60	72.58	78.39	64.51	67.26	55.69
1150	79.30	73.19	76.95	64.77	65.64	53.93
1200	76.13	76.83	77.21	66.84	64.74	53.01
1250	73.99	71.82	78.86	66.13	64.63	51.13
1300	70.86	72.29	74.62	67.26	65.43	49.79
1350	77.75	72.13	75.49	65.47	62.70	49.72
1400	75.30	70.32	72.88	65.14	62.02	47.18
1450	75.73	63.87	72.15	68.13	61.36	46.28
1500	78.76	70.25	74.32	64.65	59.88	45.60
1550	68.70	70.46	74.60	64.53	60.04	42.66
1600	72.98	66.39	73.85	62.51	58.89	43.30
1650	65.71	67.85	72.32	63.73	60.21	41.65
1700	72.13	71.35	72.79	62.11	57.78	41.11
1750	69.14	68.27	70.25	61.62	57.52	41.56
1800	71.96	68.84	71.14	62.93	57.24	39.42
1850	71.26	67.68	72.58	61.97	55.76	38.36
1900	66.20	66.34	69.85	59.67	56.11	35.21
1950	64.79	67.54	71.12	57.74	55.29	34.34
2000	71.05	69.43	69.64	58.68	54.47	33.65
2050	70.51	69.31	69.21	57.50	52.09	31.51
2100	70.62	65.69	70.04	57.15	52.21	32.55
2150	71.19	59.95	68.34	56.25	51.67	31.51
2200	63.71	69.12	68.06	55.71	52.40	28.97
2250	67.66	65.87	70.95	56.09	50.23	27.70
2300	68.74	67.00	70.77	56.44	50.59	28.22
2350	67.21	62.35	66.96	54.44	51.08	25.02
2400	68.48	63.29	68.34	54.68	49.11	25.12
2450	66.72	68.48	64.53	53.22	48.89	24.06
2500	68.67	63.29	68.04	54.02	47.48	23.12

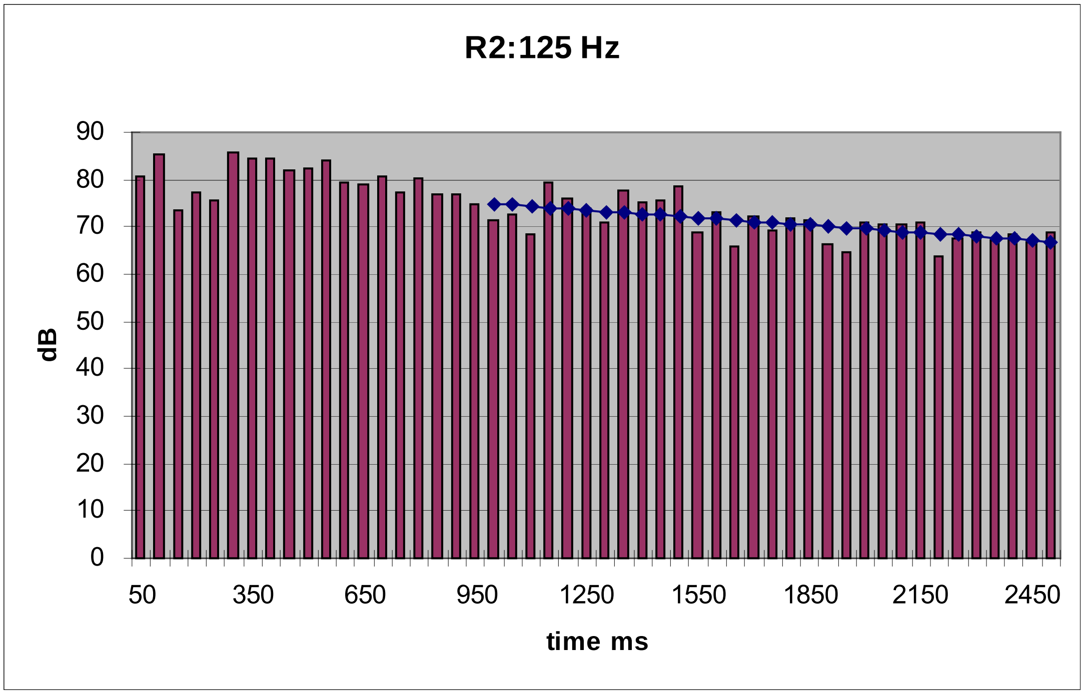

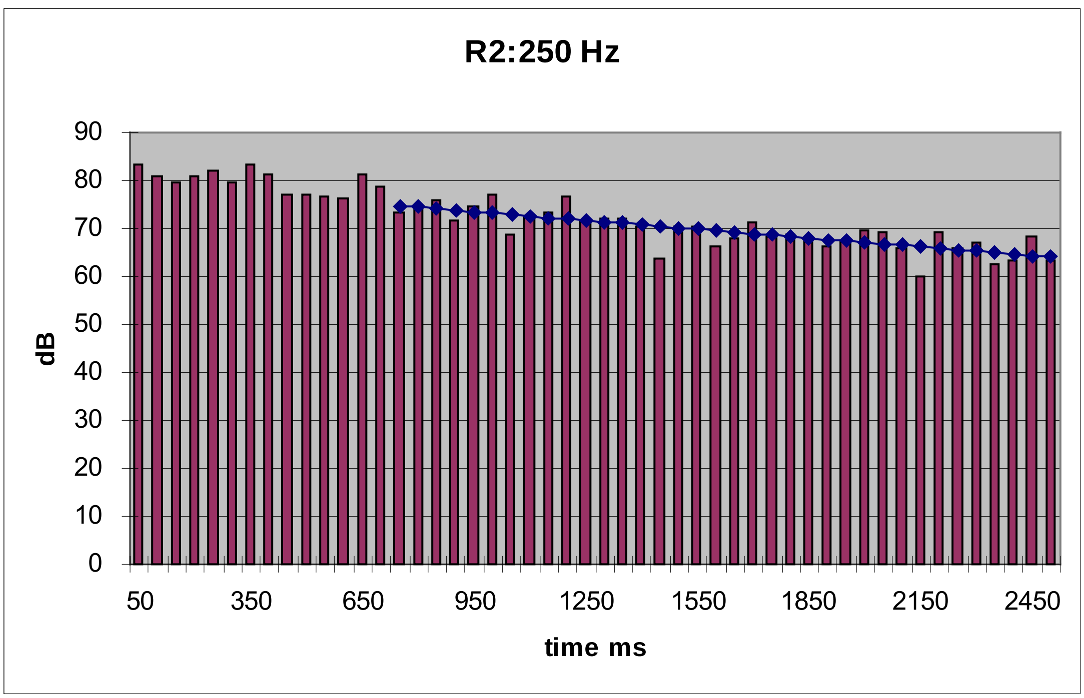

Figure A.28 Decay and Fit for T30 for 125 and 250 Hz at R2S1 in Süleymaniye.

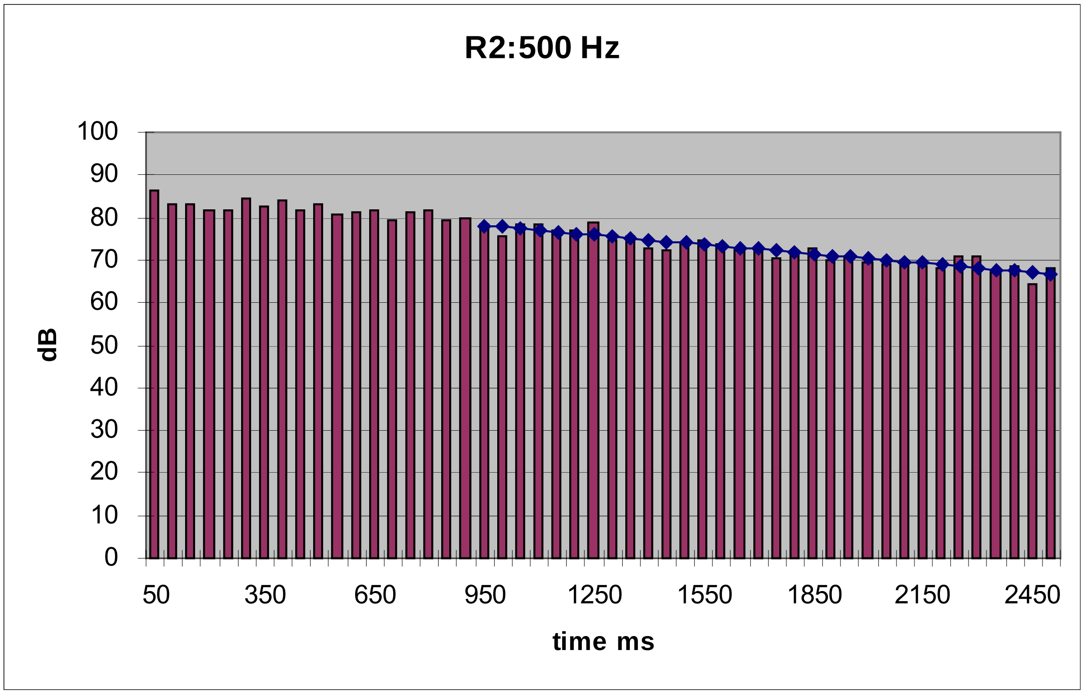

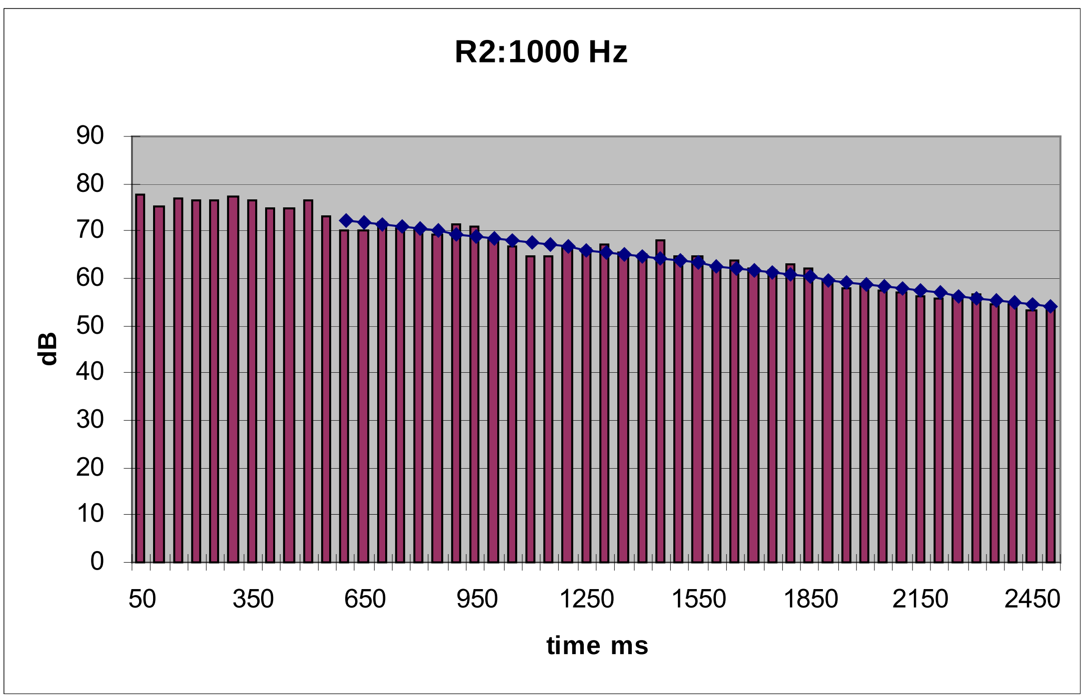

Figure A.29 Decay and Fit for T30 for 500 and 1000 Hz at R2S1 in Süleymaniye.

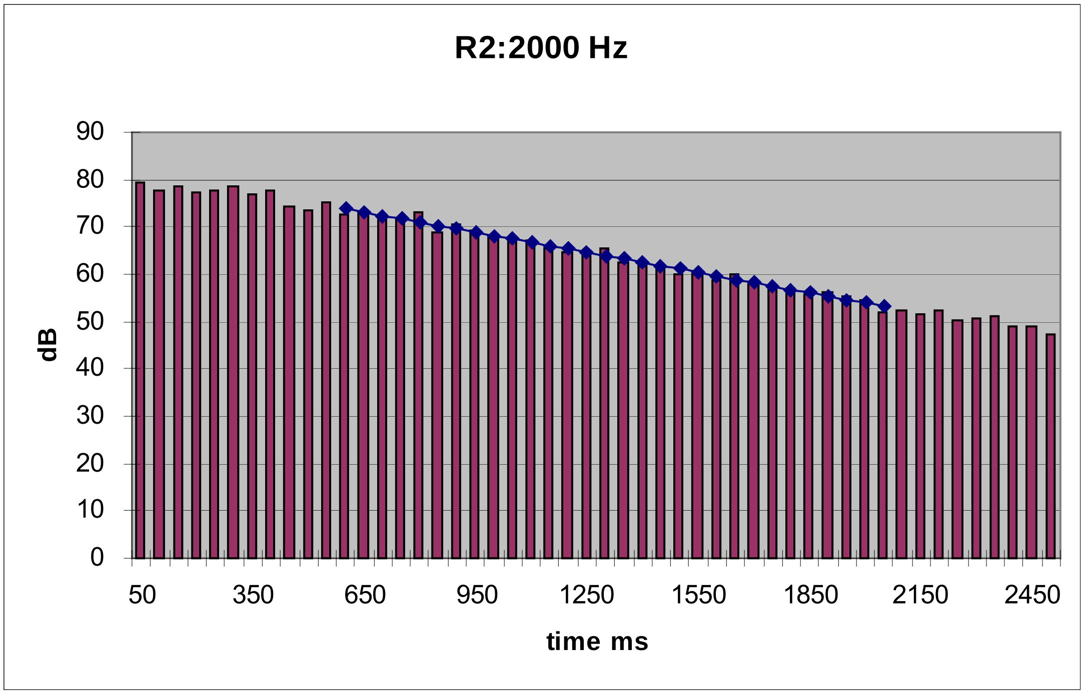

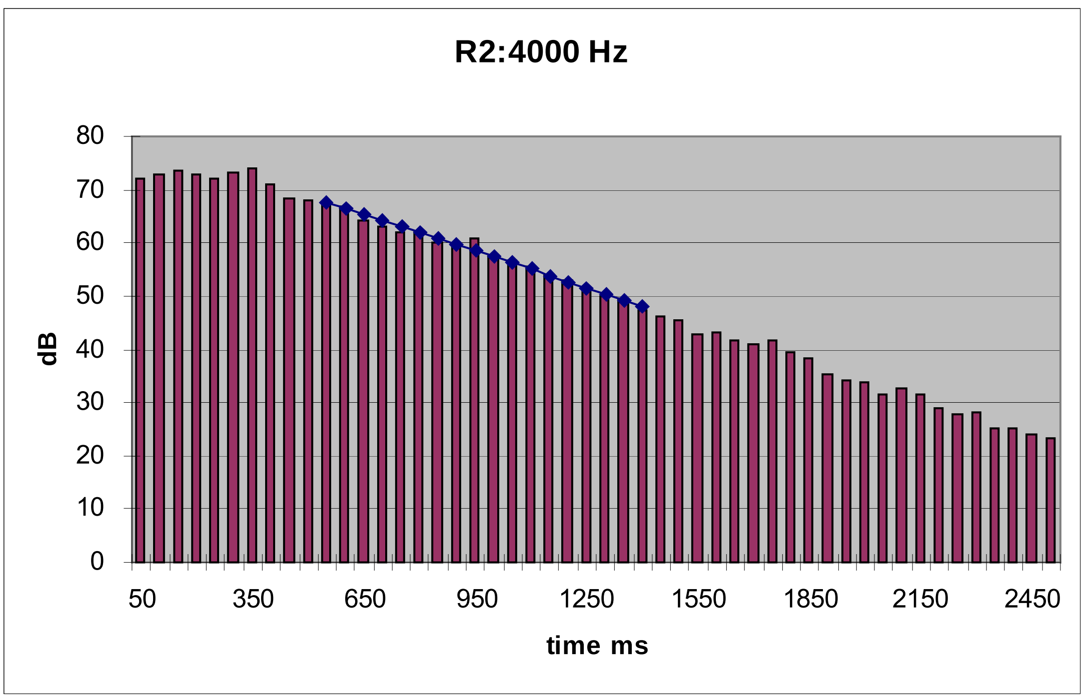

Figure A.30 Decay and Fit for T30 for 2 and 4 kHz at R2S1 in Süleymaniye.

Table A.11 Measurements at R3 in Süleymaniye

time	dB					
ms	**125**	**250**	**500**	**1000**	**2000**	**4000**
50	77.73	79.54	81.87	76.29	79.07	74.76
100	80.48	76.79	82.95	73.89	78.20	72.79
150	79.16	79.09	85.16	74.48	78.13	74.22
200	84.24	80.17	86.76	73.75	78.24	71.52
250	78.67	82.92	84.31	72.84	79.23	72.39
300	79.87	77.44	86.12	75.49	76.97	74.34
350	74.55	81.75	84.10	76.62	76.97	72.86
400	82.83	77.75	84.31	75.12	75.09	69.19
450	80.27	75.42	83.89	73.00	75.33	68.91
500	81.98	72.51	80.48	73.35	75.96	68.06
550	82.38	71.45	83.47	72.08	73.68	66.77
600	77.84	77.80	81.18	72.88	73.19	66.79
650	76.15	79.80	78.46	71.89	73.54	65.76
700	79.56	73.47	78.03	69.94	72.25	63.19
750	75.33	78.10	76.88	71.80	71.42	61.85
800	78.71	78.64	78.48	70.08	71.89	61.43
850	76.88	74.36	78.97	69.00	70.37	59.55
900	75.96	73.49	78.48	70.32	69.57	57.95
950	73.35	67.05	78.90	67.47	67.59	56.40
1000	78.03	71.05	77.23	69.05	67.05	57.57
1050	73.66	72.34	79.23	68.51	68.30	55.01
1100	72.81	70.72	73.49	67.14	67.12	53.48
1150	78.69	75.38	73.63	68.55	67.00	52.92
1200	71.68	70.30	76.36	67.05	64.91	51.10
1250	68.63	70.04	72.41	66.13	64.32	50.78
1300	71.99	65.78	73.61	65.50	62.68	48.26
1350	76.20	72.67	74.58	65.87	62.96	48.45
1400	70.60	71.59	76.79	66.98	63.73	47.01
1450	75.52	69.54	75.38	64.44	62.49	43.74
1500	74.86	71.26	73.87	63.78	61.73	44.87
1550	74.95	69.71	72.65	64.49	59.45	44.17
1600	75.77	66.56	72.04	62.68	60.04	42.87
1650	74.53	67.61	69.38	60.91	60.49	41.58
1700	70.84	67.71	68.48	60.75	59.41	41.34
1750	63.55	68.32	75.96	61.05	58.16	39.23
1800	70.84	66.51	71.52	61.52	58.70	38.78
1850	69.43	70.11	71.45	61.03	56.51	36.31
1900	71.09	67.05	74.06	59.69	54.42	36.01
1950	69.73	62.68	69.00	59.95	54.96	34.08
2000	69.68	65.24	67.66	59.74	53.55	33.82
2050	68.08	68.48	72.36	61.01	54.59	32.05
2100	67.40	64.84	67.90	56.07	52.77	32.17
2150	66.77	65.33	69.66	55.24	51.88	30.36
2200	60.11	67.66	68.77	59.41	52.26	30.03
2250	65.14	65.33	68.84	56.94	50.85	28.32
2300	66.20	66.34	68.06	54.16	50.75	27.26
2350	68.08	64.04	68.55	55.69	49.03	26.34
2400	69.05	63.10	64.16	55.48	46.24	24.74
2450	67.94	59.83	67.00	52.80	46.61	23.66
2500	67.52	65.07	68.39	54.56	47.55	23.19

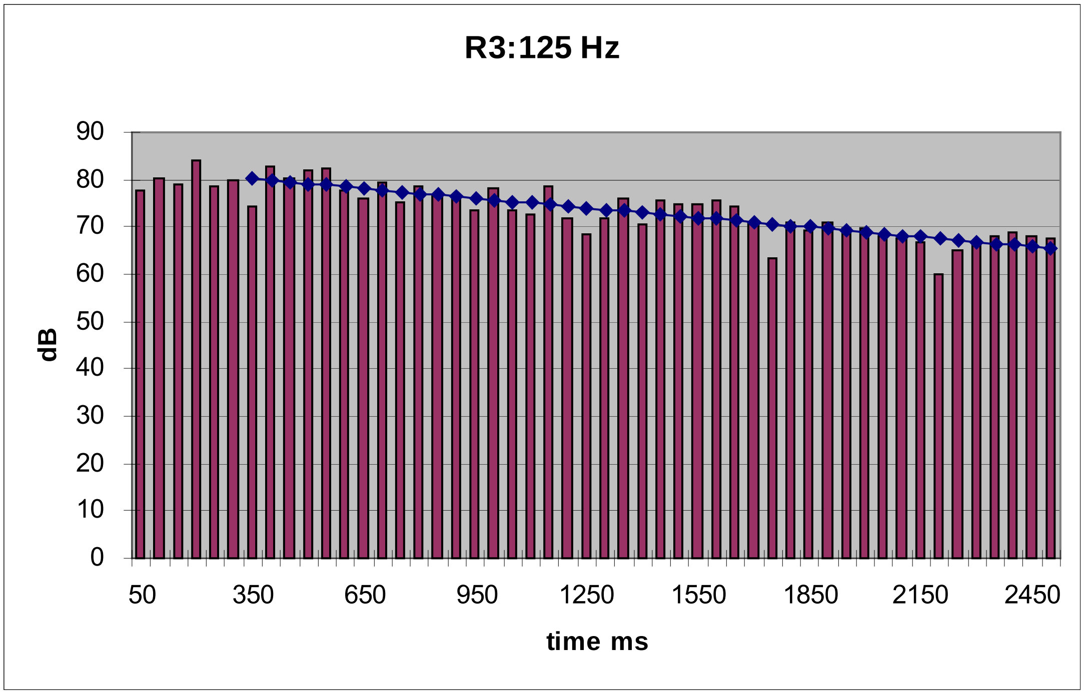

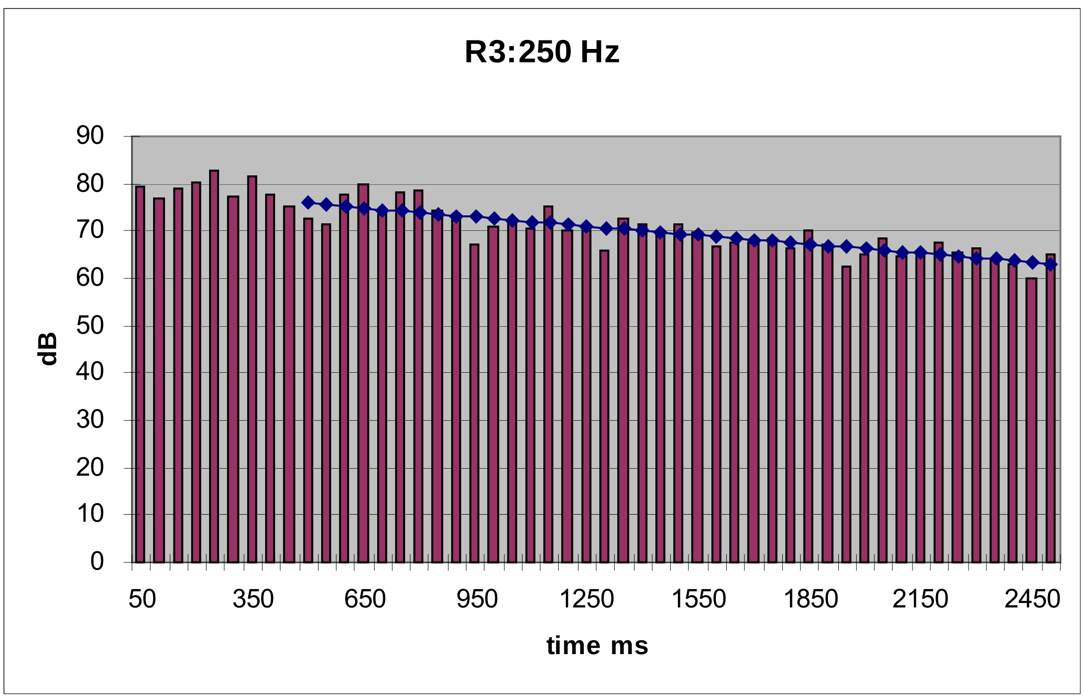

Figure A.31 Decay and Fit for T30 for 125 and 250 Hz at R3S1 in Süleymaniye.

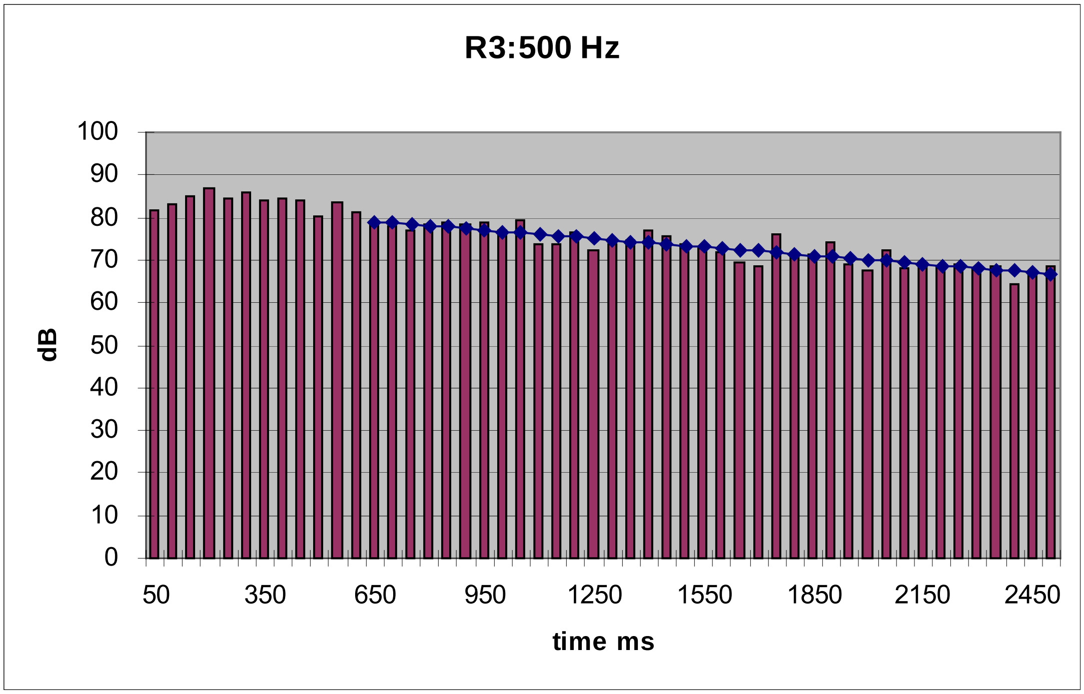

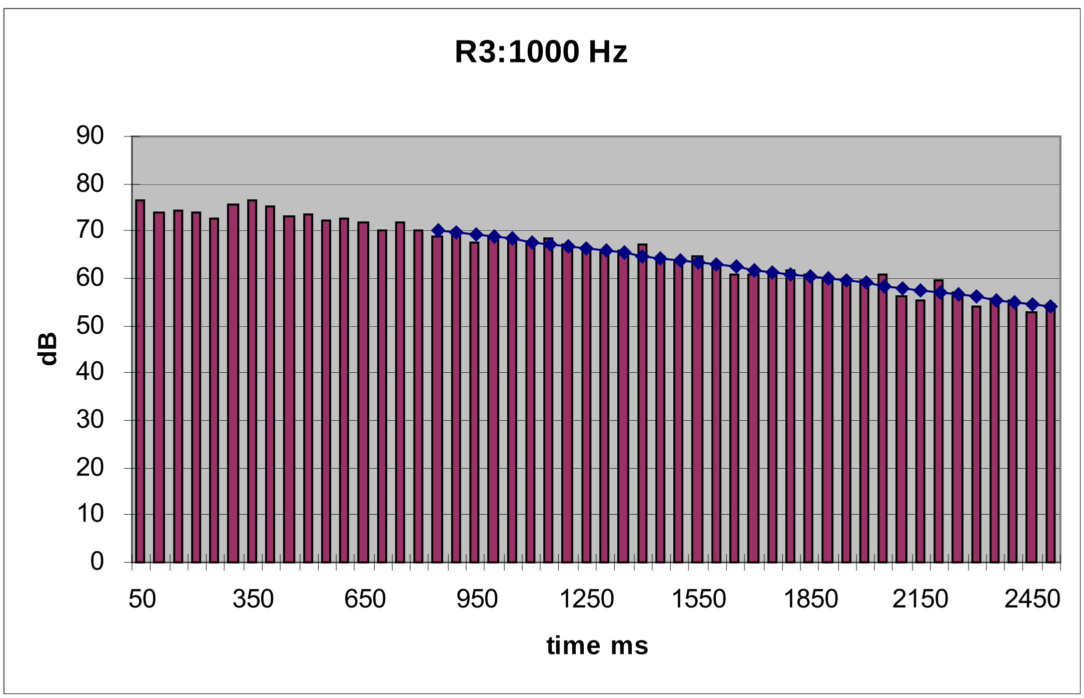

Figure A.32 Decay and Fit for T30 for 500 and 1000 Hz at R3S1 in Süleymaniye.

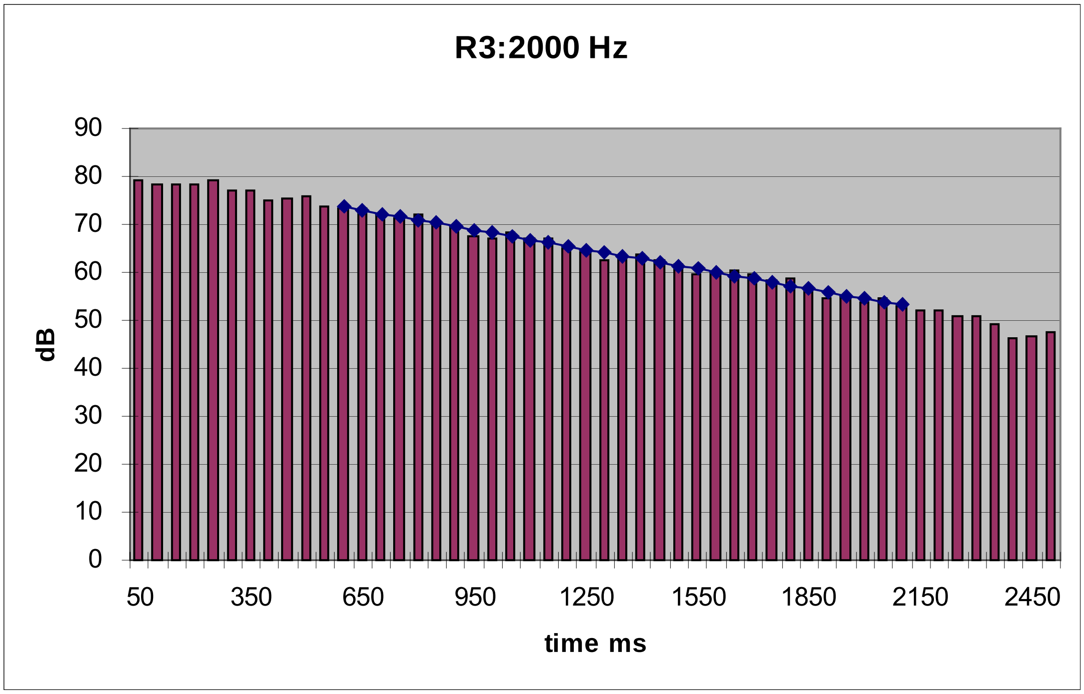

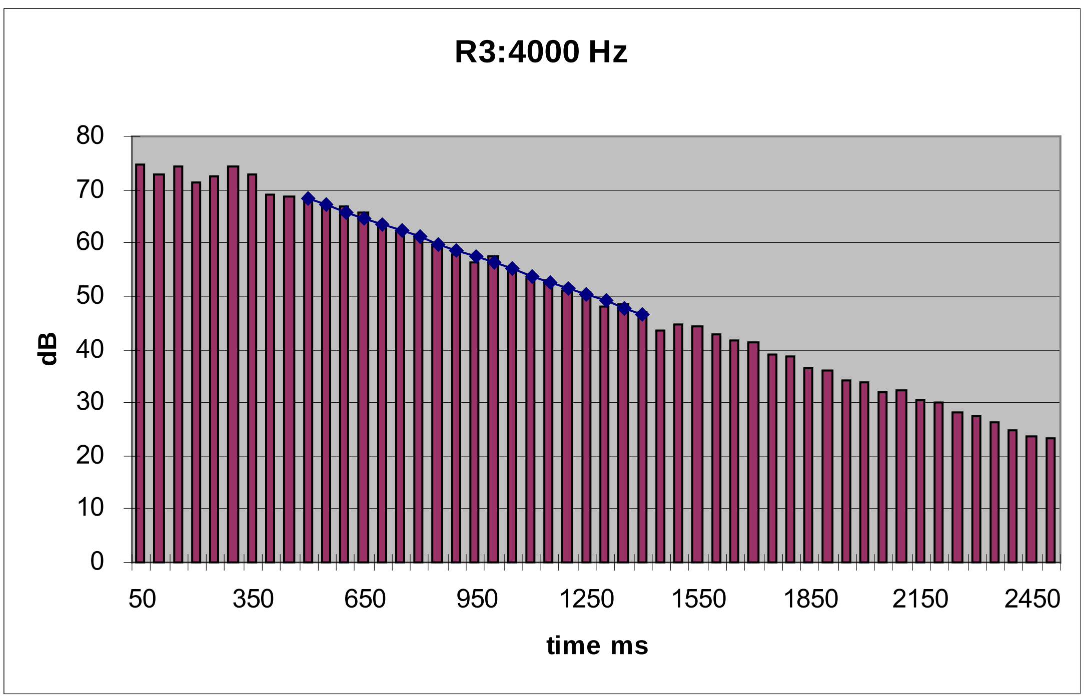

Figure A.33 Decay and Fit for T30 for 2 and 4 kHz at R3S1 in Süleymaniye.

Table A.12 Measurements at R4 in Süleymaniye

time	dB					
ms	125	250	500	1000	2000	4000
50	83.25	83.44	84.78	76.36	78.39	71.09
100	82.15	81.75	84.64	73.45	78.74	72.36
150	83.61	80.85	84.15	73.49	77.70	71.71
200	83.96	80.71	85.53	76.22	78.24	70.34
250	80.43	83.25	81.89	74.53	77.44	71.33
300	80.55	79.82	83.25	74.06	77.04	71.49
350	78.74	80.13	84.83	76.20	77.14	72.11
400	78.03	80.38	81.37	75.07	76.81	68.41
450	82.67	80.55	83.47	74.62	75.05	67.45
500	78.15	79.40	80.85	74.08	75.85	68.20
550	78.03	80.53	81.04	73.94	75.80	66.60
600	83.51	77.56	79.40	71.45	74.50	65.69
650	83.11	80.17	80.69	72.13	72.15	64.70
700	80.71	74.83	79.49	70.44	71.99	63.31
750	74.69	73.61	80.76	69.61	70.98	61.83
800	79.23	72.55	76.34	69.68	71.35	60.63
850	73.92	78.60	81.25	70.30	70.01	61.08
900	78.60	78.46	79.07	69.40	68.48	59.17
950	74.18	75.85	79.80	70.37	71.00	57.95
1000	76.90	69.92	82.17	68.32	69.21	55.67
1050	75.12	72.44	76.86	68.91	67.21	56.40
1100	75.75	75.28	79.33	68.16	66.89	54.07
1150	73.26	71.14	75.38	67.80	63.97	53.29
1200	74.29	69.38	79.07	67.59	64.06	52.26
1250	71.73	71.78	75.30	66.96	64.35	51.60
1300	74.20	66.84	78.39	66.32	63.22	49.98
1350	73.26	69.68	77.02	64.65	62.49	49.69
1400	67.21	71.45	73.40	66.65	60.70	47.76
1450	73.02	70.30	74.39	65.07	62.23	45.98
1500	72.62	70.84	73.33	64.98	61.01	46.78
1550	71.92	70.86	71.49	63.55	60.04	44.17
1600	69.10	64.84	71.92	60.91	58.98	44.12
1650	68.81	70.13	73.71	62.53	59.34	41.58
1700	70.34	72.81	73.33	62.18	58.61	42.05
1750	73.33	67.71	69.35	61.59	56.49	37.86
1800	67.94	68.81	73.75	60.32	57.03	38.50
1850	61.90	68.51	65.40	59.81	55.22	37.23
1900	72.25	67.76	71.40	61.41	56.11	36.17
1950	69.14	69.75	72.62	59.74	54.28	35.35
2000	72.95	60.91	72.51	59.01	53.95	32.97
2050	68.08	62.32	67.87	61.10	53.64	32.38
2100	68.25	62.13	69.87	58.79	52.26	31.87
2150	63.31	66.49	70.37	58.68	52.52	31.26
2200	67.80	68.06	68.63	55.81	52.30	30.34
2250	69.17	67.61	67.24	53.88	52.54	27.70
2300	68.30	65.62	69.57	56.11	49.69	28.64
2350	67.05	64.93	70.72	56.47	49.32	27.75
2400	67.24	65.83	69.50	54.37	48.35	26.46
2450	68.65	60.68	66.58	53.34	47.84	24.91
2500	67.00	64.82	69.24	55.27	48.00	25.82

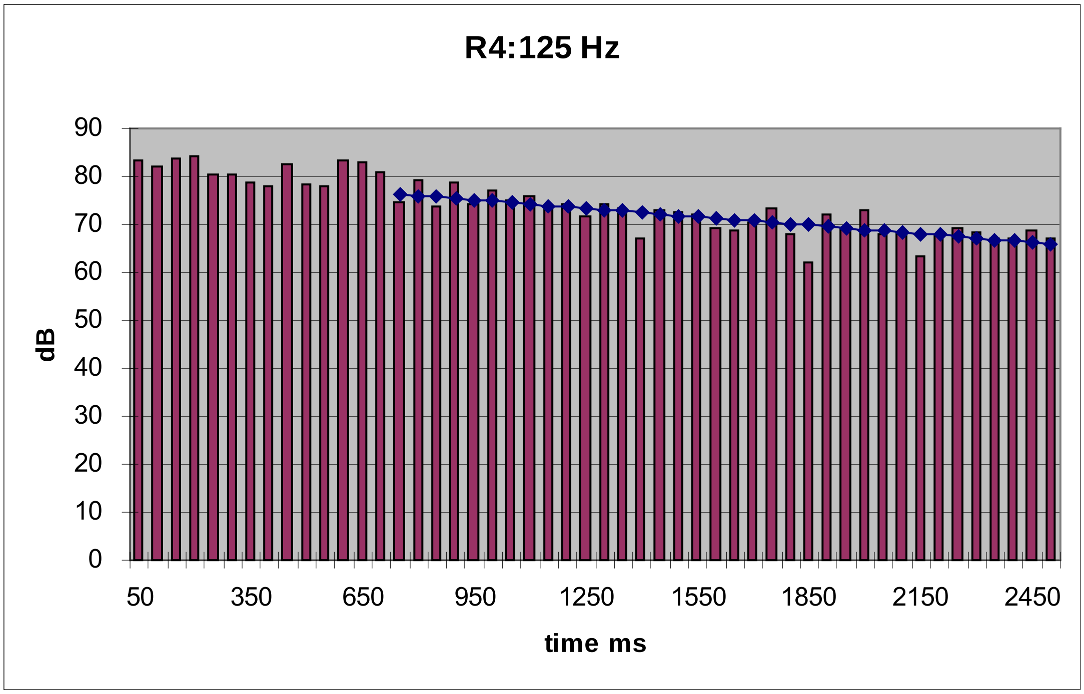

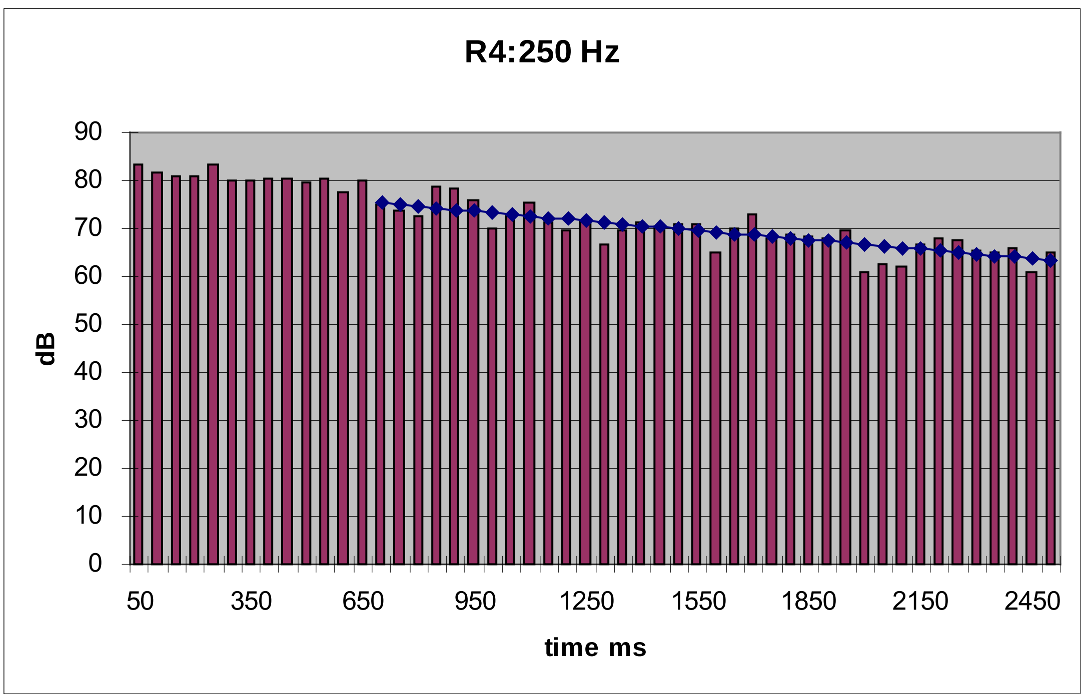

Figure A.34 Decay and Fit for T30 for 125 and 250 Hz at R4S1 in Süleymaniye.

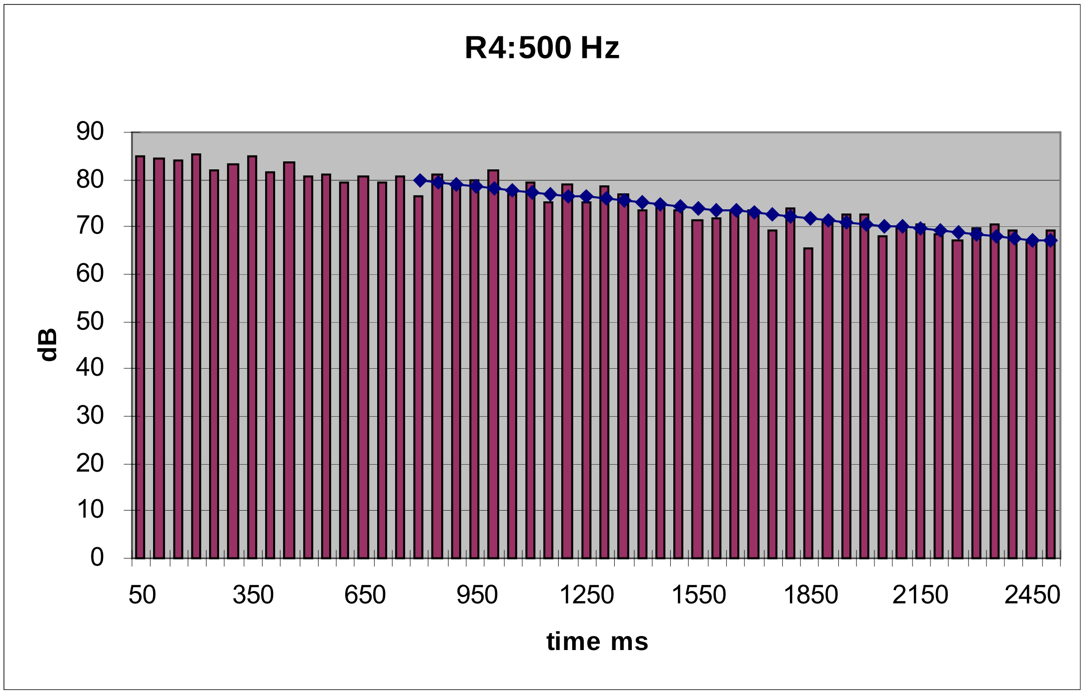

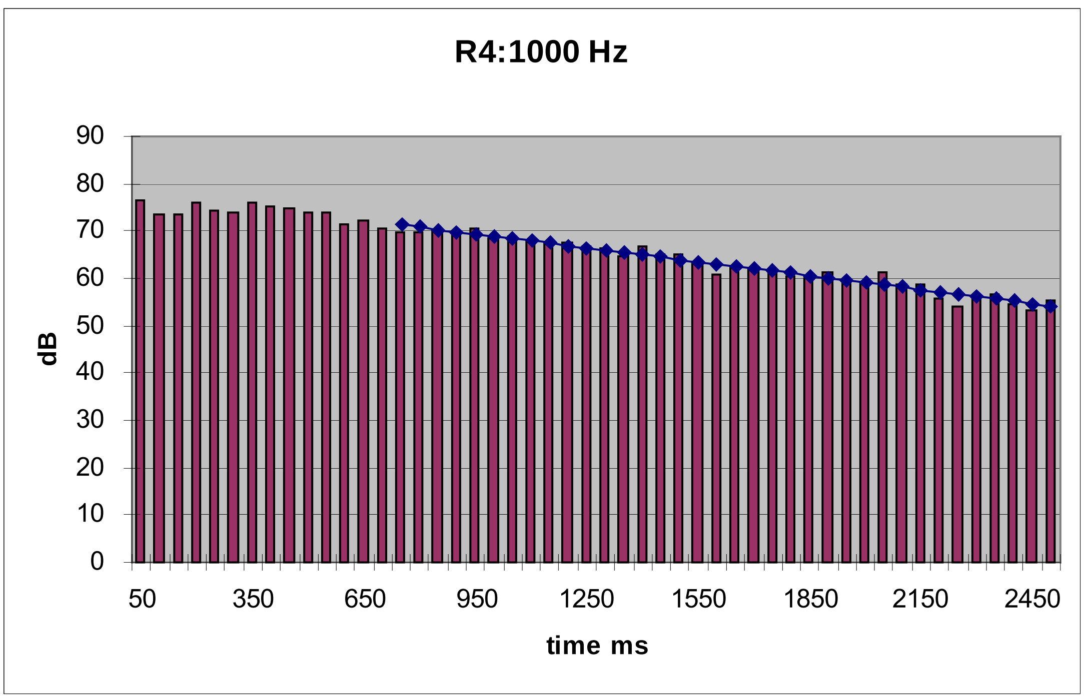

Figure A.35 Decay and Fit for T30 for 500 and 1000 Hz at R4S1 in Süleymaniye.

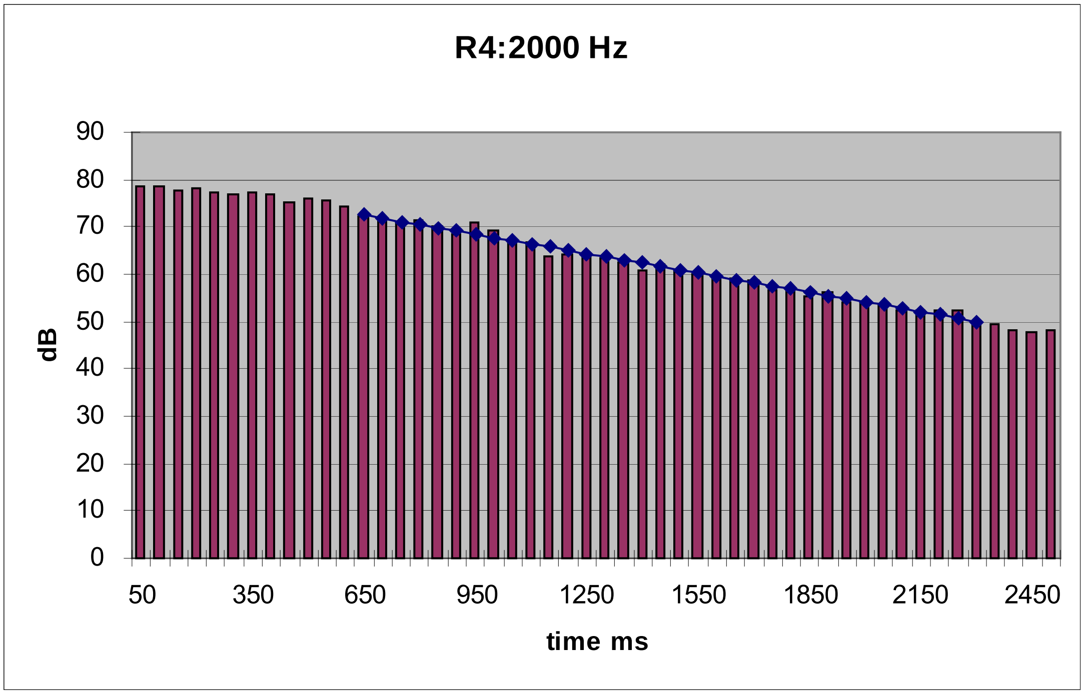

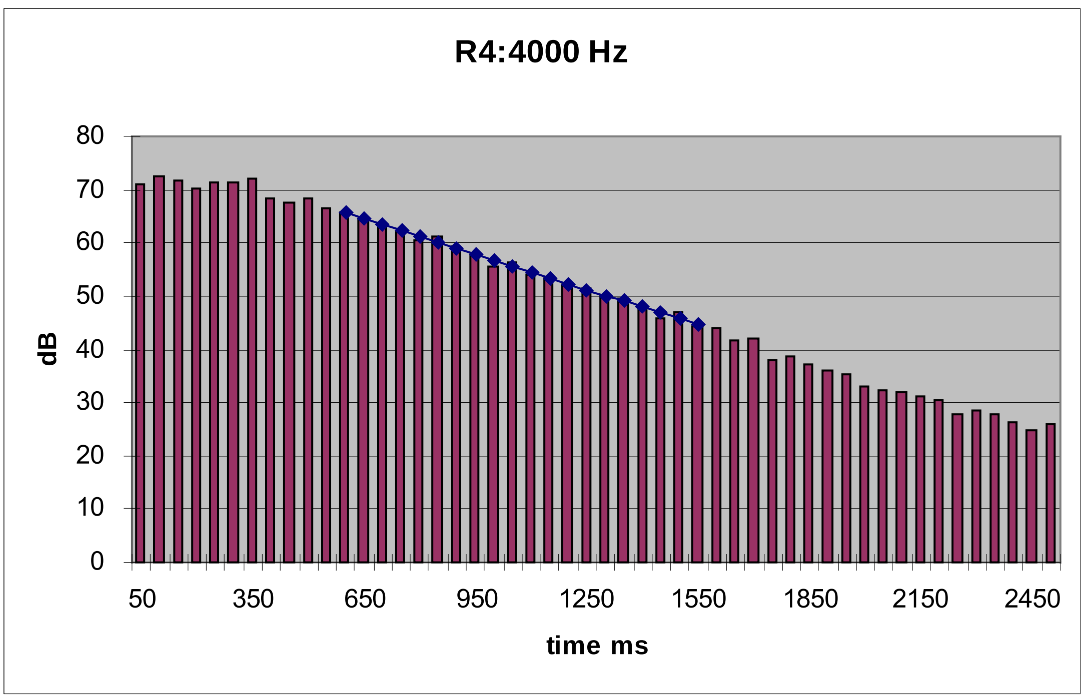

Figure A.36 Decay and Fit for T30 for 2 and 4 kHz at R4S1 in Süleymaniye.

Table A.13 Measurements at R5 in Süleymaniye

time	dB					
ms	**125**	**250**	**500**	**1000**	**2000**	**4000**
50	82.48	83.61	83.54	71.68	78.13	72.88
100	85.77	83.44	86.62	76.83	78.10	72.76
150	81.56	80.29	84.48	75.28	79.09	73.68
200	80.24	81.30	85.44	76.74	79.00	71.80
250	82.10	77.75	84.76	73.99	78.24	73.45
300	84.10	75.68	83.63	74.34	79.11	72.18
350	82.08	82.55	81.51	74.69	77.02	73.49
400	84.22	82.67	83.25	74.15	76.57	69.17
450	83.96	77.07	81.65	74.74	76.48	68.67
500	79.77	78.60	82.48	74.69	73.80	68.23
550	72.98	79.07	80.17	71.94	73.19	67.17
600	70.81	75.21	79.35	73.02	73.40	65.40
650	79.87	77.23	81.30	71.49	72.32	65.10
700	82.78	79.26	80.20	72.72	72.84	64.02
750	79.11	74.74	82.99	70.60	70.74	61.97
800	79.14	74.36	80.88	70.72	70.74	60.32
850	80.10	76.10	78.39	69.92	68.84	59.41
900	81.16	76.90	79.04	70.62	69.21	58.96
950	79.07	72.34	77.94	69.31	68.70	57.83
1000	76.86	71.21	77.84	68.58	68.72	55.86
1050	76.55	72.13	78.81	65.94	66.98	54.42
1100	74.22	70.62	77.35	67.45	67.12	54.66
1150	79.91	64.09	75.07	66.30	66.37	53.79
1200	76.08	72.53	75.07	66.56	65.22	51.95
1250	76.10	68.95	76.79	67.07	63.78	50.42
1300	76.15	69.43	73.02	66.70	63.08	50.26
1350	76.25	67.78	75.77	68.58	62.11	48.05
1400	76.48	70.39	72.91	65.07	62.77	47.34
1450	77.09	69.03	76.29	63.99	62.11	46.00
1500	68.20	71.38	68.51	63.00	60.94	44.47
1550	72.84	66.86	70.98	62.58	60.23	42.83
1600	72.48	73.23	72.93	62.91	59.03	42.05
1650	71.05	66.98	73.45	63.40	59.03	41.23
1700	69.90	70.46	71.99	63.15	58.61	40.07
1750	70.86	67.17	72.04	62.70	57.76	37.02
1800	74.74	66.81	72.34	61.81	56.91	38.01
1850	62.53	68.95	73.19	61.36	56.47	37.11
1900	68.74	68.20	70.22	60.54	54.89	35.91
1950	70.37	63.59	71.00	61.92	55.48	33.96
2000	67.66	64.89	71.05	59.88	55.57	34.20
2050	73.12	65.62	68.32	59.10	52.80	31.82
2100	66.86	65.85	68.60	58.44	52.70	30.97
2150	68.08	63.19	68.93	58.40	51.93	29.21
2200	68.08	64.58	69.78	57.62	51.83	29.19
2250	66.65	61.95	69.17	55.69	50.63	27.00
2300	66.16	61.59	69.10	55.60	49.91	26.65
2350	68.72	64.37	67.31	57.52	48.75	26.83
2400	67.31	62.25	67.26	54.51	48.85	24.15
2450	63.33	66.41	66.01	52.56	48.49	23.99
2500	66.46	61.64	68.23	51.81	46.47	23.56

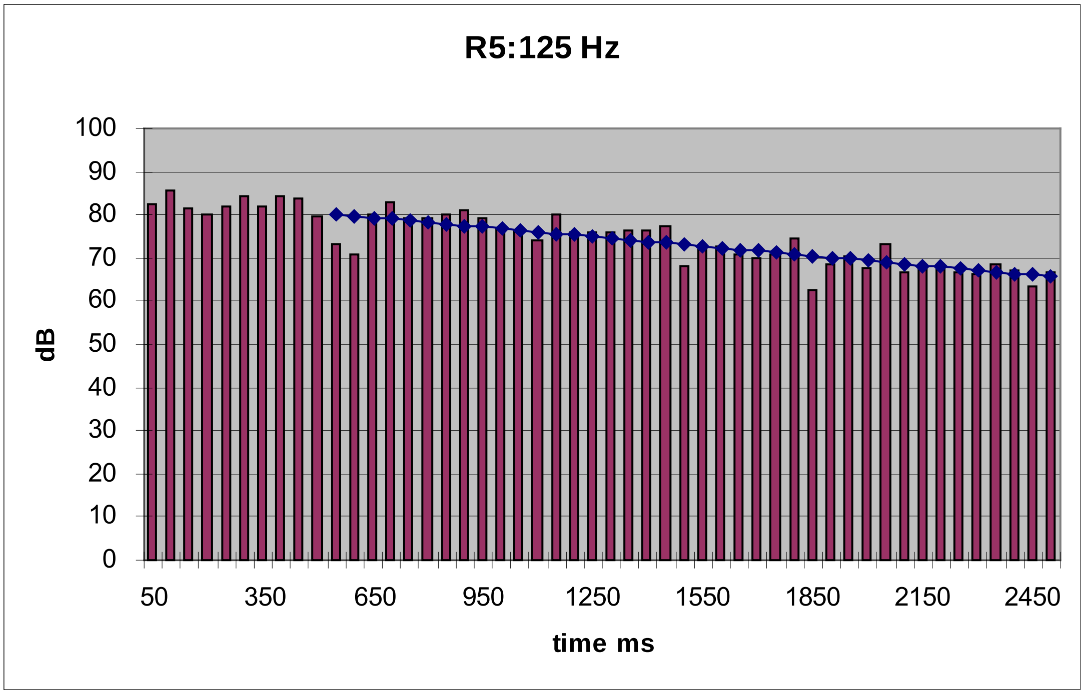

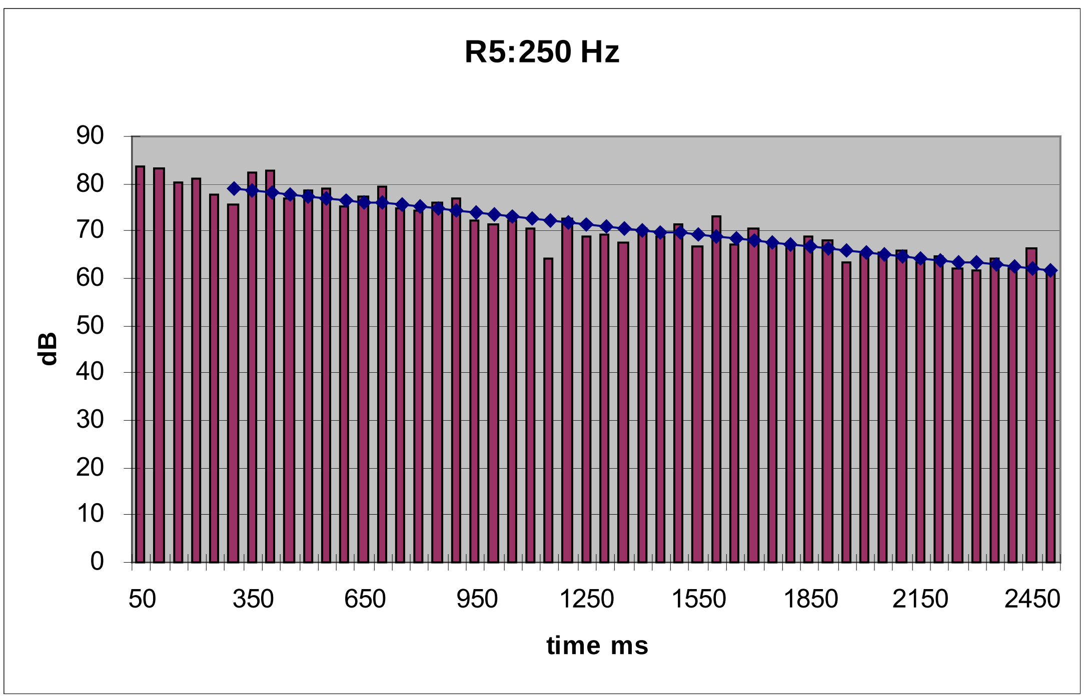

Figure A.37 Decay and Fit for T30 for 125 and 250 Hz at R5S1 in Süleymaniye.

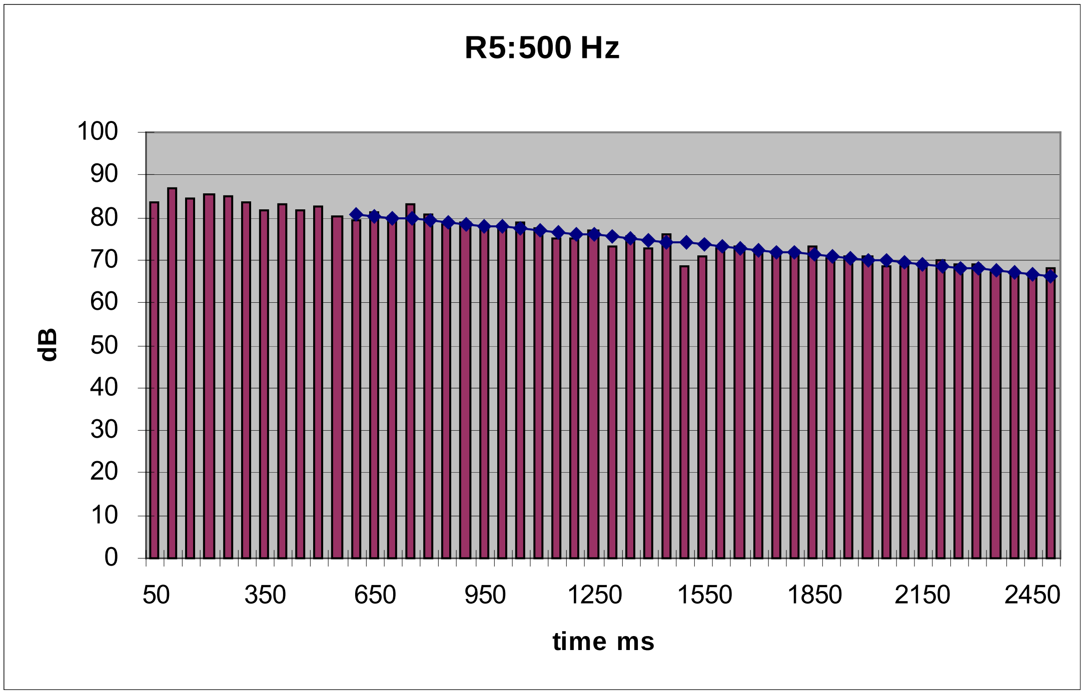

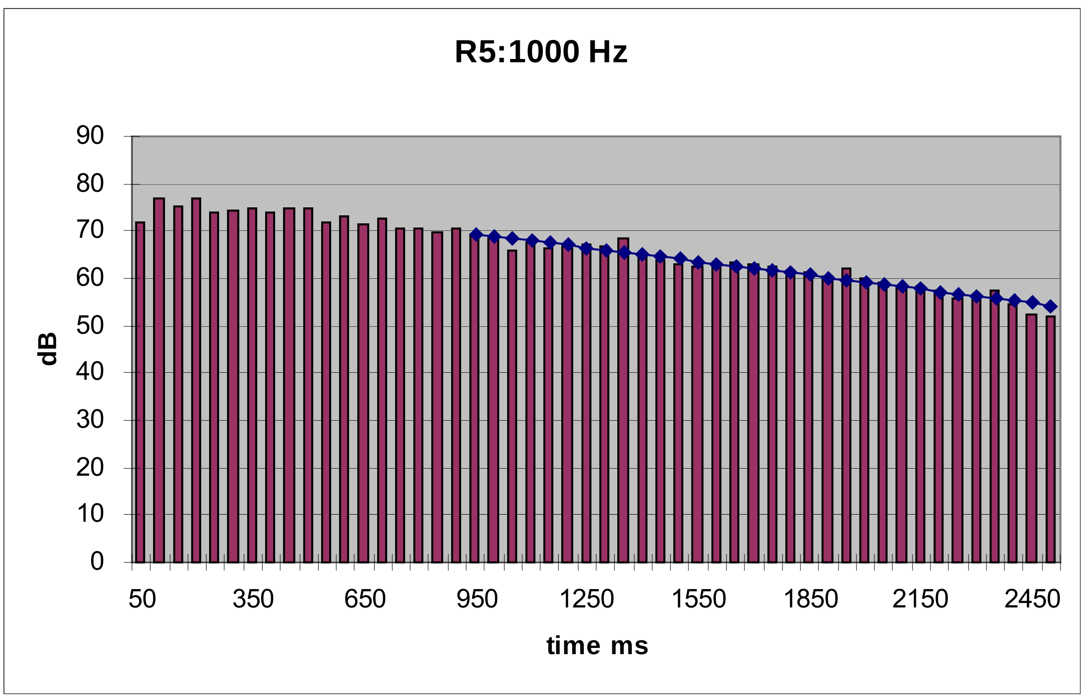

Figure A.38 Decay and Fit for T30 for 500 and 1000 Hz at R5S1 in Süleymaniye.

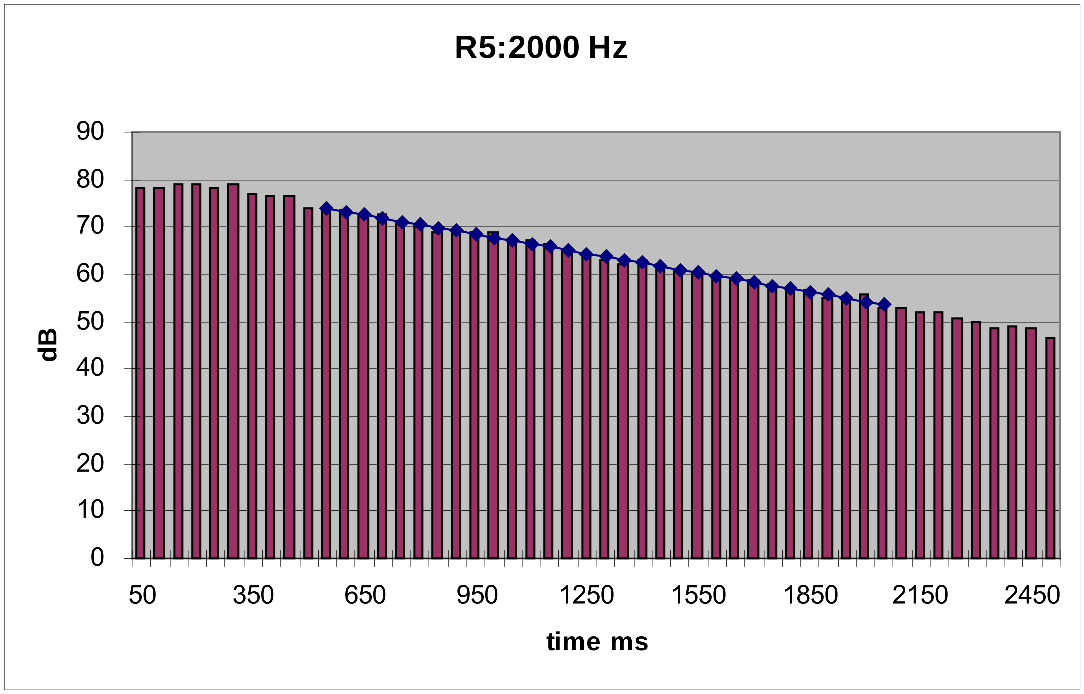

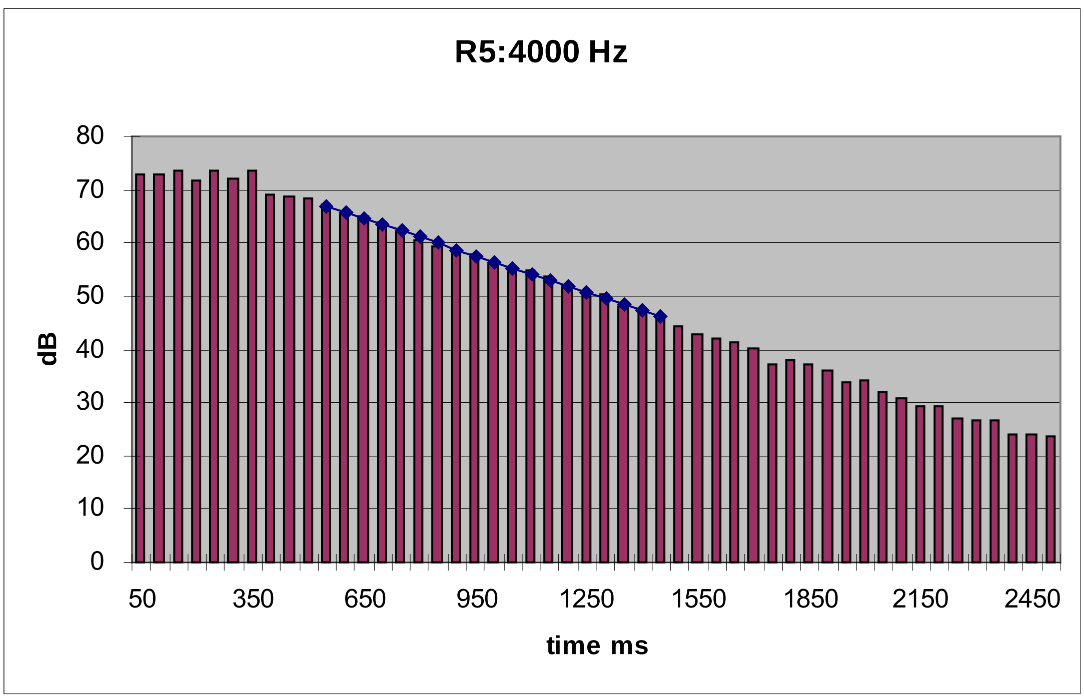

Figure A.39 Decay and Fit for T30 for 2 and 4 kHz at R5S1 in Süleymaniye.

Table A.14 Measurements at R6 in Süleymaniye

time	dB					
ms	125	250	500	1000	2000	4000
50	74.46	81.94	82.34	75.99	81.28	76.69
100	82.10	80.64	85.75	79.37	81.04	76.36
150	85.86	79.23	86.66	77.66	79.68	77.59
200	86.48	82.17	84.38	77.23	81.09	77.96
250	82.38	85.79	86.78	76.55	81.14	76.27
300	87.49	84.62	86.52	77.37	80.78	76.29
350	85.32	76.03	87.37	78.50	80.13	76.03
400	83.23	82.12	83.39	73.80	75.82	71.07
450	81.40	75.23	83.11	74.62	75.61	67.10
500	79.56	78.53	83.25	73.00	73.66	68.16
550	81.11	74.86	79.89	72.25	73.35	66.93
600	83.25	77.37	82.10	71.21	73.73	65.50
650	81.47	75.40	78.57	72.55	75.26	65.24
700	80.03	75.21	79.00	73.09	72.72	63.19
750	78.31	76.57	78.69	70.98	71.00	62.28
800	73.14	73.71	81.72	71.35	71.09	61.26
850	69.78	72.51	80.20	68.13	72.72	60.98
900	79.42	73.71	82.12	68.30	69.52	59.36
950	80.74	73.94	80.93	70.37	69.21	58.63
1000	75.12	78.06	80.71	68.51	68.74	56.54
1050	77.87	73.00	79.00	66.51	67.28	55.55
1100	75.75	77.16	75.16	67.61	66.72	54.21
1150	75.19	74.55	75.49	66.25	66.41	52.16
1200	74.58	73.35	77.47	65.33	63.97	51.48
1250	71.05	72.22	76.15	66.37	64.63	50.96
1300	72.41	72.44	75.99	65.94	63.76	50.14
1350	79.82	72.67	76.57	65.62	63.10	50.00
1400	72.25	67.19	76.60	64.25	63.15	45.23
1450	79.56	71.89	74.22	62.72	60.68	46.85
1500	72.74	71.49	74.53	64.74	60.65	43.93
1550	77.47	70.27	77.33	62.89	58.96	42.83
1600	78.13	66.34	75.07	62.30	59.50	44.21
1650	71.05	70.30	73.19	62.39	60.70	42.99
1700	73.14	66.89	74.60	59.62	57.57	41.46
1750	70.48	68.67	71.78	62.86	58.40	38.05
1800	73.63	65.57	74.06	60.18	55.08	37.98
1850	71.52	65.14	69.45	57.01	57.36	37.65
1900	69.00	61.83	73.31	58.89	56.70	35.86
1950	75.23	64.51	71.78	59.71	55.36	34.74
2000	68.34	62.70	71.31	58.61	54.96	32.95
2050	73.26	64.39	70.95	57.88	52.70	32.97
2100	71.99	64.23	69.80	57.52	51.46	31.07
2150	73.47	62.79	71.21	57.03	51.22	31.49
2200	69.45	61.62	70.39	57.92	51.53	29.54
2250	65.62	60.94	70.98	56.56	51.29	27.80
2300	69.26	62.51	68.79	53.79	50.82	26.83
2350	68.91	64.49	66.67	55.81	48.75	25.68
2400	66.41	60.32	70.46	52.40	48.31	26.79
2450	67.28	63.38	67.59	55.46	46.92	25.16
2500	65.94	63.33	68.67	54.51	47.86	24.58

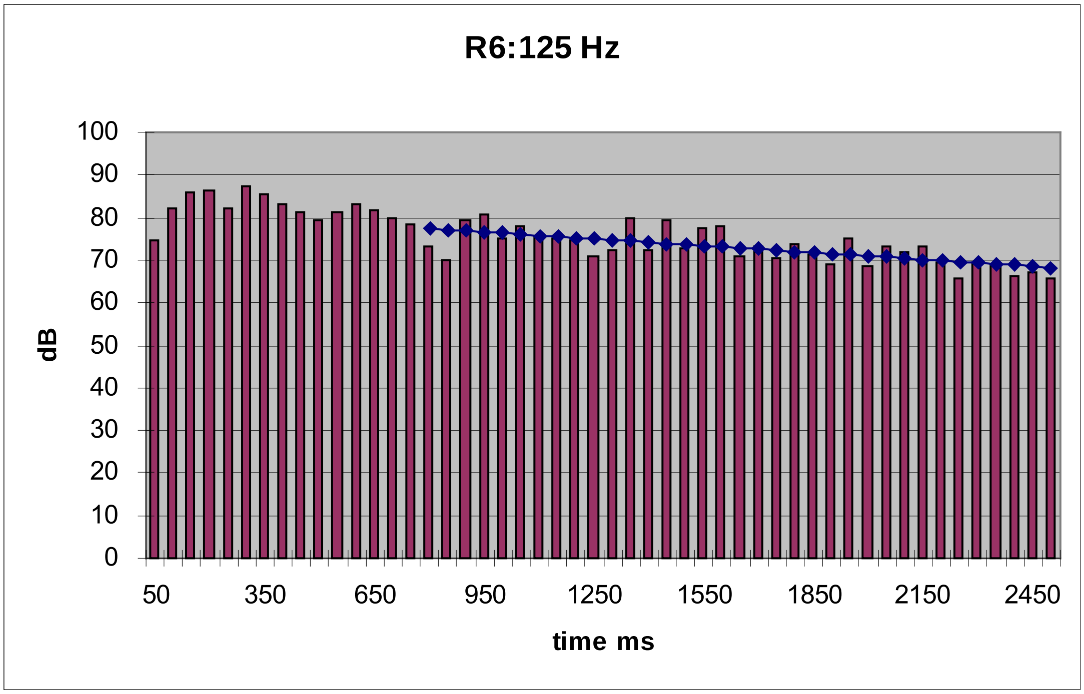

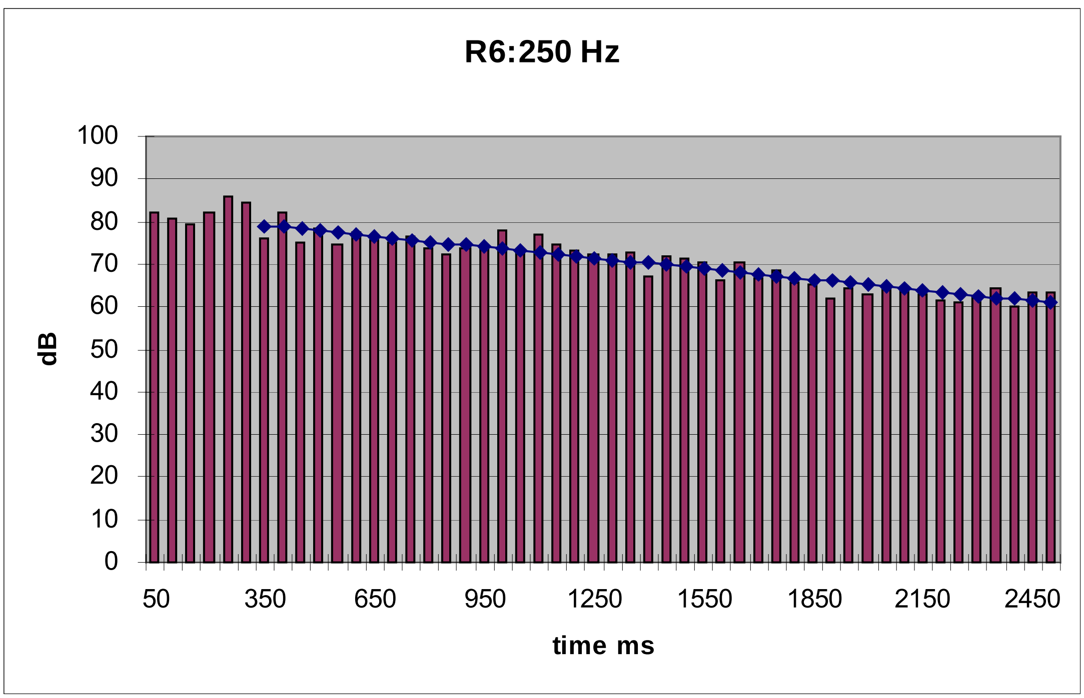

Figure A.40 Decay and Fit for T30 for 125 and 250 Hz at R6S1 in Süleymaniye.

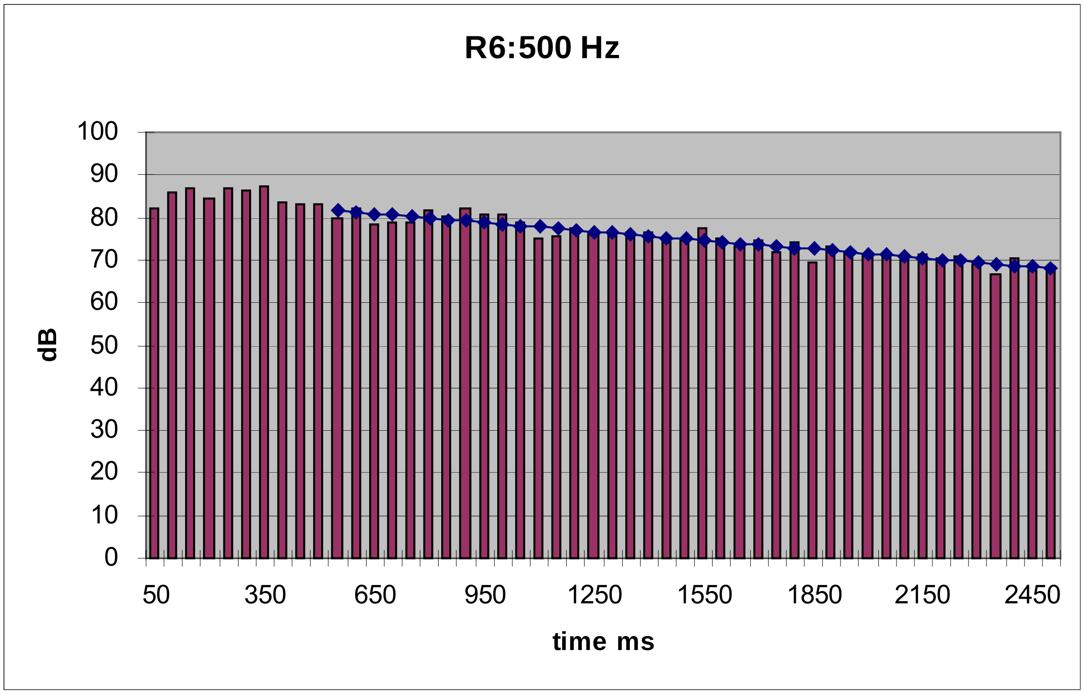

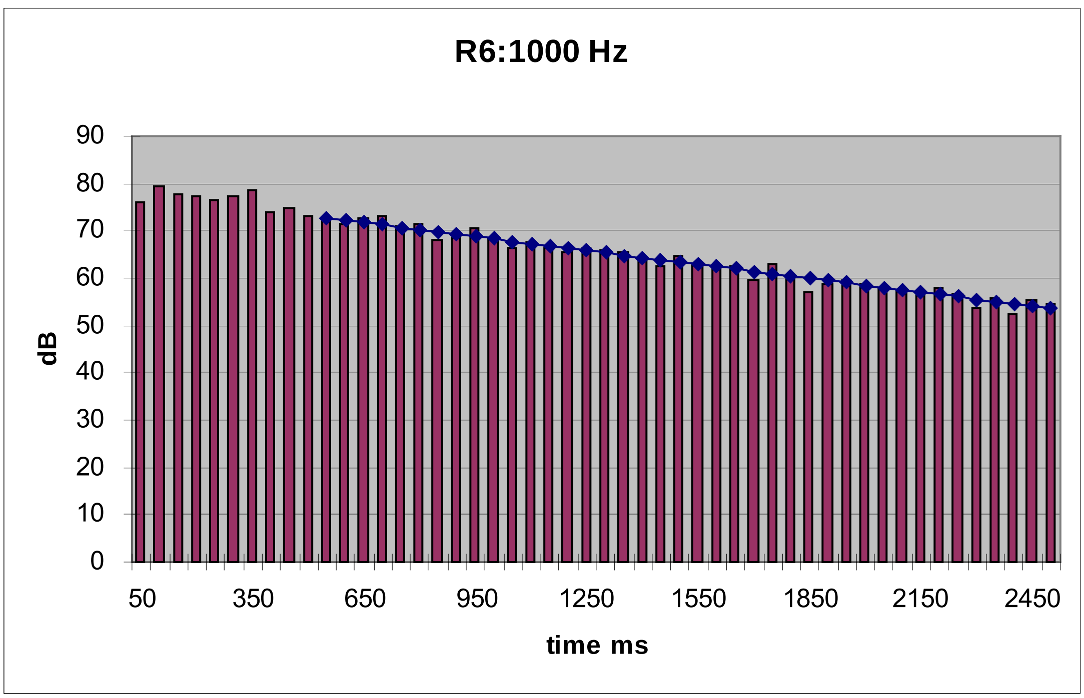

Figure A.41 Decay and Fit for T30 for 500 and 1000 Hz at R6S1 in Süleymaniye.

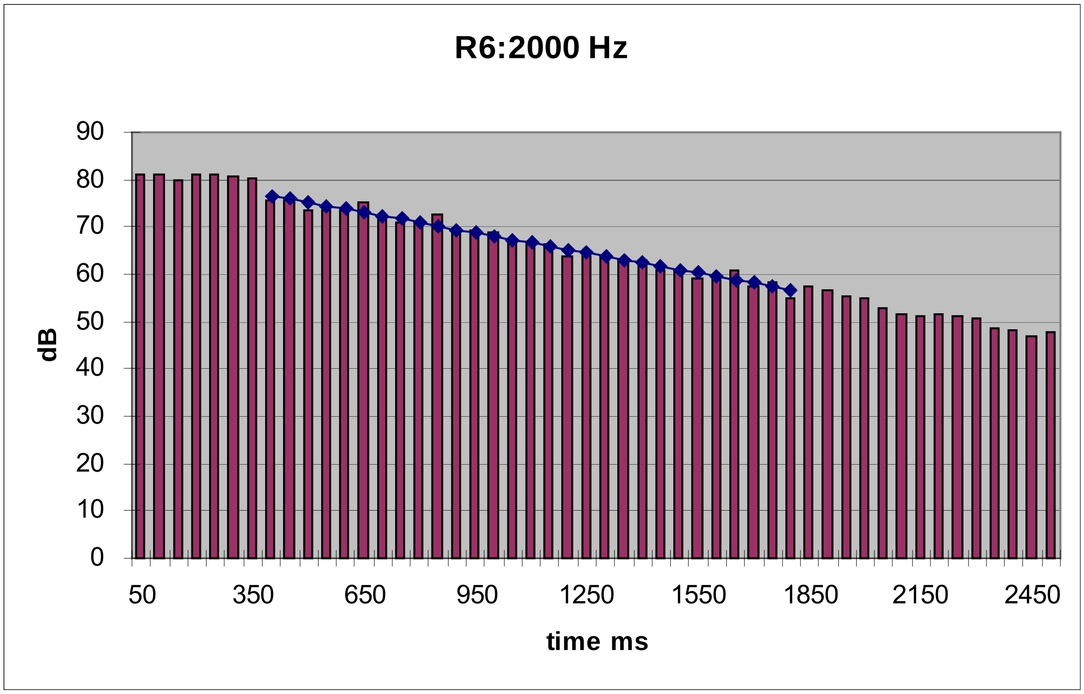

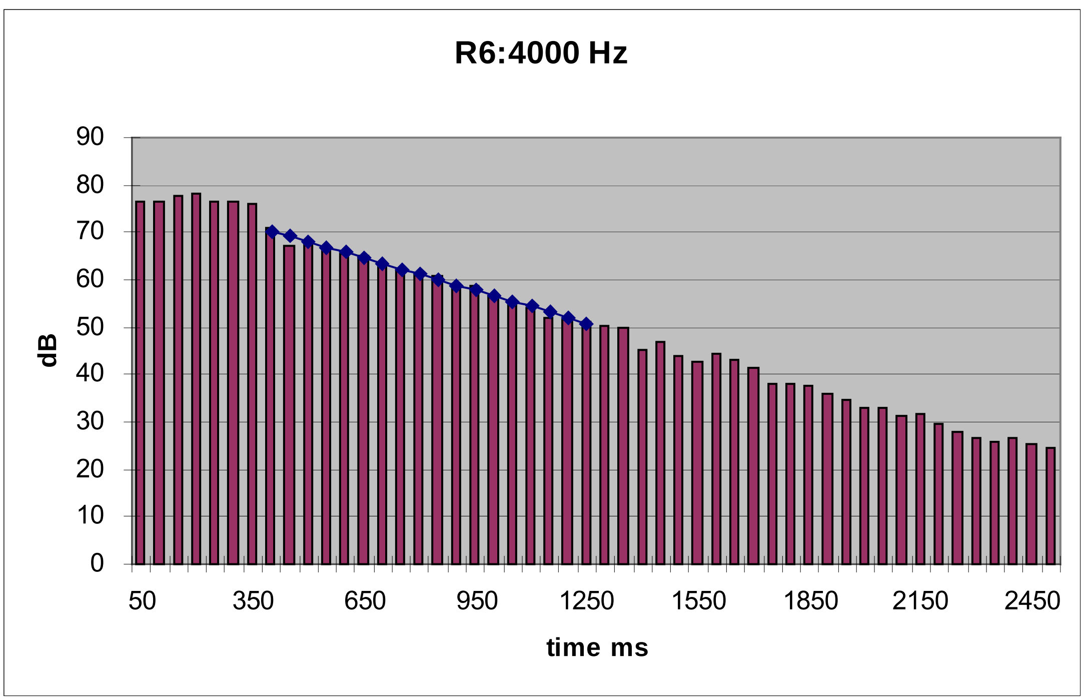

Figure A.42 Decay and Fit for T30 for 2 and 4 kHz at R6S1 in Süleymaniye.

Table A.15 Measurements at R1S2 in Süleymaniye

time	dB					
ms	125	250	500	1000	2000	4000
50	81.00	77.87	82.83	73.23	77.54	71.96
100	77.23	79.42	83.11	73.63	78.10	71.05
150	77.35	81.21	82.01	74.74	77.23	72.72
200	80.76	81.56	82.36	70.62	77.94	72.79
250	83.39	76.15	83.98	73.40	77.02	71.87
300	83.14	78.41	81.35	73.96	76.76	73.68
350	79.80	79.89	82.81	73.68	77.89	73.40
400	84.88	73.09	82.67	75.26	74.06	68.20
450	75.19	71.73	80.45	72.79	74.53	66.20
500	76.46	78.50	80.76	70.93	74.06	66.89
550	81.14	77.37	80.95	73.87	72.44	66.56
600	77.75	77.70	81.14	72.04	73.14	65.33
650	70.37	76.65	82.36	73.56	72.93	65.54
700	78.93	71.12	81.09	71.07	71.52	63.59
750	78.01	73.33	80.27	72.15	71.05	63.19
800	76.48	73.40	78.95	71.78	70.86	61.41
850	72.27	71.68	80.03	70.44	70.44	59.29
900	75.28	69.05	77.44	71.35	69.31	58.40
950	74.46	69.52	79.30	68.58	69.43	57.97
1000	77.96	73.19	78.60	69.82	68.32	56.28
1050	73.94	70.69	78.74	69.17	67.85	55.62
1100	80.55	68.86	71.87	66.56	65.71	55.55
1150	75.82	72.76	78.55	67.45	65.66	52.66
1200	74.43	71.85	77.59	68.44	65.03	53.01
1250	70.46	73.52	75.85	66.60	63.73	51.46
1300	76.27	69.92	75.54	65.19	63.45	50.49
1350	67.94	70.95	79.42	64.23	63.85	48.02
1400	74.95	69.47	75.45	62.53	61.52	47.51
1450	70.46	68.55	76.25	64.77	62.91	45.39
1500	72.34	71.12	74.50	63.29	62.65	43.25
1550	73.28	67.94	72.53	63.40	59.38	43.96
1600	73.80	69.57	74.08	61.03	59.19	41.67
1650	70.27	68.44	71.68	62.84	59.99	41.53
1700	71.14	66.25	71.14	62.11	57.27	40.36
1750	67.21	72.58	75.12	61.83	58.51	39.56
1800	68.63	68.86	73.68	60.79	58.23	37.37
1850	68.32	65.73	72.67	62.04	56.28	36.83
1900	66.60	68.04	71.35	60.44	56.09	36.45
1950	71.09	64.23	73.45	60.39	56.47	34.05
2000	70.79	67.80	72.62	58.21	54.26	34.62
2050	69.10	63.15	73.54	55.57	52.54	33.23
2100	67.61	61.64	70.44	59.45	53.15	30.29
2150	67.54	60.68	70.34	57.67	51.95	30.39
2200	70.44	65.73	71.33	56.07	52.56	30.62
2250	72.06	66.18	67.43	55.74	50.33	27.52
2300	67.36	64.25	69.43	54.42	50.21	26.90
2350	70.44	61.41	66.96	55.13	48.75	25.61
2400	70.74	65.85	69.66	53.93	48.71	26.34
2450	67.38	61.76	69.57	53.50	47.32	24.98
2500	67.21	64.09	65.71	52.40	45.81	24.93

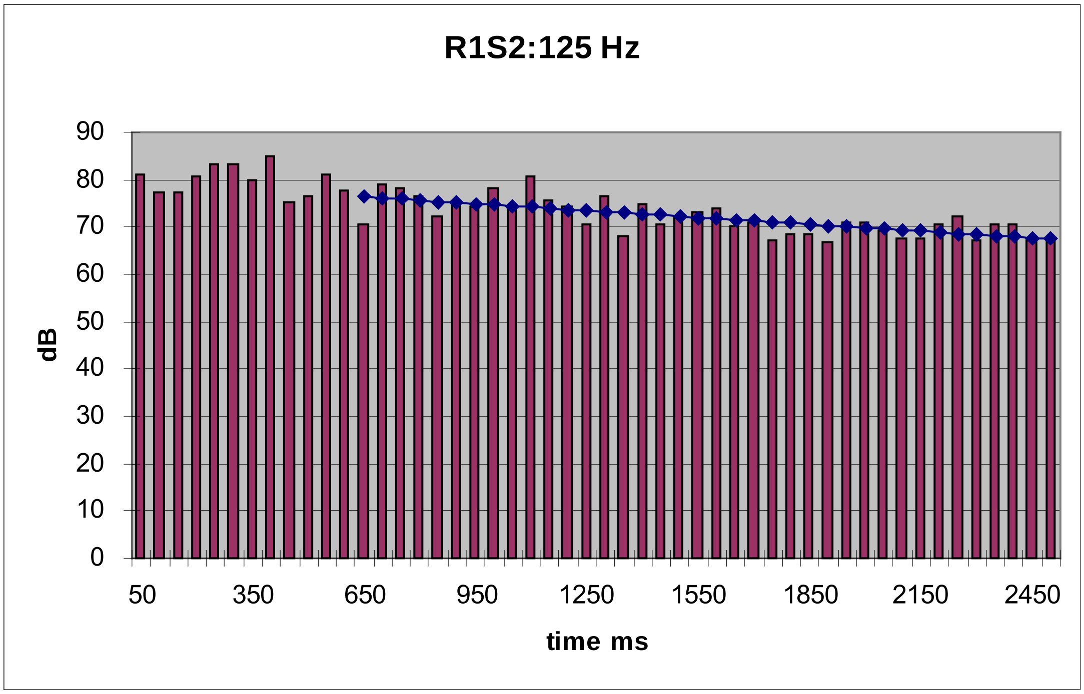

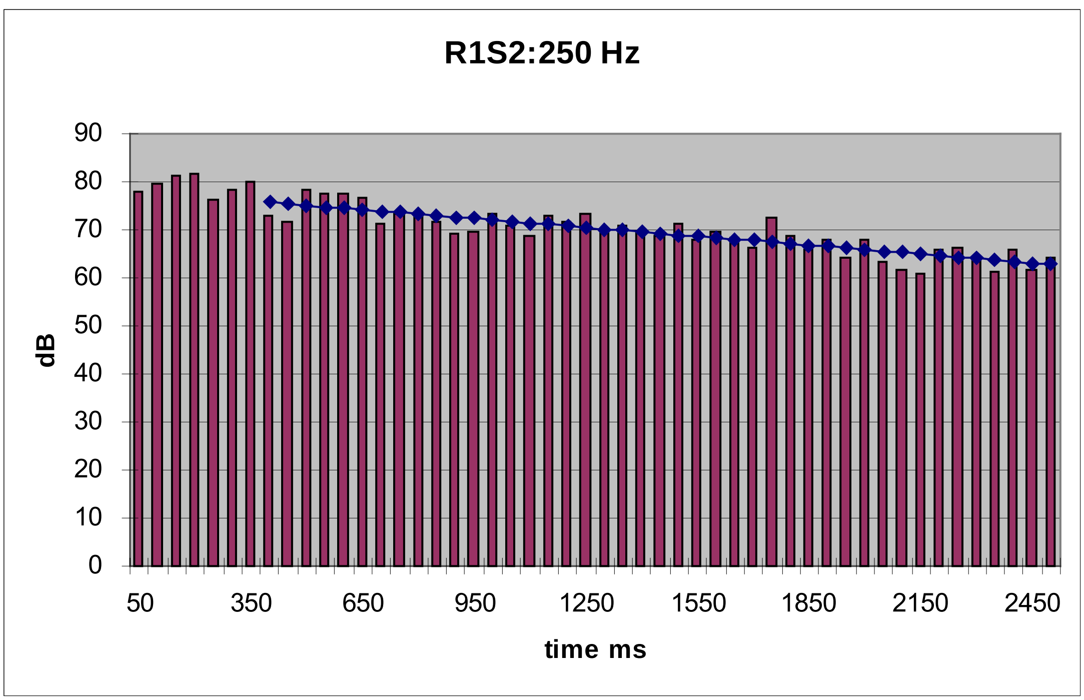

Figure A.43 Decay and Fit for T30 for 125 and 250 Hz at R1S2 in Süleymaniye.

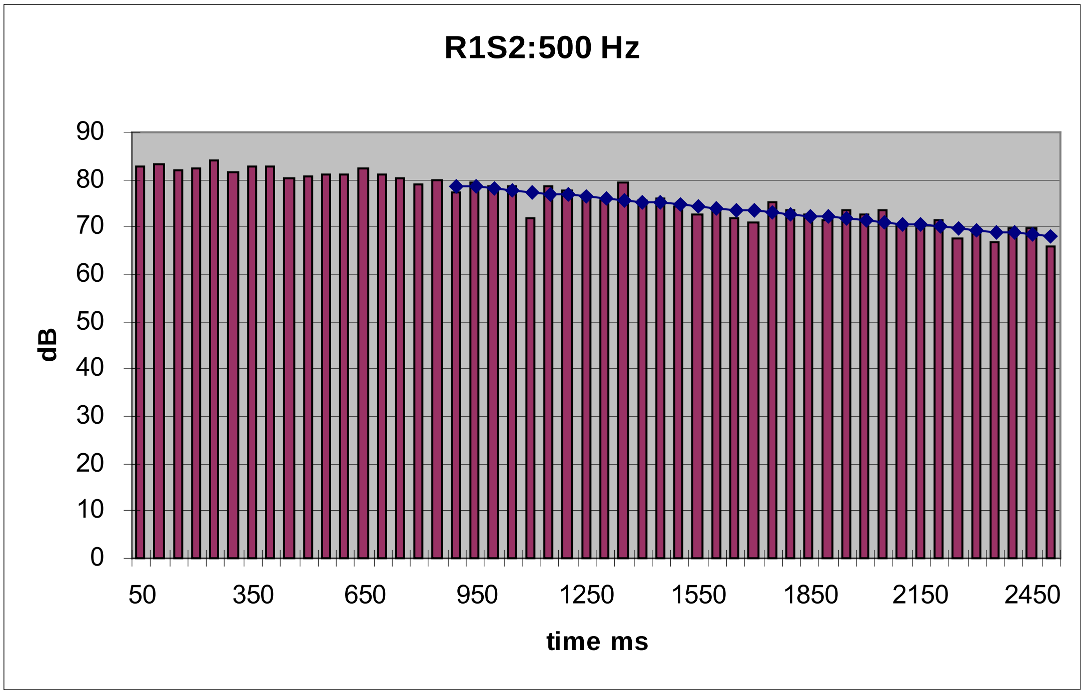

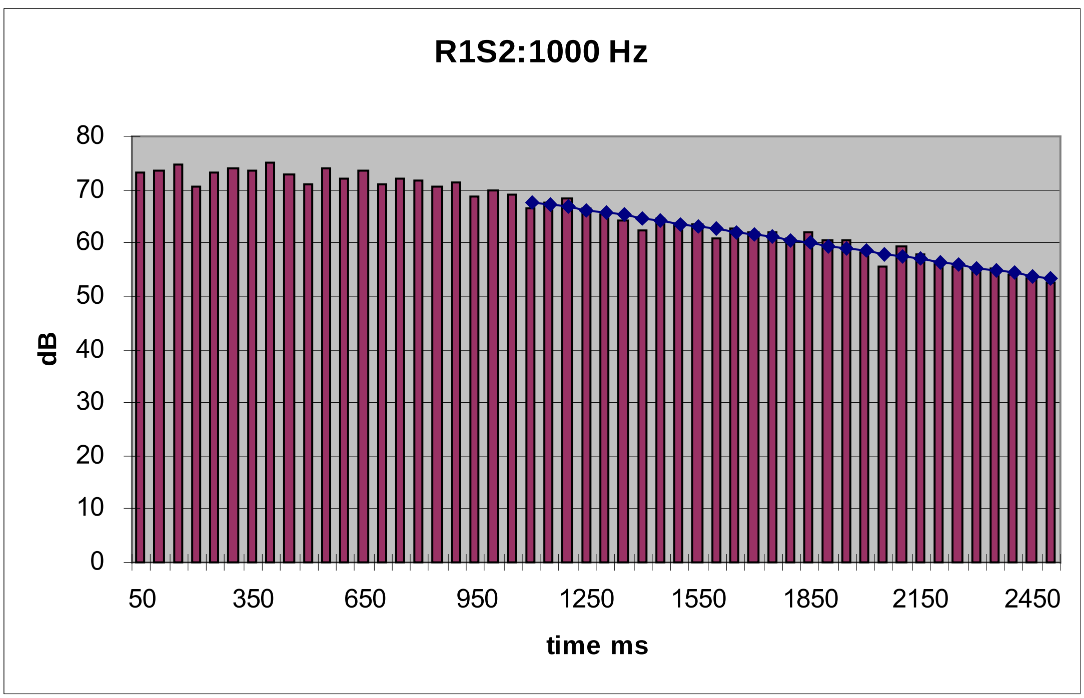

Figure A.44 Decay and Fit for T30 for 500 and 1000 Hz at R1S2 in Süleymaniye.

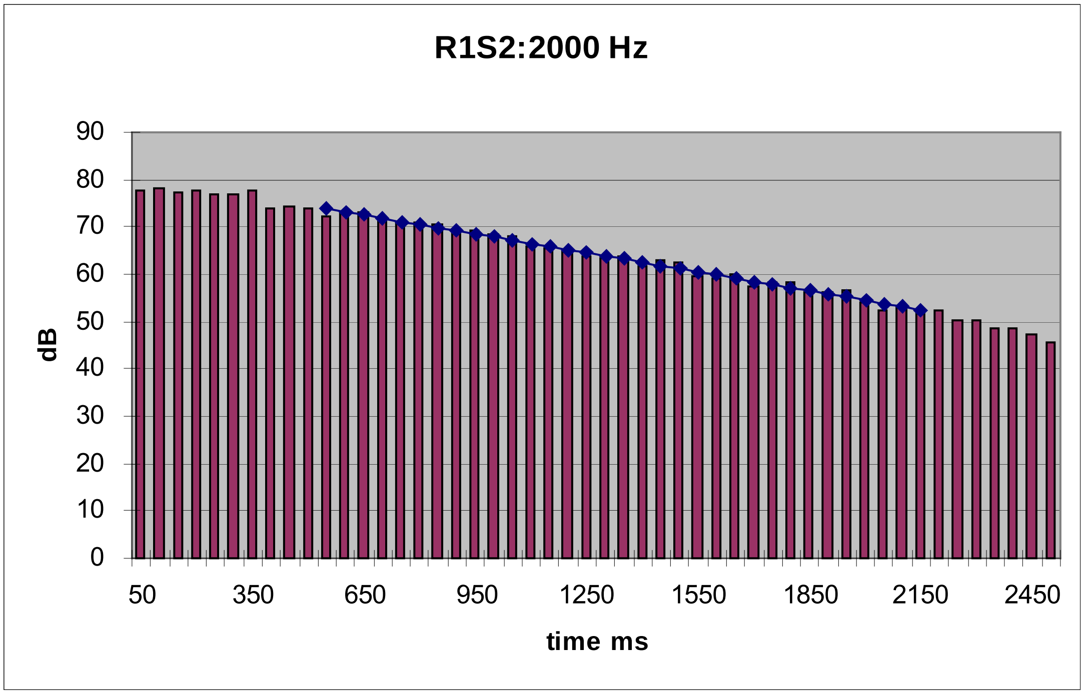

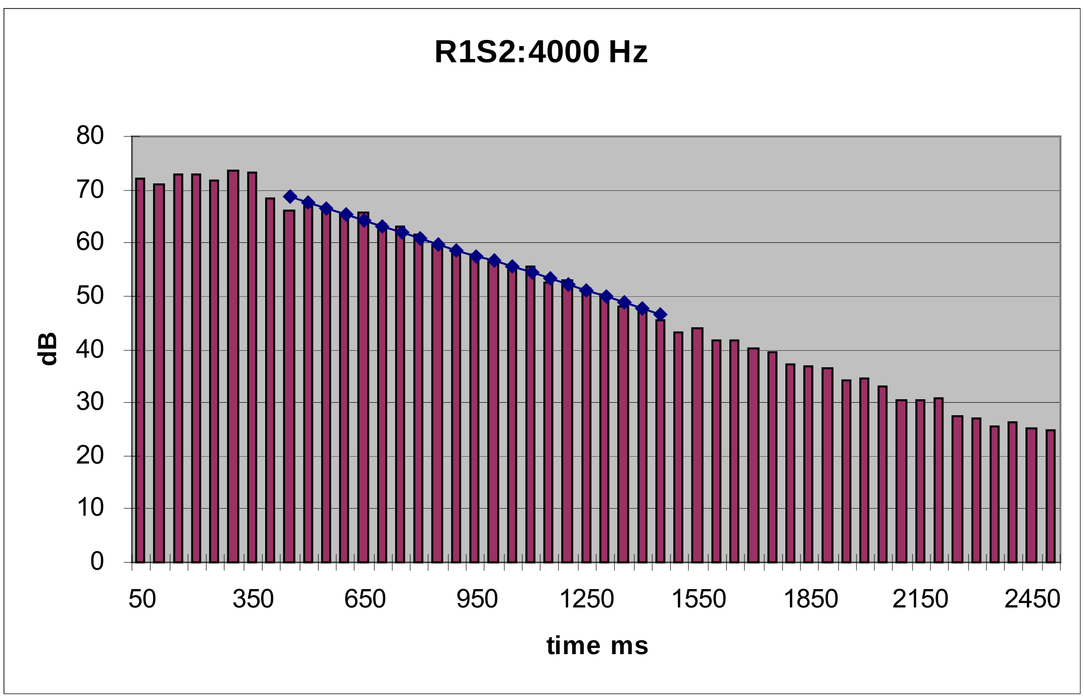

Figure A.45 Decay and Fit for T30 for 2 and 4 kHz at R1S2 in Süleymaniye.

Table A.16 Measurements at R2S2 in Süleymaniye

time	dB					
ms	125	250	500	1000	2000	4000
50	86.80	79.75	83.87	74.20	77.56	72.67
100	80.83	83.79	82.92	73.87	76.65	74.18
150	84.12	77.87	81.98	74.46	77.04	74.67
200	83.16	79.37	82.88	75.33	78.48	74.11
250	83.39	81.98	82.29	73.23	78.83	72.51
300	76.20	82.97	83.89	73.52	78.03	74.58
350	81.91	79.49	81.89	73.78	76.03	74.22
400	85.72	81.70	81.28	72.67	76.08	70.01
450	72.22	77.19	84.52	73.00	75.33	68.32
500	76.57	73.75	78.20	73.19	75.66	67.68
550	78.06	75.09	80.34	73.94	75.30	67.21
600	77.07	65.31	80.43	74.01	71.05	65.90
650	75.80	76.67	80.74	73.82	74.18	64.39
700	81.44	76.74	81.14	70.67	73.40	64.98
750	79.16	73.49	77.68	72.04	71.87	63.66
800	79.33	74.01	78.71	70.37	71.07	61.99
850	72.41	75.87	77.59	68.23	70.93	60.25
900	71.07	74.86	77.40	69.28	69.10	59.78
950	75.96	73.23	73.68	68.25	69.07	58.18
1000	72.67	72.36	79.75	68.91	66.86	56.77
1050	77.61	70.86	76.90	68.30	67.10	55.88
1100	77.28	73.52	76.97	68.44	66.25	53.69
1150	74.15	68.18	78.64	65.90	66.79	53.62
1200	79.68	72.48	77.84	66.98	65.90	52.68
1250	76.76	67.50	76.62	65.29	63.19	50.14
1300	70.84	74.83	76.60	66.91	65.03	50.23
1350	74.53	72.22	71.42	65.00	60.75	48.19
1400	74.53	72.88	74.22	65.94	61.99	47.18
1450	77.37	72.25	73.47	65.43	61.15	46.14
1500	77.23	69.78	75.45	64.42	62.11	44.35
1550	71.40	72.65	73.63	61.48	60.79	44.75
1600	78.34	69.03	75.99	60.14	61.62	42.92
1650	74.01	69.33	76.20	60.06	58.47	41.20
1700	68.18	70.30	73.47	60.11	58.84	41.44
1750	71.94	70.60	73.49	60.32	58.70	37.53
1800	70.72	68.81	71.71	60.77	57.13	38.66
1850	66.60	65.14	72.60	58.02	56.00	38.12
1900	73.38	68.67	69.82	58.91	55.22	34.29
1950	66.58	68.46	70.58	58.25	55.41	34.43
2000	67.19	66.51	70.91	58.58	54.73	34.81
2050	65.03	63.15	70.58	58.79	52.87	33.07
2100	66.18	64.58	68.95	57.22	53.43	31.51
2150	69.07	68.20	70.25	56.61	50.33	30.39
2200	63.12	65.78	70.30	55.20	49.62	29.47
2250	69.19	68.46	69.90	57.60	51.27	28.06
2300	63.85	62.53	70.65	56.30	50.99	27.14
2350	67.03	66.70	69.73	56.09	48.96	25.40
2400	69.17	61.52	69.64	53.39	49.86	26.34
2450	70.37	58.14	66.53	54.42	48.80	24.08
2500	67.61	57.90	65.57	53.79	45.98	24.48

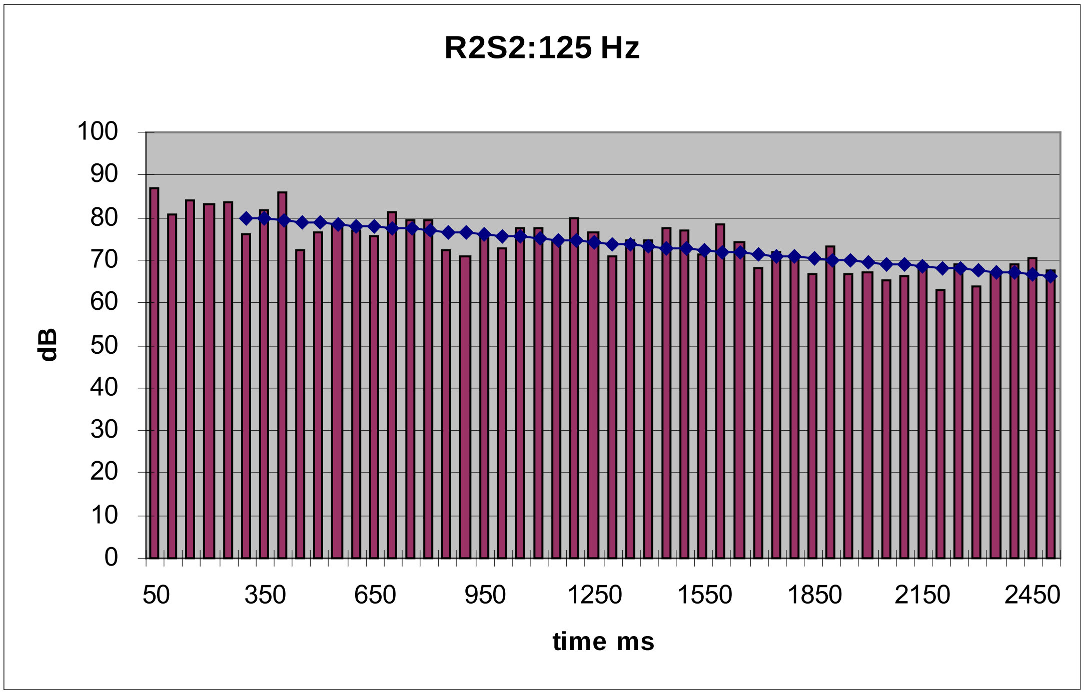

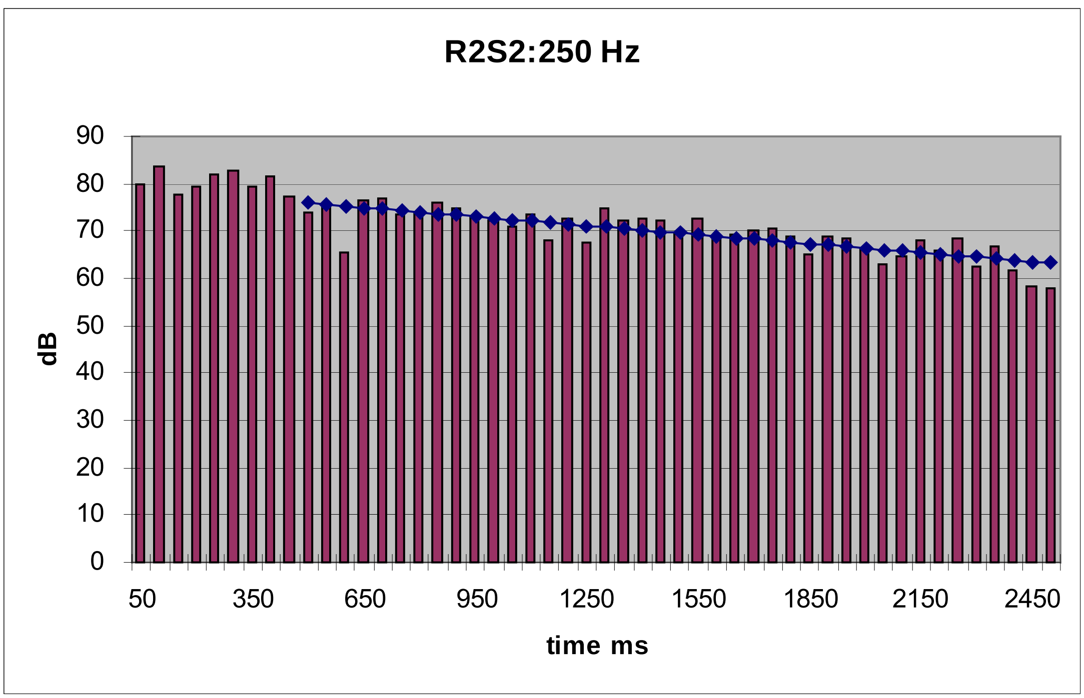

Figure A.46 Decay and Fit for T30 for 125 and 250 Hz at R2S2 in Süleymaniye.

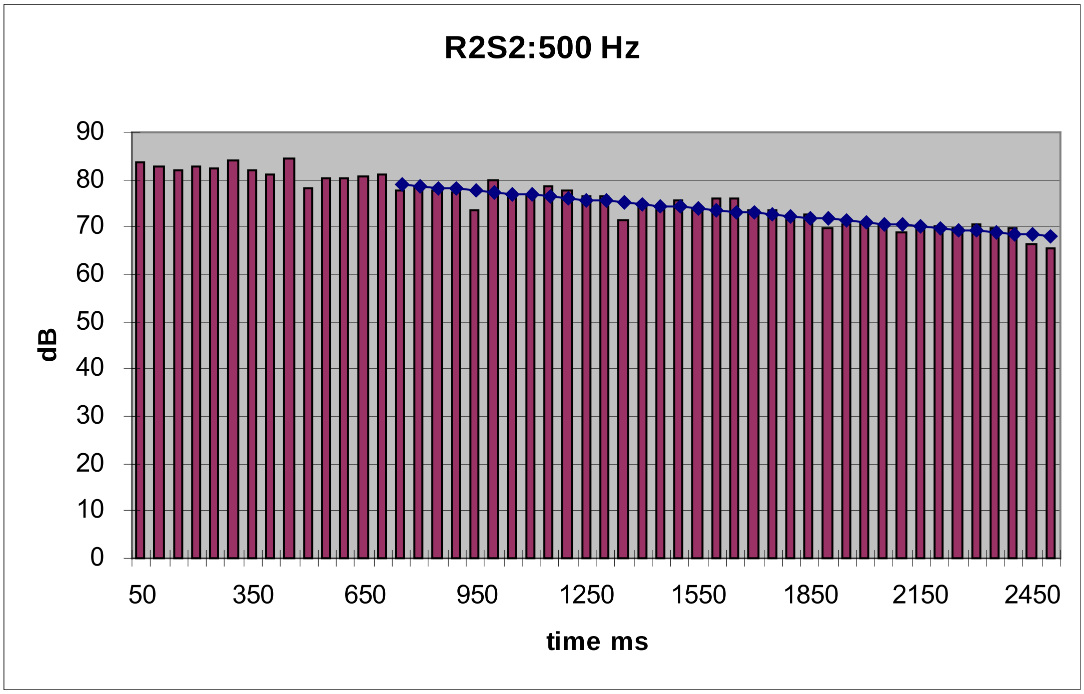

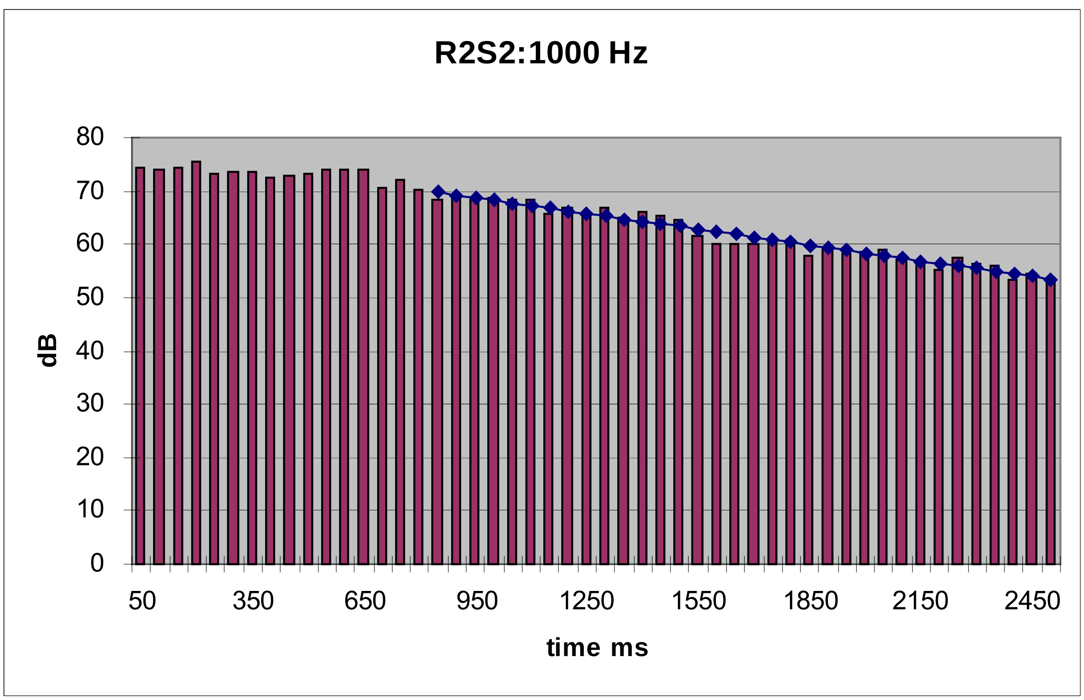

Figure A.47 Decay and Fit for T30 for 500 and 1000 Hz at R2S2 in Süleymaniye.

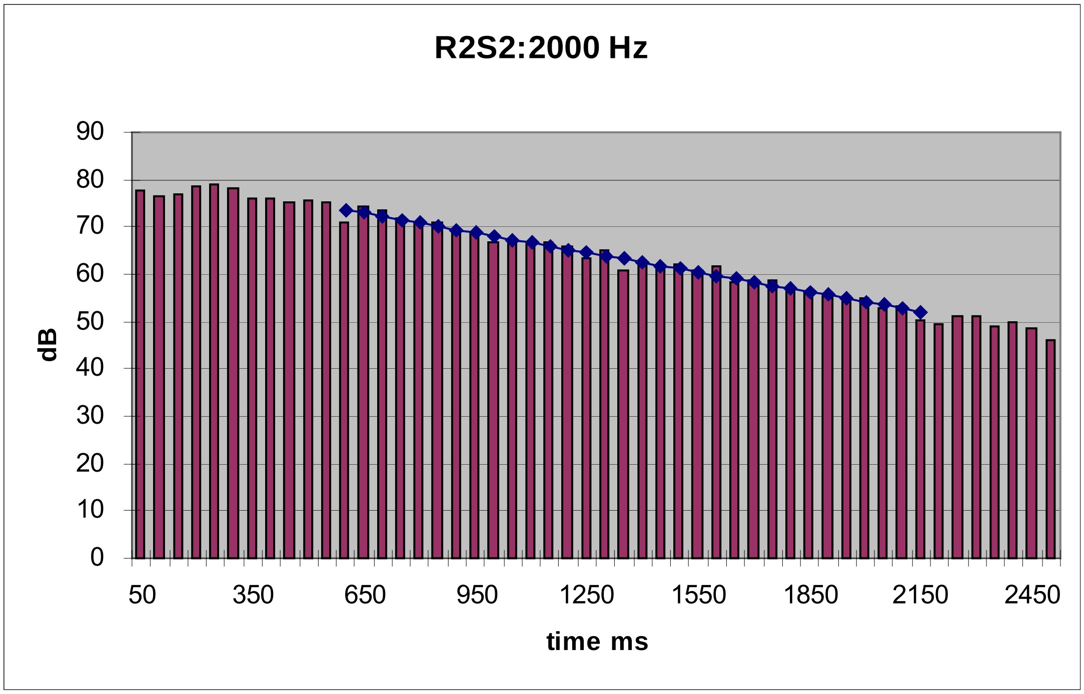

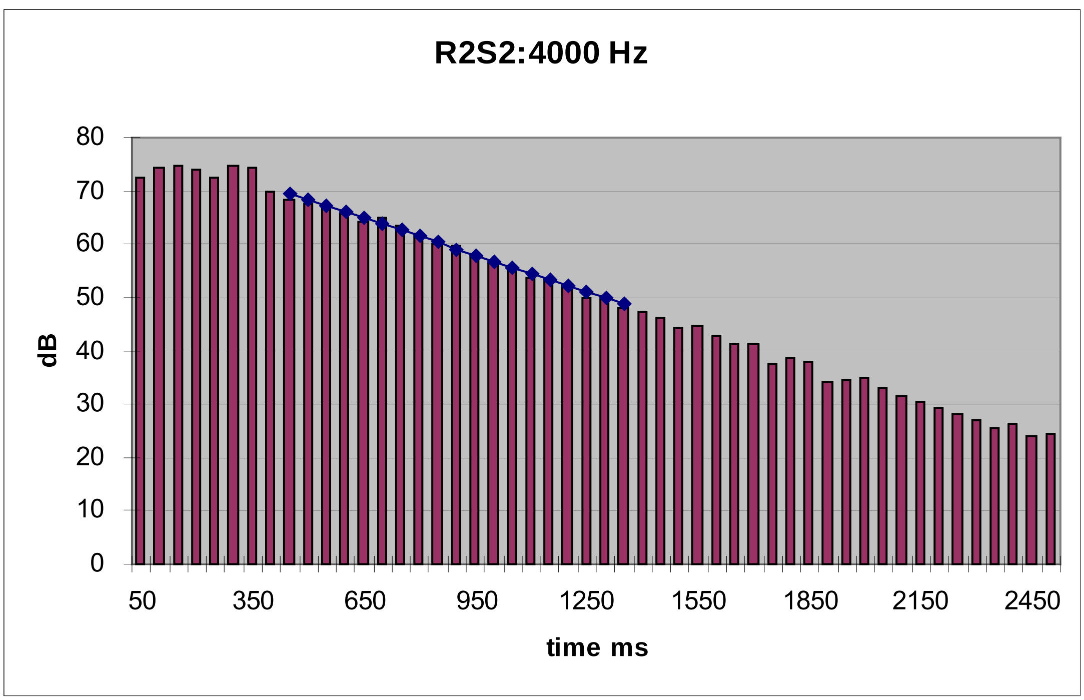

Figure A.48 Decay and Fit for T30 for 2 and 4 kHz at R2S2 in Süleymaniye.

Table A.17 Measurements at R1 in Rüstem Pasa

time	dB					
ms	125	250	500	1000	2000	4000
50	67.64	75.94	79.98	71.59	76.10	72.04
100	72.76	78.15	80.36	70.77	74.29	71.80
150	74.83	77.56	76.81	71.28	72.46	72.62
200	69.78	76.43	79.09	72.08	74.01	73.56
250	79.14	77.70	80.06	72.11	74.60	72.58
300	72.93	77.94	73.56	70.65	74.08	72.55
350	65.94	78.15	78.01	71.07	73.59	72.74
400	75.30	73.35	79.16	69.17	74.13	68.86
450	74.41	73.09	74.06	69.87	72.46	67.57
500	76.57	68.20	72.91	71.24	71.82	67.47
550	72.41	72.08	77.63	71.78	70.65	64.56
600	71.19	73.47	75.30	69.80	69.54	61.78
650	70.95	69.19	76.29	67.03	68.91	60.25
700	72.15	70.20	74.50	67.24	65.80	59.55
750	72.29	72.91	75.23	66.53	65.97	57.27
800	72.67	71.75	72.74	66.34	66.67	56.28
850	73.23	70.98	70.55	65.73	65.80	53.97
900	68.74	69.59	72.13	63.55	63.66	51.95
950	65.38	68.55	72.25	63.64	62.23	50.96
1000	61.95	66.16	69.03	64.02	61.15	49.88
1050	65.10	66.53	71.33	61.76	61.26	47.32
1100	66.56	67.97	67.61	59.83	57.74	47.15
1150	69.47	64.46	70.51	59.43	59.55	46.05
1200	68.77	68.41	68.41	57.76	58.77	42.99
1250	65.85	64.20	66.44	58.94	56.42	41.02
1300	59.88	64.84	66.60	57.29	55.31	39.42
1350	64.32	63.45	67.50	59.34	54.21	39.49
1400	60.61	62.32	64.70	57.48	53.22	37.61
1450	57.41	60.77	63.43	53.36	52.89	36.19
1500	62.86	60.89	63.71	56.84	50.92	34.17
1550	60.51	61.08	61.81	53.36	50.23	31.42
1600	62.68	59.50	62.93	51.25	47.04	30.43
1650	63.15	61.31	61.55	51.72	46.07	29.61
1700	63.90	63.69	60.94	47.76	46.26	28.64
1750	60.14	60.16	62.11	49.58	45.15	26.43
1800	59.05	59.95	61.08	50.14	44.57	25.26
1850	57.15	58.61	59.22	48.59	43.51	24.04
1900	60.35	60.46	59.19	45.79	42.26	23.47
1950	59.38	62.09	57.08	45.15	41.42	20.70
2000	55.17	59.08	54.56	46.26	41.46	21.75
2050	50.92	55.34	56.42	45.04	40.43	20.34
2100	54.91	52.89	51.55	43.51	38.05	19.45
2150	47.91	54.16	55.41	44.03	37.93	17.97
2200	55.22	55.43	55.24	41.56	37.25	20.41
2250	60.89	52.16	54.04	42.94	37.09	17.97
2300	51.10	51.22	51.88	42.40	33.51	17.73
2350	54.68	54.09	52.37	38.50	33.77	17.07
2400	53.46	55.08	52.42	37.91	32.78	15.03
2450	50.96	52.80	53.57	37.53	29.94	16.79
2500	53.50	52.00	49.95	36.36	30.41	16.58

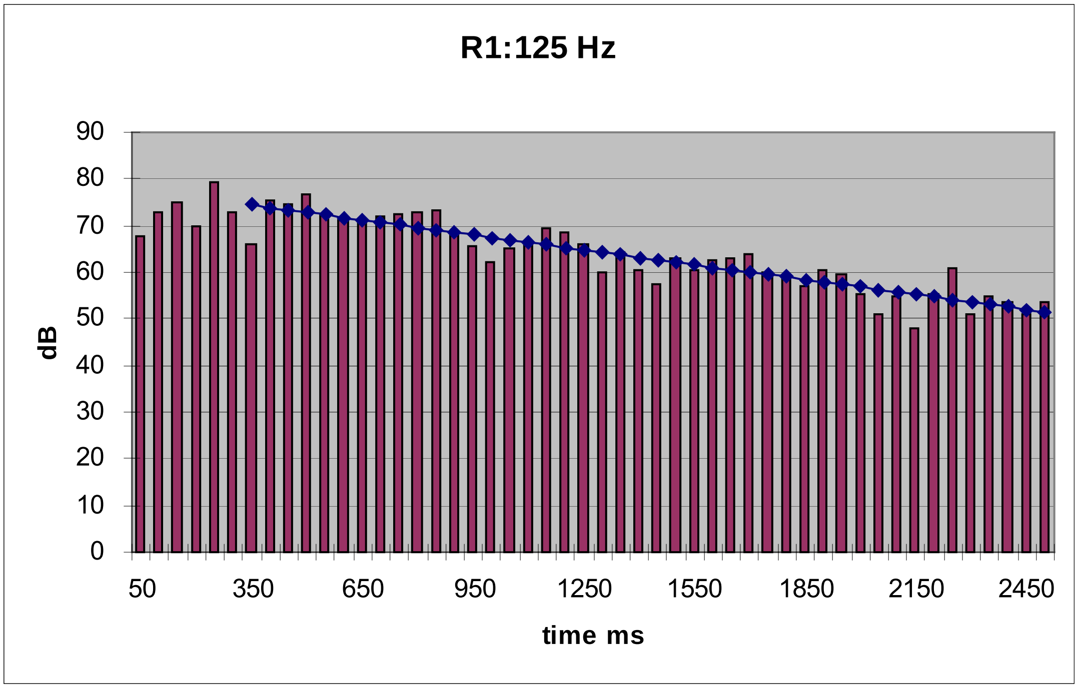

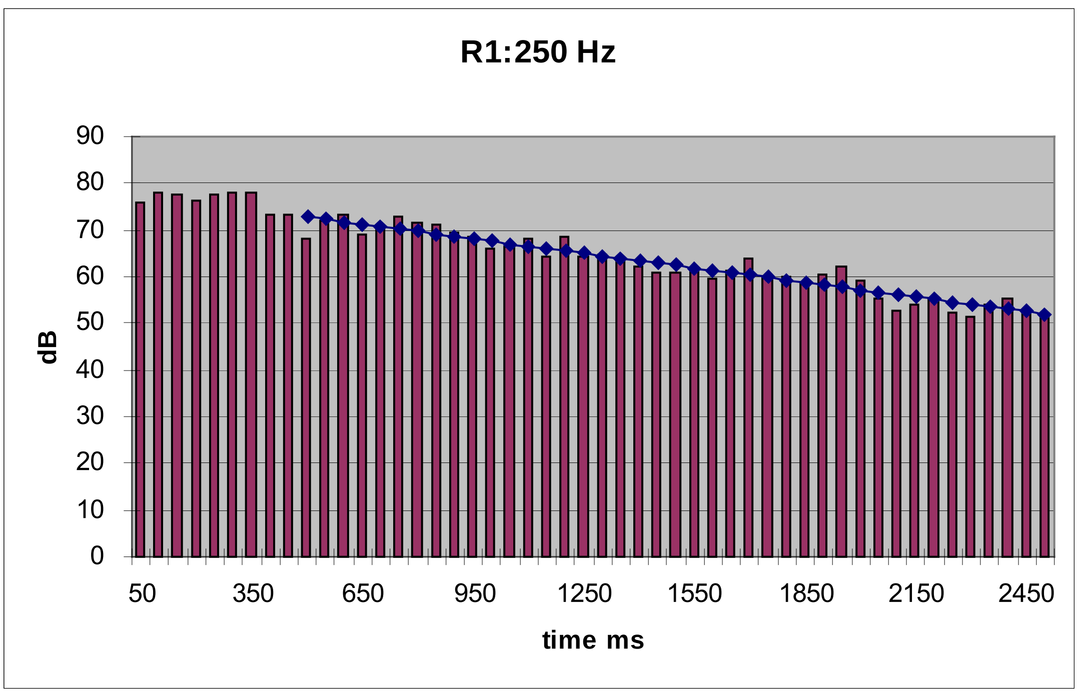

Figure A.49 Decay and Fit for T30 for 125 and 250 Hz at R1 in Rüstem Pasa

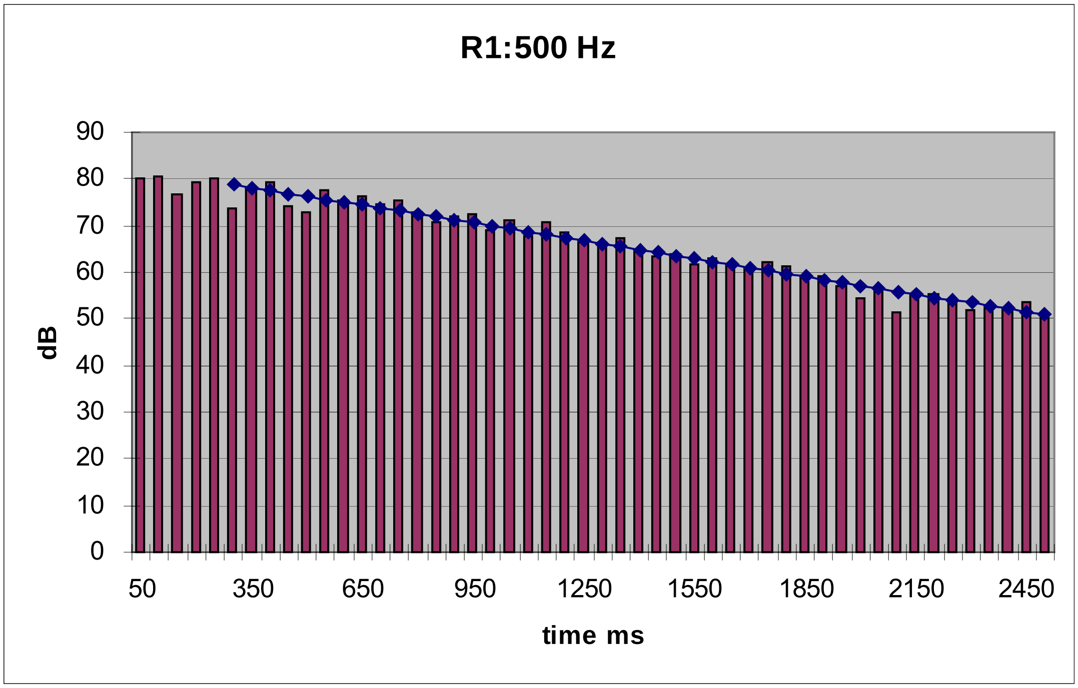

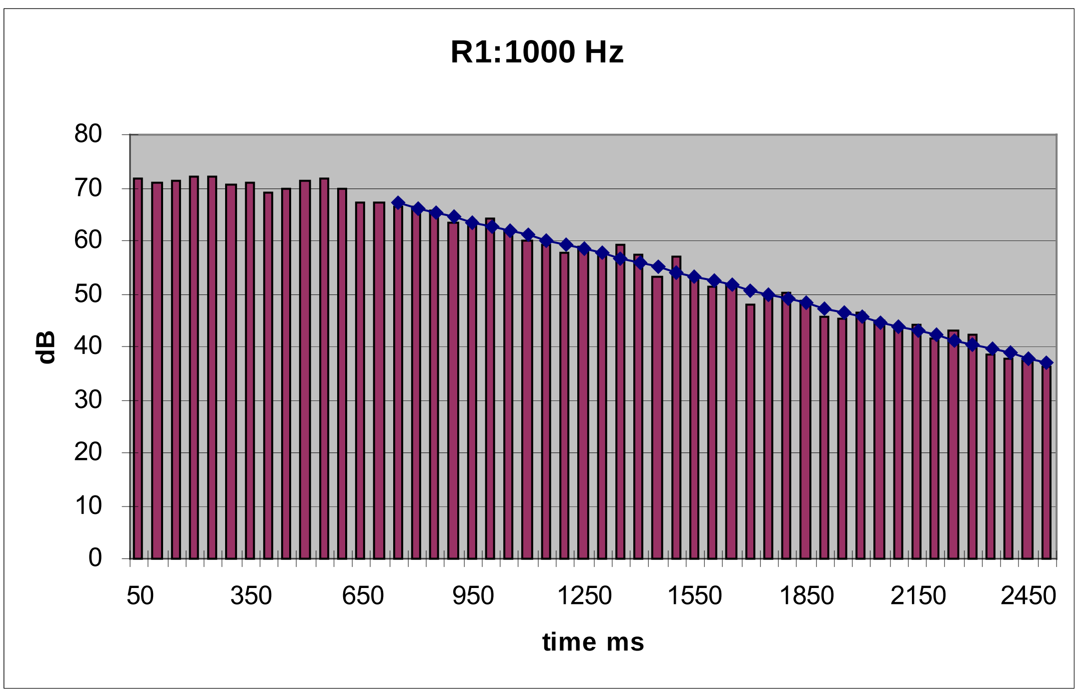

Figure A.50 Decay and Fit for T30 for 500 and 1000 Hz at R1 in Rüstem Pasa

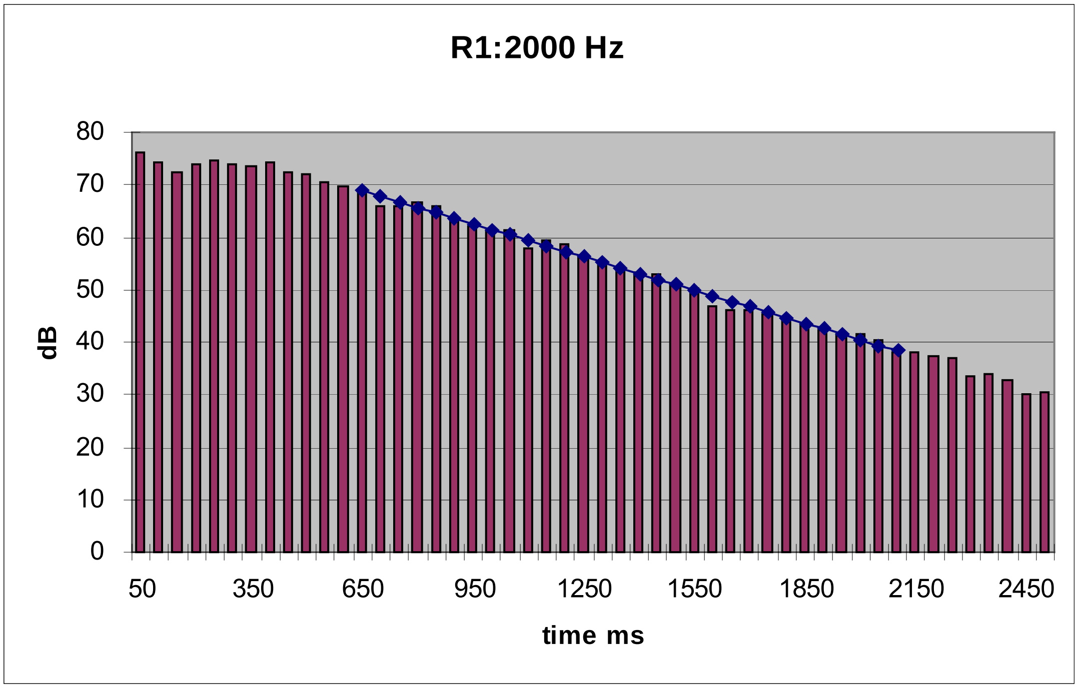

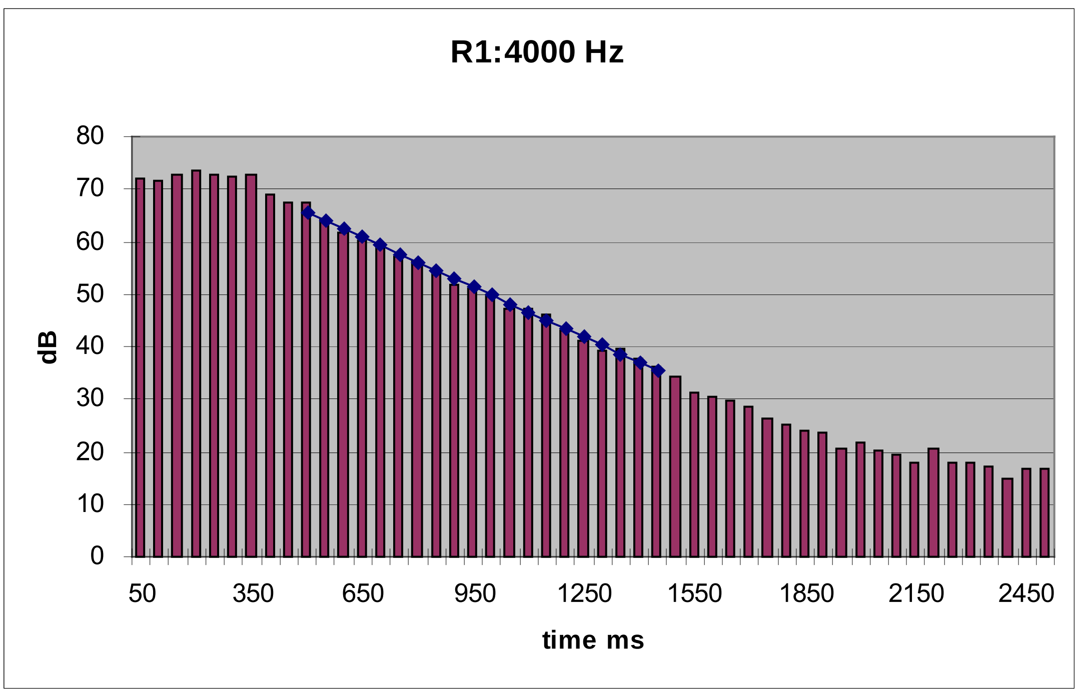

Figure A.51 Decay and Fit for T30 for 2000 & 4000 Hz at R1 in Rüstem Pasa

Table A.18 Measurements at R2 in Rüstem Pasa

time	dB					
ms	125	250	500	1000	2000	4000
50	74.32	80.90	80.78	73.56	74.53	74.55
100	74.95	77.02	81.33	73.94	76.57	73.28
150	80.85	82.31	79.63	72.76	75.96	74.18
200	75.80	80.60	80.06	74.93	74.74	75.02
250	72.98	81.35	80.34	75.99	77.33	73.96
300	80.06	78.90	78.10	74.41	76.03	74.18
350	79.21	79.00	82.97	74.86	75.49	72.22
400	78.90	78.79	77.75	72.44	75.52	68.55
450	79.42	79.04	77.82	75.38	73.85	68.04
500	69.07	78.15	74.69	72.51	74.50	66.18
550	71.38	74.08	75.16	72.01	72.88	65.50
600	69.87	77.04	77.75	71.33	72.01	63.19
650	76.17	74.34	76.41	70.04	71.07	60.25
700	75.80	77.23	75.63	67.45	68.25	61.01
750	68.67	73.05	72.36	66.77	68.01	57.08
800	70.15	73.40	74.29	68.32	67.61	57.36
850	76.55	74.32	72.76	66.49	66.96	55.67
900	69.07	75.45	72.08	67.45	65.71	52.82
950	76.67	73.26	71.92	64.98	65.03	50.23
1000	69.57	71.14	73.82	64.37	62.63	50.40
1050	75.14	74.20	72.06	63.64	61.41	49.03
1100	73.92	71.38	70.46	63.73	61.45	47.13
1150	68.30	71.68	71.02	62.53	60.65	46.97
1200	71.38	67.10	66.72	62.79	58.49	44.83
1250	64.84	70.60	70.44	59.62	59.22	43.01
1300	64.86	67.21	69.52	60.28	54.84	42.64
1350	67.17	63.55	67.17	59.43	56.54	40.29
1400	66.41	68.77	64.91	58.11	55.81	38.97
1450	68.04	61.50	67.00	57.41	53.97	36.83
1500	68.48	66.44	66.89	55.90	53.86	36.03
1550	63.76	61.64	65.59	54.84	50.96	33.75
1600	61.19	64.96	61.85	53.88	49.62	31.14
1650	66.11	63.55	64.51	52.21	49.98	30.57
1700	63.38	62.82	61.43	52.84	48.68	29.30
1750	59.62	66.20	61.92	53.10	46.35	28.34
1800	63.55	64.02	62.68	51.50	45.81	27.47
1850	63.40	56.54	57.74	50.00	44.99	26.79
1900	59.90	59.52	60.18	49.91	43.93	23.12
1950	58.70	62.63	60.18	49.03	42.78	23.89
2000	57.92	60.68	60.21	49.20	42.78	20.44
2050	60.28	63.00	56.75	45.79	40.94	21.05
2100	58.96	62.18	54.26	46.19	40.73	21.40
2150	61.48	57.05	57.05	44.31	39.42	21.14
2200	58.82	60.39	55.06	44.90	38.90	17.57
2250	54.77	56.33	54.02	44.31	37.93	18.04
2300	58.00	58.63	56.35	43.18	36.36	19.07
2350	54.70	56.96	53.55	40.69	35.37	16.72
2400	50.33	58.11	53.10	42.14	34.41	19.07
2450	59.24	58.68	49.74	41.51	32.24	20.95
2500	60.39	55.46	53.01	41.06	33.40	19.07

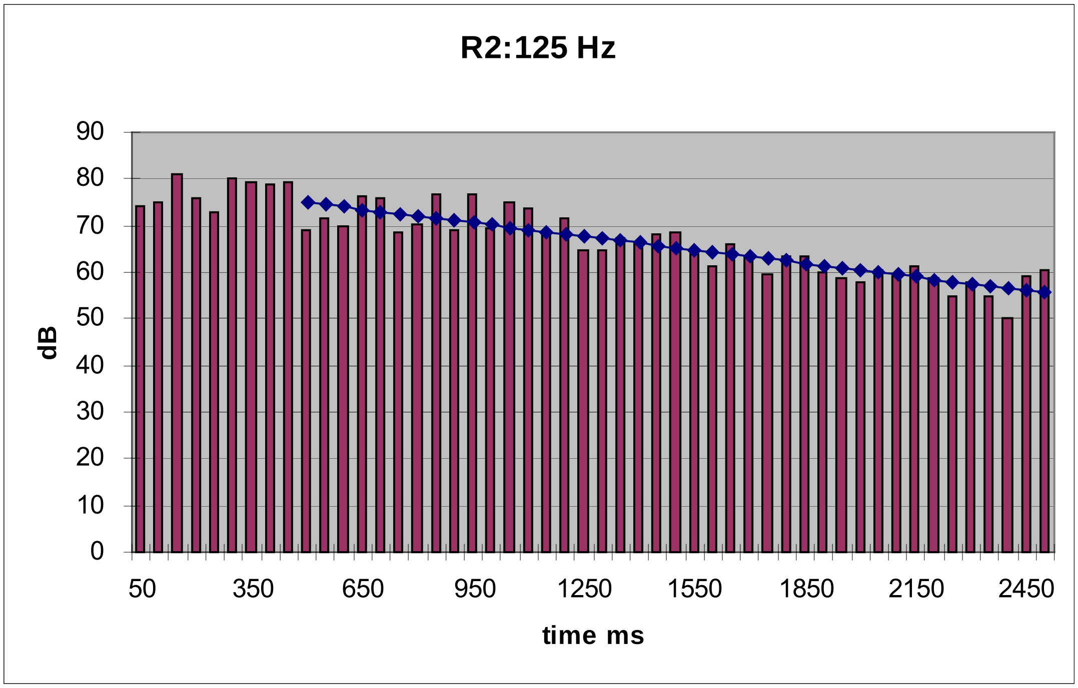

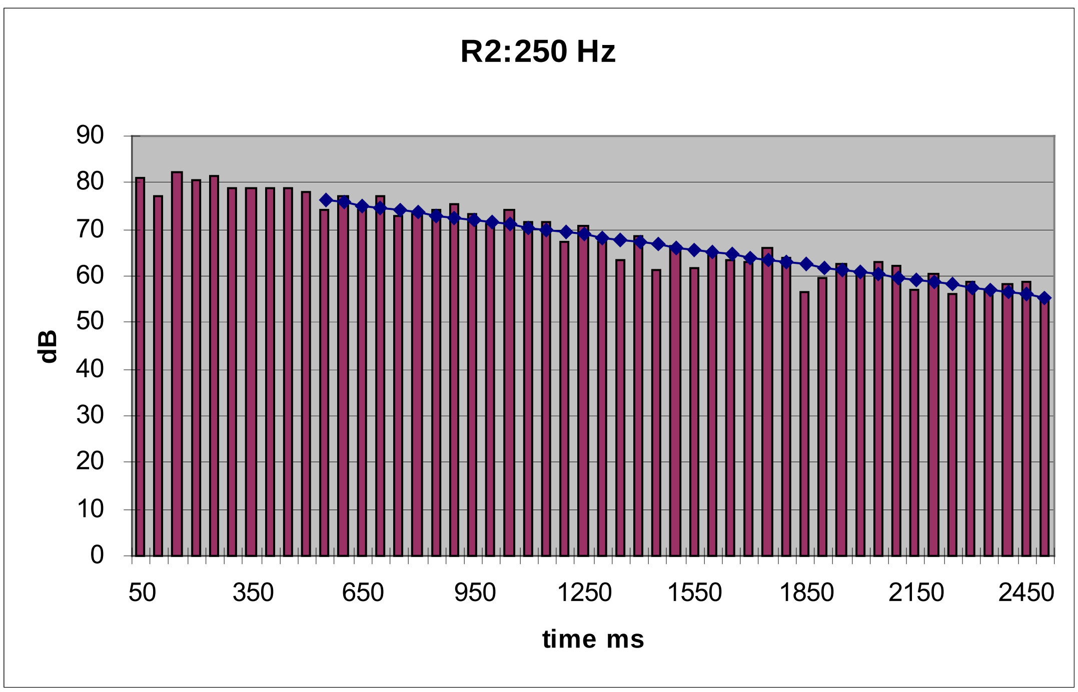

Figure A.52 Decay and Fit for T30 for 125 and 250 Hz at R2 in Rüstem Pasa

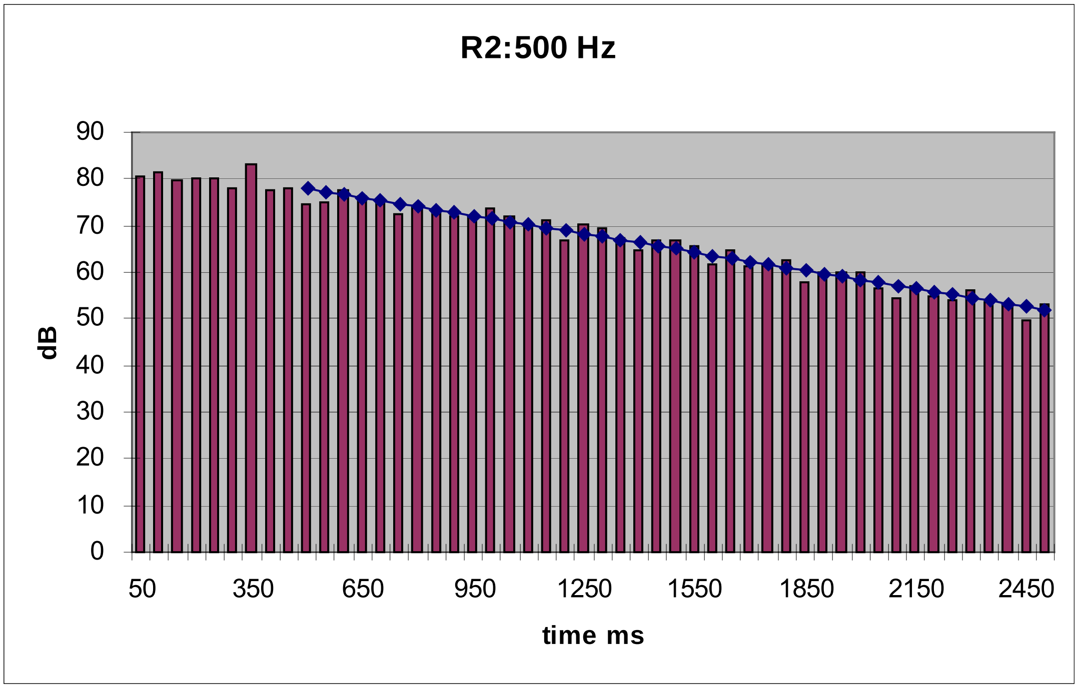

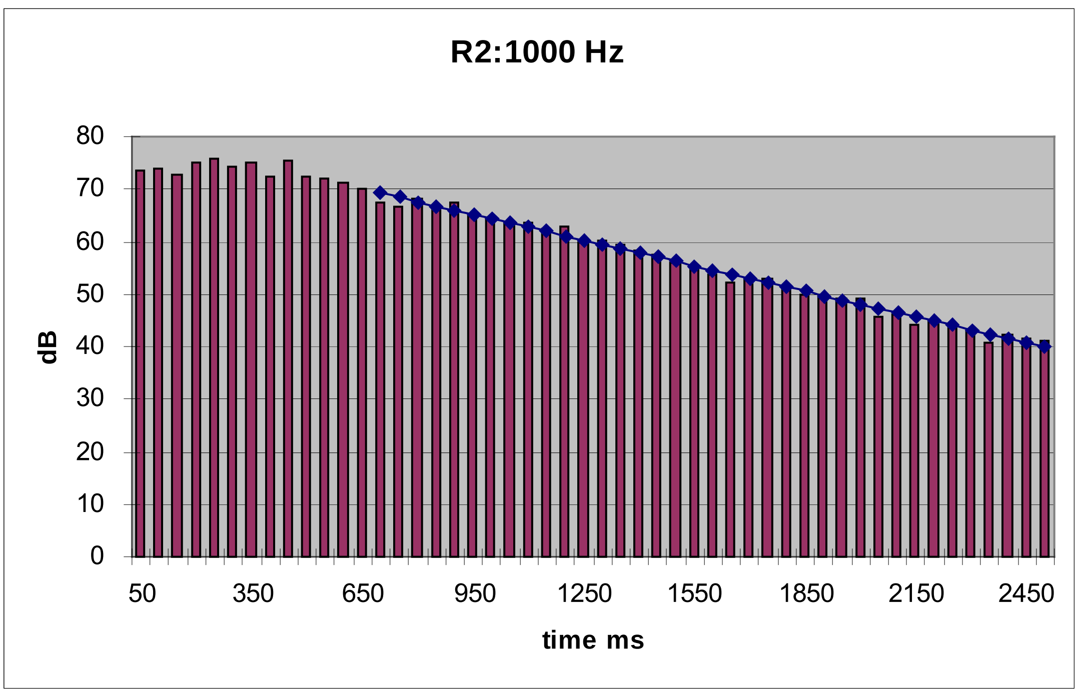

Figure A.53 Decay and Fit for T30 for 500 and1000 Hz at R2 in Rüstem Pasa

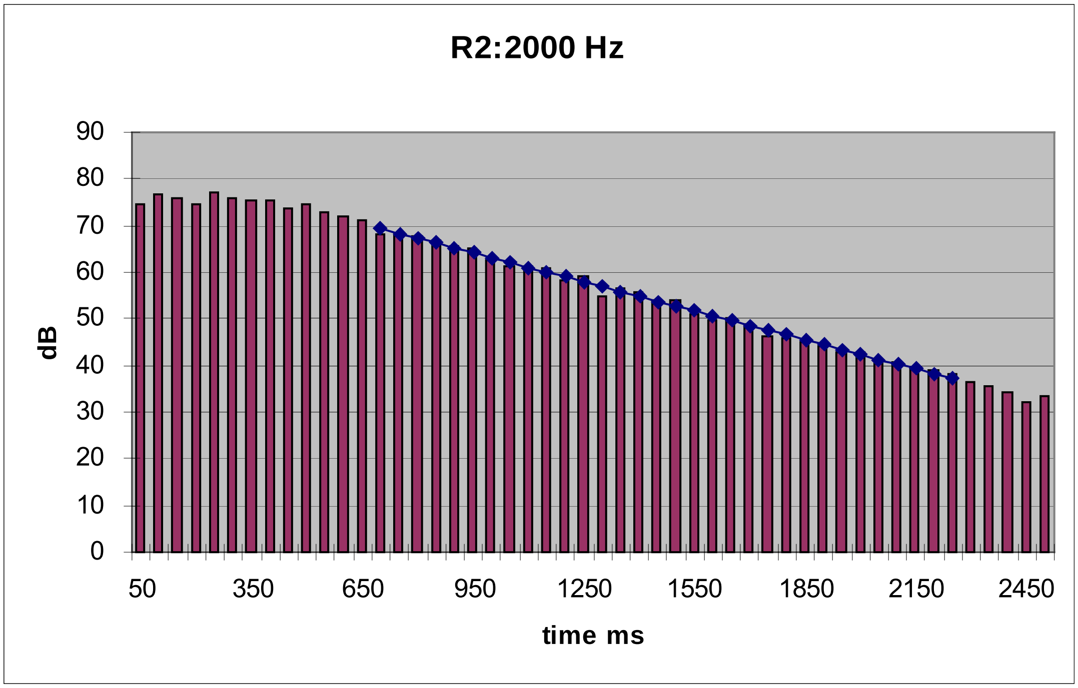

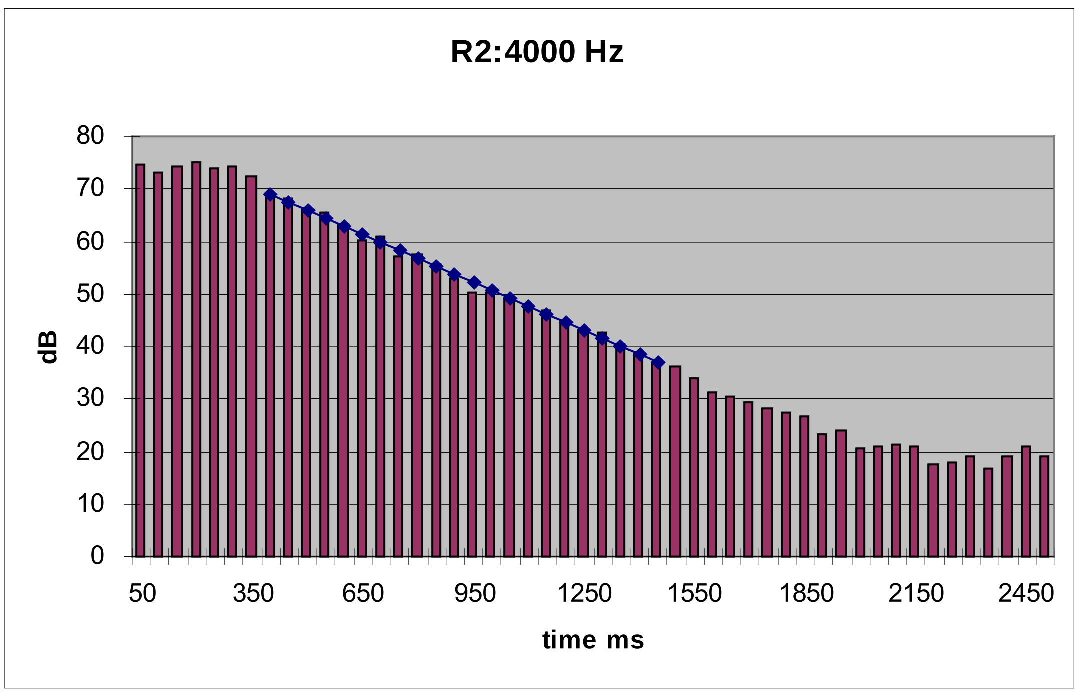

Figure A.54 Decay and Fit for T30 for 2 and 4 kHz at R2 in Rüstem Pasa

Table A.19 Measurements at R3 in Rüstem Pasa

time	dB					
ms	125	250	500	1000	2000	4000
50	74.74	78.20	80.34	72.15	73.42	73.80
100	81.84	80.71	78.64	71.71	74.08	71.85
150	78.53	77.56	82.20	73.61	73.89	74.13
200	73.68	82.31	82.64	74.22	75.49	72.79
250	76.93	74.76	81.33	73.21	73.35	71.73
300	74.58	74.65	78.81	69.92	71.71	73.33
350	74.22	81.51	77.63	73.05	73.94	72.06
400	73.99	77.02	82.50	71.47	73.23	70.27
450	73.71	77.16	78.53	72.20	73.05	66.65
500	73.31	78.71	75.99	71.59	71.99	65.76
550	73.19	69.82	79.96	71.38	71.26	63.45
600	70.01	73.66	76.50	70.04	70.22	62.56
650	68.32	70.69	76.46	68.01	68.67	62.09
700	75.33	74.22	76.50	66.39	67.64	58.79
750	66.27	75.07	72.51	65.38	67.38	58.47
800	74.22	75.77	75.30	64.70	65.73	56.49
850	74.36	73.49	73.16	64.67	65.03	55.48
900	71.57	70.08	72.76	63.92	63.66	54.59
950	77.42	68.18	74.60	63.33	62.60	52.61
1000	72.27	68.88	72.32	62.46	61.41	51.01
1050	70.01	69.50	70.41	63.12	58.77	48.33
1100	65.90	68.88	70.84	59.57	60.09	46.82
1150	65.36	67.19	65.97	59.29	58.04	47.51
1200	69.50	63.95	70.62	56.54	56.96	45.01
1250	68.18	68.30	69.90	58.47	56.87	42.14
1300	67.94	65.05	70.04	58.75	55.71	41.23
1350	64.18	65.17	67.36	57.97	55.76	40.50
1400	69.75	69.33	67.80	56.11	53.32	38.19
1450	66.16	62.42	67.97	52.66	53.48	37.18
1500	62.30	66.67	63.59	54.14	51.41	35.84
1550	62.21	66.53	59.29	52.84	52.05	33.82
1600	60.14	62.56	64.32	53.34	49.22	32.74
1650	66.91	59.27	61.22	52.99	49.41	31.77
1700	66.98	64.89	60.63	49.62	47.91	30.79
1750	59.88	62.32	61.66	50.28	45.70	27.05
1800	61.66	59.78	61.48	49.88	45.15	26.67
1850	54.23	64.30	59.15	47.32	43.30	25.31
1900	54.21	59.90	58.56	47.32	41.96	22.79
1950	56.21	62.82	60.14	47.65	42.03	23.38
2000	59.34	59.74	57.92	46.45	41.53	20.39
2050	55.97	57.92	57.90	46.87	39.72	20.51
2100	58.07	55.64	52.80	43.32	39.98	18.65
2150	56.65	58.25	56.54	44.97	39.63	17.07
2200	57.01	57.78	58.98	43.65	36.17	18.51
2250	58.11	57.52	59.19	42.57	36.17	16.98
2300	55.15	55.06	53.22	40.90	36.05	17.50
2350	58.40	56.58	54.56	40.64	33.07	15.17
2400	53.43	56.80	51.29	40.59	35.35	18.04
2450	51.43	52.47	53.88	38.26	32.17	18.77
2500	52.16	48.85	57.22	38.78	32.69	16.79

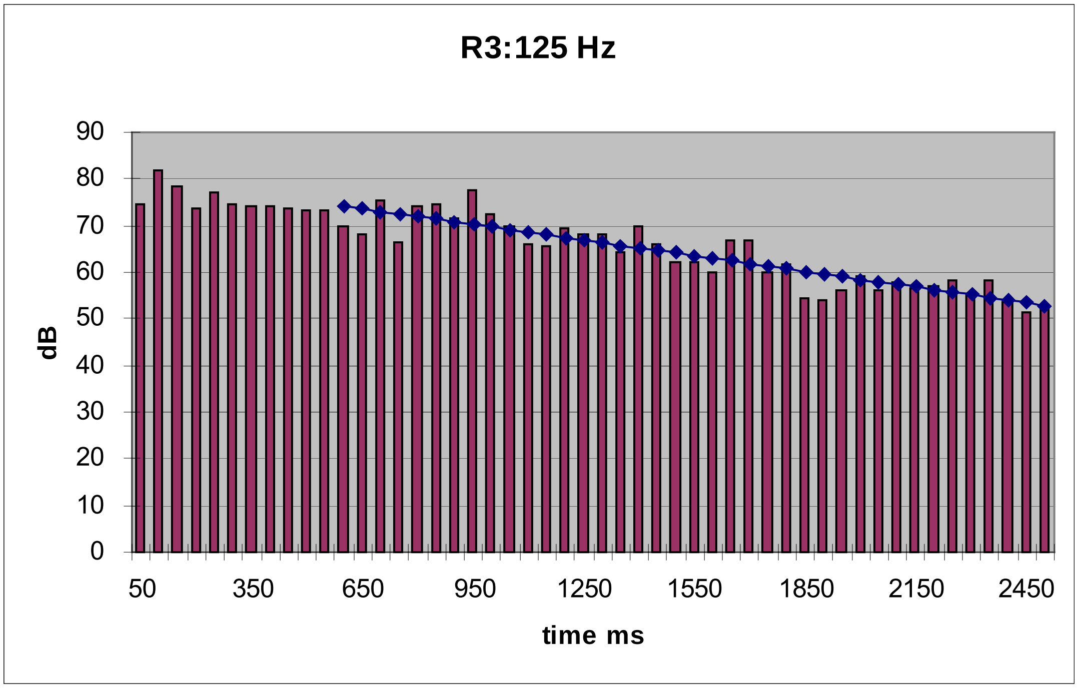

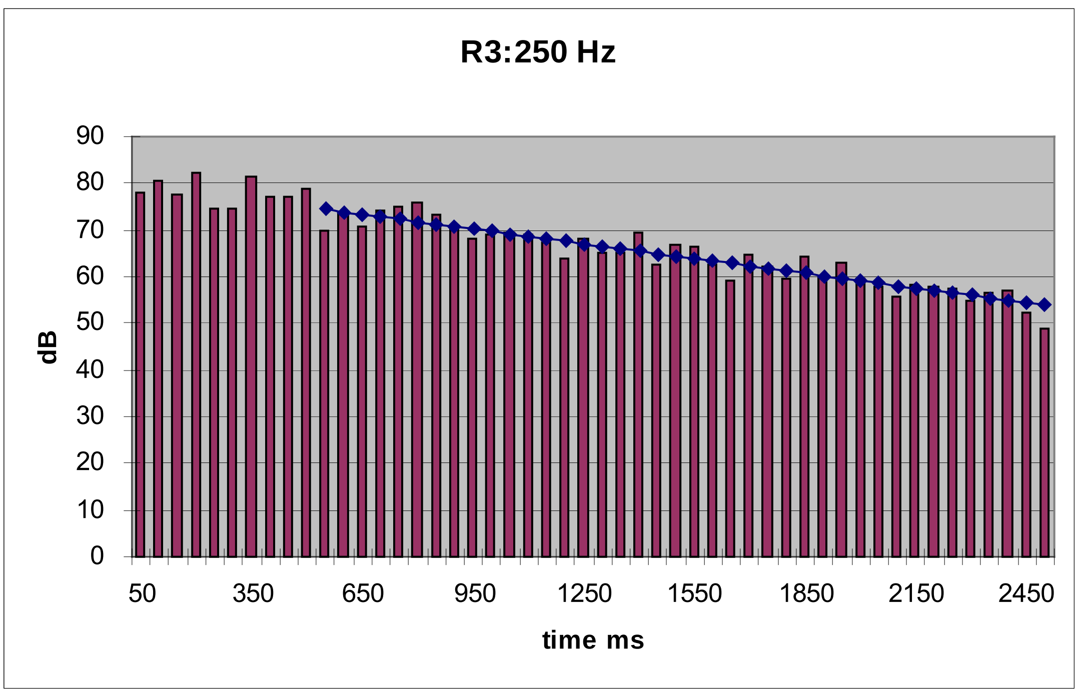

Figure A.55 Decay and Fit for T30 for 125 and 250 Hz at R3 in Rüstem Pasa

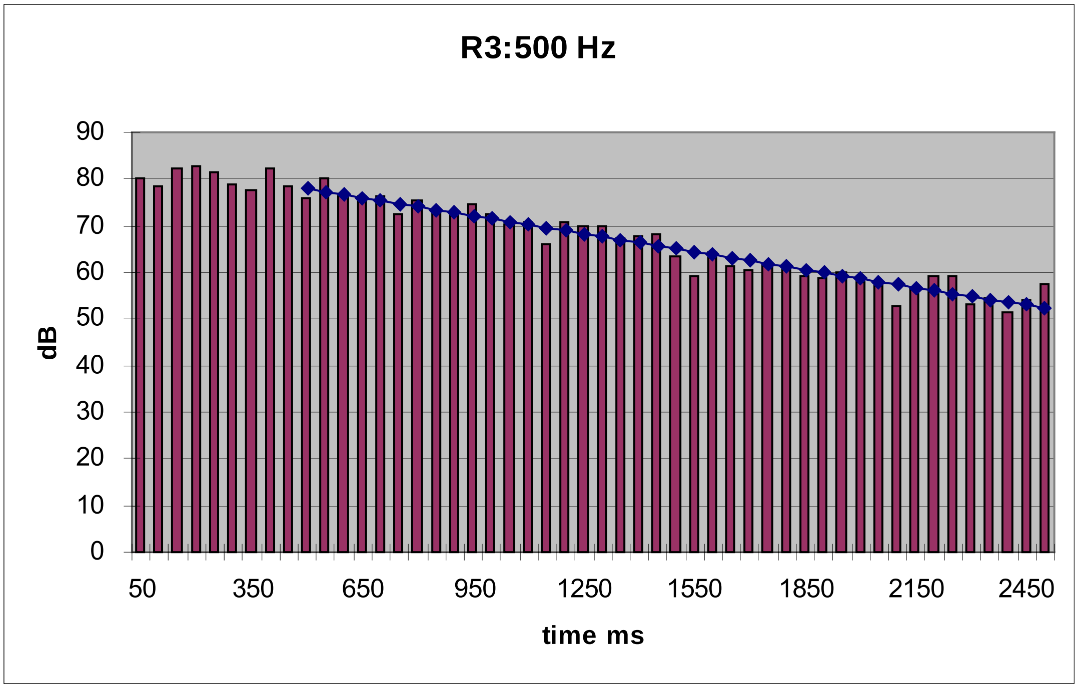

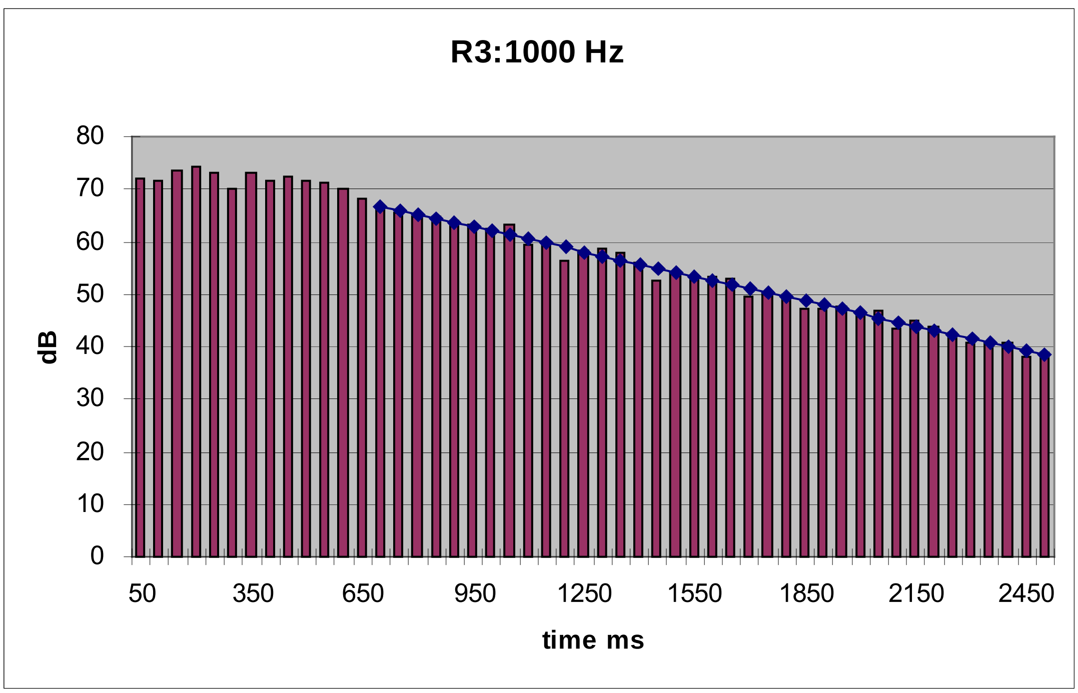

Figure A.56 Decay and Fit for T30 for 500 and 1000 Hz at R3 in Rüstem Pasa

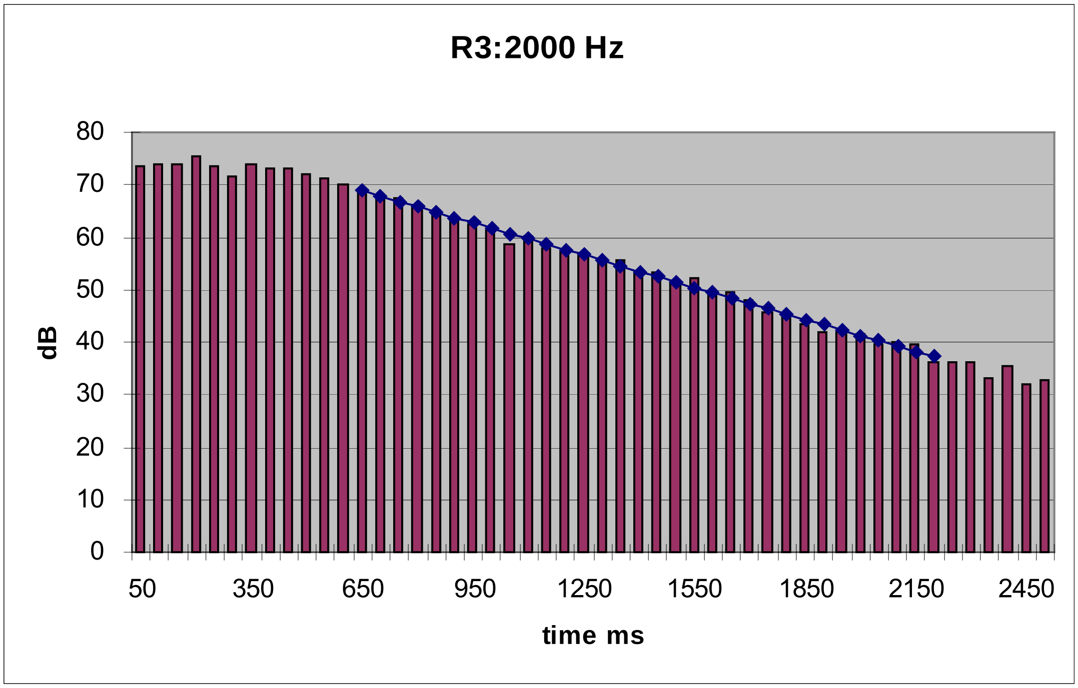

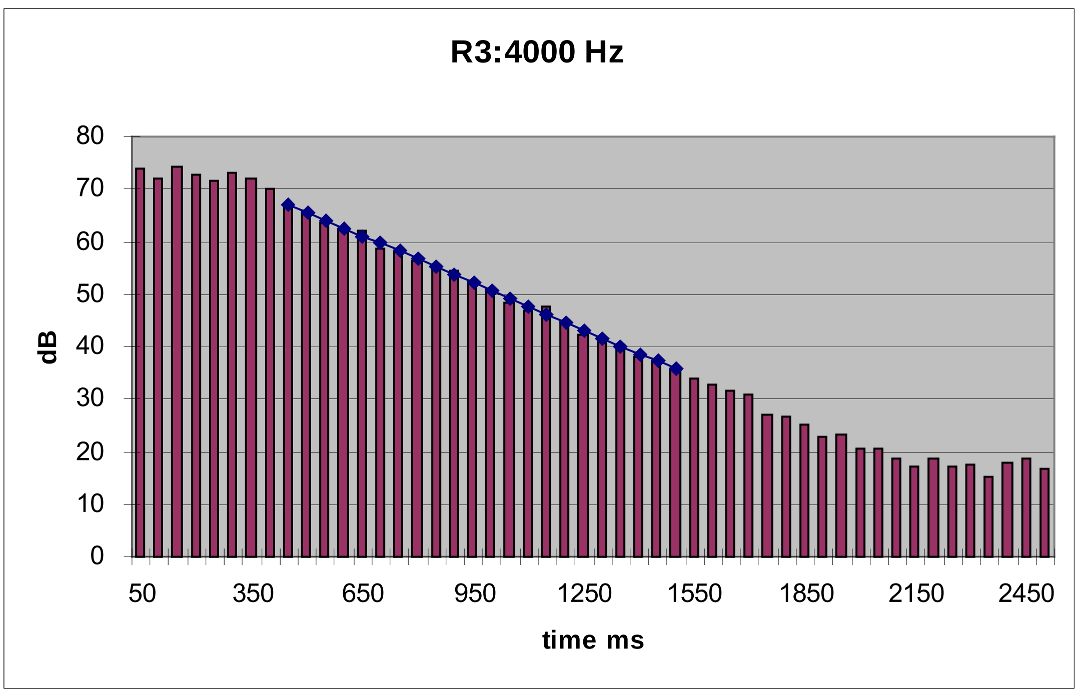

Figure A.57 Decay and Fit for T30 for 2 and 4 kHz at R3 in Rüstem Pasa

Table A.20 Measurements at R4 in Rüstem Pasa

time	dB					
ms	**125**	**250**	**500**	**1000**	**2000**	**4000**
50	75.70	81.33	78.67	70.74	76.22	75.14
100	73.75	79.94	82.74	73.52	76.06	72.06
150	81.89	80.55	79.54	72.27	75.05	74.41
200	81.09	77.84	84.99	71.07	75.49	73.52
250	73.56	80.06	77.40	74.22	75.66	74.32
300	77.89	83.18	81.07	70.60	73.12	73.52
350	82.12	76.13	82.57	71.07	76.08	74.03
400	77.94	75.94	79.09	71.09	75.49	68.95
450	74.83	76.39	80.71	73.80	74.03	67.78
500	70.48	78.67	81.16	71.78	72.29	66.34
550	76.10	74.62	78.81	70.30	72.72	63.52
600	73.73	73.59	76.79	70.01	71.09	61.85
650	68.53	78.95	81.72	68.41	69.12	62.02
700	76.86	70.79	78.17	67.90	67.50	59.38
750	73.28	74.90	76.06	65.33	67.33	56.61
800	75.80	69.52	76.32	66.16	66.58	55.13
850	75.82	71.35	74.34	64.98	66.16	54.84
900	67.45	75.80	74.11	64.70	64.65	54.49
950	67.24	72.60	74.46	62.91	63.87	52.05
1000	69.00	69.78	73.23	62.42	61.92	50.73
1050	70.88	72.01	68.63	65.24	60.68	47.79
1100	64.96	70.69	72.15	60.84	60.89	47.51
1150	69.38	70.39	69.64	61.33	59.19	45.32
1200	72.76	69.10	70.27	61.38	57.15	43.44
1250	68.67	65.97	68.06	59.38	57.52	42.47
1300	67.64	70.93	68.60	59.55	55.10	40.40
1350	64.09	68.27	67.57	57.78	54.44	39.72
1400	68.58	64.06	64.30	57.45	54.21	37.89
1450	63.10	65.33	65.03	56.37	53.13	35.68
1500	68.53	63.24	63.47	55.57	53.32	35.96
1550	66.60	66.18	64.30	53.20	52.16	32.95
1600	67.07	65.66	63.12	53.93	49.72	29.96
1650	70.62	66.77	63.15	53.20	48.75	31.02
1700	64.11	62.16	62.75	52.07	48.33	28.53
1750	62.49	61.62	59.76	49.13	46.07	27.09
1800	65.29	60.96	62.56	50.75	45.48	26.34
1850	62.86	58.18	60.04	50.66	44.54	23.66
1900	59.59	62.51	60.46	49.06	44.38	22.86
1950	65.07	59.83	59.17	49.29	43.23	22.20
2000	64.93	59.01	57.95	47.79	41.37	21.19
2050	56.47	60.70	56.58	45.65	41.96	19.28
2100	54.75	58.75	58.23	46.02	40.83	16.89
2150	53.24	58.18	57.64	45.65	39.46	18.18
2200	60.11	58.58	58.32	43.86	37.21	18.88
2250	57.34	55.20	54.44	39.51	38.05	16.89
2300	60.30	55.29	52.33	40.97	36.29	15.31
2350	48.96	55.93	55.20	42.78	35.30	15.43
2400	53.08	58.40	54.44	41.20	33.02	15.31
2450	53.29	53.88	53.83	37.09	32.85	13.69
2500	47.41	56.51	53.48	37.39	31.96	15.69

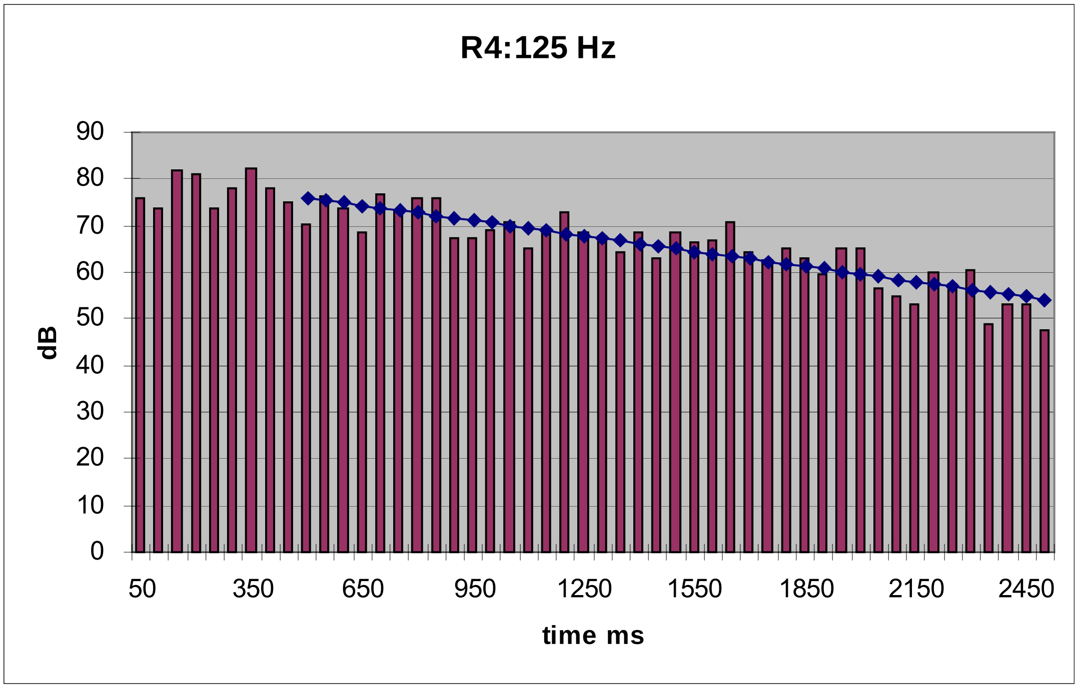

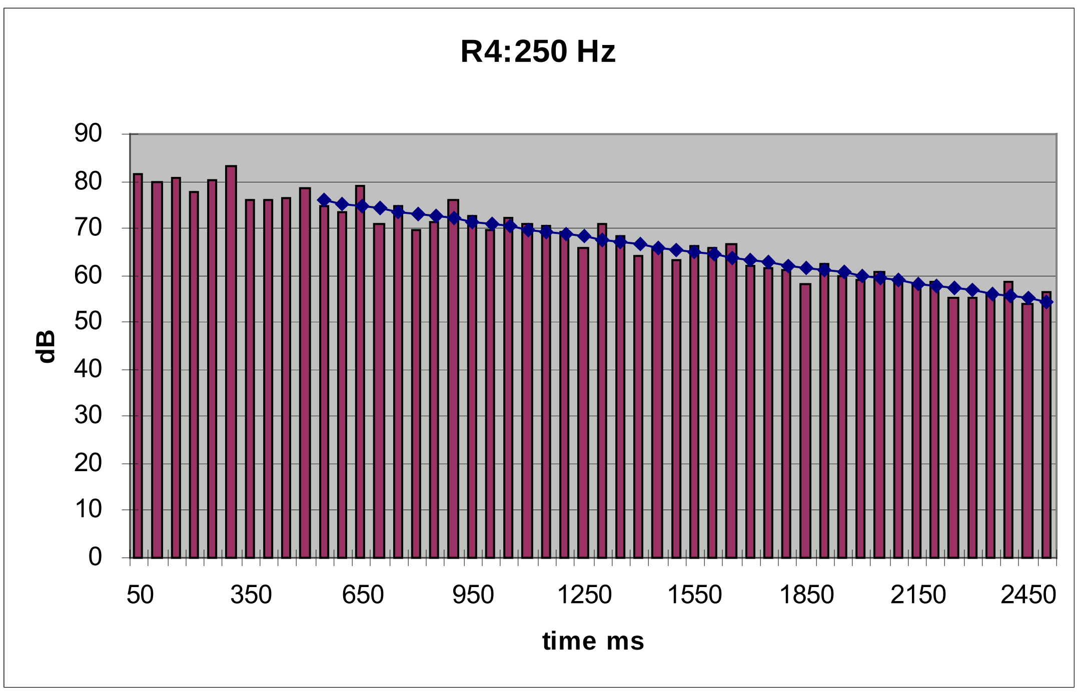

Figure A.58 Decay and Fit for T30 for 125 and 250 Hz at R4 in Rüstem Pasa

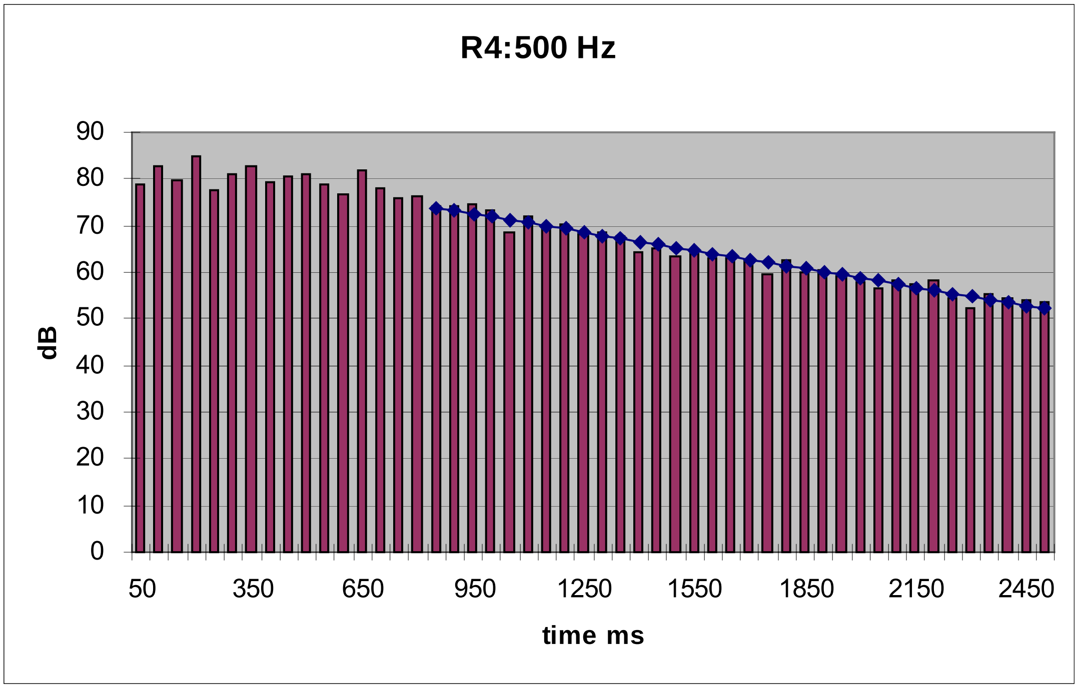

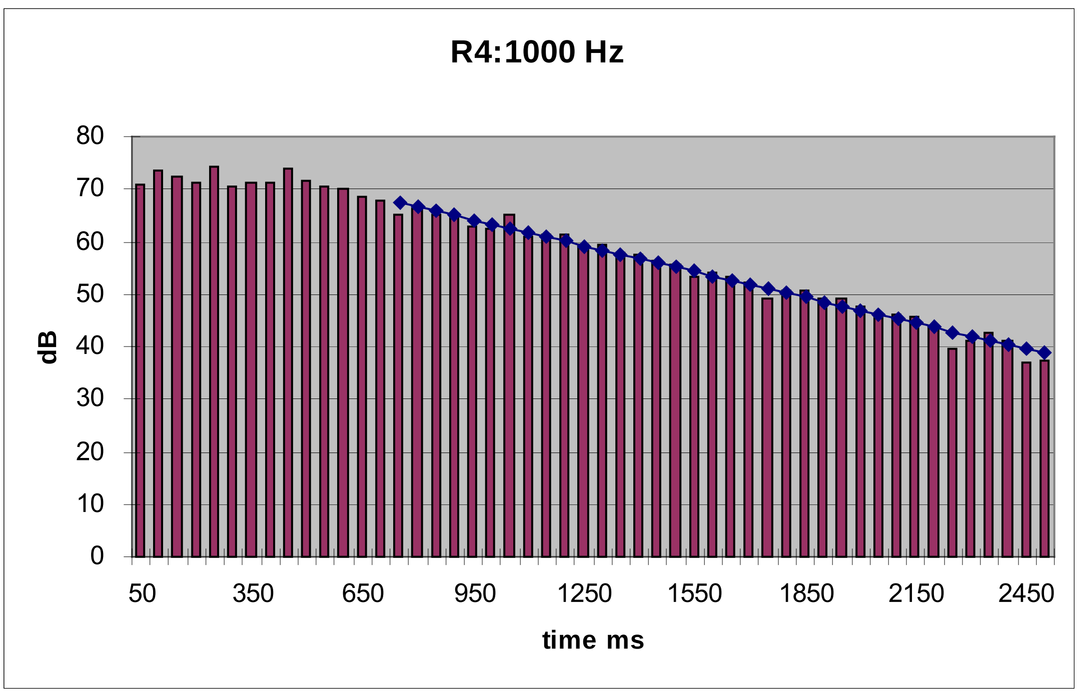

Figure A.59 Decay and Fit for T30 for 500 and 1000 Hz at R4 in Rüstem Pasa

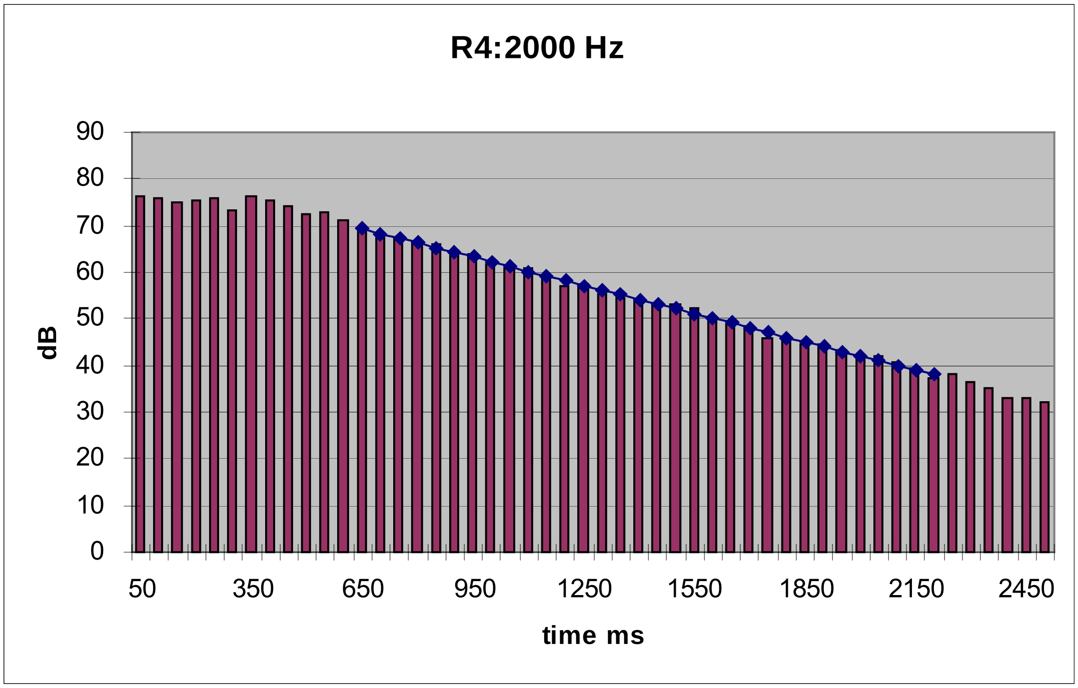

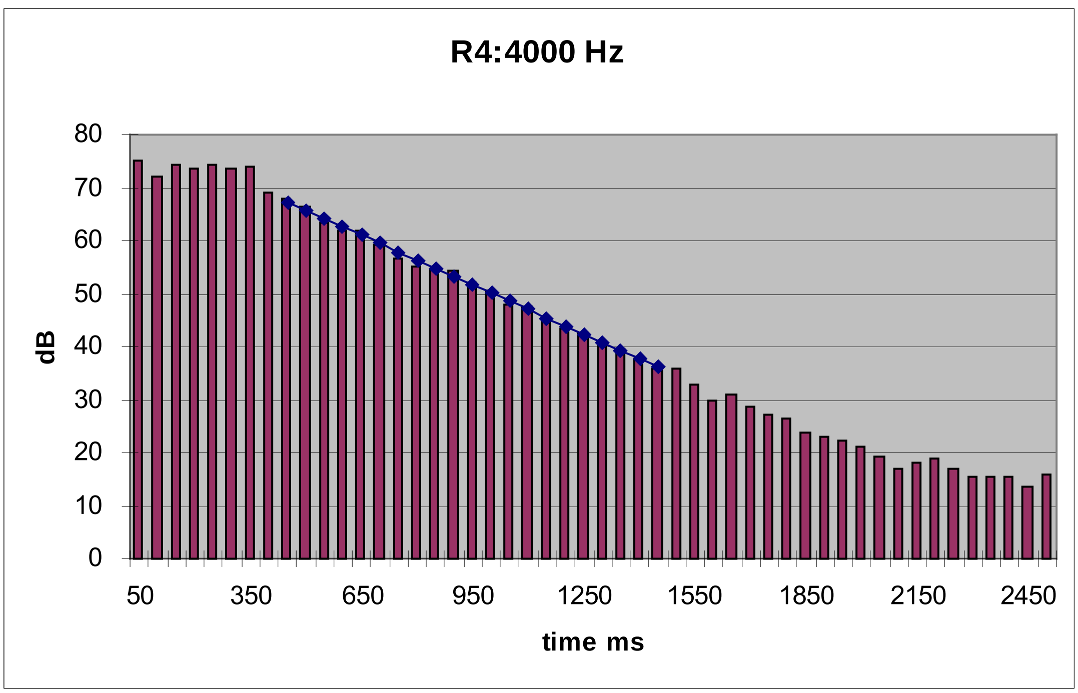

Figure A.60 Decay and Fit for T30 for 2 and 4 kHz at R4 in Rüstem Pasa

Table A.21 Measurements at R5 in Rüstem Pasa

time	dB					
ms	125	250	500	1000	2000	4000
50	74.22	81.61	76.81	72.22	76.41	73.05
100	74.22	78.50	77.63	73.12	74.62	70.39
150	80.60	76.83	79.96	75.63	76.41	71.28
200	75.85	79.77	79.70	75.02	74.55	71.19
250	71.92	77.04	78.93	75.80	75.63	72.76
300	72.01	77.04	78.03	75.49	73.49	71.33
350	69.90	80.22	79.56	73.63	75.54	72.79
400	75.07	74.39	79.96	72.62	73.49	70.60
450	75.05	76.03	79.63	72.06	71.85	67.36
500	72.13	79.26	80.13	71.61	73.61	64.96
550	73.73	75.33	81.44	71.31	71.02	63.76
600	72.88	69.52	76.25	71.17	68.72	61.50
650	68.06	73.54	76.55	70.18	68.20	61.22
700	71.47	73.61	77.12	68.81	66.60	59.95
750	69.40	67.45	75.73	67.90	67.85	58.00
800	67.45	67.54	75.92	67.38	65.54	57.08
850	73.02	70.81	74.15	64.16	66.27	55.03
900	69.07	64.93	75.99	63.85	64.91	52.77
950	70.37	71.73	73.26	63.73	63.19	51.50
1000	66.23	72.58	71.73	62.89	62.18	49.91
1050	69.21	68.13	74.39	63.55	60.79	49.48
1100	71.28	68.60	71.21	63.69	59.81	47.62
1150	65.17	67.07	72.58	59.81	59.10	45.53
1200	68.13	69.71	67.26	60.54	55.64	43.18
1250	61.95	66.60	60.75	59.52	58.14	42.03
1300	68.55	66.72	67.07	57.31	54.91	40.29
1350	66.06	63.85	66.70	56.56	53.81	39.91
1400	61.71	64.09	68.84	57.36	53.95	38.48
1450	62.37	59.05	65.59	55.31	51.60	36.90
1500	61.08	65.38	66.60	56.56	53.41	34.81
1550	67.03	64.67	64.44	54.07	49.76	34.24
1600	59.52	64.82	61.97	54.26	50.54	33.11
1650	61.01	62.98	60.28	53.24	50.02	31.26
1700	54.16	64.51	62.53	49.83	48.12	28.90
1750	63.73	60.42	62.65	51.15	45.65	27.47
1800	58.82	54.96	63.76	51.55	44.24	27.26
1850	52.68	60.25	63.12	49.55	44.24	25.31
1900	56.51	64.51	59.71	48.07	43.46	25.00
1950	56.61	58.42	61.99	48.00	42.10	23.52
2000	53.97	60.49	60.11	47.98	41.91	22.22
2050	57.52	59.83	58.65	45.81	41.30	21.14
2100	58.40	58.00	55.97	44.85	41.06	20.84
2150	55.48	59.67	59.90	44.78	37.91	21.71
2200	51.29	55.67	54.26	44.85	37.16	20.32
2250	56.21	58.91	54.30	44.05	37.11	19.87
2300	61.01	58.42	56.96	42.00	36.29	20.32
2350	58.72	58.72	54.56	41.91	35.63	19.07
2400	58.98	55.43	56.25	40.40	34.15	20.04
2450	52.47	57.41	53.15	38.22	33.40	19.21
2500	54.47	58.94	52.59	38.08	32.24	19.57

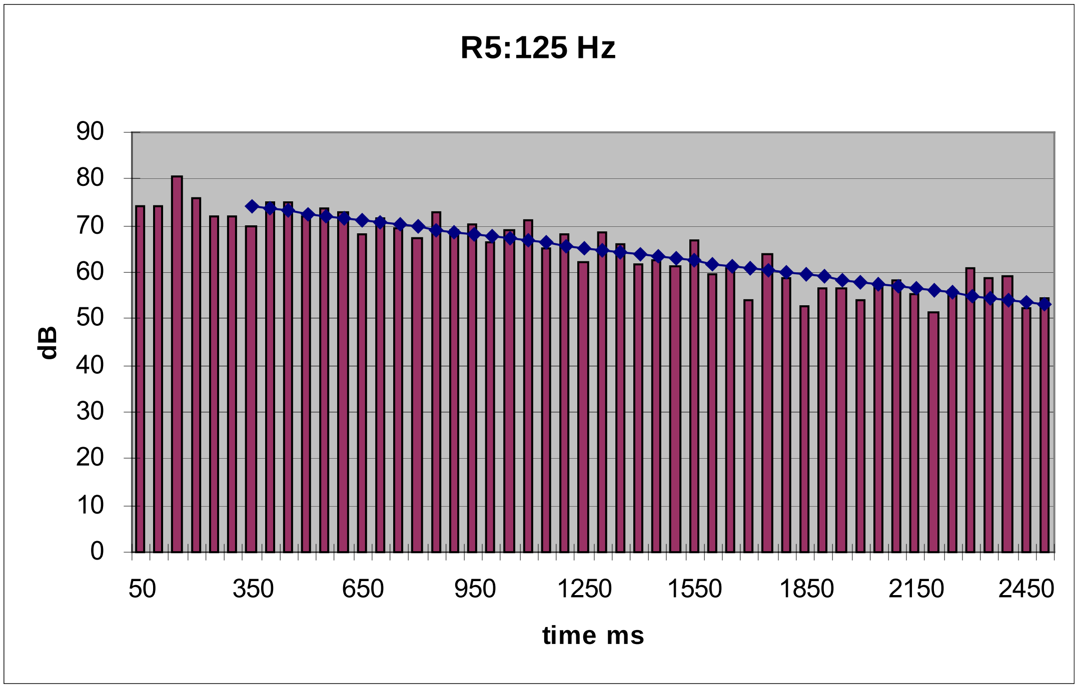

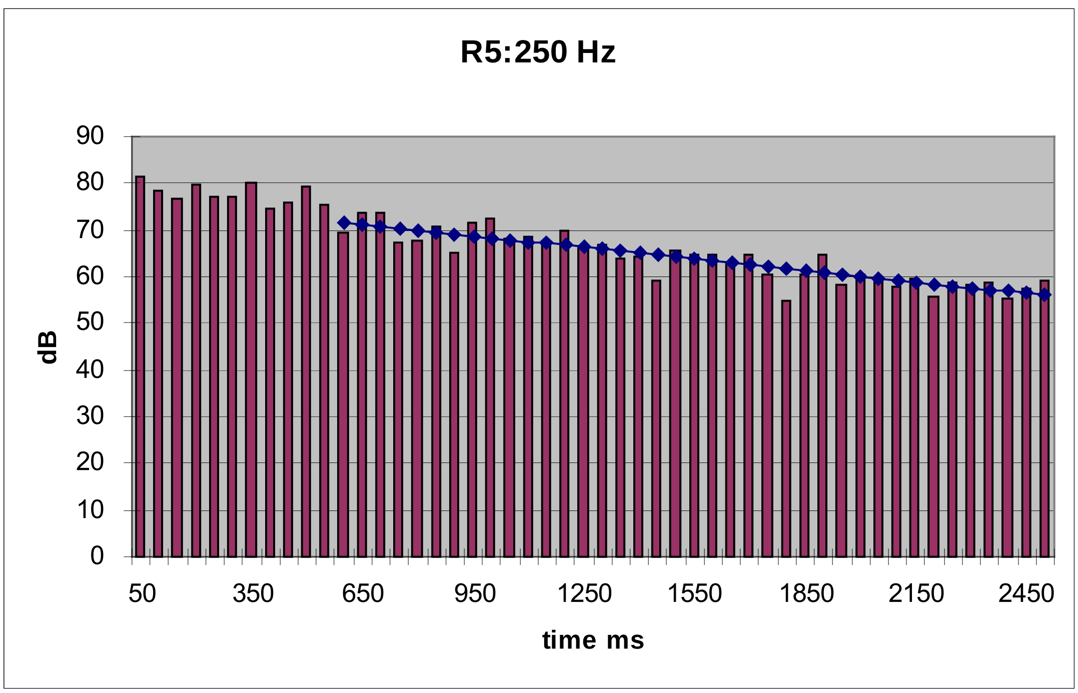

Figure A.61 Decay and Fit for T30 for 125 and 250 Hz at R5 in Rüstem Pasa

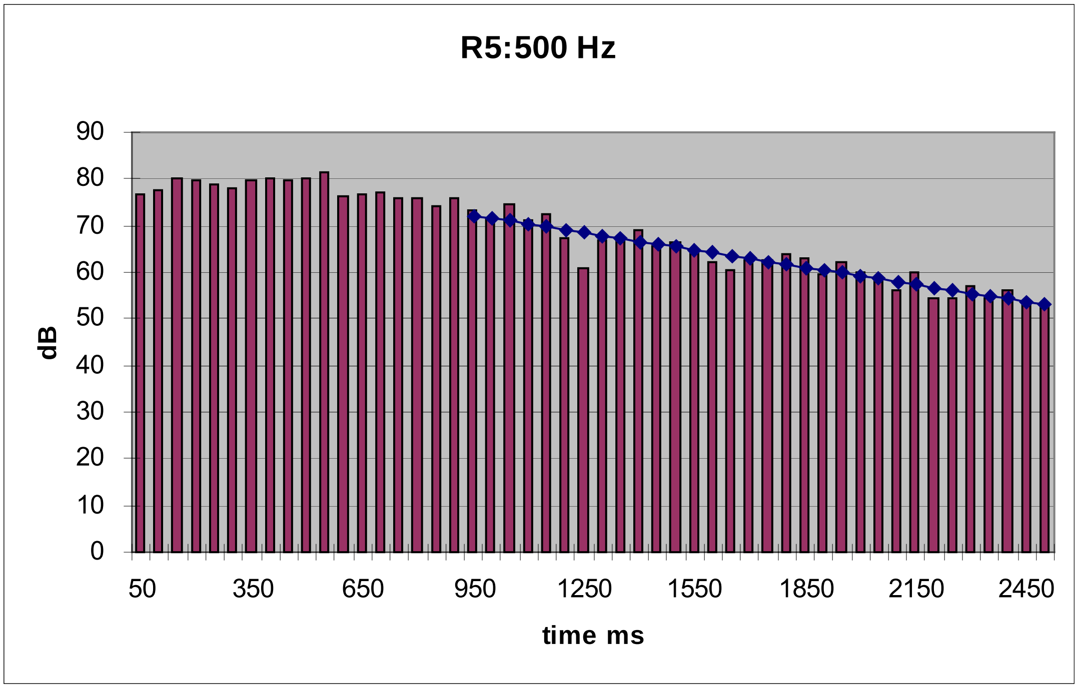

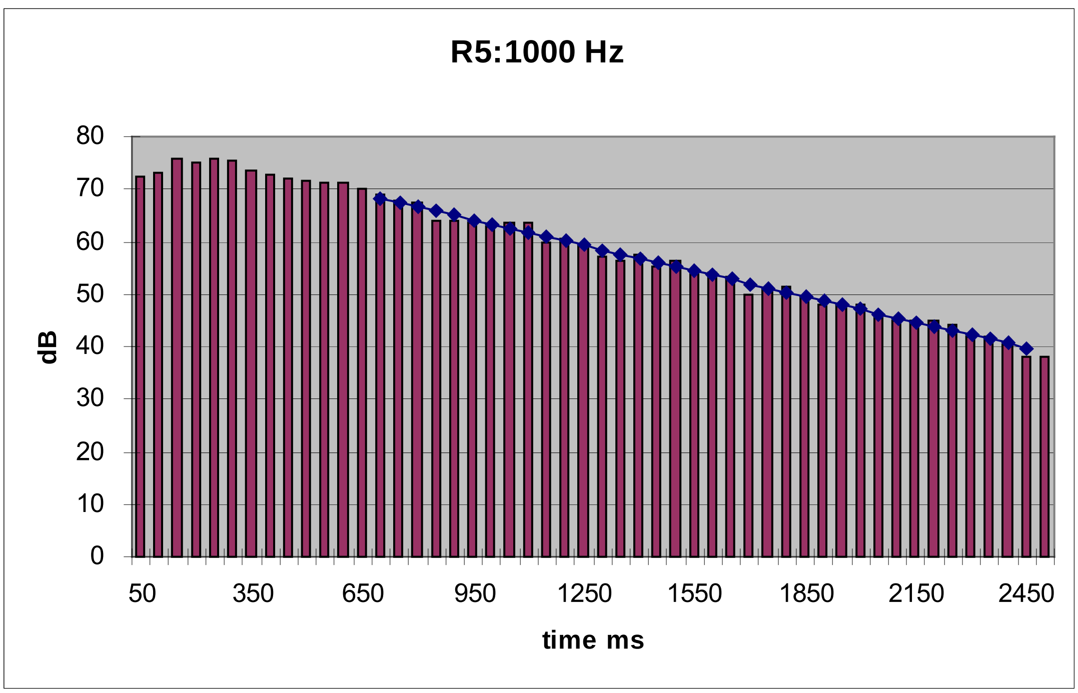

Figure A.62 Decay and Fit for T30 for 500 and 1000 Hz at R5 in Rüstem Pasa

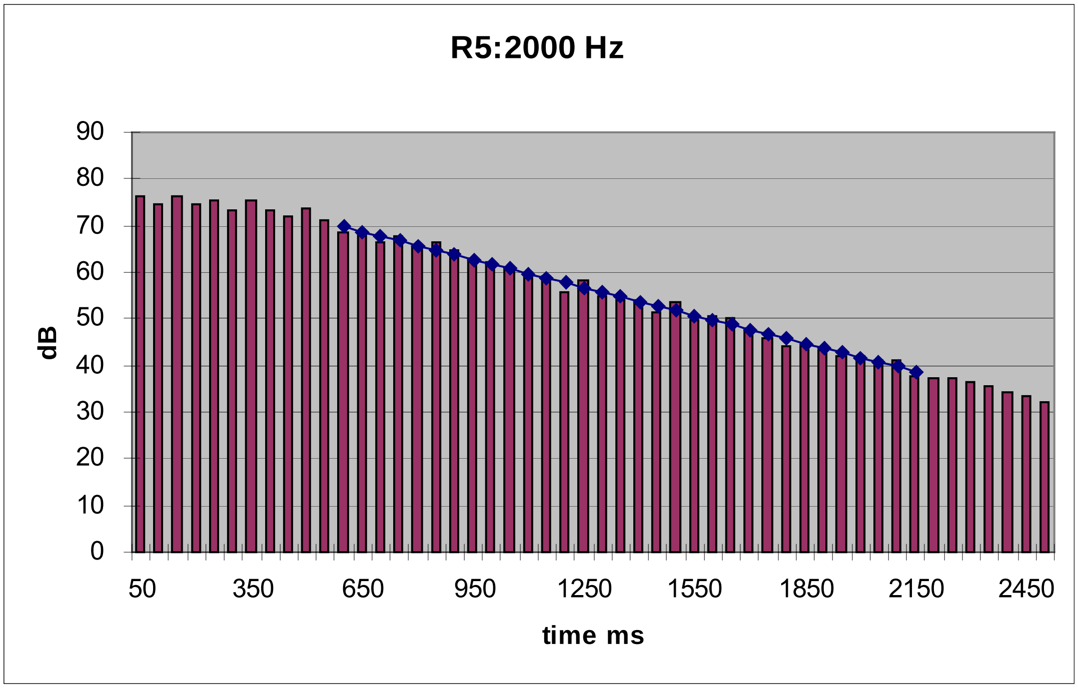

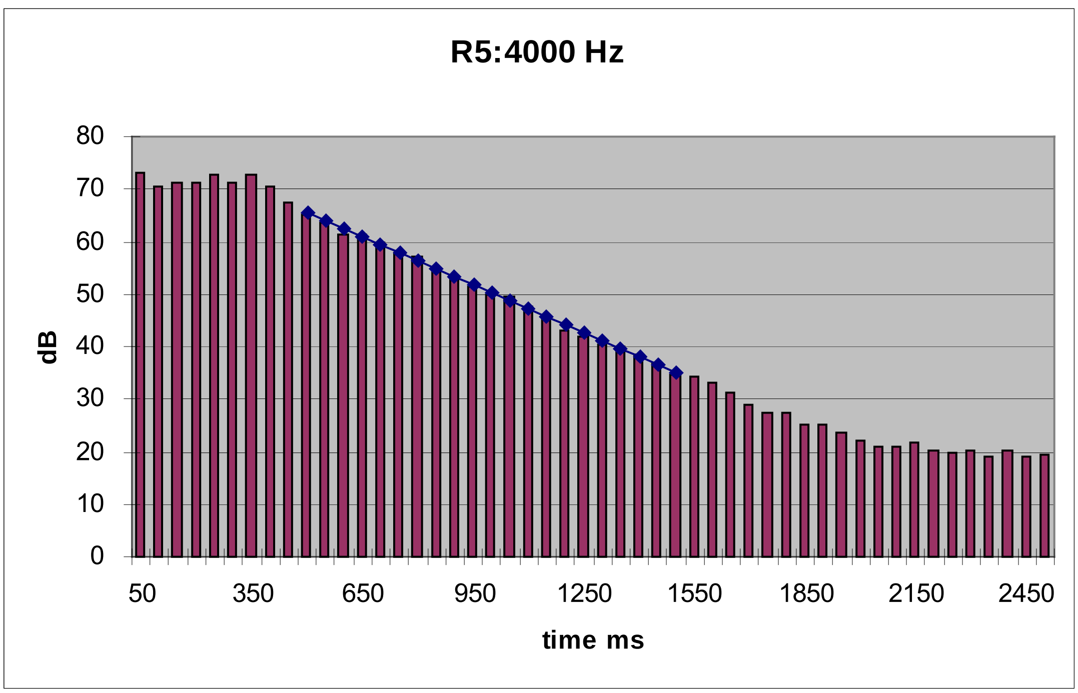

Figure A.63 Decay and Fit for T30 for 2 and 4 kHz at R5 in Rüstem Pasa

Table A.22 Measurements at R6 in Rüstem Pasa

time	dB					
ms	125	250	500	1000	2000	4000
50	71.96	79.00	78.74	73.56	75.21	71.31
100	78.22	80.81	79.73	74.48	76.76	69.40
150	78.24	78.20	80.76	76.17	74.43	72.06
200	72.46	76.22	82.22	73.63	77.12	71.92
250	76.22	76.46	80.64	73.38	75.07	72.55
300	74.74	78.27	82.41	76.10	76.22	71.02
350	79.61	81.33	81.23	75.94	74.90	71.89
400	76.93	77.89	79.68	74.18	75.54	70.13
450	77.30	79.51	76.48	72.20	72.86	67.78
500	74.58	72.60	78.15	73.16	72.48	67.57
550	77.07	71.52	76.32	70.86	72.34	65.52
600	76.36	72.18	79.84	69.47	72.18	64.27
650	67.54	74.62	77.44	67.68	70.55	60.96
700	69.85	73.07	77.75	67.00	69.92	59.99
750	72.51	70.51	75.14	66.91	68.11	58.68
800	71.35	68.23	73.78	67.78	67.73	57.24
850	72.08	72.15	74.29	66.06	66.77	55.27
900	73.59	73.89	71.05	66.60	64.13	55.36
950	67.31	71.57	71.42	65.50	63.33	53.32
1000	67.07	68.37	72.93	63.08	62.32	52.09
1050	69.31	69.50	71.96	63.33	61.97	50.02
1100	66.98	66.18	68.01	62.23	61.57	47.76
1150	70.44	65.17	66.46	60.77	58.79	47.51
1200	67.14	64.35	68.01	62.44	59.90	45.11
1250	70.27	60.04	69.52	60.32	57.76	44.12
1300	68.55	66.60	67.19	59.01	55.88	41.44
1350	64.86	67.92	66.53	55.64	55.24	41.70
1400	68.46	66.27	68.30	57.48	54.61	38.31
1450	66.58	63.92	67.85	57.08	53.55	37.35
1500	68.20	64.11	65.50	53.08	52.30	36.50
1550	64.39	64.58	65.80	53.67	51.62	35.42
1600	60.14	60.46	64.77	54.51	50.28	33.32
1650	64.79	59.01	62.96	53.46	48.82	30.43
1700	59.05	61.90	67.52	53.76	48.82	29.96
1750	62.79	64.46	60.46	51.46	47.39	30.13
1800	63.31	64.13	62.51	52.84	45.25	26.86
1850	52.07	61.03	62.63	50.70	45.60	26.93
1900	59.90	64.25	62.98	48.19	44.35	26.55
1950	59.31	61.73	60.32	47.32	43.91	25.42
2000	60.11	58.70	57.92	49.48	41.74	24.60
2050	56.68	59.41	58.37	44.66	42.64	23.52
2100	63.10	58.70	60.51	46.26	40.76	22.32
2150	58.47	58.37	58.87	44.68	39.46	24.06
2200	58.04	57.45	59.90	43.32	39.86	23.47
2250	57.97	50.28	58.47	42.36	38.10	21.07
2300	54.47	54.14	56.91	42.54	36.26	21.85
2350	58.23	52.37	53.86	40.64	35.56	21.28
2400	55.41	54.26	54.35	41.93	33.30	20.08
2450	54.87	54.89	52.37	40.03	33.91	20.30
2500	57.10	54.33	54.37	38.26	32.41	20.79

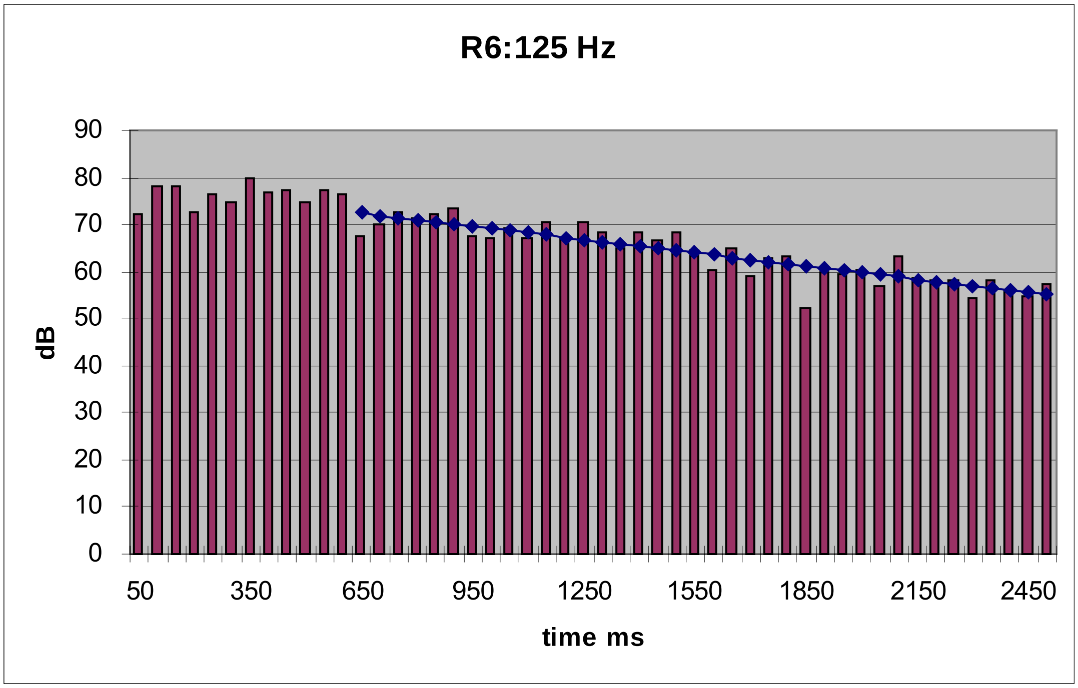

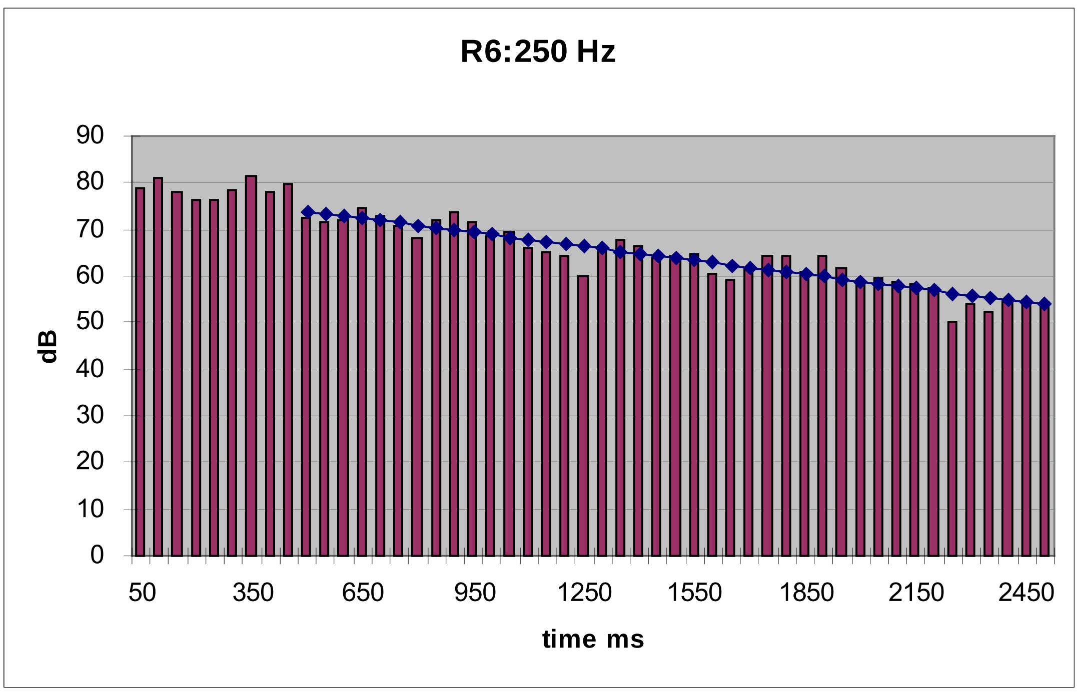

Figure A.64 Decay and Fit for T30 for 125 and 250 Hz at R6 in Rüstem Pasa

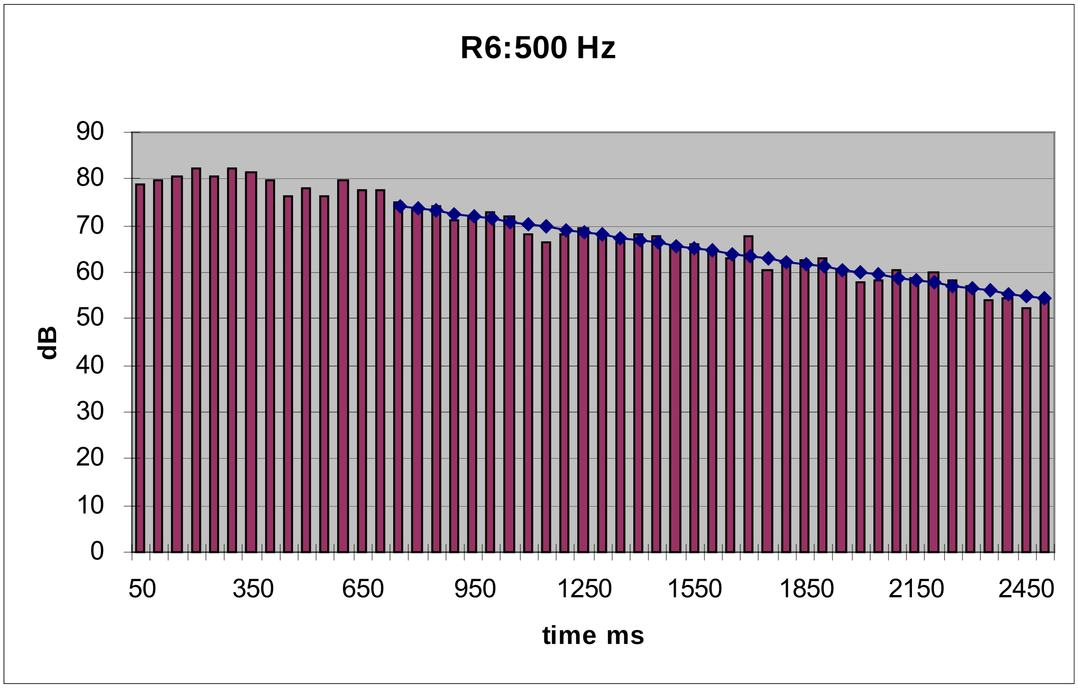

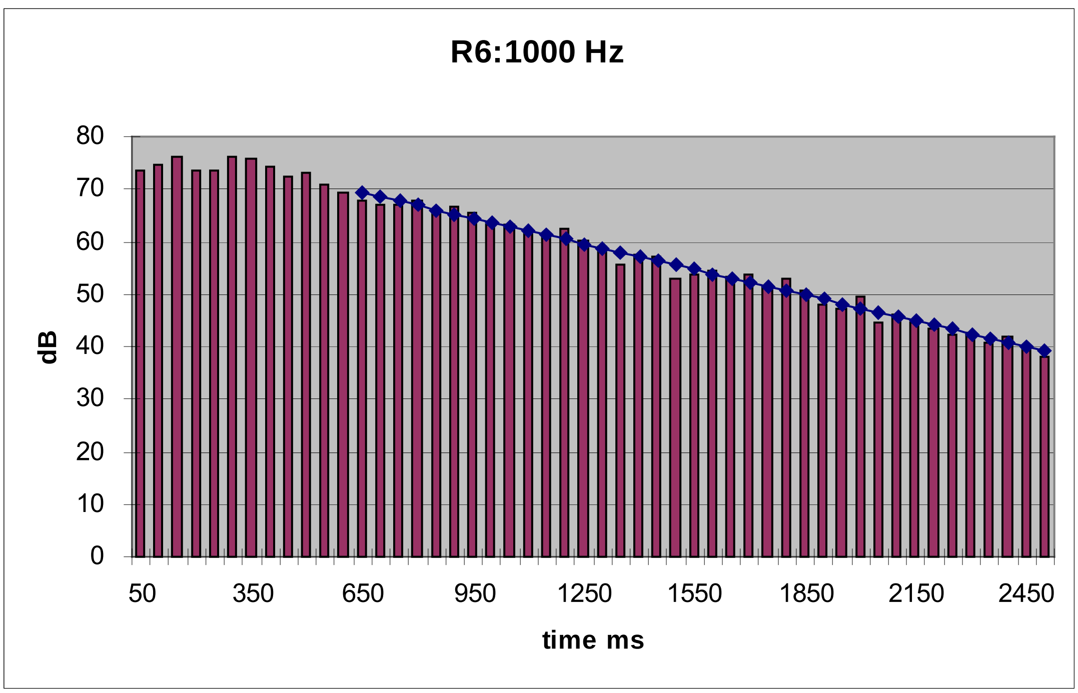

Figure A.65 Decay and Fit for T30 for 500 and 1000 Hz at R6 in Rüstem Pasa

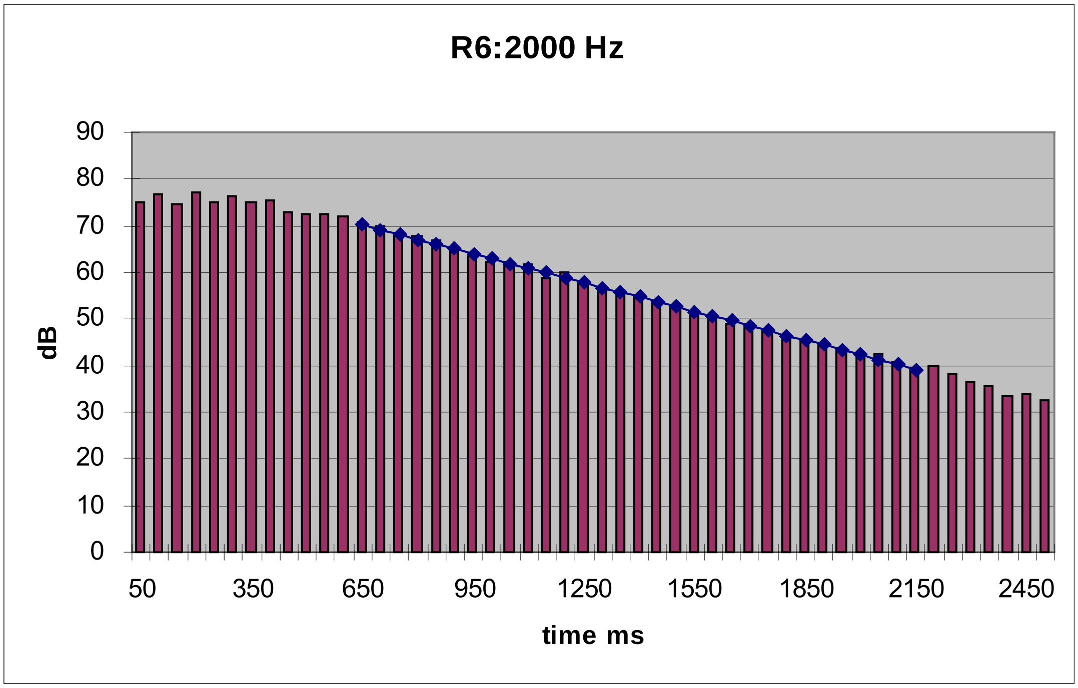

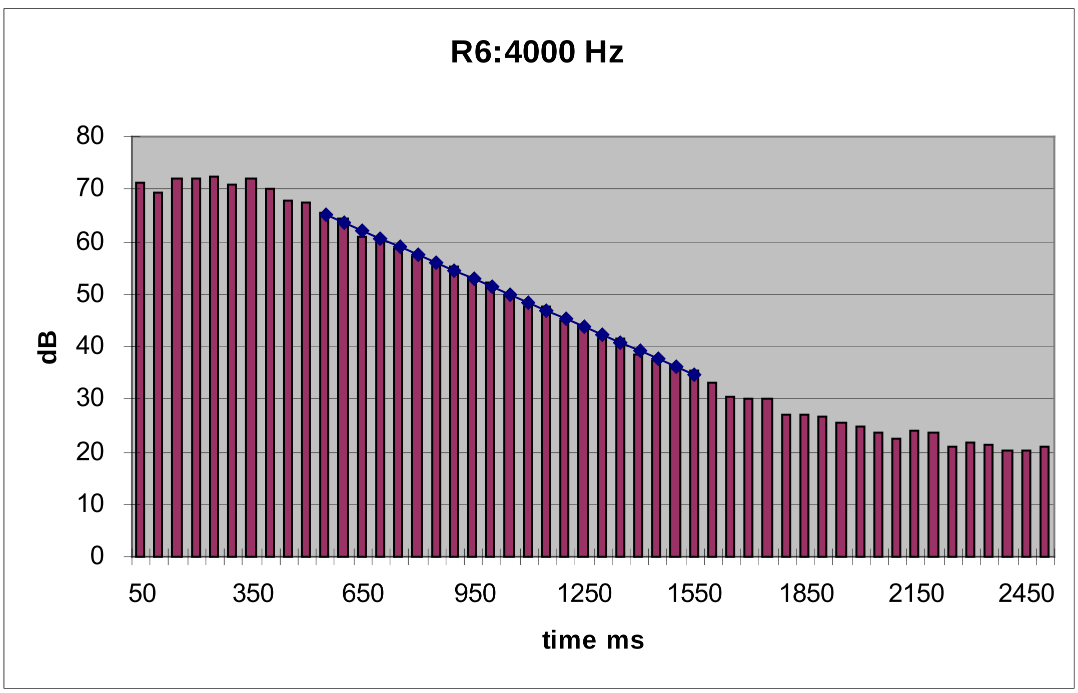

Figure A.66 Decay and Fit for T30 for 2 and 4 kHz at R6 in Rüstem Pasa

Table A.23 Measurements at R7 in Rüstem Pasa

time	dB					
ms	125	250	500	1000	2000	4000
50	77.75	77.75	79.00	72.39	73.92	71.31
100	74.88	77.87	77.30	72.29	74.41	71.00
150	68.72	80.08	80.69	72.53	73.40	70.27
200	77.07	77.99	79.47	71.66	74.03	70.81
250	78.31	78.95	80.24	72.51	74.67	71.05
300	77.56	79.07	76.86	72.79	75.52	70.60
350	74.76	82.48	81.61	72.41	74.69	69.66
400	79.26	77.99	80.22	73.68	71.75	67.78
450	78.62	76.79	81.49	73.56	72.06	67.47
500	75.61	77.61	79.94	69.61	72.08	65.00
550	69.87	79.89	78.10	69.61	72.11	63.59
600	73.31	76.55	74.39	71.28	71.40	61.88
650	77.77	78.48	76.36	68.86	69.57	59.17
700	71.85	78.76	79.94	68.55	66.70	58.18
750	74.11	73.99	77.59	67.85	65.85	56.87
800	74.39	77.52	75.42	67.19	65.69	56.16
850	71.24	74.50	71.94	66.49	65.14	53.22
900	78.41	71.45	69.07	67.03	64.51	52.09
950	70.51	69.75	72.39	64.46	62.79	50.07
1000	71.28	72.25	70.79	63.95	60.86	49.69
1050	71.64	70.74	72.69	61.66	59.71	48.75
1100	70.93	70.08	68.04	60.72	57.69	45.60
1150	67.76	68.81	70.15	59.27	58.00	44.57
1200	73.23	67.43	70.98	58.49	57.29	42.52
1250	69.99	60.09	66.01	59.78	55.64	41.06
1300	67.90	67.87	69.12	57.41	55.78	41.37
1350	69.35	64.93	66.16	56.40	54.94	39.63
1400	63.64	66.77	67.36	55.31	52.45	37.53
1450	61.41	61.33	64.63	52.82	52.21	36.48
1500	64.70	65.97	63.15	53.69	49.27	36.03
1550	69.99	68.32	66.25	53.60	49.69	33.89
1600	64.20	60.09	65.31	53.15	50.12	32.45
1650	64.02	62.70	64.96	48.94	46.97	30.10
1700	66.30	66.46	65.12	50.82	46.73	28.76
1750	57.29	58.77	63.69	50.26	45.53	28.55
1800	58.65	63.05	63.64	48.16	44.59	25.75
1850	59.41	61.69	59.31	50.23	44.35	24.29
1900	63.50	60.65	61.26	48.02	42.69	23.68
1950	65.03	62.28	62.60	45.79	43.04	23.42
2000	61.57	60.54	58.18	47.58	39.77	22.30
2050	63.83	60.72	56.18	44.61	37.65	21.61
2100	53.97	58.09	56.77	42.69	38.62	18.18
2150	61.55	60.54	58.47	42.19	38.83	20.30
2200	59.45	60.77	53.41	42.73	37.61	19.45
2250	52.47	58.70	54.70	42.78	36.45	19.80
2300	52.12	60.28	49.32	42.78	34.74	20.55
2350	52.82	57.43	53.74	39.63	36.17	19.33
2400	54.73	54.73	51.93	40.26	33.87	25.52
2450	51.46	60.28	51.83	40.50	32.22	20.51
2500	49.86	55.01	52.07	37.09	31.51	20.79

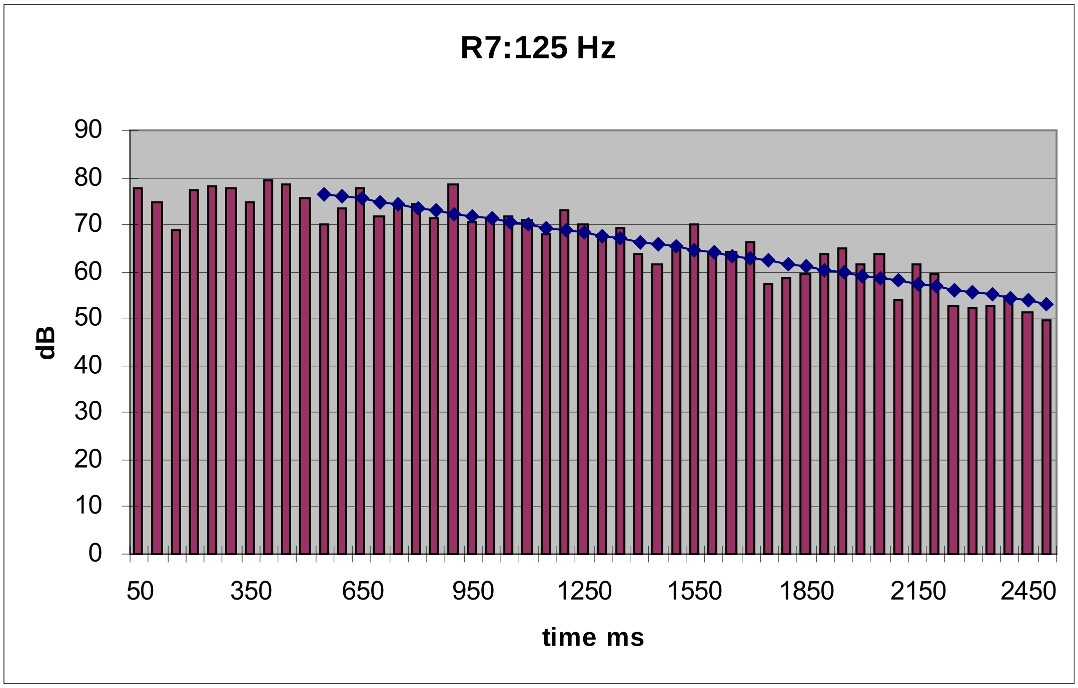

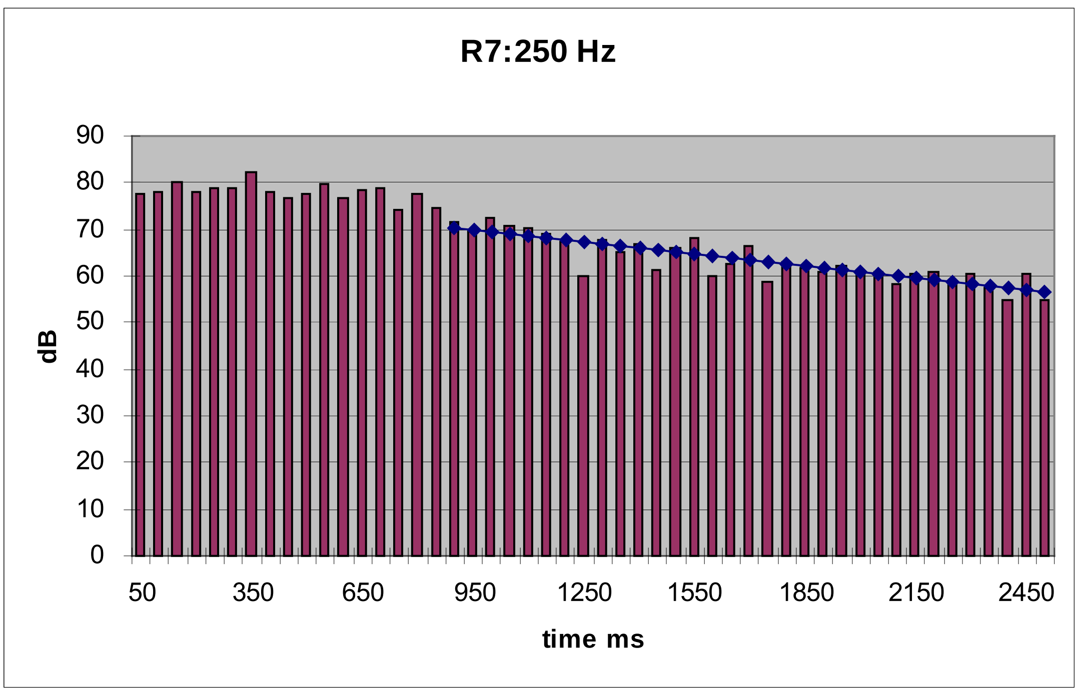

Figure A.67 Decay and Fit for T30 for 125 an d250 Hz at R7 in Rüstem Pasa

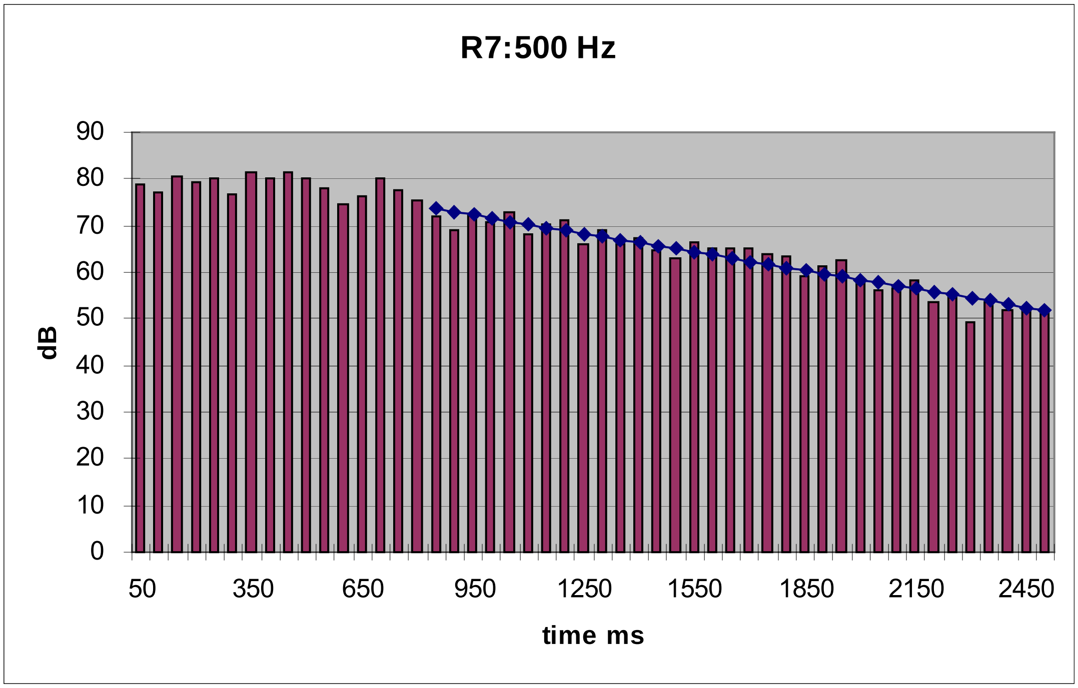

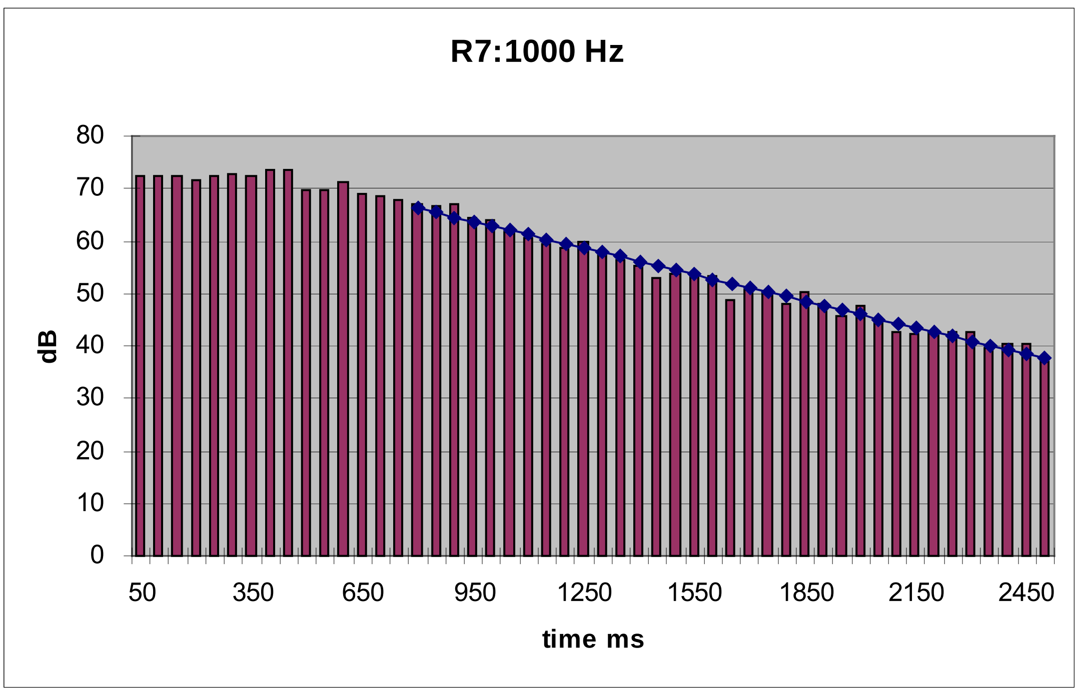

Figure A.68 Decay and Fit for T30 for 500 and 1000 Hz at R7 in Rüstem Pasa

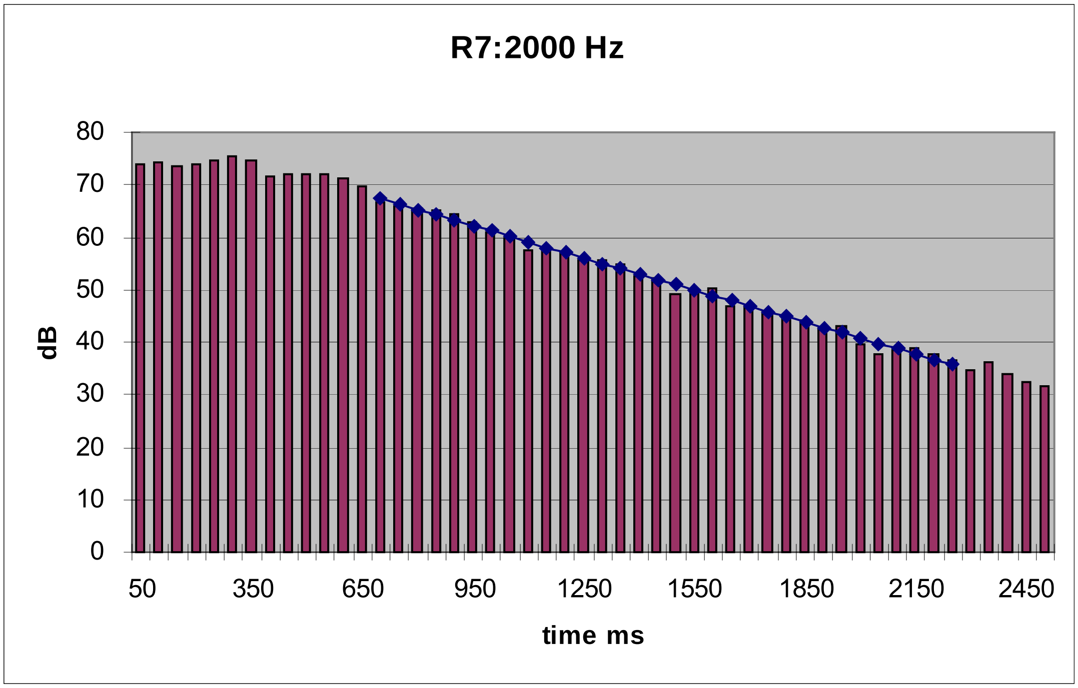

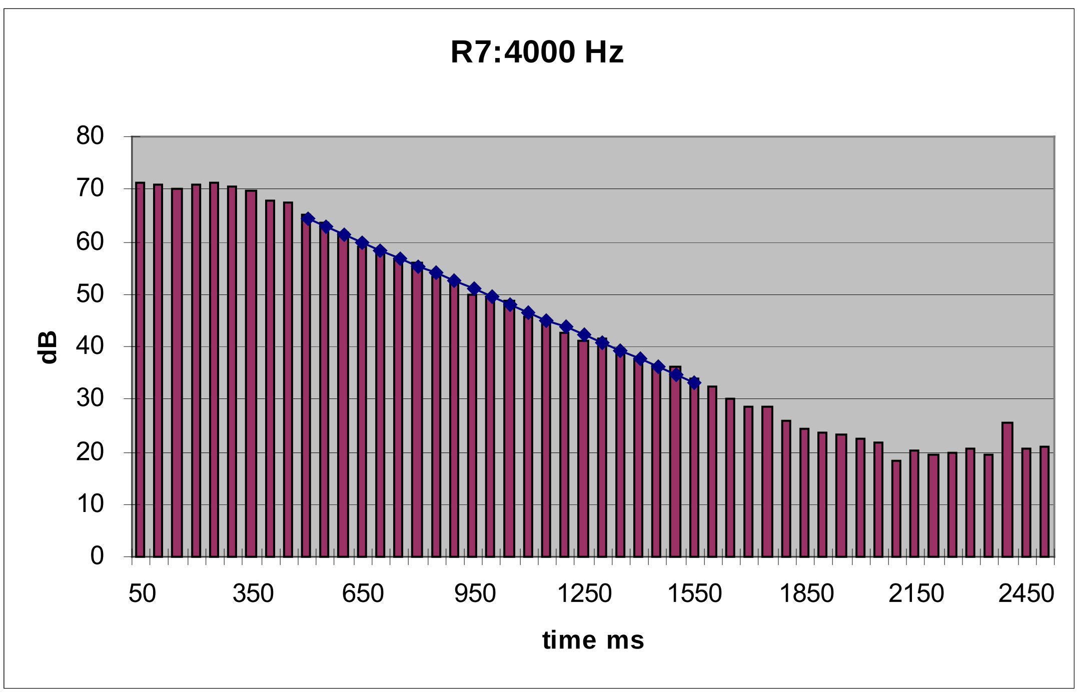

Figure A.69 Decay and Fit for T30 for 2 and 4 kHz at R7 in Rüstem Pasa

Table A.24 Measurements at R8 in Rüstem Pasa

time	dB					
ms	125	250	500	1000	2000	4000
50	73.23	75.16	75.96	71.78	71.66	69.10
100	70.95	71.68	77.14	71.12	71.85	70.06
150	71.40	72.84	77.14	70.30	73.94	69.28
200	76.15	75.80	78.10	69.50	72.18	70.60
250	75.38	77.23	78.62	71.19	70.95	69.61
300	77.49	79.87	78.46	68.74	72.36	70.72
350	73.02	78.81	77.33	70.86	73.09	69.43
400	66.44	77.37	76.13	71.02	71.31	67.92
450	74.67	73.47	78.67	70.79	70.08	62.51
500	70.95	75.30	78.76	68.46	69.50	63.00
550	68.79	74.65	78.76	68.86	67.66	59.74
600	63.87	70.58	77.33	68.27	67.12	58.75
650	71.82	74.34	74.74	67.38	66.46	57.31
700	66.86	69.52	74.27	66.98	65.43	56.82
750	72.36	72.36	74.41	65.10	64.09	55.01
800	65.66	73.38	73.14	64.46	62.86	53.36
850	69.87	69.33	73.21	64.11	61.99	50.33
900	57.05	72.62	68.86	61.73	60.89	49.03
950	58.18	69.33	70.55	60.23	61.19	48.05
1000	62.11	69.57	71.14	61.99	61.50	48.02
1050	65.85	69.73	72.39	59.05	56.18	46.47
1100	63.24	61.88	70.01	59.19	57.83	43.56
1150	65.05	68.25	67.73	58.56	57.01	41.49
1200	59.74	66.18	70.65	57.13	55.38	40.90
1250	63.50	65.00	67.33	56.09	53.32	39.39
1300	64.11	64.86	67.87	55.69	51.39	38.10
1350	57.78	63.55	68.95	52.63	51.57	35.25
1400	60.35	60.28	63.52	53.50	51.18	34.83
1450	62.42	64.72	66.01	53.10	51.90	34.15
1500	60.94	66.18	63.38	49.83	48.73	32.36
1550	58.16	67.14	66.44	51.03	47.11	30.69
1600	57.57	61.10	61.73	50.82	47.81	29.16
1650	60.46	64.42	60.91	49.53	45.39	28.97
1700	59.67	63.73	61.08	51.97	44.54	27.30
1750	56.94	62.72	61.55	48.89	42.26	25.00
1800	58.63	62.89	60.32	47.22	41.67	23.78
1850	59.29	59.83	61.26	46.97	41.96	23.14
1900	58.32	60.21	57.88	46.17	40.17	21.90
1950	58.04	59.05	62.30	45.18	39.39	21.28
2000	59.43	55.67	58.37	44.75	38.33	21.19
2050	57.15	58.42	55.53	42.59	37.91	20.55
2100	59.71	56.58	58.23	44.00	35.91	19.50
2150	58.04	55.31	56.07	42.24	35.96	19.45
2200	55.03	58.25	56.75	40.69	34.74	20.13
2250	51.55	54.73	56.28	40.05	32.81	20.58
2300	53.06	57.92	54.47	40.38	31.98	20.39
2350	46.00	55.71	51.10	38.05	31.94	22.51
2400	52.94	56.18	52.80	37.77	32.83	21.59
2450	48.56	51.46	52.35	36.81	30.62	21.33
2500	46.73	47.93	51.43	37.56	30.10	21.33

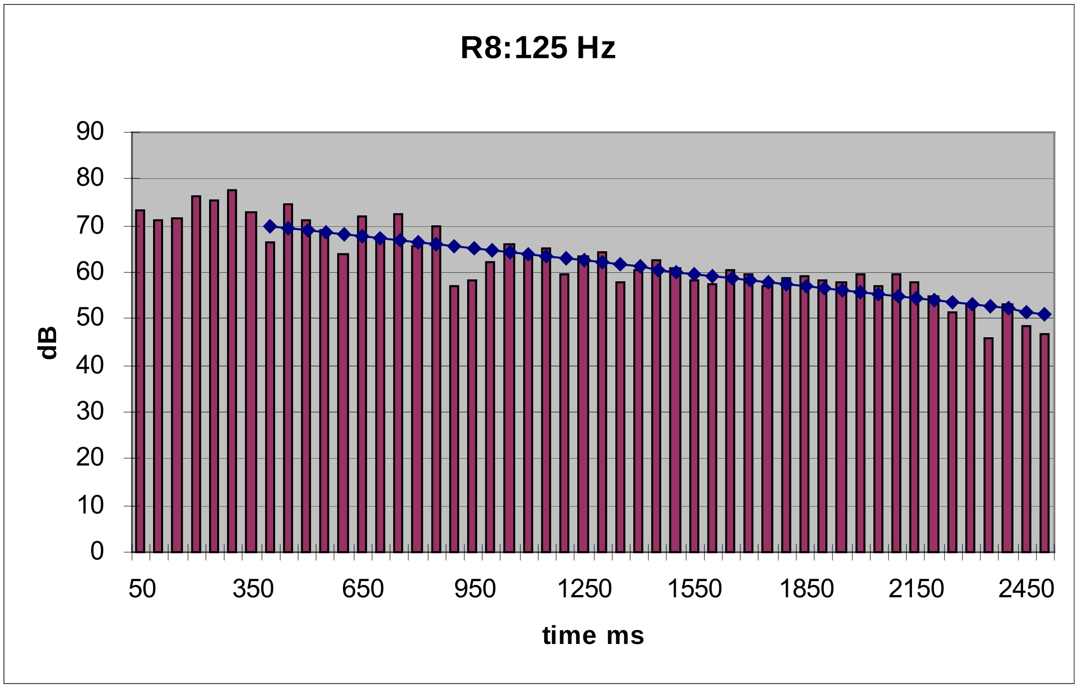

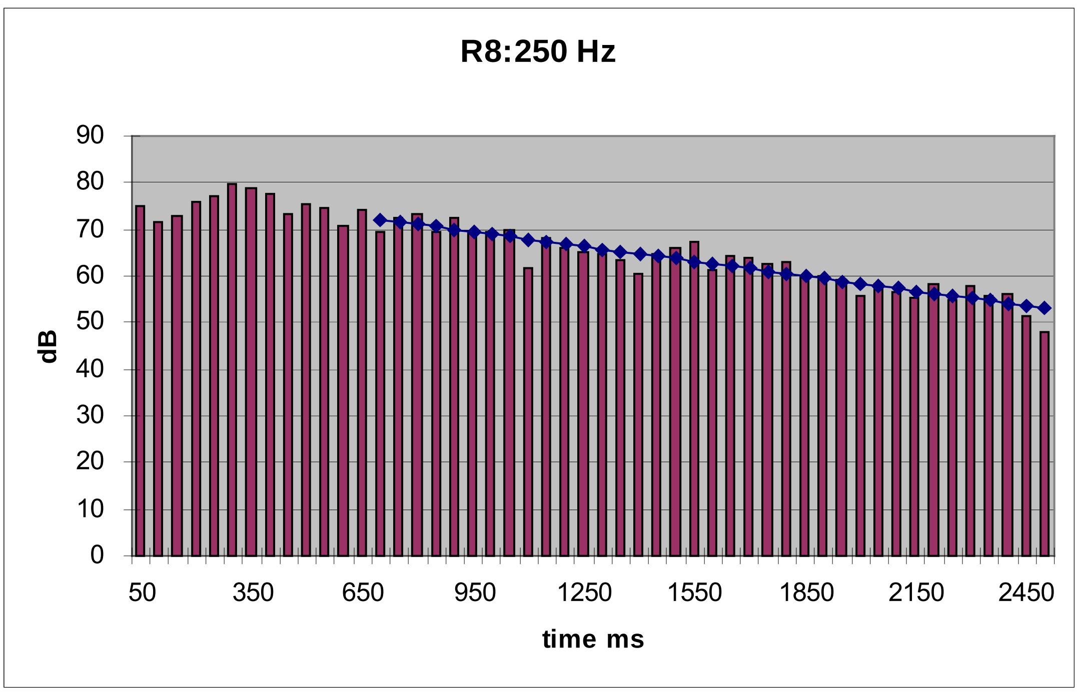

Figure A.70 Decay and Fit for T30 for 125 and 250 Hz at R8 in Rüstem Pasa

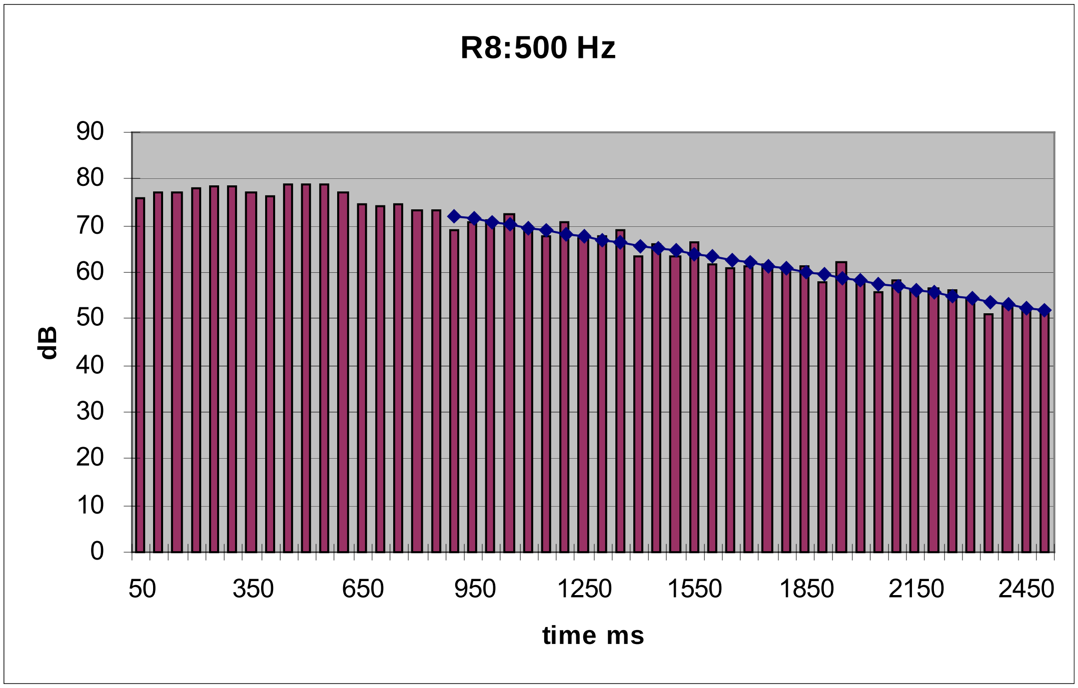

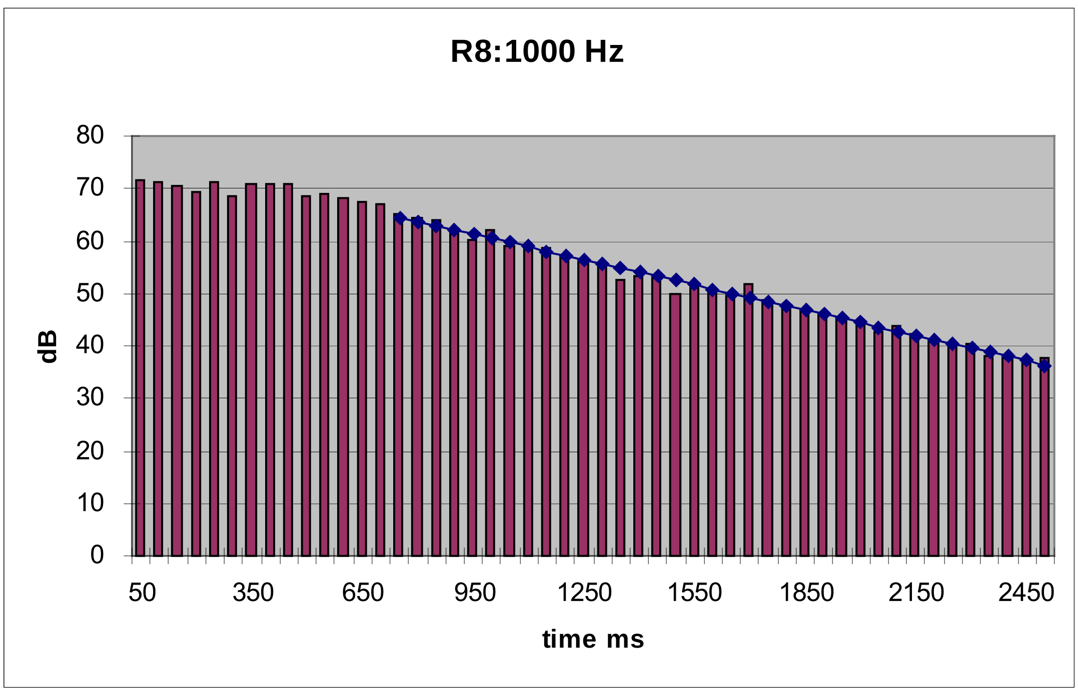

Figure A.71 Decay and Fit for T30 for 500 and 1000 Hz at R8 in Rüstem Pasa

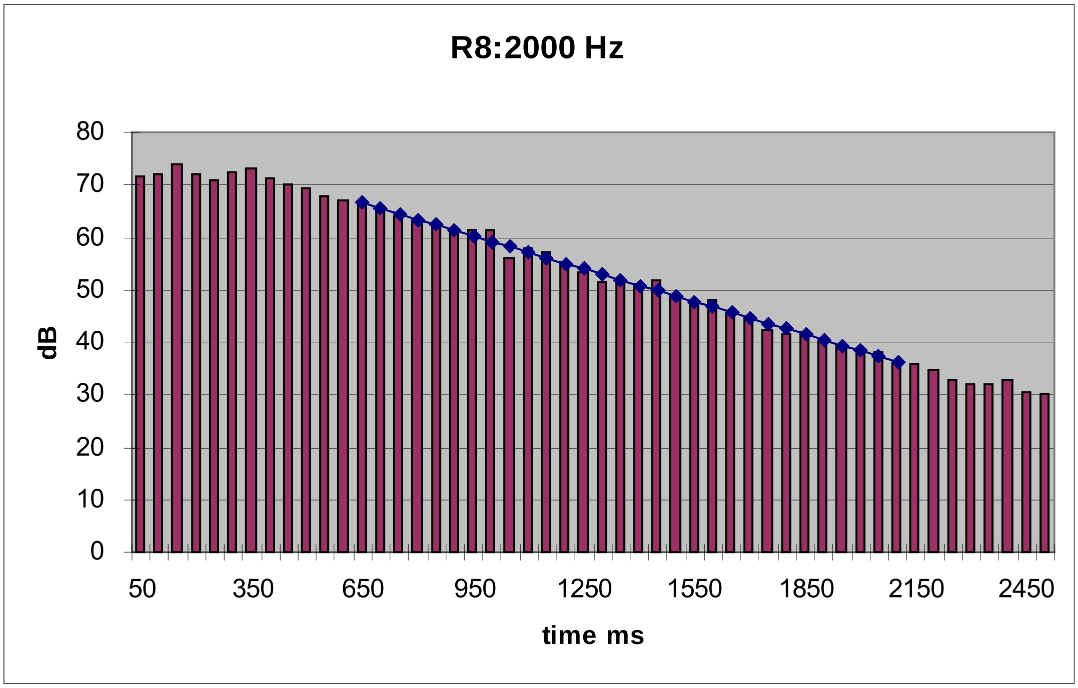

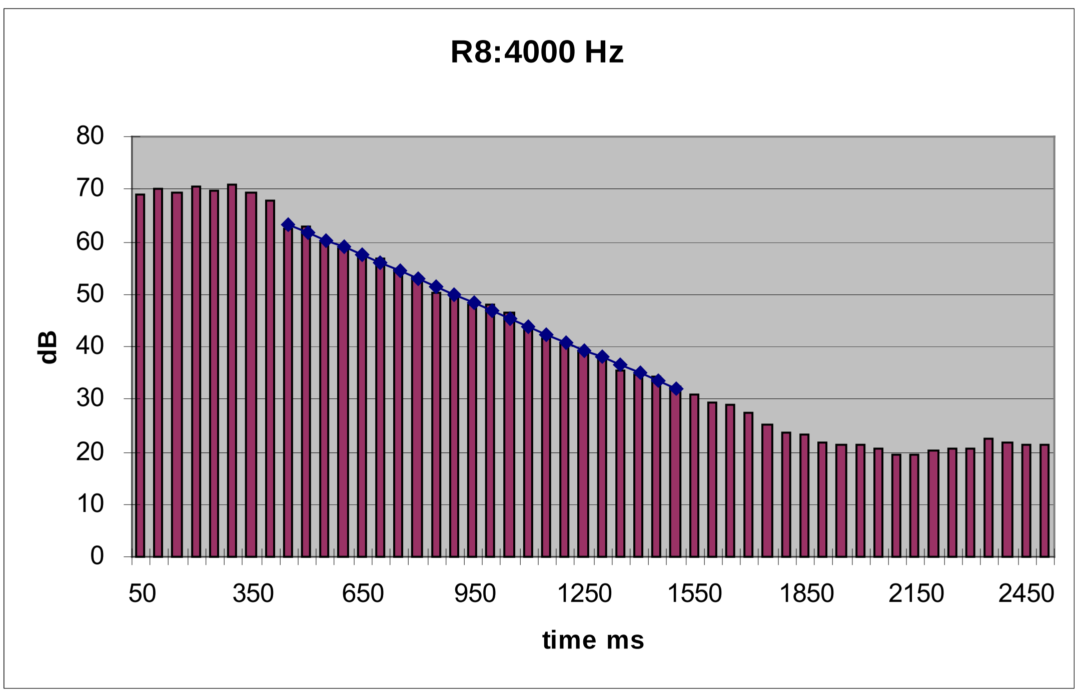

Figure A.72 Decay and Fit for T30 for 2 and 4 kHz at R8 in Rüstem Pasa

Table A.25 Measurements at R9 in Rüstem Pasa

time	dB					
ms	125	250	500	1000	2000	4000
50	77.07	76.32	77.91	68.63	71.17	66.81
100	77.89	72.79	78.27	69.68	72.84	65.76
150	68.74	75.80	75.92	71.02	71.28	65.07
200	76.41	78.10	75.38	69.61	69.54	66.74
250	76.46	78.90	75.73	66.89	70.55	66.53
300	76.69	71.02	75.99	66.96	71.89	65.80
350	78.67	74.62	74.01	66.18	70.15	67.10
400	76.32	70.44	77.02	67.59	70.30	67.14
450	70.81	77.40	78.24	69.90	69.35	64.98
500	74.81	74.32	74.69	67.66	69.59	63.95
550	72.67	73.80	73.26	67.19	68.51	61.48
600	70.37	73.94	76.13	65.12	69.05	60.65
650	67.33	70.55	73.40	66.04	68.63	58.70
700	68.98	68.81	74.74	63.33	66.58	57.05
750	67.31	74.22	72.08	65.64	64.79	55.90
800	69.33	70.39	72.98	64.98	65.52	54.02
850	70.98	72.88	71.21	64.06	63.47	52.49
900	68.72	71.21	69.52	60.79	63.95	50.75
950	66.06	68.46	71.05	62.91	61.17	48.33
1000	68.63	68.48	71.61	60.39	60.11	48.47
1050	65.38	69.17	67.03	59.74	59.67	45.23
1100	68.55	67.03	69.64	60.21	59.17	43.70
1150	63.45	65.12	67.92	57.10	56.77	43.86
1200	69.05	68.84	70.65	57.85	56.87	41.30
1250	65.92	65.10	68.65	58.00	57.29	41.42
1300	62.68	64.32	70.53	53.57	55.41	38.29
1350	57.85	65.14	67.92	54.84	54.11	35.28
1400	60.61	63.19	65.14	56.21	53.08	36.41
1450	64.63	65.64	62.70	52.14	49.48	34.74
1500	60.46	63.55	66.60	51.46	51.01	33.02
1550	59.17	61.26	65.83	51.72	48.78	31.23
1600	59.64	65.73	63.22	49.72	45.39	30.39
1650	58.25	62.65	60.46	51.27	45.60	27.94
1700	60.75	59.92	61.26	49.93	45.51	26.65
1750	57.74	63.43	63.76	48.96	44.26	25.05
1800	54.98	56.16	59.45	48.26	42.61	24.08
1850	57.85	56.96	62.77	48.47	42.31	21.80
1900	54.44	61.52	57.83	47.32	40.59	21.14
1950	56.16	56.87	57.78	44.97	40.59	19.52
2000	57.50	53.15	60.21	44.94	39.86	17.54
2050	57.78	62.98	58.40	44.94	38.19	20.11
2100	55.93	59.17	56.49	42.54	37.32	19.31
2150	59.17	54.00	54.84	42.50	36.99	15.83
2200	55.29	56.73	55.13	41.06	37.70	15.59
2250	53.06	56.94	51.79	40.76	34.62	14.65
2300	47.84	55.38	51.53	38.73	31.80	15.40
2350	53.74	53.34	52.80	37.72	33.49	15.59
2400	52.23	52.54	53.15	39.39	29.96	15.31
2450	46.12	53.46	51.90	38.64	32.27	15.24
2500	52.02	51.22	49.13	36.17	30.60	15.31

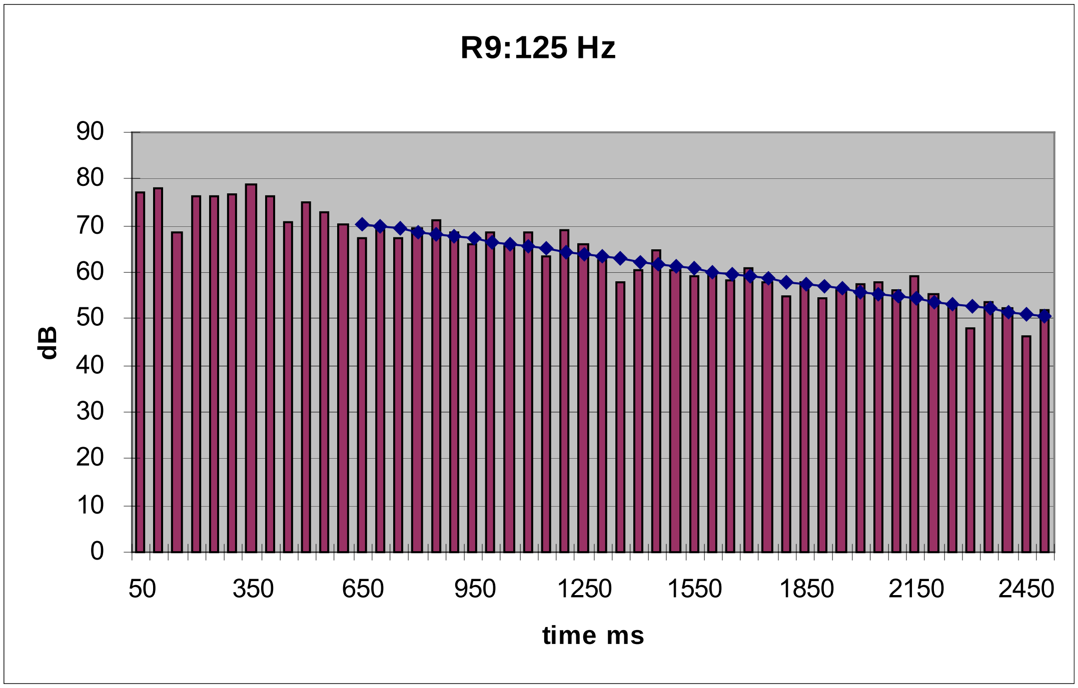

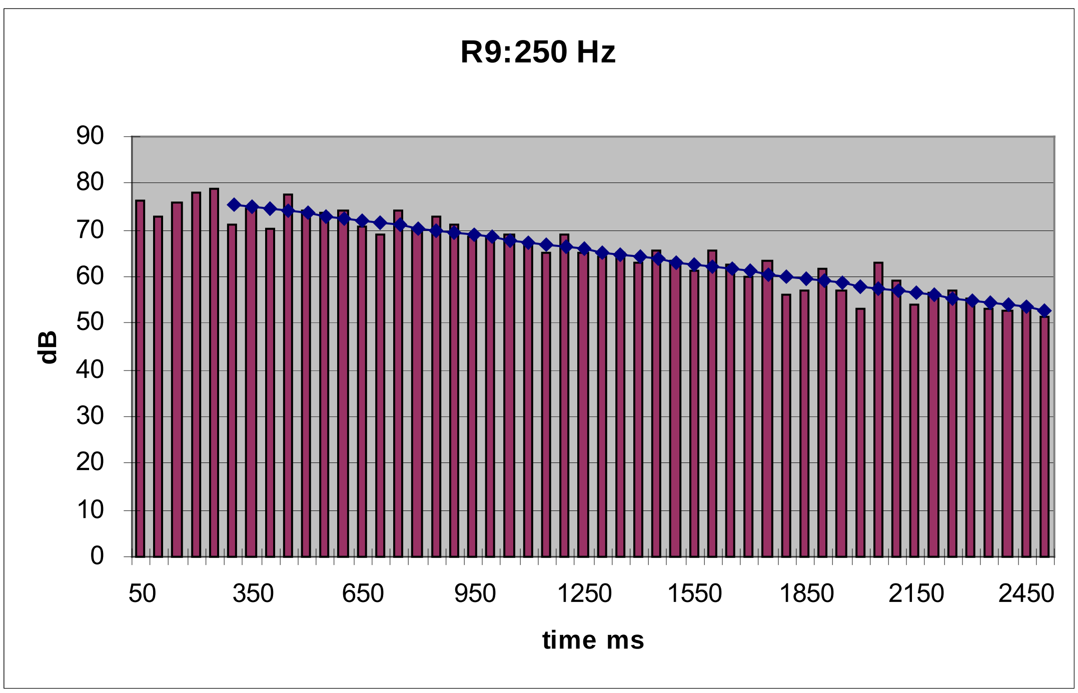

Figure A.73 Decay and Fit for T30 for 125 and 250 Hz at R9 in Rüstem Pasa

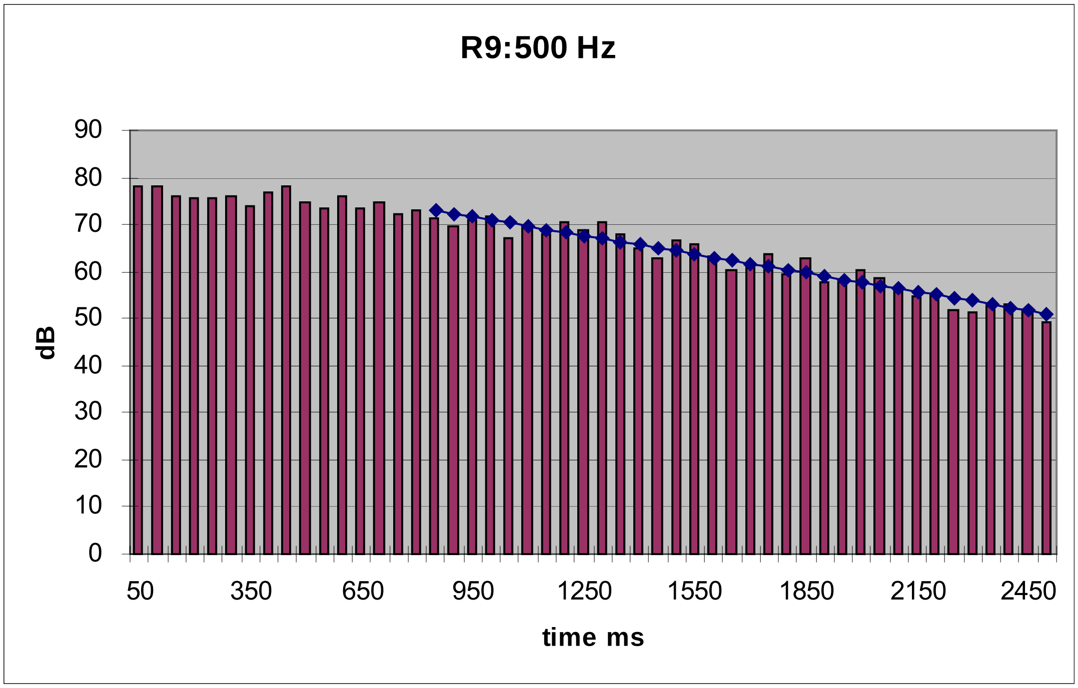

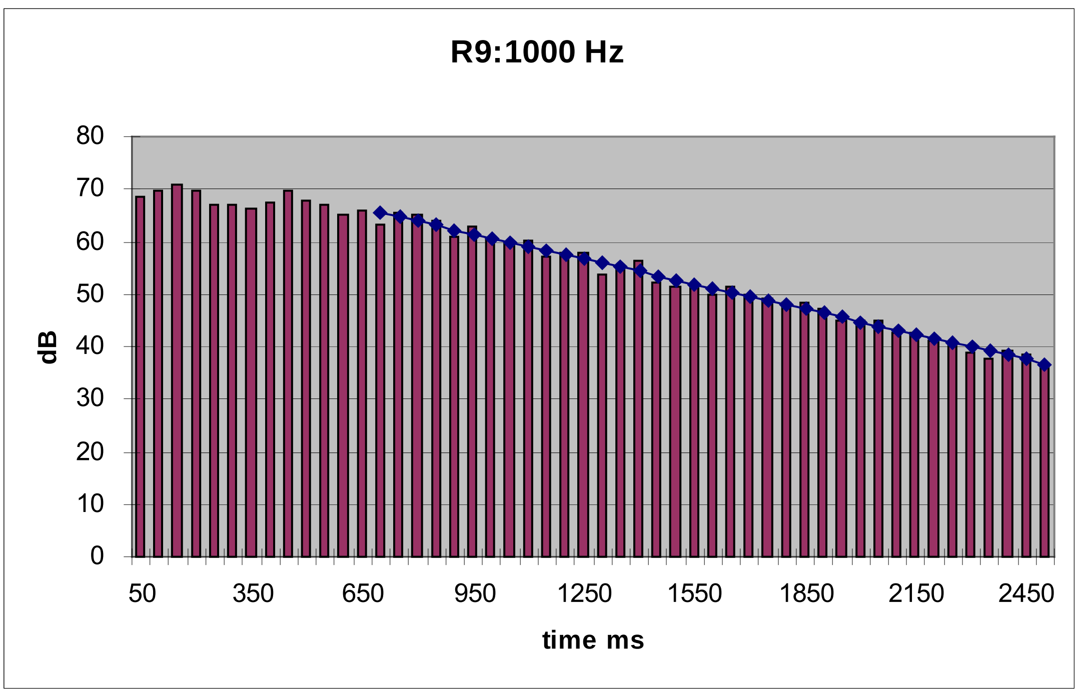

Figure A.74 Decay and Fit for T30 for 500 and 1000 Hz at R9 in Rüstem Pasa

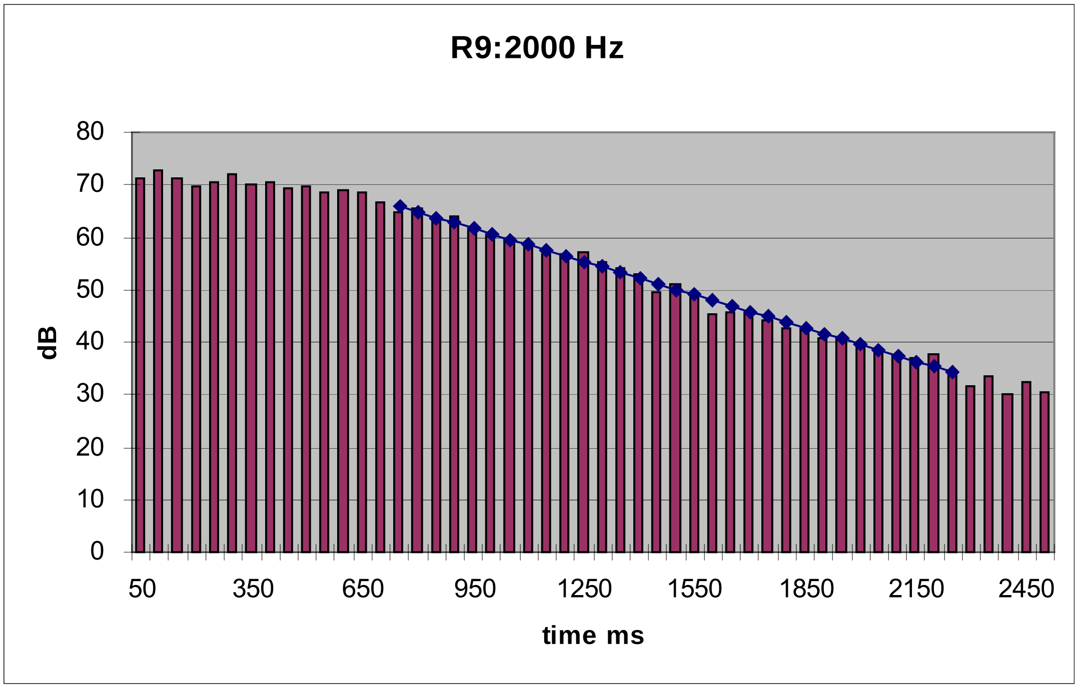

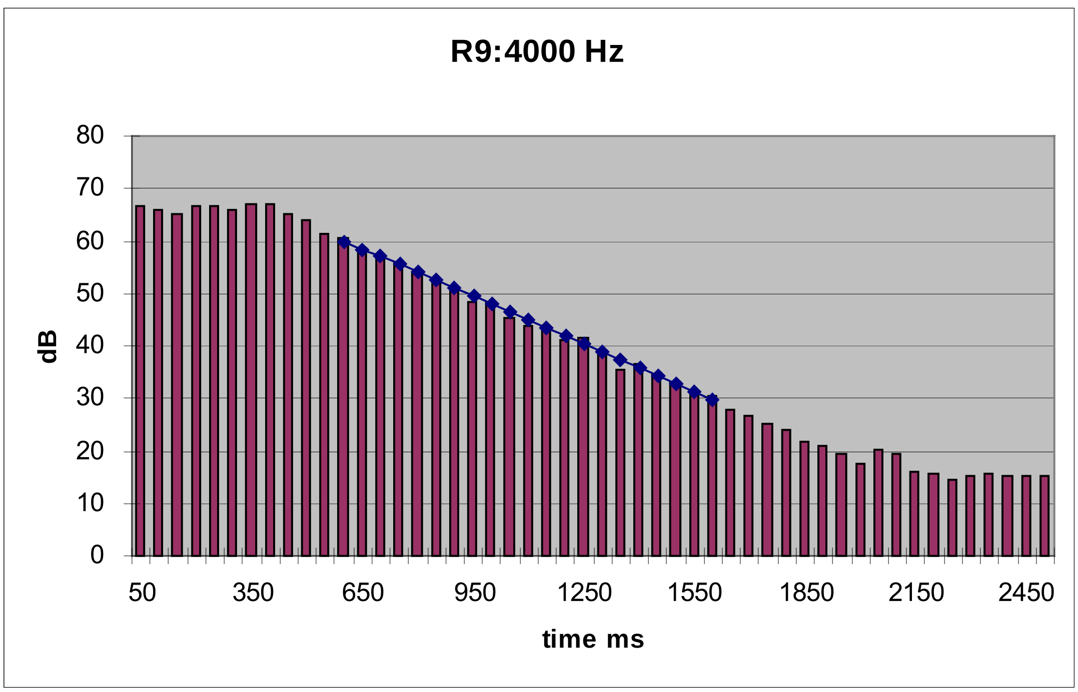

Figure A.75 Decay and Fit for T30 for 2 and 4 kHz at R9 in Rüstem Pasa

Table A.26 Measurements at R10 in Rüstem Pasa

time	dB					
ms	**125**	**250**	**500**	**1000**	**2000**	**4000**
50	75.33	77.70	80.45	72.95	75.68	69.12
100	75.85	80.62	80.27	73.35	74.20	69.14
150	76.25	82.29	83.28	72.06	73.63	69.50
200	76.53	78.13	83.72	74.01	75.33	69.43
250	77.59	73.71	81.70	73.61	74.74	68.46
300	79.21	71.57	82.81	73.00	74.58	68.55
350	78.60	80.45	80.85	73.66	74.86	69.24
400	70.18	75.19	79.35	74.22	74.15	67.43
450	77.16	75.85	78.74	71.09	73.47	65.33
500	77.80	77.73	82.43	71.14	72.93	63.10
550	79.54	70.65	78.95	71.35	69.87	63.33
600	74.18	76.13	80.31	70.69	71.12	62.58
650	69.71	73.82	79.21	68.88	69.59	59.85
700	75.12	72.22	78.83	65.12	67.78	56.84
750	73.28	77.47	76.39	67.10	67.31	56.44
800	75.40	70.06	76.69	64.77	64.77	54.66
850	71.35	65.94	73.19	63.85	63.87	52.84
900	67.45	72.53	73.45	64.44	63.55	52.07
950	70.46	71.12	70.67	63.08	62.13	48.92
1000	71.14	70.65	69.90	62.42	62.77	48.75
1050	64.82	71.68	68.60	62.13	60.46	46.92
1100	65.92	71.78	69.78	61.92	59.57	45.67
1150	73.05	69.10	70.72	61.43	57.88	44.47
1200	67.83	62.53	66.70	58.42	57.50	42.21
1250	67.50	67.66	69.57	58.35	55.38	41.81
1300	68.11	63.95	67.03	59.10	53.90	38.99
1350	68.27	67.31	66.53	56.04	54.59	39.20
1400	56.30	63.99	64.37	55.03	52.00	36.66
1450	61.19	66.25	65.76	55.17	53.22	35.63
1500	62.93	65.12	64.63	54.91	50.30	33.80
1550	67.14	64.20	61.64	54.11	49.06	32.20
1600	63.76	61.01	65.87	53.22	48.14	30.29
1650	61.57	63.78	65.29	53.29	45.86	29.23
1700	61.41	63.08	65.59	52.16	46.92	26.41
1750	62.68	60.06	59.27	53.29	45.06	26.95
1800	65.22	61.92	61.62	51.46	44.73	24.51
1850	63.05	64.09	59.27	51.10	43.58	23.92
1900	63.85	60.68	62.68	48.16	41.79	23.82
1950	60.28	63.10	60.18	47.69	42.57	22.95
2000	59.76	58.14	59.03	46.24	40.66	19.73
2050	57.31	56.84	58.14	44.28	39.16	20.67
2100	58.44	58.56	60.77	46.24	37.32	18.44
2150	59.03	57.34	58.49	43.51	36.43	19.57
2200	56.77	55.88	58.30	44.05	35.65	18.88
2250	55.03	57.27	55.38	43.51	34.78	17.38
2300	59.34	57.52	55.69	40.64	35.61	20.67
2350	57.74	51.72	53.41	40.38	32.93	19.73
2400	56.89	58.07	51.97	39.79	32.71	19.47
2450	56.96	56.75	51.81	37.77	33.51	15.97
2500	61.05	53.81	53.74	37.49	32.34	18.53

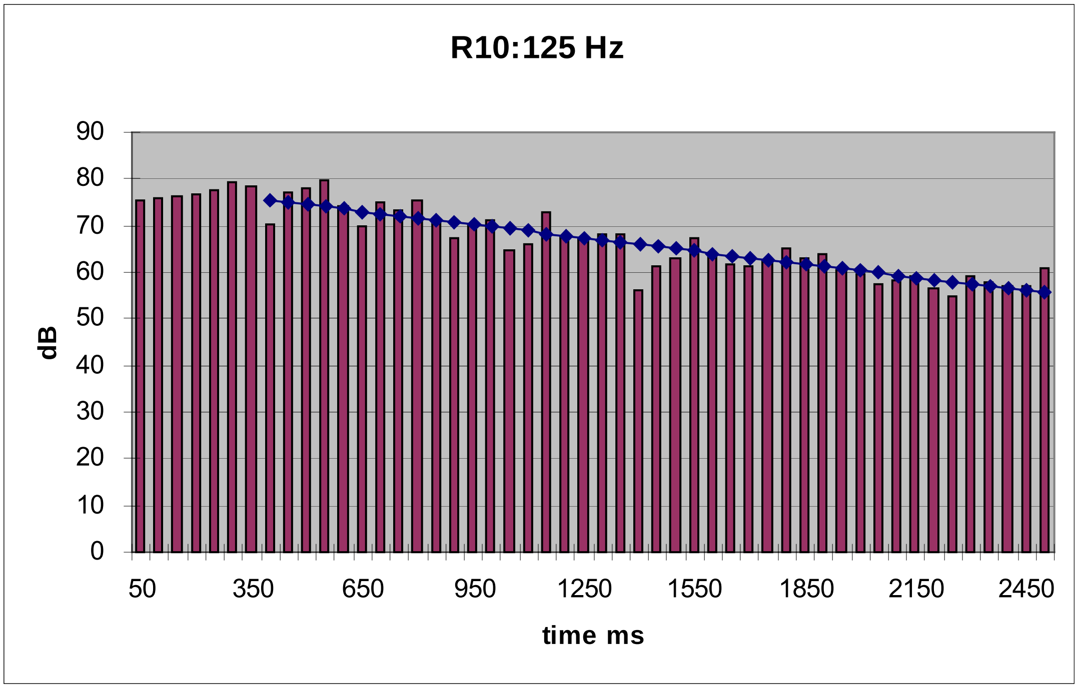

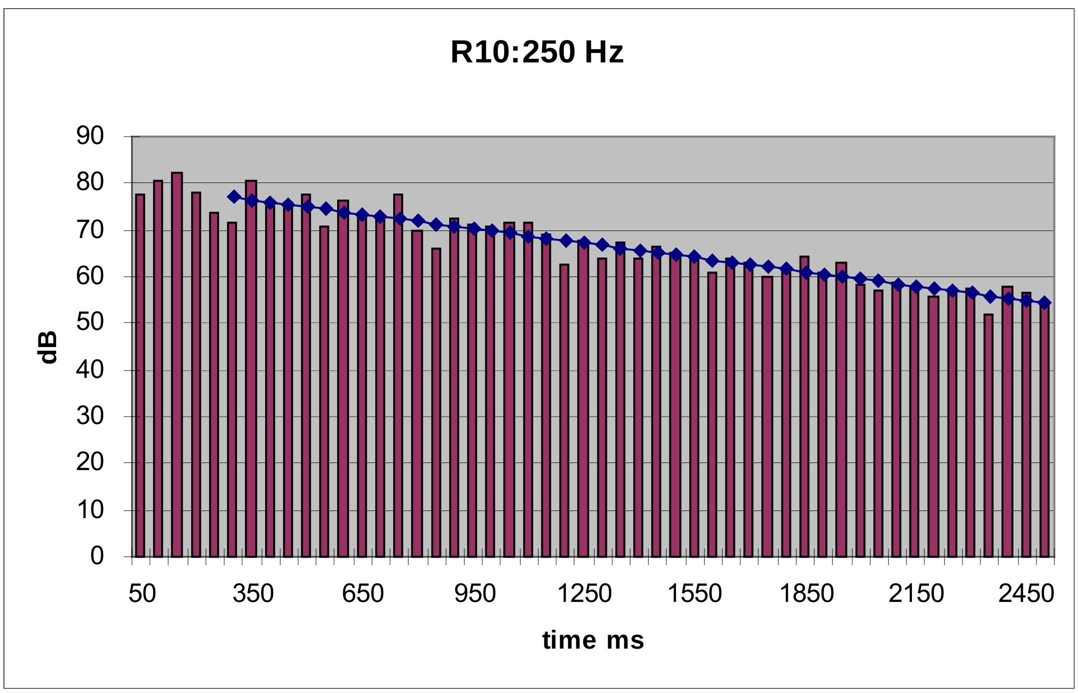

Figure A.76 Decay and Fit for T30 for 125 and 250 Hz at R10 in Rüstem Pasa

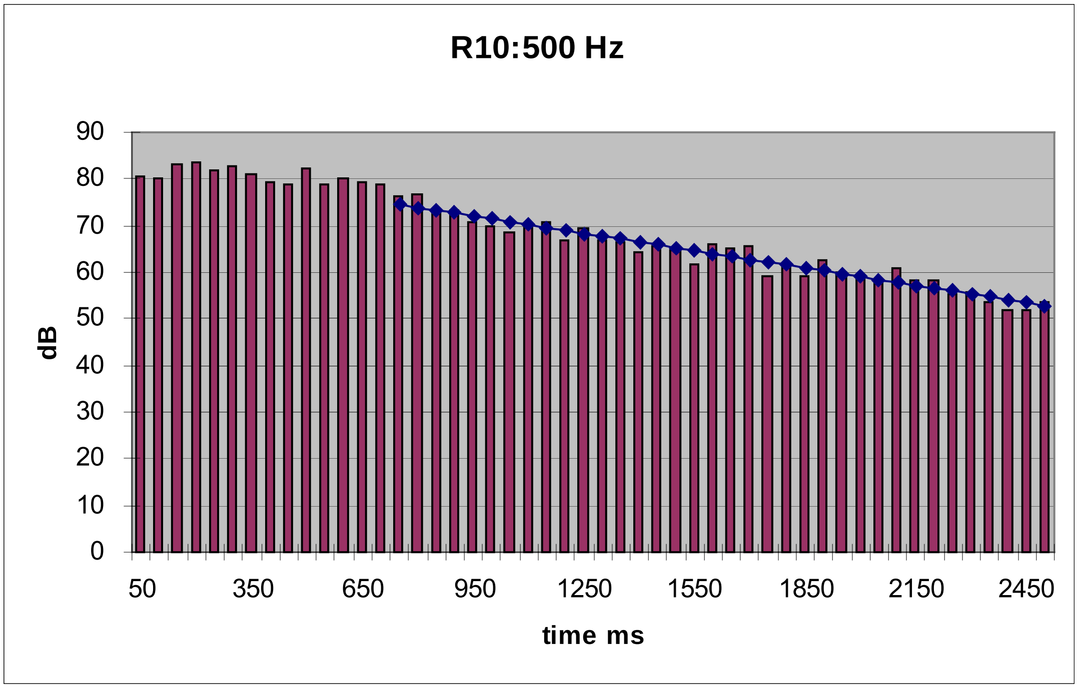

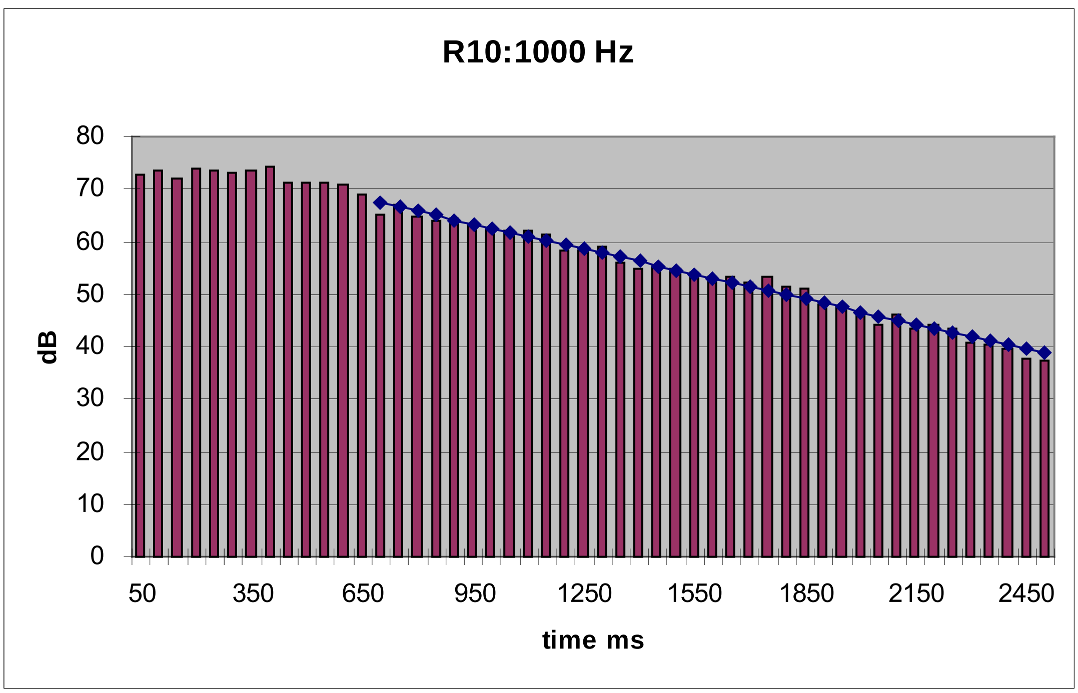

Figure A.77 Decay and Fit for T30 for 500 and 1000 Hz at R10 in Rüstem Pasa

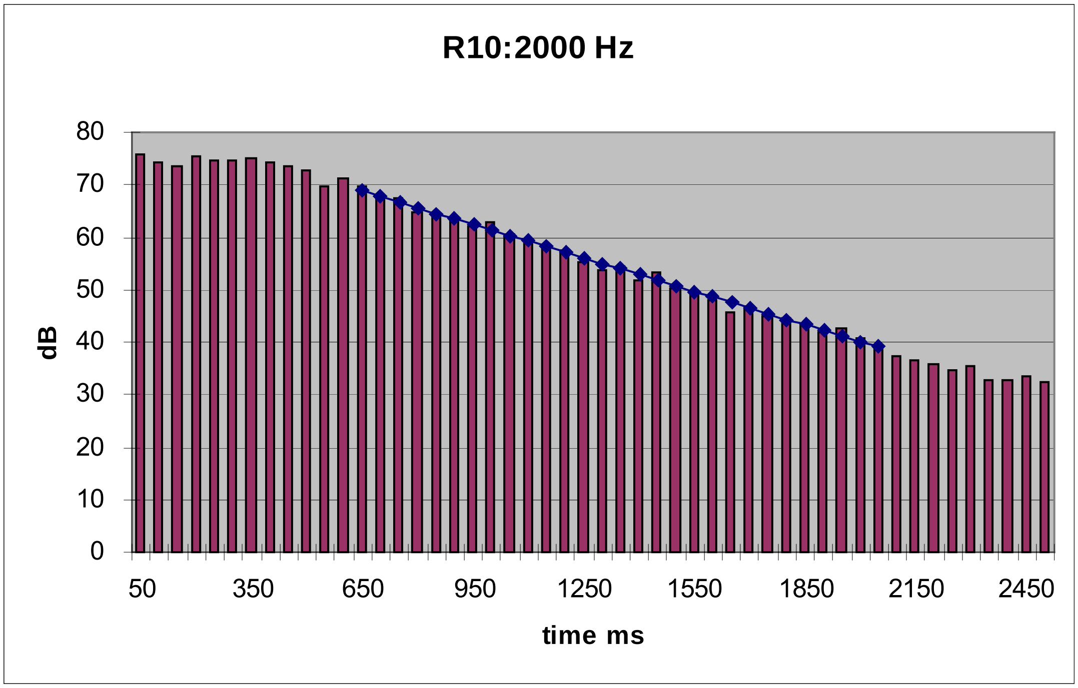

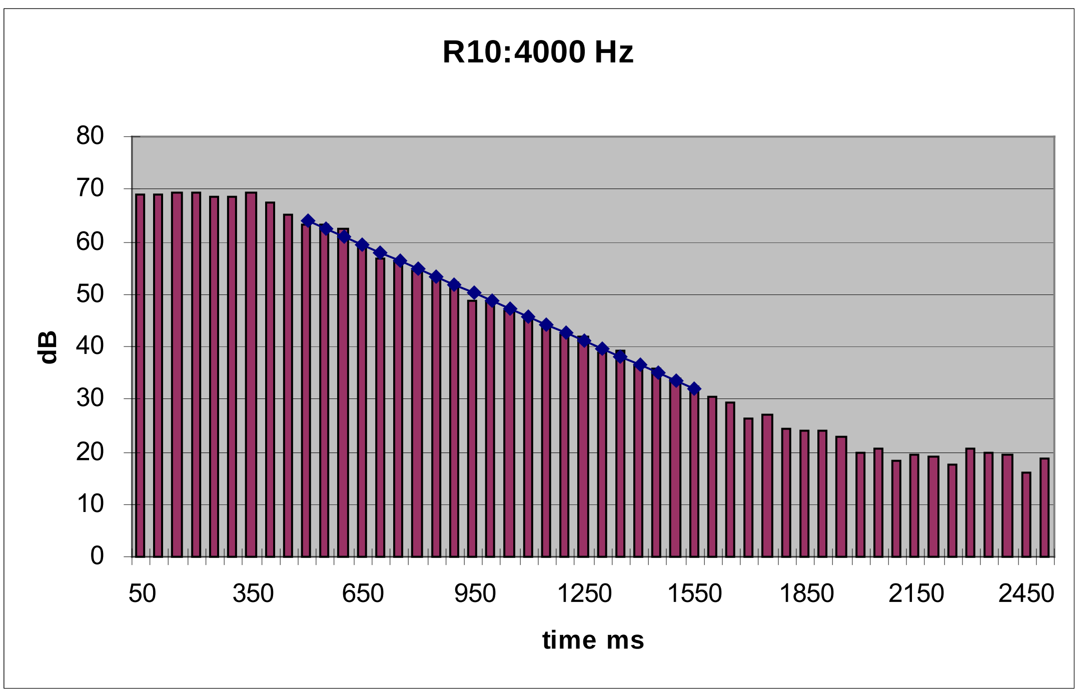

Figure A.78 Decay and Fit for T30 for 2 and 4 kHz at R10 in Rüstem Pasa

APPENDIX B

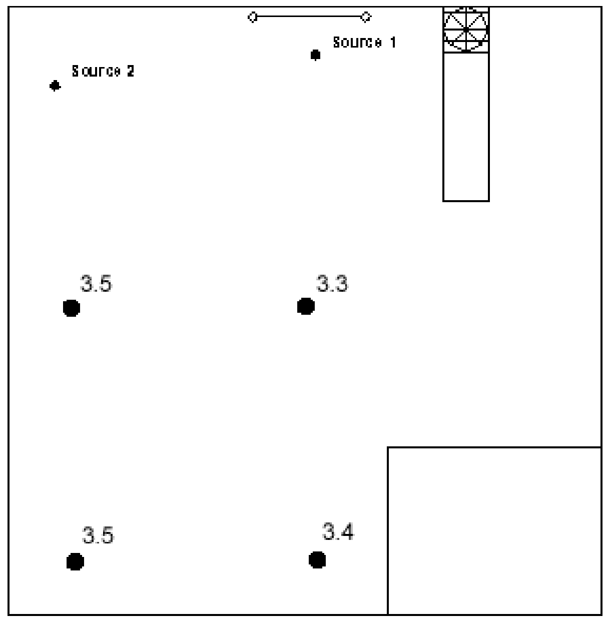

Figure B.1 RT30 distribution for 1000 Hz in Cenabi Ahmet Pasa Mosque

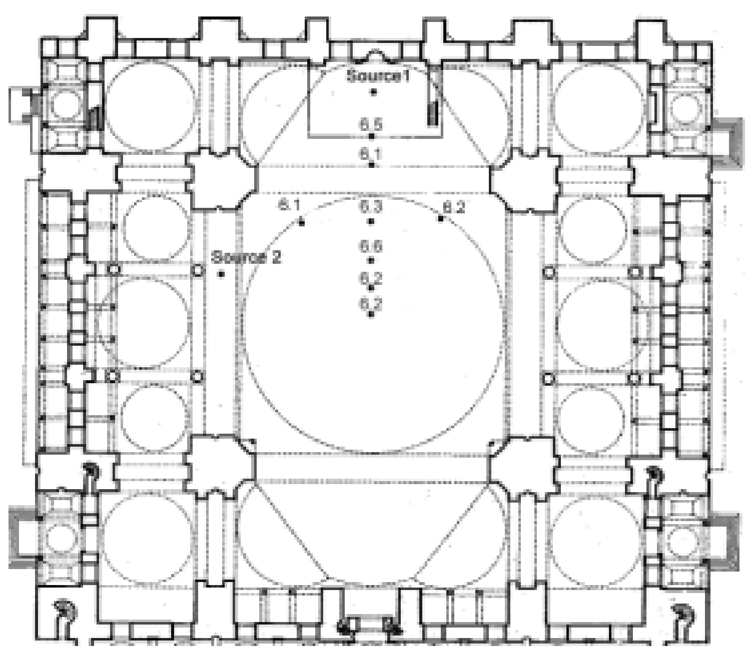

Figure B.2 RT30 distribution for 1000 Hz in Suleymaniye Mosque

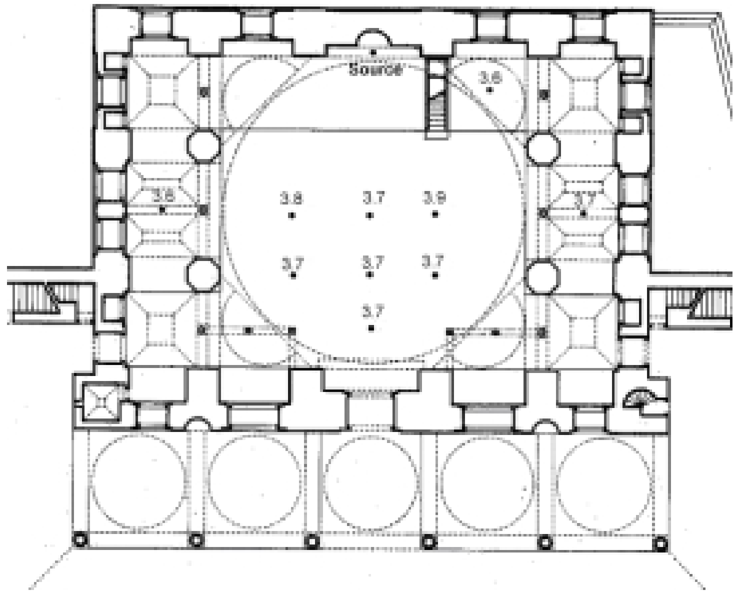

Figure B.3 RT30 distribution for 1000 Hz in Rustem Pasa Mosque

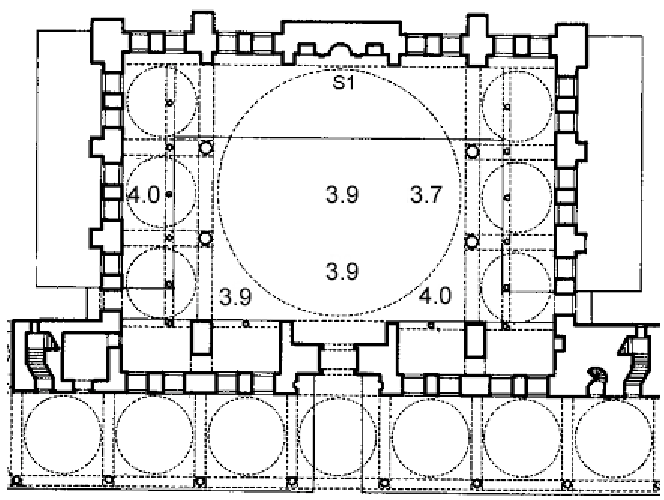

Figure B.4 RT30 distribution for 1000 Hz in Mihrimah Sultan Mosque

VITA

I.Levent Topaktaş was born in Ankara on September 09, 1964. He received his B.S. degree in July 1987 and M.S. degree in July 1990 in Mechanical Engineering from the Middle East Technical University. He worked in Alarko Alfenaş as an engineer from 1998 to 1991. After then he worked as research assistant and instructor in the Department Architecture from 1991 to 1997. Since then he is working in Intergraph Middle East company. He started to work in Ankara office, continued with Bahrain office and currently he is in Dubai office as Technical Development Manager. His main areas of interest are software development, geographical information systems and database design.